The Development and Evaluation of Extracellular Vesicles as a Biocompatible Anti-Infective Drug Delivery System

Dissertation

zur Erlangung des Grades

des Doktors der Naturwissenschaften

der Naturwissenschaftlichen-Technischen Fakultät

der Universität des Saarlandes

von

Eilien Heinrich

(geb. Schulz)

Saarbrücken

2021

Tag des Kolloquiums:	05. Mai 2021
Dekan:	Prof. Dr. Jörn Walter
Berichterstatter:	Junior Prof. Dr. Gregor Fuhrmann
	Prof. Dr. Rolf Müller
Vorsitz:	Prof. Dr. Alexandra Kiemer
Akademischer Mitarbeiter:	Dr. Anna Kühn

Die vorliegende Arbeite wurde von Februar 2018 bis Februar 2021 unter der Leitung von Herrn Junior Prof. Dr. Gregor Fuhrmann am Helmholtz-Institut für Pharmazeutische Forschung Saarland (HIPS) in der Abteilung Biogene Nanotherapeutika (BION) angefertigt.

Table of Contents

I. Summary I
II. Zusammenfassung II
III. Graphical Abstract III
IV. Abbreviations IV
1. Introduction 1
1.1. Challenges in treating bacterial infections 1
1.2. Extracellular vesicles and outer membrane vesicles 8
1.2.1. Biology 8
1.2.2. OMVs derived from myxobacteria 11
1.2.3. Therapeutics based on extracellular vesicles 12
1.3. Gastrointestinal Tract 18
1.3.1. GIT Infections 18
1.3.2. *Shigella* Infections 19
1.3.3. GIT Models 22
1.3.4. Nanotherapeutics against gastrointestinal infections 22
1.4. Zebrafish 25
1.4.1. Anatomy, development and importance in research 25
1.4.2. Infection models in zebrafish 26
1.4.3. Nanotherapeutics in zebrafish 27
2. Aim 29
3. Main Findings 30
3.1. Characterization of EVs and OMVs 30
3.2. Storage Stability 32
3.3. Biocompatibility 33
3.4. Uptake 36
3.5. Antimicrobial Activity 37
4. Conclusion and Outlook 40
5. References 42
6. List of publications, oral and poster presentations 55
7. Scientific Output 56
7.1. Biocompatible bacteria-derived vesicles show inherent antimicrobial activity 56
7.2. Hot EVs - How temperature affects extracellular vesicles 92
7.3. Myxobacteria-Derived Outer Membrane Vesicles: Potential Applicability Against Intracellular Infections 116
7.4. A biocompatible carrier system against GI infections: Ciprofloxacin loaded Extracellular Vesicles inhibit the growth of *Shigella flexneri* 151
8. Acknowledgements 200

I. Summary

Approximately 700,000 people worldwide die from infections with antimicrobial-resistant bacteria annually. Extracellular vesicles (EVs) can help to delay or even prevent the development of this resistance by releasing high concentrations of antimicrobial agents specifically at the site of infection. In this context, vesicles derived from immune cells and myxobacteria were tested for the use as anti-infective drug delivery systems. Five main research objects were investigated: i) **characterization** of the vesicles, ii) storage **stability** iii) **biocompatibility**, iv) **uptake** in bacteria and cells and v) their **antimicrobial activity** against bacterial pathogens.

The vesicles exhibited sufficient stability and showed exceptional biocompatibility with low endotoxin levels, minor cytokine release by primary immune cells and no toxicity in zebrafish larvae. Vesicles were taken up into bacteria, cells and the epithelial layer of a 3D gastrointestinal co-culture model. An inherent antibacterial effect against *Escherichia coli* was observed with vesicles derived from *Cystobacter velatus*. Non-inherently active vesicles were successfully loaded with a broad-spectrum antibiotic, which thus inhibited the growth of *Shigella flexneri*.

The findings in this work demonstrate the exceptional properties of EVs to treat infections and provide the foundation for a successful translation towards clinical application.

II. Zusammenfassung

Weltweit sterben jährlich ca. 700.000 Menschen an einer Infektion mit antimikrobiell resistenten Bakterien. Extrazelluläre Vesikel (EVs) können dazu beitragen, die Entwicklung der Resistenzen zu verzögern oder gar zu verhindern, indem sie gezielt am Ort der Infektion hohe Konzentrationen an antimikrobiellen Wirkstoffen freisetzen. In diesem Zusammenhang wurden Vesikel, von Immunzellen und Myxobakterien, auf ihre Verwendung als antiinfektive Wirkstofftransportsysteme getestet. Fünf Hauptforschungspunkte wurden untersucht: i) **Charakterisierung** der Vesikel, ii) **Stabilität** iii) **Biokompatibilität**, iv) **Aufnahme** in Bakterien und Zellen und v) ihre **antimikrobielle Aktivität** gegenüber Pathogenen.

Die Vesikel wiesen eine ausreichende Stabilität auf und zeigten hohe Biokompatibilität mit niedrigen Endotoxinwerten, geringer Zytokinfreisetzung durch primäre Immunzellen und keine Toxizität in Zebrafischlarven. Die Vesikel wurden in Bakterien, Zellen und in die Epithelschicht eines 3D-Gastrointestinalen Kokulturmodells aufgenommen. Eine inhärente antibakterielle Wirkung gegen *Escherichia coli* wurde mit Vesikeln von *Cystobacter velatus* beobachtet. Nicht inhärent aktive Vesikel wurden erfolgreich mit einem Breitspektrum-Antibiotikum beladen, welche so das Wachstum von *Shigella flexneri* hemmten.

Die Ergebnisse dieser Arbeit weisen auf die außergewöhnlichen Eigenschaften von EVs zur Behandlung von Infektionen und bilden die Grundlage für eine erfolgreiche Translation in die klinische Anwendung.

III. Graphical Abstract

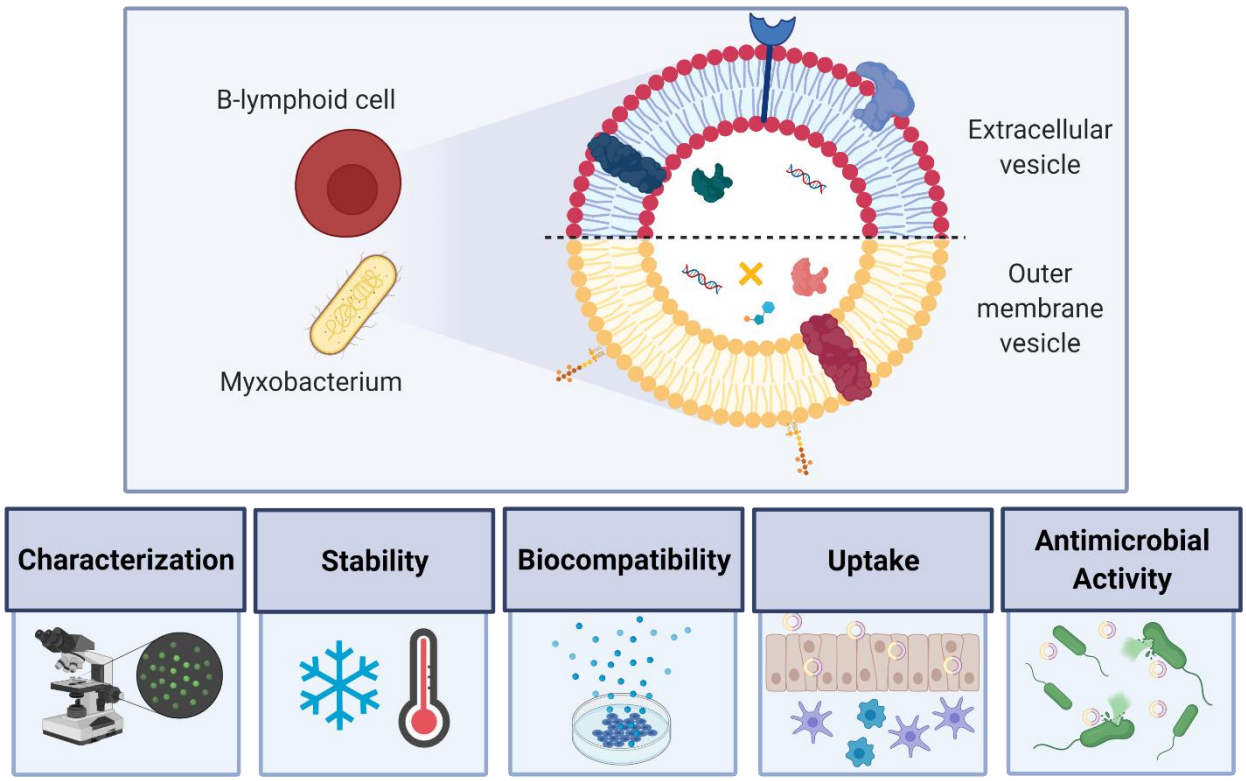

IV. Abbreviations

AMR	Antimicrobial Resistance
Cbv-OMVs	Outer Membrane Vesicles derived from Cbv034 myxobacteria
CPX	Ciprofloxacin
CFU	Colony Forming Unit
Cryo-EM	Cryo-Electron-Microscopy
EVs	Extracellular Vesicles
GI	Gastrointestinal
IL	Interleukin
LC MS	Liquid Chromatography coupled Mass Spectrometry
LPS	Lipopolysaccharide
MIC	Minimal Inhibitory Concentration
MTC	Maximal Tolerated Concentration
NPs	Nanoparticles
NTA	Nanoparticle Tracking Analysis
OD	Optical Density
OMVs	Outer Membrane Vesicles
PBMCs	Peripheral Blood Mononuclear Cells
PBS	Phosphate Buffered Saline
RO_{CPX}-EVs	Extracellular Vesicles derived from RO Cells loaded with ciprofloxacin
RO-EVs	Extracellular Vesicles derived from RO Cells
SB_{CPX}-OMVs	Outer Membrane Vesicles derived from SBSr073 myxobacteria loaded with ciprofloxacin
SB-OMVs	Outer Membrane Vesicles derived from SBSr073 myxobacteria
SEC	Size Exclusion Chromatography
TNF	Tumor Necrosis Factor

1. Introduction

1.1. Challenges in treating bacterial infections

Bacterial infections were one of the leading causes of death and increased morbidity, before the first antibiotic penicillin was discovered in 1928. The commercialization of the β-lactam inhibitor marked the breakthrough of a new chapter of modern medicine: the golden era of antibiotics. Pioneering drugs such as vancomycin, tetracycline or streptomycin were discovered, which also had an impact on other disciplines, *i.e*., in surgery, where highly complicated and longer lasting operations could now be carried out (1). However, shortly after each newly approved drug, antimicrobial resistant pathogens were isolated (***Figure 1***).

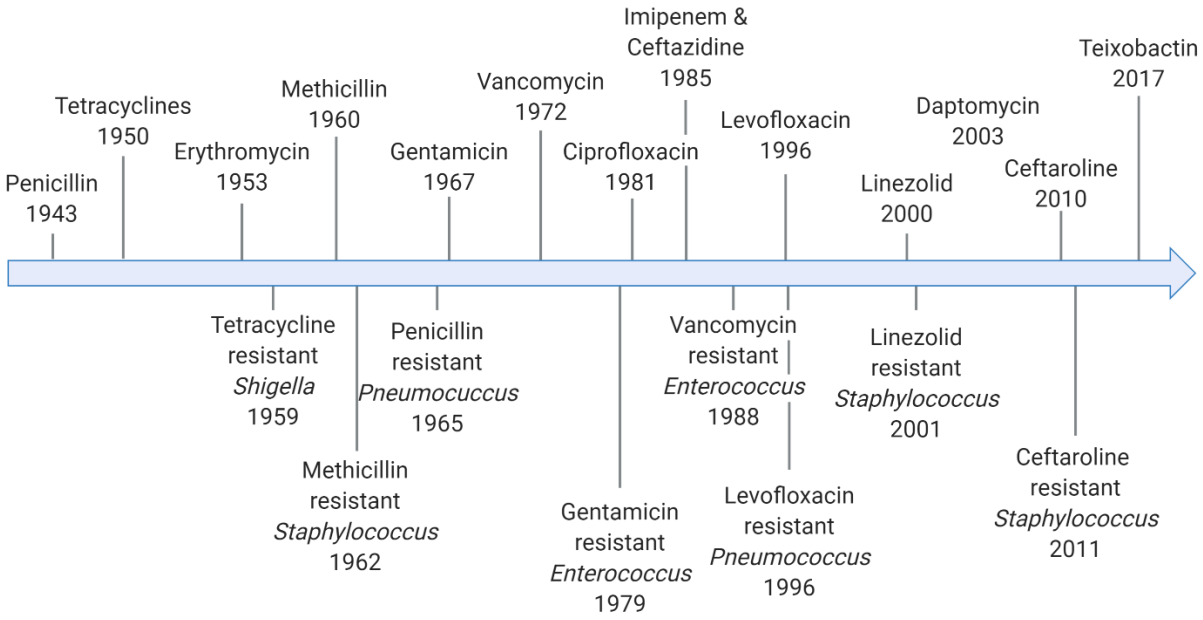

Figure 1 Timeline of the development of antibiotics and the occurrence of resistant pathogens *(2)*

Alexander Fleming himself, warned about antimicrobial resistance in his acceptance speech of the Nobel Prize in 1945: "It is not difficult to make microbes resistant to penicillin in the laboratory by exposing them to concentrations not sufficient to kill them, and the same thing has occasionally happened in the body" (3). The tools to develop resistance are ubiquitous, but the extensive and unwary use of antibiotics within the last decades leads to the probability that we will be facing an antibiotic resistance crisis. Today, approximately 700,000 people die annually due to antimicrobial resistant (4) bacteria worldwide (**Figure 2a**) (5). In Europe alone, 33,000 people die each year of multidrug-resistant pathogens, increasing healthcare costs up to 1.5 billion Euro (6, 7). In Germany, the number of deaths due to AMR infections increased

to 2,400 annually (8). By 2050, the number could rise up to 10 million worldwide each year, surpassing cancer mortality rates (5). Especially gastrointestinal (GI) infections are a matter of concern. The 2019 Center for Disease Control Report estimates, 212,500 non-thyphoidal *Salmonella* infections, for instance and 77,000 *Shigella* infections annually, only in the US within the next years (9). Simultaneously, the number of ciprofloxacin or azithromycin resistant *Shigella* has more than doubled between 2016 and 2018 (**Figure 2b**).

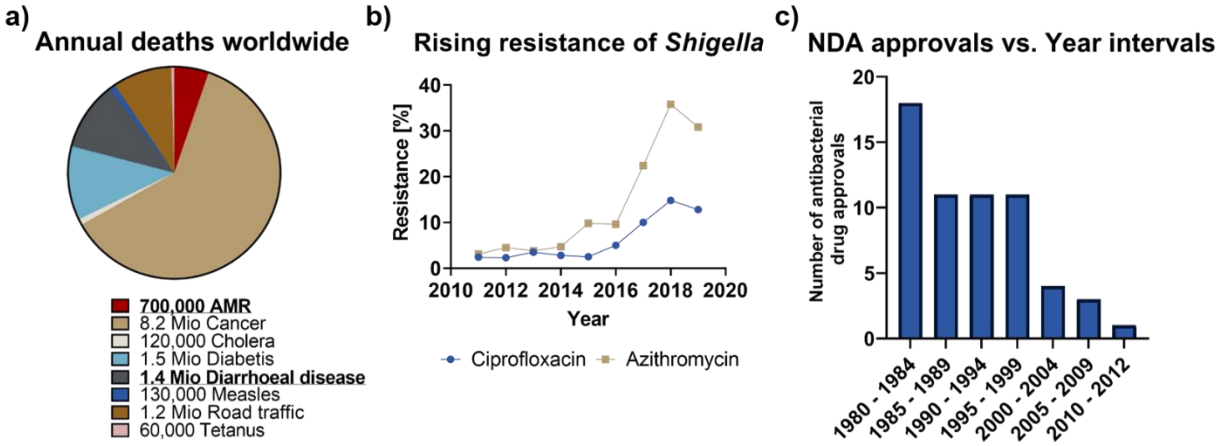

***Figure 2 The threat of antimicrobial resistance in numbers**. a) Annual deaths worldwide (5) b) Rising resistance rates of Shigella spp. to ciprofloxacin and azithromycin in the US (9) c) Number of antibacterial drug (NDA) approvals from 1980 to 2012 (2)*

In order to combat AMR, it is important to understand the mechanisms behind it. There are two different classes of resistance: i) intrinsic resistance, which relies on the structure and functions of bacteria and ii) acquired resistance, which has developed over time (10). An example for intrinsic resistance is the one against vancomycin. This antibiotic is only active against gram-positive bacteria and cannot affect gram-negative due to their lack of the target peptide D-Ala-D-Ala (10). Acquired resistance can be classified into three main modes of action: i) The minimization of intracellular concentration of the antibiotic, ii) the modification of the target structure, or iii) the inactivation of the antibiotic. To minimize intracellular antibiotic concentrations, efflux pumps actively transport undesired compounds outside the pathogen. An overexpression of either substrate specific or wide range pumps (*e.g.,* multidrug resistance efflux pumps), due to mutations in the regulator network result in AMR. These mutations can also be passed between bacteria via plasmid transfer (11). In addition to efflux pumps, poor penetration of the antibiotic through the outer membrane in gram-negative bacteria can be manipulated by a downregulation of porin expression (12). Therefore, it is important to establish gram-negative bacterial membrane models to screen new antibiotics in a high content manner (13). However, even if the antibiotic is able to penetrate through the cell wall, the target structure can change either via genetic mutation or modification (10). Alternatively,

enzymes can alter or degrade the compound, resulting in a loss of efficacy (10). One example of each mechanism of antibiotic resistance can be found in **Table 1**.

Table 1 Examples of different mechanisms of antibiotic resistance in pathogens and its affected antibiotic.

Mechanism of antibiotic resistance	**Pathogen**	**Antibiotics**	**Reference**
Reduced permeability	*Klebsiella pneumonia*	Ceftaroline, Ceftaroline-avibactam	(14)
Efflux	*Salmonella enterica*	Ciprofloxacin	(15)
Mutation in target structure	*Staphylococcus aureus*	Daptomycin	(16)
Inactivation of antibiotic	*Klebsiella pneumonia*	Carbapenem	(17)

Besides the development of antimicrobial resistance, bacteria can also escape antibiotic treatment by invading human cells or by the formation of a biofilm. In the latter, individual cells adapt to a multicellular lifestyle by first attaching to a surface and then forming an extracellular polymeric substance, altogether mediated by quorum sensing signalling (18). Due to the matrix barrier and low metabolic activity within the biofilm, higher doses of antibiotics need to be administered in order to successfully eliminate the pathogens (19). Unfortunately, higher doses often do not cure patients as these drugs often poorly penetrate the biofilm. They can even promote the development of resistance, in addition to increased risk of side effects.

In general, AMR progresses when the antibiotic is not sufficiently effective and is not able to eliminate the pathogen until complete eradication. This may be due, to the use of broad-spectrum antibiotics or the implementation of an incorrect antibiotic therapy, mainly with unspecific therapeutics that can favour the progress and spread of resistance (20). Moreover, compliance problems, when the therapeutic is not administered regularly can provoke the development of AMR. To the end, this will lead to lower drug concentrations on the side of infection, resulting in non-effective eradication of naturally resistant pathogens, which can then spread though the human body, unhindered (**Figure 3**).

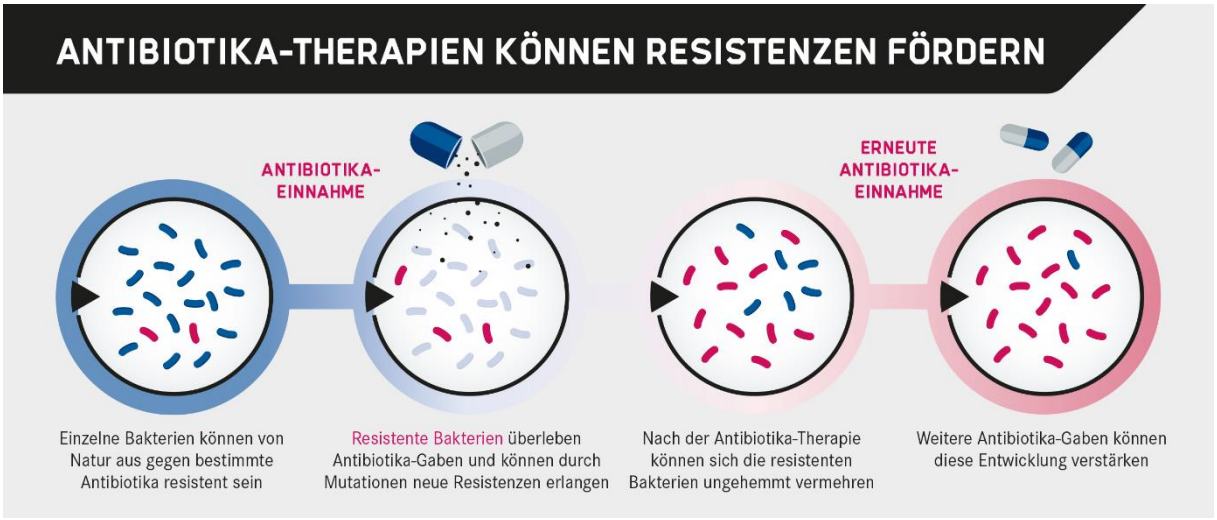

***Figure 3 How an antibiotic therapy can provoke the development of resistance**. Copyright Helmholtz-Zentrum für Infektionsforschung GmbH (21)*

Generally, besides education and stricter hygiene regulations, there are two ways to prevent the spread and development of AMR: First, the design of new antimicrobial drugs with alternative modes of action and higher efficacy, and second the improvement of well-established compounds. Unfortunately the number of newly approved antimicrobial drugs has decreased within the last decades and fewer pharmaceutical companies are interested in their research and development (**Figure 2c**) (2, 22, 23). This leaves the second alternative, to improve and repurpose known antibiotics. Nanotechnology, for example, bares great potential to be used as a tool to combat resistance as therapeutics, vaccines or diagnostic tools (24, 25). So-called nanoantibiotics, antibiotics encapsulated into nanoparticles or liposomes or inherent antimicrobial nanomaterials, can take advantage by simultaneously acting on multiple mechanisms. Briefly, they can target specifically the site of infection, actively or passively, increase antimicrobial uptake, decrease efflux, tackle biofilm formation and target intracellular pathogens (19, 24) (**Figure 4**).

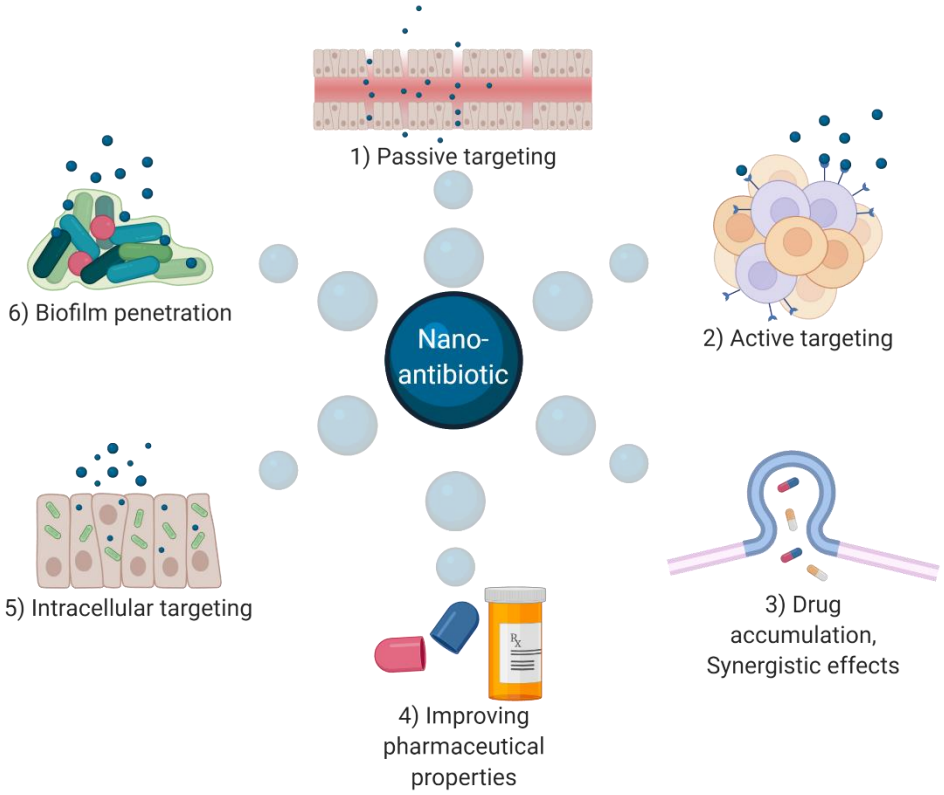

Figure 4 Principle of nanoantibiotics. *Nanoantibiotics can combat antimicrobial resistance on a multi-dimensional level, by 1) passively and 2) actively targeting the side of infection and 3) by increasing drug accumulation in target cells and allow synergistic effects of multiple drugs. Moreover, they are able to 4) improve pharmaceutical properties such as solubility, bioavailability or storage stability, 5) combat intracellular pathogens and 6) penetrate biofilms. By releasing high dosages of antibiotic into the (bacterial) cell, resistance patterns can be inhibited or overstrained.*

To target the site of infection passively, nanotherapeutics can utilize the enhanced permeation and retention effect (EPR-effect). It is known that bacterial components as well as bacteria themselves trigger various inflammation mediators released by immune cells. These stimuli lead to leaky barriers and thus, enhanced permeability, directing the particles to the site of infection, where they accumulate (26). In addition to inflammation, lower pH, higher levels of hydrogen peroxide and the existence of specific proteins characterize the microenvironment of the site of infection. This can provide new opportunities for pH, H_2O_2 or enzyme responsive drug delivery (27). Active targeting can be established by the decoration of particles with ligands with a higher surface area to volume ratio, such as antibodies or components that can specifically react with the target (28). Active targeting can also be beneficial in eliminating intracellular microorganism. Pathogens such as *Shigella* and Rotavirus mainly invade intestinal epithelial cells, whereas *Salmonella*, HIV and Leishmaniasis invade macrophages,

tuberculosis alveolar macrophages, dendritic and HPV urogenital epithelial cells (29). The high local dose at the site of infection can be established by specific reactions of the nanoparticle with the membrane of the infected cell *e.g.,* via invasin or mannose decorated liposomes (30, 31). Antimicrobial uptake can be increased by fusion of nanotherapeutic membranes with either bacterial or human cell membranes. Efflux will then be decreased because of a saturation of efflux pumps, as high concentrations of the drug accumulate in the microorganism. The bioavailability of poorly soluble drugs can be improved, as well as pharmacokinetics and pharmacodynamics via prolonged release (28). Thus, nanoformulations are unlikely to trigger resistance development, while at the same time reduce toxic side effects due to unspecific targeting of the drug (19). More examples of nanotherapeutics against bacterial infections are listed in **Table 2**.

Table 2 List of selected nanotherapeutics to combat bacterial infections.

Nanotherapeutic	***Pathogen(s)***	**Advantage**	**Reference**
Ciprofloxacin submicrocarrier	*Pseudomonas aeruginosa, Escherichia coli*	Increased solubility, growth inhibition	(32)
Tobramycin solid lipid NPs	-	Increased bioavailability	(33)
Poly(butylcyanoacrylate)-moxifloxacin-NPs	*Mycobacterium tuberculosis*	Intracellular growth inhibition	(34)
Ampicillin multilamellar liposomes	*Micrococcus luteus*	Enhanced stability	(35)
Vamcomycin/ teicoplanin liposomes	*MRSA*	Intracellular growth inhibition	(36)
Extracellular vesicle coated-NPs	*S. aureus*	Active targeting	(37)
Magnetic Eugenol microspheres	*S. aureus, P. aeruginosa*	Inhibition of biofilm formation	(38)
Chlaritromycin PLGA nanocapsules	*S. aureus, M. absessus*	Intracellular growth inhibition	(39)
Chitosan-ceftriaxone-NPs	*Salmonella typhimurium*	Intracellular growth inhibition	(40)
Liposomal ciprofloxacin	*Salmonella dublin*	More effective than free drug, accumulation on side of infection	(41)
Invasin functionalized gentamycin liposomes	*Y. pseudotuberculosis, S. aureus*	Intracellular growth inhibition	(30)

Liposomal amphotericin B (AmBisome®), for instance was one of the first antimicrobial liposomal formulations approved by the FDA and EMA. By encapsulating the antimycotic into a lipid formulation, the toxic profile, which limited the treatment of invasive fungal diseases, was significantly reduced (42). MAT2501 is another promising nanoformulation, where

amikacin is encapsulated into lipid-nanocrystals, currently investigated in phase I clinical trials. The formulation fuses with infected cells and due to a lower calcium concentration within the cell, releases amikacin in high dosages, targeting intracellular pathogens and potentially reducing side effects of the drug (43).

In contrast to their promising characteristics to combat infections, the clinical impact of nanotherapeutics, however has been modest in the field of antimicrobial therapeutics. This may be due to a lack of understanding their *in vivo* interactions and fate, resulting in little apprehension of their toxicity to the human body as well as the consequence for the environment. For example, silver nanoparticles, although active against several hazardous pathogens, show increased eco-toxicological risks and increased resistance patterns, due to releasing sub-toxic levels of silver ions and an accumulation of silver in aquatic animals (44). Moreover, nanoparticles targeting the gastrointestinal tract can, like common antibiotics, negatively influence its microbiota (45). Additionally, because of their efficient cellular uptake, the accumulation of NPs *e.g.,* in the brain, heart, liver, spleen and lymphatics can results in organ nanotoxicity (25). A new strategy in the field of nanotherapeutics is in taking advantage of the potential of extracellular vesicles (EVs) as carrier systems or therapeutics themselves. Many methods and characterization protocols used in nanotherapeutic research, such as loading techniques or size determination can be adapted to EVs. Briefly, they are capable of protecting their cargo, overcome biological barriers, show low immunogenicity, can be engineered for targeted delivery and have inherent therapeutic potential (46, 47). Although the research of EVs still requires extensive efforts and multidisciplinary cooperation, several advantages and promising possibilities of EV-therapeutics, in combination with nano-characteristics, have already been discovered and will be discussed in the following chapter (48).

1.2. Extracellular vesicles and outer membrane vesicles

1.2.1. Biology

Extracellular vesicles (EVs) are nano-sized particles with a phospholipid bilayer released from mammalian cells. There are several subtypes of EVs, which, depending on their biogenesis or physico-chemical characteristics are characterized in three main classes: i) exosomes, ii) microvesicles or iii) apoptotic bodies. Exosomes originate from multivesicular endosomes within the cell, microvesicles from budding of the cell membrane and apoptotic bodies are formed during the apoptosis of a cell (49). However, as determining the origin and exact biogenesis of the vesicle is difficult to ascertain, the International Society of Extracellular Vesicles recommends using the comprehensive term “extracellular vesicles” (EVs) (4). Unless the biogenesis can be caught in the act *e.g.,* by live cell imaging techniques or determined by specific marker, the designated term can be used (4).

Extracellular vesicles are released by all different kinds of healthy or pathological cells, such as intestinal epithelial cells, fibroblasts, immune cells, tumor cells or neuronal cells. *In vivo*, EVs can be isolated from various fluids, such as saliva, blood, breast milk or urine (50). Hence, EVs play an important role in the human body, marking them excellent tools in understanding, *i.e.,* pathophysiological or immunological processes (51).

Similar to their origin, vesicles can be decorated with membrane proteins or particular receptors and are able to carry enzymes, proteins or nucleic acid, controlled by and specific to their producer (**Figure 5**) (52, 53). Tetraspanins, such as CD9 and CD63 for instance, are typically and ubiquitously associated with EVs, whereas CD45 is specific for immune cell, TSPAN8 for epithelial cells and ERBB2 for breast cancer cell derived EVs (4).

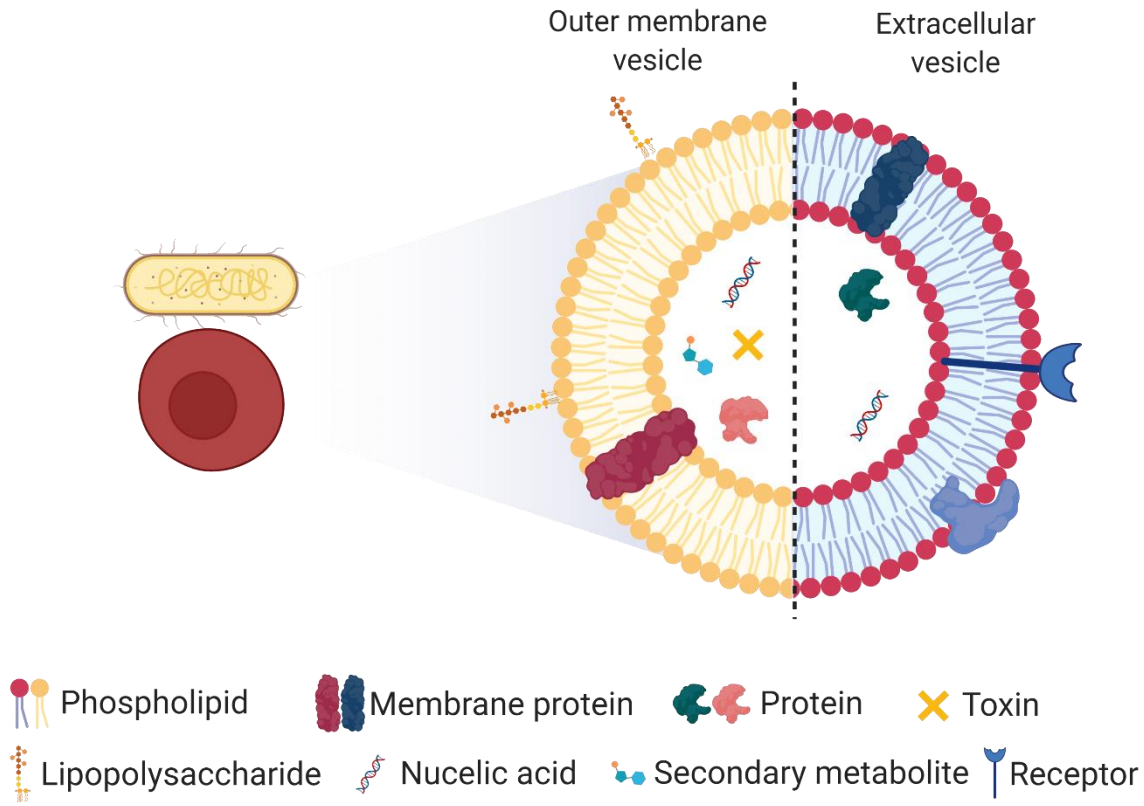

Figure 5 Structure of Outer Membrane Vesicles and Extracellular Vesicles

As mentioned above, two possible pathways of EV formation are possable: either vesicles are formed within the cell and secreted into the extracellular space (exosomes), or the vesicles are directly formed by budding of the cellular plasma membrane (microvesicles) (54). Both mechanisms involve sorting machineries such as endosomal sorting complexes required for transport (ESCRT) (55). The complex biogenesis and cargo packing involves several components such as small GTPase ADP-ribosylation factor 6 or membrane type 1- matrix metalloprotease 1, making it difficult to clearly reveal the entire process and thus, explicitly identify the type of EVs dealt with (55). Nevertheless, typical characteristics and the basic structure, can be identified and often give information on the cellular source.

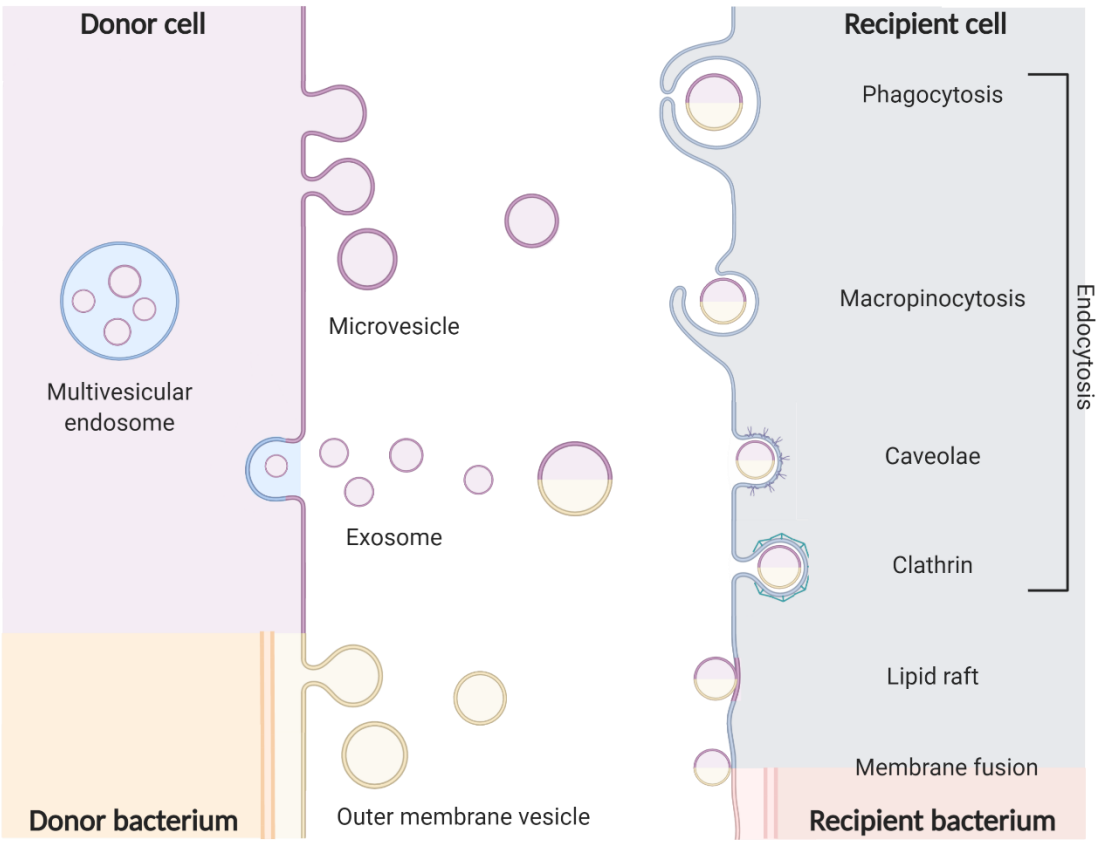

Figure 6 Biogenesis, secretion and uptake of extracellular and outer membrane vesicles in host cells or bacteria.

As the biogenesis and origin of EVs is versatile, so is their content and biological function. They can be involved in tissue repair, coagulation, balancing body fluids and play a crucial role in the immune response (56). In general, EVs are transport vehicles, carrying information from one cell to another through the extracellular environment and can consequently be described as “signalosomes” (52). To transport this information to acceptor cells, EVs need to be actively or passively be taken up. There are 5 ways in which EVs can interact with recipient cells, which may also occur simultaneously: phagocytosis, macropinocytosis, caveolin-dependent endocytosis, clathrin-mediated endocytosis and lipid raft-mediated endocytosis (**Figure 6**) (57). These, as endocytosis classified mechanisms are energy depended, fast and involve receptor and protein interaction. For instance, tetraspanins such as CD63 and CD9, integrins, proteoglycans, lectins or immunoglobulins and possibly lipids may play leading roles in cellular uptake of vesicles (57). Whether uptake is cell specific or generic is still unclear, as different publications support one or the other (58-60). Thus, it mainly depends on EV characteristics, complicated by their heterogeneity and targeted cell type. In addition to active uptake, there is the possibility of passive uptake via fusion of the two membranes. However, it can be argued that this process is unlikely, as EV uptake is most likely a fast process, which cannot be fulfilled by slow passive fusion (57).

Outer membrane vesicles (OMVs) are a different type of extracellular vesicles, where the phospholipid-bilayer nano-structures originating from budding of the outer membrane of gram-negative bacteria (61). In addition to membrane proteins, lipopolysaccharides cover the surface of the vesicles and toxins, as well as secondary metabolites can be incorporated within the vesicles (**Figure 5**) (62). For instance, OMV isolated from *Shigella dysenteriae* carry the characteristic virulence factor shiga toxin (63), whereas enterotoxic *Escherichia coli* secretes heat liable enterotoxin in OMVs (64). Similar to EVs, the main function of OMVs is to deliver content in proximity, distance and in different environments. For example, genetic information such as resistance genes or lysing components for predatory nutrient acquisition can be distributed among the colony or interspecifically (65, 66). The formation of biofilm and the removal of toxins or misfolded proteins are further tasks involved with OMV secretion (67). OMVs are able to deliver content to host cells similar to the mechanism of EV delivery, via endocytosis or membrane fusion (68). However, the exact machinery of exchange of information between donor and acceptor bacteria is unknown. Fusion of membranes and recognition via LPS may be linked to specific targeting, but has not been unambiguously confirmed yet (69, 70). The involvement of fusogenic enzymes such as GAPDH may also play a crucial role in OMV uptake in acceptor cells (71).

Their versatile components and characteristics allow EVs and OMVs to take on diverse roles in the environment and the human body, emphasizing this field of research to explore several possibilities in fundamental research and understanding diseases as well as gaining knowledge for applied sciences. Thus, vesicles display interesting tools in pharmaceutical research *e.g.,* as targets, diagnostic markers, or as therapeutics themselves.

1.2.2. OMVs derived from myxobacteria

Myxobacteria are gram-negative, soil living bacteria with versatile characteristics. Among only a few prokaryotes, they are able to lyse and ‘hunt’ prey in order to use them as a source for nutrients, such as essential three-branched amino acids (72). Yet, they do not detect and prey as individuals, they hunt as a “wolfpack” (73). Chemo- or predataxis stimulates the colony to move forward, lysing their prey and eliminating even 20 *E.coli* cells individually. In addition to antimicrobial compounds such as myxovirescin, thuggacin and cystobactamid, myxobacteria are producer of a variety of other pharmaceutical relevant secondary metabolites. For instance, anti-fungal compounds play a major role in the development of active drugs derived from myxobacteria (74). Their OMVs play a significant part in the transport of these secondary metabolites. *Myxococcus xanthus* OMVs for example, carry antimicrobial agents such as

myxalamid or cittilin (75). *Corallococcus* sp. OMVs on the other hand can transport β-1,6-glucanases, an antifungal membrane β-barrel protein, gaining advantages on the hostile soil environment by feeding on fungi (76). Moreover, it is believed that myxobacteria in general generate an abundant yield of OMVs for intra- and interspecies communication (77). This is especially beneficial for the establishment of OMVs as therapeutics, as they seem to be an unlimited source for pharmaceutical relevant OMV production. Although cellular uptake behavior of OMVs has been studied, this primarily applies to OMVs derived from pathogenic bacteria such as *Helicobacter pylori*, ETEC or *Campylobacter jejuni* (68). However, the uptake behavior and mechanism of OMVs derived from myxobacteria with human cells lacks precise comprehension.

1.2.3. Therapeutics based on extracellular vesicles

Extracellular vesicles and outer membrane vesicles have interesting features that can be utilized in vesicle-based therapies. Some studies focus on the evaluation of EVs and OMVs in diagnostics, as they are involved in the regulation of intercellular communication and are easily accessible. Samples can be drawn from various tissues, such as blood plasma or urine with little to small invasiveness. With this, suitable markers can be established to diagnose certain diseases, which evidently display pathological conditions more distinctively according to the parent cell. For example, specific miRNA detected in EVs derived from plasma can help identify early stages of psoriatic arthritis with little variation in proportion compared to commonly used markers (78). The analysis of tears from cancer patients, may also bare the potential of a fast, non-invasive and early-stage method for recognizing the development and aggressiveness of cancer. With nanocavity sEV sensing chips, Takeuchi et al. were able to detect specific antibody positive EVs in cancer patients, establishing a new approach for customized rapid and non-invasive tear EV diagnostics (79). OMVs also play a role in detecting *e.g.,* infectious pathogens more efficiently. For instance, peptides related to *Mycobacterium tuberculosis* OMVs isolated from plasma are sensitive indicators of latent tuberculosis, accelerating early onset diagnosis, subsequent therapy and reducing the spread of the disease (80). More recent examples of EVs used as diagnostic marker in diseases *in vivo* and *in vitro* are listed in **Table 3**.

Table 3 EVs as diagnostic marker

EV origin	Diagnosis for	Marker	Reference
Preimplantation bovine embryos	Embryo development	Concentration and size	(81)
Syncytiotrophoblasts	Preeclampsia	Lower expression of syncytin-1	(82)
Tears	(Breast) cancer	Anti-Her2, Anti-GGT1	(79)
Plasma	Psoriatic arthritis	miRNA	(78)
Plasma	Latent tuberculosis infection	*M. tuberculosis* peptides in serum extracellular vesicles	(80)

Vesicles can furthermore be utilized as therapeutics or adjuvants in vaccines. Due to their nano-structure and membrane composition, they can for example, harness the EPR effect and are able to target cells specifically (83). In addition, they have not the ability of self-replication, which abolishes side effects such as uncontrolled and unwanted cellular and bacterial growth or spreading. Moreover, EVs and OMVs represent a new biogenic drug-delivery opportunity compared to synthetically produced nanoparticles. In some cases, EVs or OMVs even have an inherent therapeutic effect, emphasized in **Table 4**.

.

Table 4 EVs and OMVs with inherent therapeutic effect

EV/OMV origin	Therapeutic	Mode of action	Reference
Human adipose MSCs	Prevention of hypertrophic scars	Suppressing myofibroblast aggregation and collagen deposition	(84)
IFN-γ-primed mouse mesenchymal stem cells	Amyotrophic lateral sclerosis	EV miRNA affects genes in the p38 MAPK to decrease microglial production of pro-inflammatory cytokines	(85)
Monkey derived bone marrow- MSCs	Recovery after cortical injury	Hypothesis: expression of ramified microglia, which promotes repair and anti-inflammatory processes	(86)
Embryonic stem cell	Vascular dementia	EV miRNAs inhibits mTORC1 activation	(87)
Neutrophils	Antibacterial	Unknown multiple factors	(88)
Urine derived stem cells	Prevent diabetic nephropathy in diabetis	Hypothesis: EV incorporated growth factor β1, angiogenin and bone morphogenetic protein-7	(89)
Human breast milk	Necrotizing enterocolitis	Antiapoptotic and proproliferative effects in intestinal epithelial cells	(90)
Pseudomonas aeruginosa	Antibacterial	OMV incorporated Peptidoglycan hydrolases	(65)
Myxococcus xanthus	Antibacterial	OMV incorporated Myxalamid	(71)
Corallococcus spp	Anti-fungal	OMV incorporated β-1,6-glucanases	(76)

Unfortunately, some EVs or OMVs do not have inherent therapeutic effects. However, their physiological origin and size can be harnessed to create a low immunogenic nanocarrier system. Therefore, different strategies to load vesicles have been developed. These loading strategies can be divided into exogenous and endogenous methods (**Figure 7**). In exogenous loading, cells, either bacteria or human cells are co-incubated with the desired drug. It is believed, that cells then incorporate those drugs that diffuse or permeate the cell, into the vesicles and release them either as “trash” or for other, yet unknown reasons (91, 92). The exogenous loading techniques can be classified again, into passive and active. Passive loading is the simple co-incubation of the drug with the isolated vesicles. However, these methods are only effective, if the drug is able to penetrate and overcome the membrane barrier. Hence, lipophilic drug have an easier start compared to hydrophilic drugs (93). Techniques such as electroporation, saponin-assisted, osmotic shock, sonication and freeze-thaw-cycles are active loading methods, which, to some extend and for a short period damage the

membrane of the vesicles allowing the drug to penetrate. These methods seem to especially increase the loading efficiency of hydrophilic compounds (93).

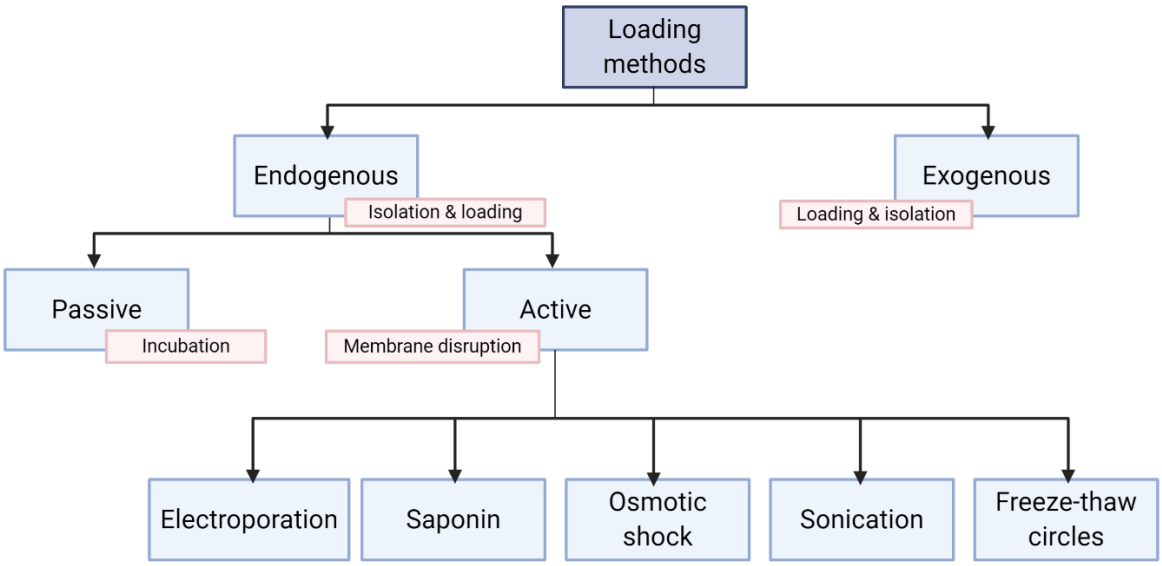

Figure 7 Different methods for loading extracellular vesicles or outer membrane vesicles

After loading, free and not encapsulated drug needs to be removed efficiently, *e.g.,* by ultra-centrifugation, tangential flow field filtration, asymmetric flow field fractionation or size exclusion chromatography. Otherwise, the therapeutic effect cannot be attributed to the loaded EVs alone, but maybe due to the free drug or a synergistic effect of both loaded vesicles and free drug. Depending on the compound used, different approaches need to be tested and evaluated, which one is more effective. In **Table 5** different examples of loaded EVs and OMVs are presented including the method to remove free compound and their therapeutic application.

Table 5 Examples of loaded and engineered EVs and OMVs

EV/OMV origin	**Drug loaded**	**Loading method**	**Removal of free drug**	**Therapeutic application**	**Reference**
A549	Paclitaxel	Passive	Ultra-centrifugation	Lung cancer treatment (*in vivo*, *in vitro*)	(94)
hMSC	Paclitaxel	Incubate cells with drug	Cell washing	Inhibition *in vitro* tumor growth	(95)
L929 cells	Methotrexate	UV stimulation of cells, incubate cells with drug	Centrifugation	Functionalized EVs to treat	(96)
Engineered Mouse	Doxorubicin	Electroporation	Ultra-centrifugation	Specific targeting of αv integrin	(97)

immature dendritic cells				positive breast cancer (*in vivo, in vitro*)	
EL-4, RAW 264.7	Curcumin	Passive	Sucrose gradient	Enhanced activity, specific targeting to activated myeloid cells against inflammation	(98)
MDA-MB231, Human umbilical vein endothelial cells, hMSC, human embryonic stem cell	Porphyrins	Passive, electroporation, saponin-assisted, extrusion, hypotonic dialysis	Size exclusion chromato-graphy	Phototoxic effect on cancer cells	(93)
Cow milk, CaCo-2	Curcumin	Passive	Size exclusion chromato-graphy	Increased bioavailability	(99)
RAW 264.7	Linezolid	Passive	centrifugation	Growth inhibition intracellular *S.aureus*	(100)
RAW 264.7	Catalase	Passive, freeze-thaw, saponin-assisted, sonication, extrusion	Size exclusion chromato-graphy	Target delivery to brain to treat Parkinson's Disease	(101)
hMSCs	Venofer (iron oxide carbohydrate nanoparticle)	Incubated with cells	Cell washing	Target delivery to tumor cells, magnetically induced hyperthermia to ablate tumor tissue	(102)
Mouse MSCs	Alendronate	Copper free click chemistry	Ultrafiltration, centrifugation	Targeted delivery to bones for osteoporosis therapy	(103)
RAW 264.7	Lysostaphin, vancomycin	Sonication	Ultrafiltration	Intracellular delivery to MRSA infected cells, *in vivo* growth reduction	(104)
Acineto-bacter baumannii	Ceftriaxone, amikacin, azithromycin, ampicillin, levofloxacin, ciprofloxacin	Incubated with bacteria in sub-toxic concentrations	Ultrafiltration, ultra-centrifugation	Reduction of bacterial load of pathogen infected mice	(92)

By bioengineering vesicles, targeting properties can be improved and clearance of vesicle-based drug delivery systems reduced. Although it already has been demonstrated, that EVs as well as OMVs have, to some degree specific targeting characteristics, due to particular lipid or protein compositions, bioengineering the surface of vesicles aids in avoiding accumulation in off-targeted organs (83). Further, PEGylation has been shown to influence circulation, reducing EV-clearance by a factor of six compared to unmodified EVs (105).

Despite extensive research and optimistic results, the translation of EV/OMV therapeutics into clinical trials seem to bare some obstacles that need to be overcome. Major problems are the up-scaled production, especially for EV therapeutics, as cells need adequate space. Furthermore, the reproducibility needs to be improved with standard operating procedures, which should already be introduced during their development (106). Storage conditions, explicit characterization and detailed information on loading and modification are crucial in order to establish and improve the development of a new vesicle-based therapeutic system. The task of the International Society of Extracellular Vesicles is to coordinate and guide this standardization, which aids to translate EV-based therapeutics into clinical trials (4).

1.3. Gastrointestinal Tract

1.3.1. GIT Infections

The definition of a gastrointestinal infection is a combination of a pathogen infestation with an inflammation of the gastrointestinal tract, including the upper and lower intestine. Typical symptoms are abdominal pain, vomiting and diarrhea, which is further classified into acute watery, invasive or persistent diarrhea (107). Pathogens predominantly invading the small intestine result in watery diarrhea, whereas pathogens favoring the large intestine often induce bloody mucoid stool (108). In 2016 over 1.65 million deaths caused by diarrheal diseases were reported globally, with 446,000 deaths in children under 5 years of age (109). A diverse variety of organisms, such as bacteria, viruses and protozoans are responsible for gastrointestinal infections. The six pathogens, in descending order attribute to moderate-to-severe diarrhea among infants and young children in 77.8 % of all diarrheal cases, according to the Global Enteric Multicenter Study: *Shigella* spp., Rotavirus, Adenovirus, *Cryptosporium* spp., enterotoxigenic *Escherichia coli* and *Campylobacter* spp. (110, 111). The main reasons for infections are contaminated food or water accompanied by poor sanitation. Children and elderly, as well as immunodeficient patients are high-risk groups and should be treated immediately. First line treatment are oral rehydration solutions, as the most hazardous outcomes of gastrointestinal infections, *e.g.,* hypovolemic shock, are caused by a loss of fluids. Antidiarrheal agents should also be taken into consideration, but not administered without an anti-infective treatment as they may decelerate pathogen excretion. Vaccines are available for cholera, rotavirus and typhus and have been proven well tolerated and efficient (109). Yet, a commercially available vaccine against *Shigella* infections has not been approved, although several candidates have undergone clinical trials (112).

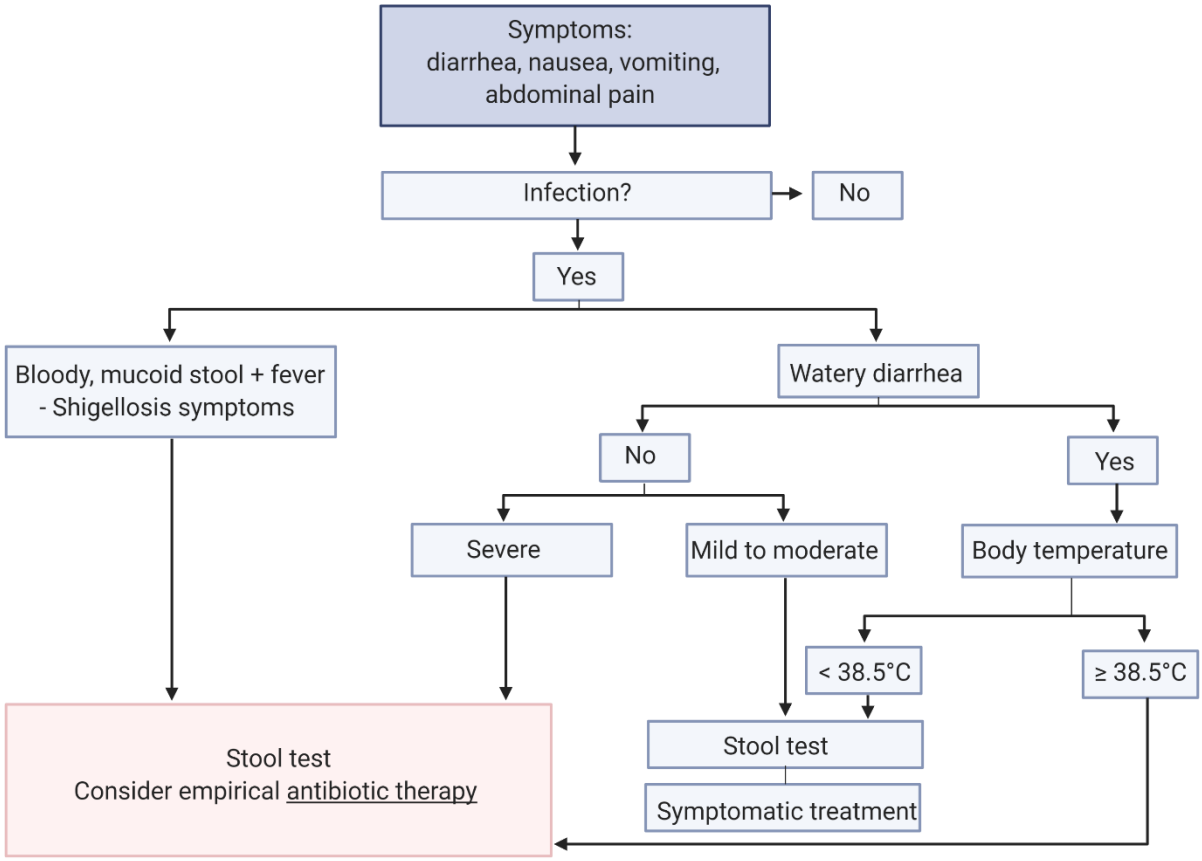

Figure 8 Decision tree for treating gastrointestinal infections. *Adapted from (113)*

However, for severe cases or high risk patients, an antimicrobial therapy is necessary, not only to reduce prolonging contagion but to shorten and dampen pathogen invasion. Here, fluoroquinolones are first-line antibiotics due to their broad-spectrum activity, in spite of increasing cases of AMR (**Figure 8**) (113). As a preventative method, a probiotic regimen with *e.g., Lactobacillus rhamnosus* is recommended, whereas immunosuppressed patient should be monitored carefully (114, 115).

Table 6 List of intracellular gastrointestinal pathogens and their niche.

Rotavirus	Intestinal epithelial cells
Salmonella	Macrophages
Shigella	Intestinal epithelial cells

1.3.2. *Shigella* Infections

Shigella spp., discovered in 1897 by Kiyoshi Shiga, are highly virulent pathogens, of which only 10 to 100 cells are able to cause an infection (116). 165 million cases of *Shigella* infections have been reported annually, resulting in 164,000 deaths worldwide (117). Common

symptoms are watery diarrhea, fever, cramping and abdominal pain accompanied by bloody mucoid stool. They are summarized under the umbrella term Shigellosis (118). Post infection complications, such as sepsis, arthritis, pneumonia and hemolytic uremic syndrome may occur due to ineffective or insufficient treatment (117). *Shigella* spreads via the fecal-oral route, through the consumption of contaminated water or food, or from person-to-person transmission, favored by poor hygiene (119). Those pathogens are able to survive the harsh conditions of the upper intestine, especially the high acidity in the stomach, due to an increased translation of acid resistance genes (120). *Shigella* spp. is classified into four species: *Shigella boydii, dysenteriae, sonnei* and *flexneri*. They belong to the gram-negative facultative anaerobe family of Enterobacteriaceae. *Shigella flexneri*, with the dominant serotype 2a has by far the highest mortality rate compared to other *Shigella* species(121).

When *Shigella* is taken up by contaminated food or water, they resist acidic conditions in the stomach and enter the lower intestine. Here, predominantly in the ileum, they enter the sub-mucosa by taking advantage of the purpose of microfold cells (M cells) (**Figure 9**). These M cells are located in the Peyer's patches and absorb antigens, which are then immediately passed onto immune cells located in the underlying germinal centers, causing an immune response. *Shigella flexneri* is able to bypass these cells and claim access to the basolateral side of the intestine by escaping the phagosome with a cocktail of different virulence factors. Now, *Shigella* is able to invade macrophages and predominantly epithelial cells. Macrophages will phagocyte the pathogen, where it will, again escape the phagosome and induce caspase-1 dependent programmed cell death and pyroptosis, subsequently releasing interleukin 1 beta and interleukin 18 (122). Epithelial cells are invaded by the activation of the type III secretion system, injecting a subset of virulence proteins (123). The injected virulence factors force the cell to take up the pathogen in a vacuole, which then induces lysis and can now freely move within the cell (124). Although *Shigella* does not express flagella it is still able to move vigorously from cell to cell, infecting large areas of the intestinal epithelium. Virulence factors destabilize microtubules and display a polymerized actin tail on one pole of the bacterium, enabling the pathogen to move (125). When epithelial cells succumb *Shigella*, they release interleukin 8, which, together with IL-1 beta results in a massive inflammatory response. This inflammation can persist over months (126). *Shigella* prevents epithelial cells from cell death by the inhibition of mitochondrial damage, caspase activation and stimulation of cell survival signaling to guarantee replication and spreading (122). One defense mechanism of the human body is the ability of so called polymorphonuclear cells, a type of granulocyte to phagocyte *Shigella* via human neutrophil elastase (127).

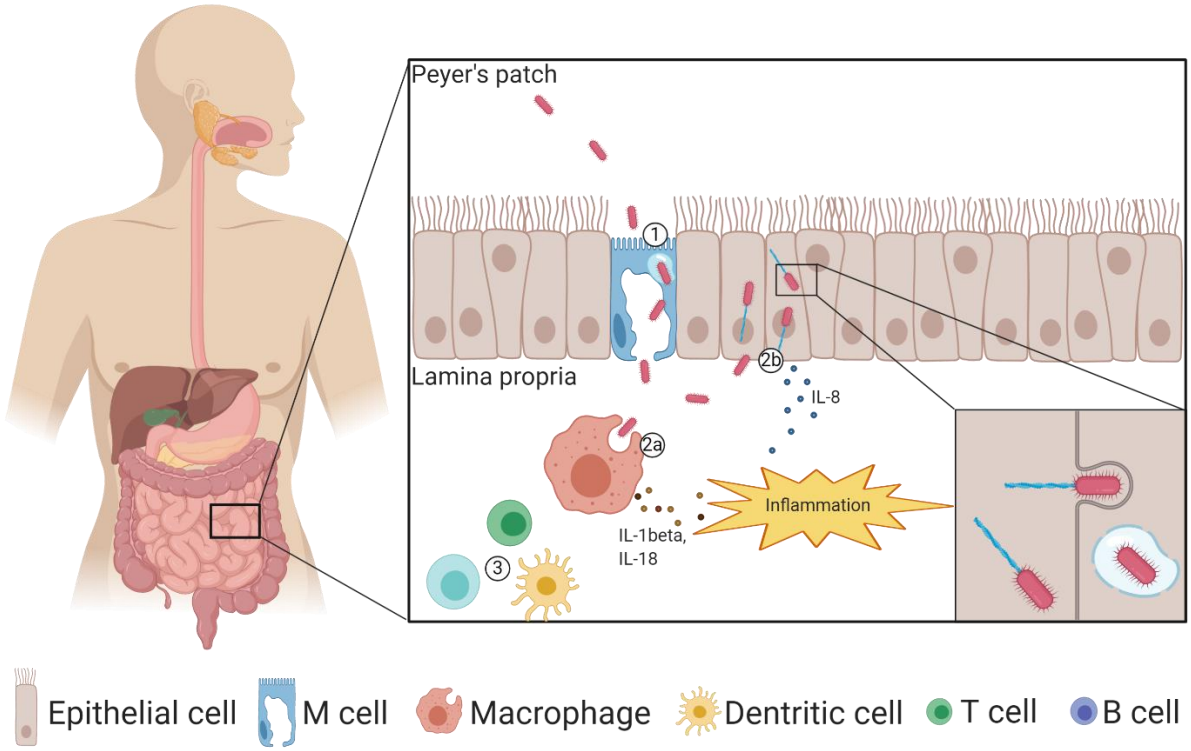

Figure 9 Mode of action of Shigella flexneri. *1) Via transcytosis, Shigella is able to enter M cells and immediately releases itself from the phagosome, entering the sub-mucosa. 2a) Macrophages phagocyte Shigella where they induce a caspase-1 dependent programmed cell death with IL-1 beta release. 2b) Shigella enters epithelial cells via type III secretion apparatus, forms a polymerized actin tail to move freely within the cell and invade neighboring cells before they release IL-8. 3) Shigella triggers T- and B-cells to migrate towards the infection. B-cells death can occur in invaded and non-invaded cells (122).*

Although rising resistance rates, antibiotic treatment is commonly used to reduce bacterial excretion, primarily with fluoroquinolones (128). Especially the use of the first line antibiotic ciprofloxacin has become more and more doubtful, as resistance in Europe with 1 % and Asia-Africa with 29 % has increased (129). For example, a Bangladesh study revealed a 44 % rise of ciprofloxacin resistant bacteria within 6 years (130). Another recent study in England publicized an increase of ciprofloxacin (28.3 %) and azithromycin (53.1 %) resistant *Shigella* infections, revealing significant public health concerns even in high-income countries (131). Second line antibiotics are pivmecillinam, ceftriaxone or azithromycin along with rehydration (132). Endeavor towards vaccines wind up in clinical trials, with no successful launches on healthcare markets, mainly due to the obstacle of protecting patients with all serotypes. However, promising innovative candidates are now in the pipeline (112). An interesting approach towards *Shigella* vaccines is a nanoparticle based system, composed of outer membrane vesicles derived from *Shigella flexneri* and encapsulated into nanoparticles. The formulation was orally administered to mice, which were later infected with a lethal dose of

Shigella. Protection rates increased from 40 to almost 100 % (133). To the best of my knowledge, only one approach has been taken to combat a *Shigella* infection by utilizing nanomedicine. Mukherjee et al. produced calcium-phosphate nanoparticles loaded with tetracycline and found, that colonization and inflammation of mice, infected with *Shigella flexneri* 2a was reduced significantly (134).

1.3.3. GIT Models

Gastrointestinal co-culture models are highly advanced models, which imitate the barrier of the intestine and can be used *e.g.,* for nanoparticle safety or efficiency testing. Several models, which take advantage of functions of specific cell lines or primary cells exist and have already been studied (135-137). Here, properties of nanoparticles such as size, surface charge, hydro- and lipophilicity with the interaction of different physiologies of the model can be simulated (137). In addition to this, models with common GI pathogens have been established. With this, the adherence, invasion and signaling of host cells can be studied intensively (138, 139). For instance, Lindén et al. investigated several gastric and intestinal cell lines with important characteristics for the development of an authentic human GI model. They examined the continuous layer formation, mucin expression and pH resilience, investigated the colonization of *H. pylori* and *C. jejuni* and were able to select cell lines more suitable for GI modelling than others (139). In general, advantages of those (pathogen) cell culture models are the well-controlled conditions for precise assessment of the impact of therapeutics or pathogen interaction. In addition, *in vivo* models are highly versatile and depend on the genetic disposition of the animal, which can then influence the pharmaceutical outcome leading to vague and sometimes misleading propositions. The lower complexity compared to animal models aids in the development and improvement of those therapeutics and makes *in vivo in vitro* correlation more predictable.

1.3.4. Nanotherapeutics against gastrointestinal infections

Nanotherapeutics designed to be effective against gastrointestinal infections need to withstand several challenges, such as different and extreme pH changes, enzymatic digestion or the contest to overcome tight barriers. Therefore, they need to be able to reach the designated area of the gastrointestinal tract and deliver a sufficient amount of drug with escaping rapid clearance (140). Following oral delivery, the first challenge is to escape enzymatic digestion. For instance, lipid based nanotherapeutics will encounter lipase and bile salts when reaching

the duodenum and secreted pancreatic fluids (141). Using different gastro-resistant coatings or polymers, the low pH in the stomach can to be bypassed (142). Once reaching the lower intestinal area, another challenge is to penetrate through the mucus layer, consisting of large glycoproteins of the mucin family. Here, nanoparticles may be trapped via hydrophobic interactions or the mesh-like structure of the mucus (143). For instance, non-muco-adhesive or mucus-penetrating particles, consisting of polystyrene particles decorated with polyethylene glycol have been proven to successfully penetrate intestinal mucus in an *in vivo* mouse model (144). Finally, the gastrointestinal epithelial layer is the last step to deliver nanoparticles directly into or through the tight barrier by *e.g.,* using cell penetrating peptides. There are four pathways of potential nanoparticle absorption: vesicular endocytosis, receptor-mediated transport, paracellular transport and vesicular phagocytosis through M-cells (145). For instance, pathogen inspired invasion of the epithelial layer can be harnessed to deliver drug content (30). Thus, nanotherapeutics are promising formulations for gastrointestinal diseases, as they are able to passively accumulate in inflamed intestinal tissue, depending on their size (146, 147), enhance bioavailability (148), reduce toxicity, actively target single cells and are able to be taken up for intracellular targeting (149). Extracellular vesicles, can also be used as nanocarrier systems to deliver drugs specifically. Especially biomimetic EV-based nanotherapeutics show promising properties, regarding cellular uptake and transcytosis though the gastrointestinal epithelial barrier (99, 150) (see chapter 2.2). More examples of synthetic nanotherapeutics able to encounter gastrointestinal obstacles and efficiently inhibit common GI-pathogens are listed in **Table 7**.

Table 7 List of nanotherapeutics to treat gastrointestinal pathogens.

Nanotherapeutic	**Active against**	**Advantage**	**Reference**
CuO-NP	*E.coli, MRSA, S. epidermidis, P. aeruginosa*	Growth inhibition	(151)
Amoxicillin liposomes	*E.coli*	Increased encapsulation efficiency, growth inhibition	(152)
Fe_3O_4-NP	*S. aureus, Shigella flexneri, V. cholerae, B. suptilis, E.coli …*	Growth inhibition	(153)
Ciprofloxacin nanostructured lipid carrier	*B. subtilis*	Improved growth inhibition	(154)
Eap functionalized cholistin liposomes	*S. enterica*	Intracellular growth inhibition	(155)
Ciprofloxacin liposomes	*S. enterica*	Improved Biodistribution, growth inhibition *in vivo*	(156)
Cephalothin liposomes	*S. enterica*	Intracellular growth inhibition	(157)
pH-sensitive gentamycin liposomes	*S. enterica*	Intracellular growth inhibition	(158)

Ag-NP	*S. enterica*	Growth inhibition	(159)
pH-sensitive amoxicillin-NP	*H. pylori*	Growth inhibition	(160)
Liposomal linolenic acid	*H. pylori*	Growth inhibition *in vivo*, reduced cytokine release	(161)
pH-responsive Au-doxycycline liposomes	*H. pylori*	Targeted delivery to intestine	(142)
Gastric epithelial cell membrane coated-clarithromycin-NP	*H. pylori*	Targeted delivery	(162)
Silica coated flexible curcumin liposomes	-	Increased oral bioavailability	(163)
PEG-based polymer-lipid hybrid vesicles encapsulated in mucoadhesive alginate carriers	-	Mucus penetration	(164)
Tetracycline Ca_2PO_4-NP	*Shigella flexneri*	Increased efficiency *in vivo*, reduced inflammation	(134)

In addition to antibacterial nanotherapeutics, a variety of nanoparticle-based vaccines against gastrointestinal pathogens has been optimized with great potential. As mentioned in chapter 1.3.2. an OMV based vaccine against *Shigella flexneri* showed efficient protection of mice after pathogen exposure (133). Advantages of nanoparticle formulations for vaccines are the ability to protect those sensitive antigens, controlled release and to facilitate and increase the uptake of those antigens in immune cells for an effective humoral and cellular immune response (165). Further examples of nanoparticle-based vaccines are listed in **Table 8**.

Table 8 List of nanoparticle-based vaccines against gastrointestinal pathogens.

Nanovaccine	**Pathogen**	**Advantage**	**Reference**
NP encapsulated OMVs	*Shigella flexneri*	Oral and nasal administration, increased protection	(133)
Liposomes	*Shigella flexneri, E.coli*	Commercial Shigella vaccine in Phase I	(166)
Lipopolysaccharide-liposomes	*Shigella flexneri*	Enhance immune response	(167)
O-Antigen-liposomes	*S. enterica*	Significantly more effective compared to other vaccines	(168)
Fusion peptide CtUBE of cholera toxin B, *H.pylori* urease B liposomes	*H. pylori*	Oral administration	(169)

1.4. Zebrafish

1.4.1. Anatomy, development and importance in research

Animal models play an essential role in understanding diseases and testing new therapeutics. Mouse models are the most widely used animals, as they show great homology with the human genome and are similar towards their cell biology and physiology. However, scaled up analysis and high content screening in mouse are often limited to facilities, staff and budget. A low-cost and easy to maintain alternative is therefore urgently needed. The focus on zebrafish (*Danio rerio*) as a whole-animal and high throughput screening tool emerged in the 1990s (170). Nowadays, scientists use zebrafish embryos to understand embryological development, taking advantage of the optical transparency and manipulability of the larvae. With the implementation of genetic screening in the 90s, genetic manipulation via mutagenes paved the way for zebrafish as new disease models (171). To date, the genome reference consortium gives access to an updated and improved version of several animal models, including zebrafish, allowing a transparent and accessible genetic map (172). This facilitates the research and drives the development of new disease models. Despite their obvious physiological differences to mammals, these vertebrates have several similarities in cellular immunological behavior and genetic disposition and thus, gained great interest, especially in the field of pharmaceutical drug discovery and safety testing. Seven advantages play key roles in the use of zebrafish embryo: significant similarities in general and systemic biology (*i.e.,* diet and organ configuration (**Figure 10**), optical transparency, genetic homology to humans, low costs, high quantity and reproducibility and rapid ex utero embryogenesis for non-invasive imaging (170, 173). Especially the quick embryological development of zebrafish (**Figure 10**) simplifies the administration of drug via different routes. Local injections in yolk sack, hindbrain ventricle or eye enable the investigation of diseases localized in specific organs or behavior of drugs destined for specific local administration. Whereas systemic injections via the caudal vein or the duct of cuvier can mimic intravenous injections and give information, regarding the biodistribution and accumulation of the drug. In summary, more similarities between humans and zebrafish can be analyzed, offering an easy, low cost model for better understanding the pathogenesis of diseases and developing new therapeutics.

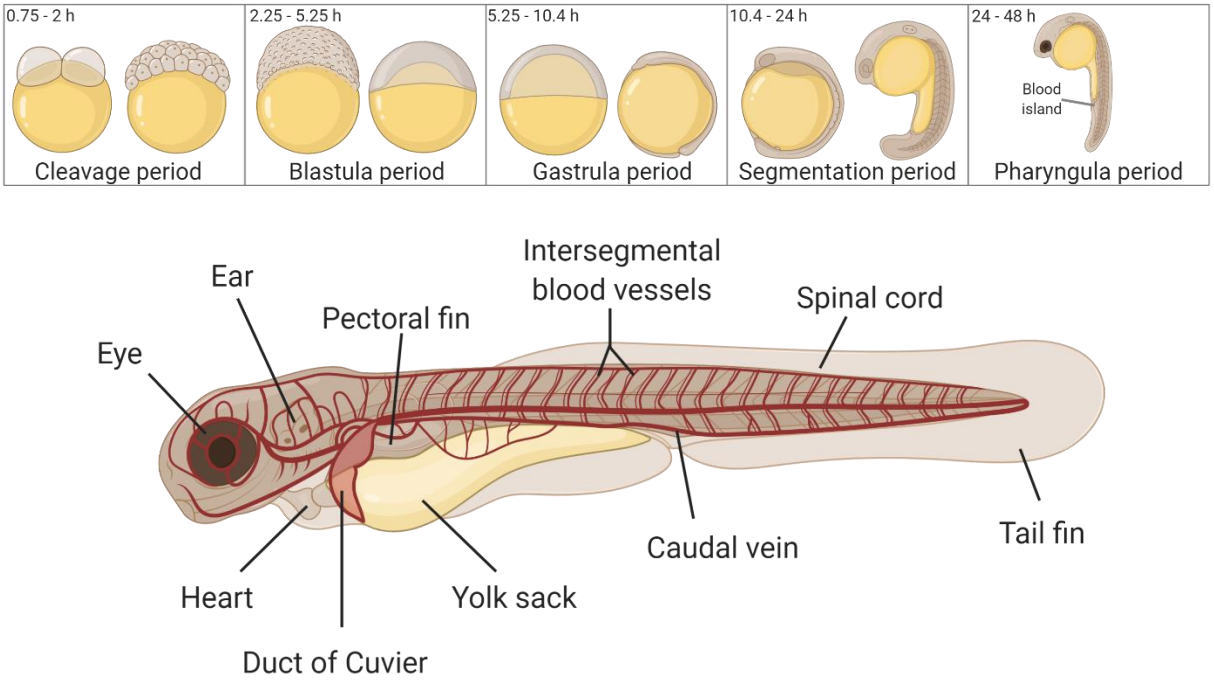

Figure 10 Development and anatomy of zebrafish larvae (174, 175)

1.4.2. Infection models in zebrafish

Zebrafish infection models, have gained great interest to study immunological and physiological effects of pathogens in real time. The ability to image and visualize infections with fluorescently labelled pathogens in transparent zebrafish larvae gives versatile information from single cells to whole animals. In addition, zebrafish help study the innate immune response exclusively, as the adaptive immune response only develops in adult fish, after 4 to 6 weeks post fertilization (176). The innate immune systems includes central features involved in host-pathogen interaction, such as macrophages and neutrophils secreting cytokines. Respectively, several cytokines, *e.g.,* IL-1 beta, TNF or IL-10 showed pronounced homology to their mammalian counterparts (177). During a real time analysis of *E.coli* infected larvae, macrophages were monitored, phagocytosing these pathogens and clearing the blood within 3 h (178). Other models, including *Pseudomonas aeruginosa* infection in zebrafish showed a virulence factor and developmental stage dependent pathogenesis, enabling the manipulation of immune response and thus creating a versatile animal model system (179). *Staphylococcus aureus* infections were also studied in zebrafish and revealed host-pathogen interactions, particularly the mode of invasion of the immune system and in which virulence factors play an important role (180). In addition to systemic infections, local application *e.g.,* of *S.aureus* onto the skin can be analyzed respectively (181). *Shigella* models showed a particular interesting

behavior of this pathogen and zebrafish larvae. Here, *S.flexneri* revealed similar behavior patterns in zebrafish compared to humans, as they invaded epithelial cells and macrophages and induced inflammation (182). In addition, experiments with *S.flexneri* in *Danio rerio* indicated the particular newly discovered role of septins, a component of the cytoskeleton, defending the host by increasing neutrophil clearance of the pathogen (183). Further, the potential therapeutic effect of *Bdellovibrio bacteriovorus* was investigated in an *S.flexneri* zebrafish model. Willis et al. were able to demonstrate the good biocompatibility of this non-pathogenic, natural predator and highlight the antimicrobial efficiency against *Shigella* in a zebrafish model (184). Besides these interesting findings, it must be kept in mind, that vertebras need 28°C, which to some extent might damped the virulent effect of some pathogens, thriving their best potential at body temperatures of 37°C. Moreover, the immunological role of the adaptive immune system is still important in host-pathogen defenses but cannot be taken into account in zebrafish larvae. However, using zebrafish to study bacterial infections is a great opportunity for high throughput and budget friendly research, narrowing down potential candidates then to be tested in higher animal models.

1.4.3. Nanotherapeutics in zebrafish

Zebrafish larvae are particularly interesting in studying nanotherapeutics, as their homologous immune system gives information about toxicity and their transparency allows real time imaging of their biodistribution. Several nanotherpeutics or hazardous nanomaterials have been studied in larvae and new insights towards their barrier crossing and organ accumulation were provided. Sieber et al., for instance established a high throughput zebrafish model to investigate liposomes (185). Different lipid and polymer compositions were tested, as well as differed fluorescent dyes to track these liposomes were analyzed. Here, the circulation time heavily depended on the transition temperature of the lipid components and the extravasation factor values on the amount of cholesterol used. Others investigated whether the size and route of administration of nanoparticles alter targeted organs and the collective amount of uptake (186). Briefly, oral exposure resulted in the highest amount of NP uptake compared to dermal uptake, whereas equal or smaller than 50 nm particles are taken up more efficiently compared to particles larger than 250 nm, which were not able to penetrate and cross the barriers. This has also been confirmed in other studies monitoring the size depended NP uptake in zebrafish larvae (187). Respectively, all polystyrene nanoparticles were taken up and distributed to several organs, finally accumulating in the liver of the larvae (186, 188).

Table 9 Nanotherapeutic efficacy analyzed in zebrafish infection models

Infection model	Nanotherapeutic	Outcome	Reference
M. marinum	Rifampicin loaded PLGA NPs	Increased embryo survival after NP treatment compared to free drug	(189)
Francisella noatunensis ssp. *orientalis*	Rifampicin/ oxolinic acid PLGA or lipid NPs	Delay of embryo mortality	(190)
S. aurues	Vancomycin gelatin nanospheres	Improved uptake in macrophages, delayed mortality	(191)
Salmonella typhi	Afzelin/ quercetrin AgNPs	Reduced toxicity	(192)
E.coli	AgNPs	Reduced toxicity	(193)
M.tuberculosis	Isoniazid/ clofazimine polymer NPs	Enhanced efficacy	(194)

A still very new and rather unexplored field of research is the combination of EVs in zebrafish larvae. Different studies, concerning live tracking and biodistribution of labelled EVs have been established (195, 196). Further, investigating the pathophysiology of diseases and the involvement of EVs brought new insides when combined with zebrafish larvae. For instance, it has been demonstrated that osteoblast derived EVs play a crucial role in osteoblast communication and the transformation in to osteoclasts (197). Moreover, plasmid loaded EVs were able to transfect zebrafish larvae with higher rates compared to common techniques, paving the way for EVs as tools for transfection and gene delivery (198). Finally, the safety of EVs was assessed in a zebrafish model. Here, milk derived EVs loaded with siRNA were incubated with 1dpf larvae with different particle concentrations in the water. Acute toxic effects such as survival, embryogenic development, hatching rate and the development of abnormalities were monitored, giving information on EV biocompatibility (198). In summary, zebrafish embryos are helpful tools for studying interaction, fate and safety of NPs. They give the possibility of live tracking, observation of an acute toxic reaction, studying the immunological impact and evaluating therapeutic efficacy.

2. Aim

The aim of this work was the overall assessment of extracellular and outer membrane vesicles as a novel biocompatible nanocarrier system against bacterial infections.

The number of antimicrobial resistant pathogens is currently at 700,000 deaths annually worldwide and rising (5). However, the number of newly approved antibiotics is decreasing (2). Thus, the improvement of common antibiotics towards efficacy, to prolong or even prevent the increase of antimicrobial resistance is essential. Nanoantibiotics are one way to address this problem, as they a) provide specific targeting b) improve solubility and bioavailability and c) increase drug accumulation in target cells (24). EVs and OMVs bare great potential in the use of therapeutics and are an advantageous alternative to synthetic nanocarrier systems. Their potentially low immunogenicity and inherent activity make them a great tool to develop nanoformulations (199, 200). Due to their size and potential inherent targeting properties, antimicrobial dosages could be reduced, as therapeutics are transported to the side of action more distinctively, minimizing side effects and prevent the spread and development of antimicrobial resistance.

In this work, extracellular vesicles derived from B-lymphoid cells and outer membrane vesicles derived from two different myxobacterial strains were investigated. The major research aims of this work were:

I) The physico-chemical **characterization** of the vesicles
II) Assessing their **stability** towards high and low temperatures
III) The assessment of their **biocompatibility** and toxicity
IV) Studying their **uptake** behavior in bacteria and cells
V) The investigation and introduction of **antimicrobial activity**

3. Main Findings

In this chapter, the main findings of three peer reviewed paper and one manuscript in preparation for submission are summarized and their impact presented. Some of the results of the individual publications were combined in this chapter for a comprehensive understanding and comparison of the data. Detailed information can be found in chapter 7.Scientific Output.

3.1. Characterization of EVs and OMVs

In this work, two strains of myxobacteria were used as a source for OMVs: i) *Cystobacter velatus* (Cbv34) and ii) an unclassified species of the suborder *Sorangiineae* (SBSr073). Extracellular vesicles were isolated from B-lymphoid RO cells, for comparative purposes and as an alternative to myxobacteria derived OMVs.

All cultures were optimized to include large volumes for the isolation of vesicles. Myxobacteria were cultivated with up to 500 mL per flask. RO cells were cultured in an upright culture flask position, increasing the volume up to 75 mL and minimizing space used for the cultivation (**Figure 11a**). The media for bacteria and cells were inexpensive and easy to produce. Further, RO cells were cultivated without serum, with an insulin-transferrin-selenium alternative, reducing effort and time due to serum depletion and unnecessary medium exchange (201). One of the problems with using vesicles, especially cell derived EVs, is the up-scalability of their production. With these optimizations, it is now possible to produce RO-EVs on a large scale approximately similar to bacteria.

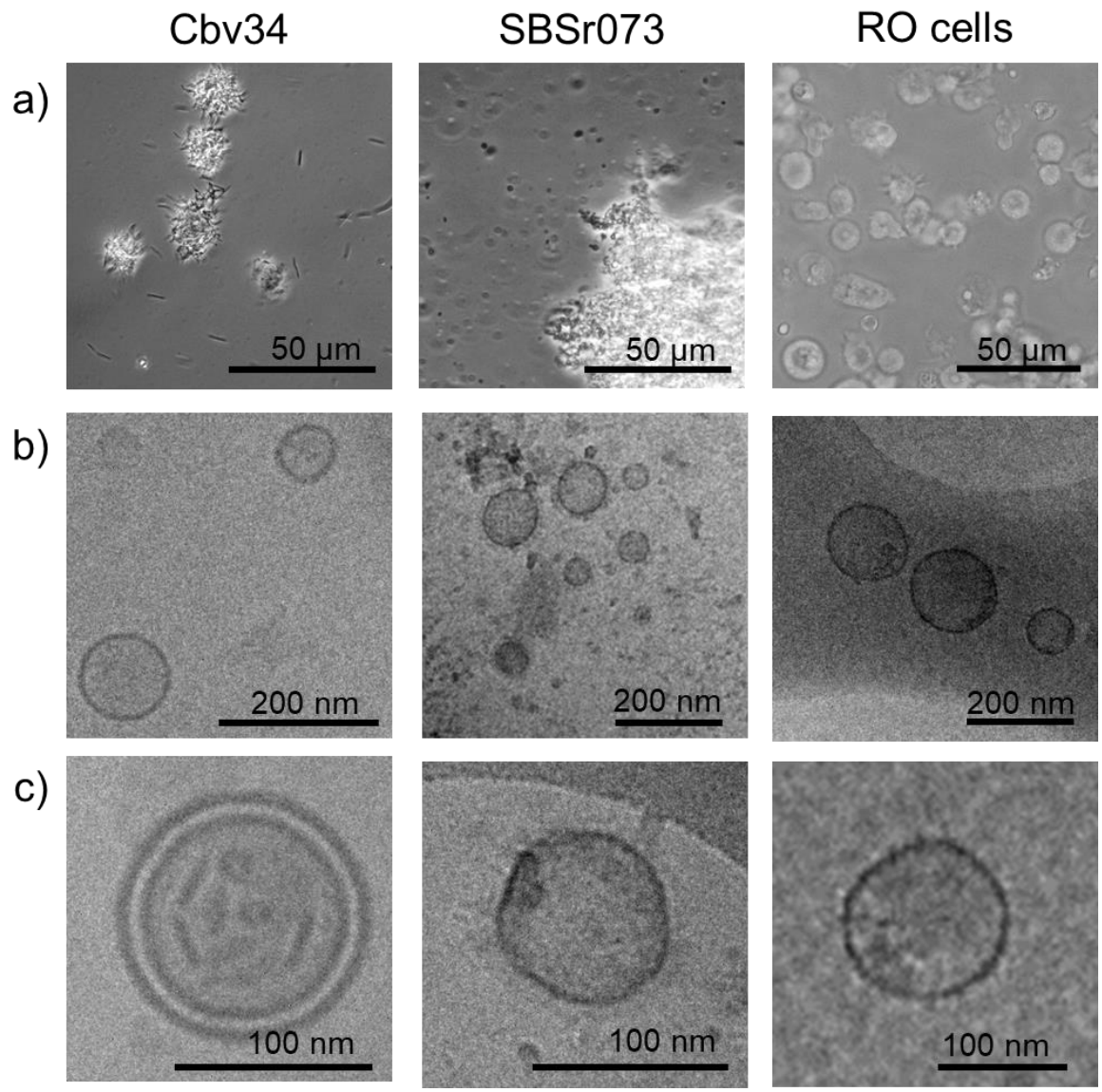

Figure 11 Microscopic images of myxobacteria, cells and their respective vesicles. *a) Microscopic images of Cbv34, SBSr073 bacteria and RO cells b) Cryo-Electron images of Cbv-OMVs, SB-OMVs and RO-EVs c) Zoomed in cryo-electron images of an individual vesicle*

Vesicles were isolated via differential ultracentrifugation, a commonly used method to isolate EVs or OMVs (4). Respectively, a size exclusion chromatography was used to remove soluble proteins and to study the vesicles without contaminations. The size and particle concentration of the vesicles was determined by nanoparticle tracking analysis (NTA). Especially particle concentrations of myxobacteria derived OMVs were particularly abundant with up to 10^{12} particles/mL. In comparison, six times the amount of RO cell supernatant had to be isolated in order to have similar particle concentrations. Thus, due to the lower volumes required to isolate high concentrations of vesicles, OMVs have a particular advantage over EVs. This could

provide a fundamental improvement for the translation of vesicles from laboratory to clinical use and should be kept in mind for further investigations.

The size of the vesicles was between 160 nm for RO-EVs and 194 nm for SB-OMVs. With that, they are most likely able to accumulate in inflamed tissue, which is beneficial towards the application against bacterial infections (202). Moreover, sizes between 100 – 200 nm may extend circulation, prolonging their therapeutic effect (203, 204). The zeta potential of the vesicles was negative, ranging from -12.8 for RO-EVs to -4.8 for Cbv-OMVs (**Table 10**). This might lead to difficulties towards the stability of the vesicles, as a lower zeta potential is often associated with the likelihood of aggregation and increased phagocytosis (203). On the contrary, we observed satisfactory stability of vesicles, which will be presented in the next chapter.

Table 10 Physico-chemical characteristics of vesicles

Vesicle source	Vesicle type	Protein/vesicle (µg/particle × 10^{-10})	Size (nm)	Zeta potential (mV)
Cystobacter velatus Cbv34	Cbv-OMVs	1.6 ± 1.2	145 ± 27	-4.8 ± 0.7
unclassified *Sorangiineae* SBSr073	SB-OMVs	3.6 ± 2.9	194 ± 18	-6.8 ± 0.6
B-lymphoid RO cells	RO-EVs	6.5 ± 1.5	160 ± 2	-12.8 ± 0.5

3.2. Storage Stability

To analyze the stability of the vesicles at different temperatures, purified SEC fractions were stored in low binding polypropylene tubes to avoid unspecific binding of the vesicles and their loss. If higher temperatures were applied, vesicles were stored in glass vials. After different time points, particle concentrations and sizes were measured by NTA to detect the loss and aggregation of vesicles.

The storage stability was evaluated at 4°C, -20°C, -80°C and upon freeze-drying after 7 and 75 days. After 7 days, an average of 54 % of vesicle yield was recovered and 46 % after 75 days (**Figure 12a**). However, a significant increase of particle sizes after 75 days was detected, suggesting an unspecific agglomeration of the vesicles. The lyophilization method exhibited the best results of all conditions with 72 % particle recovery even after 75 days of storage (**Figure 12b**).

Some reports on standardized methods for storing EVs and OMVs have been published, predominantly recommending storage at -80°C (205, 206). However, it was shown here that lyophilization of vesicles is a valid alternative. The addition of cryo-protectants could further improve the settings, nonetheless should be investigated and optimized individually (207).

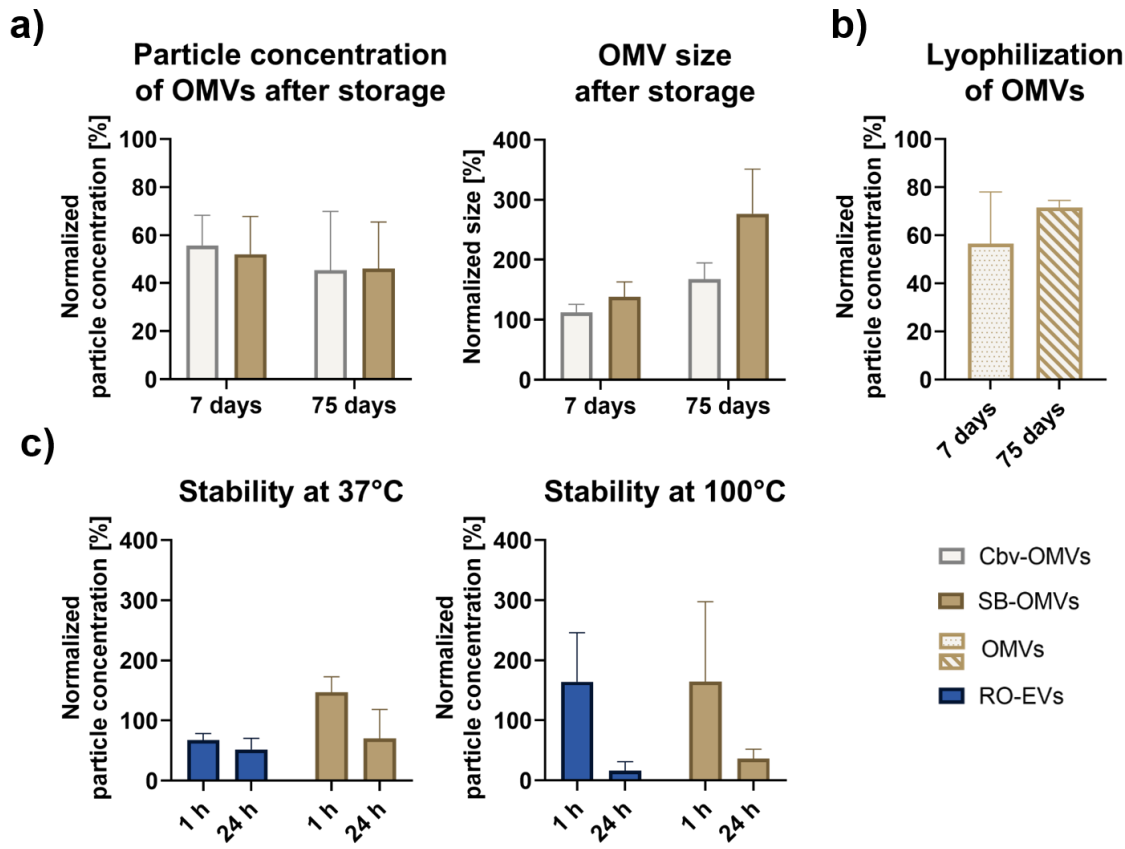

Figure 12 Stability of EVs and OMVs upon low and high temperatures. *a) Particle concentrations and sizes normalized to start measurements before storing the vesicles at 4°C, -20°C, -80°C and upon freeze-drying for 7 and 75 days b) Normalized particle concentration after lyophilization measured after 7 and 75 days c) Normalized particle concentration from vesicles incubated at 37°C and 100°C for 1 h and 24 h*

The heat stability of RO-EVs and SB-OMVs was tested at 37°C, 50°C, 70°C and 100°C, sampling after 1 h, 6 h and 24 h. Both types of vesicles were stable at 37°C even after 24 h with little to minor changes in particle concertation, protein concentration and size. Drastic physico-chemical changes were detected at temperatures up to 100°C, with altered particle and protein concentrations. When comparing EVs with OMVs, it was observable that SB-OMVs had a higher tolerance to increasing temperatures compared to RO-EVs.

Exposing vesicles to higher temperatures has certainly an effect on their physico-chemical characteristics. Although temperatures up to 37°C were tolerated, higher temperatures have an impact on the integrity of the vesicles. This should be considered during particle formulation, sterilization processes and storage.

3.3. Biocompatibility

The term biocompatibility according to Williams refers to “the ability of a biomaterial to perform its desired function with respect to a medical therapy, without eliciting any undesirable local or systemic effects in the recipient . . . ” (208). Therefore, biocompatibility of the vesicles was first evaluated using a chromogenic limulus amoebocyte lysate endotoxin assay. These assays give information on the concentration of immunostimulatory lipopolysaccharides and are

recommended by the European Medicine Agency to test pharmaceutical quality and safety of biological products, drugs and devices (209). First, SEC-purified vesicles were tested against the SEC eluent PBS, as the preparation and purification under aseptic conditions was not possible. Endotoxin concentrations were not increase compared to the PBS control (**Figure 13a**). In addition to the chromogenic test, a gel clot assay was performed. Here, the aseptically prepared, yet unpurified vesicle pellets were used for testing high concentrations of vesicles compared to diluted samples from SEC. A firm gel formation of the samples was not observed, ensuing lower LPS concentrations than 0.25 EU/mL (**Figure 13b**). Based on both tests, an inherent biocompatibility with little to no endotoxin contamination for RO-EVs, SB-OMVs and Cbv-OMVs could be proposed.

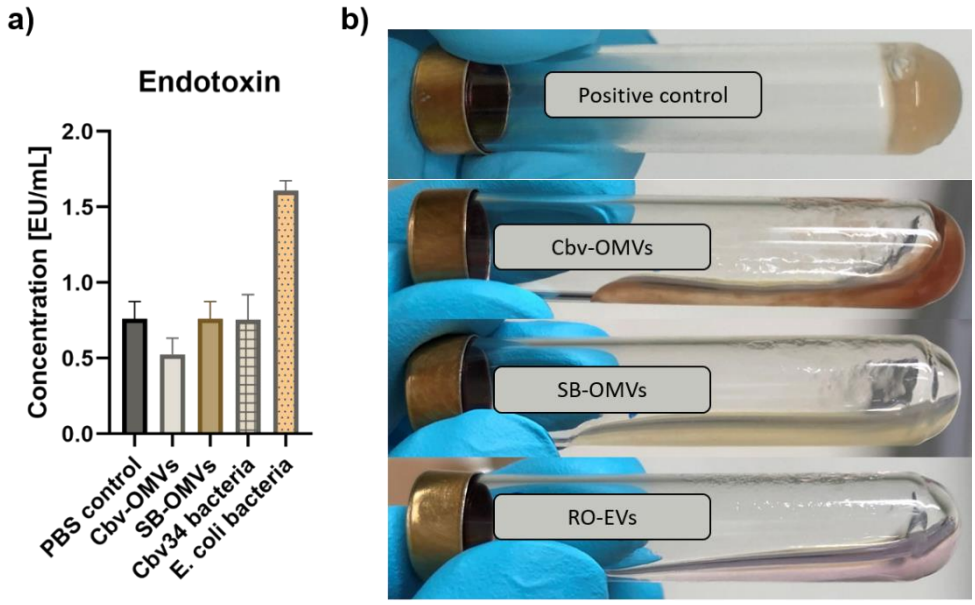

Figure 13 Detection of endotoxin in vesicles. *a) Quantification of endotoxin using a chromogenic LAL assay and SEC-purified vesicles b) Semi-quantitative detection of endotoxin using a gel clot assay and non-purified vesicle pellets.*

The immunogenic potential of the vesicles was tested on peripheral blood mononuclear cells (PBMCs). These cells were isolated from whole blood and contained T-cells, B-cells, monocytes or dendritic cells, which are involved in the innate immune response (210). The concentration of pro-inflammatory cytokines, such as interleukin 1 beta, 6, 8 and tumor necrosis factor alpha (TNF-alpha) was tested after 4 h of vesicle exposure. These cytokines are a protective response of the human body against pathogen associated molecular patterns, recognized by Toll-like receptors on respective immune cells (211). The release of the cytokines was, at any time, lower than the 1 µg/mL LPS positive control, although the vesicle concentration per cell was particularly high with up to 500,000 vesicles per cell (**Figure 14**). However, the release of pro-inflammatory cytokines by RO-EVs was profoundly lower compared to myxobacterial OMVs. It should be mentioned, that Cbv-OMVs evidently decreased the viability of PBMCs, as little to no cells were observed after an incubation with

concentration up to 10^{13} vesicles/mL or 5,000,000 vesicles per cell (7.3. supplementary data). Once a 1:10 dilution was prepared and vesicles diluted to 10^{12} vesicles/mL and respective 500,000 vesicles/cell no cytotoxic effect in microscopic images was observed. Complementary, viability and cytotoxicity assays were performed on macrophage like *d*THP-1 and epithelial cells A549. No negative effect on the viability of the cells nor cytotoxic effects were detected when concentrations up to 10,000 vesicles per cell were added for 24 h.

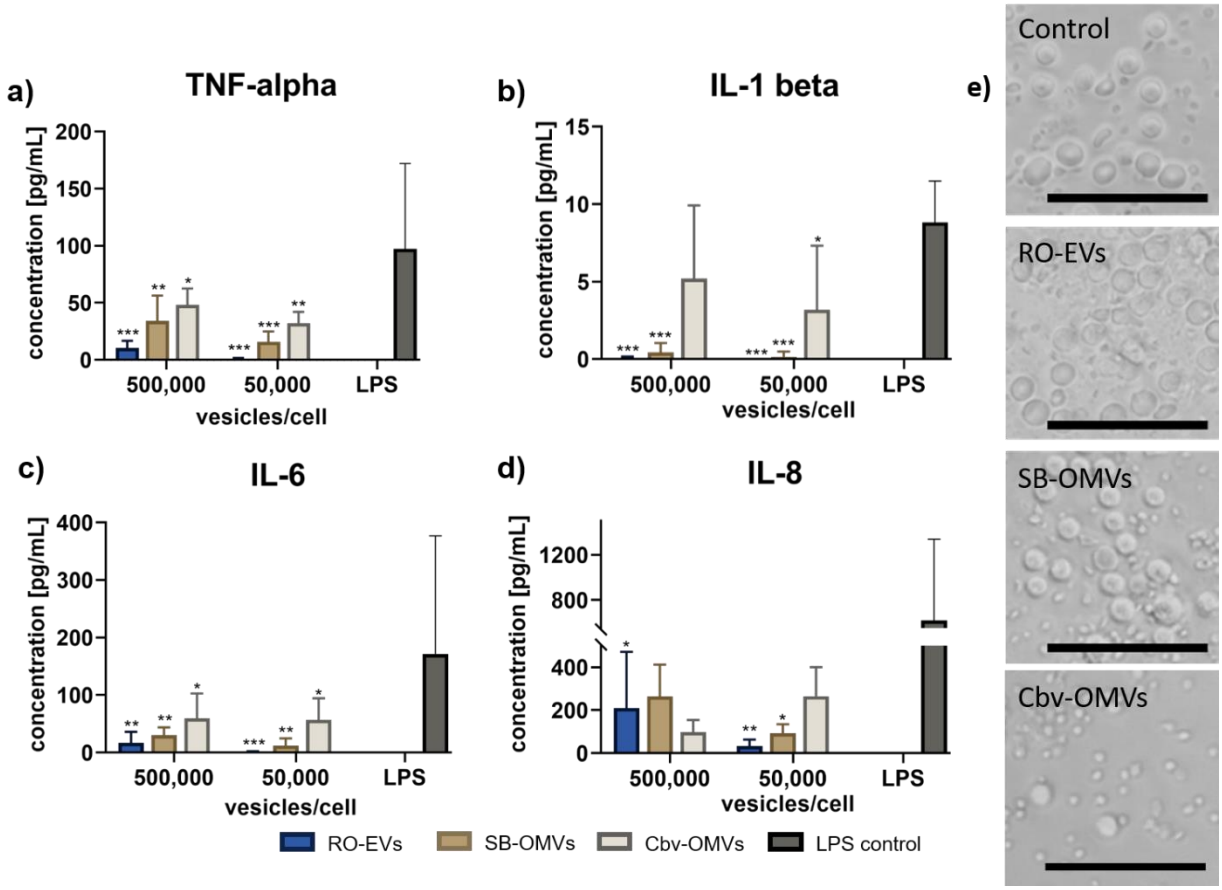

Figure 14 Cytokine release of vesicles incubated PBMCs. *a) TNF-alpha concentration after 4 h incubation with different concentrations of vesicles b) IL-1 beta release c) IL-6 release d) IL-8 release e) Microscopic images of PBMCs incubated with 500,000 vesicles per cell. Scale bar 50 µm*

Zebrafish larvae were used to assess the toxicological profile of the vesicles *in vivo*. Here, RO-EVs and SB-OMVs were tested. As zebrafish embryos have profound similarities in the innate immune system compared to humans, they are excellent and easy to maintain *in vivo* models for testing toxicological effects. The vesicles did not induce any toxic effect, nor influence the embryological development of the larvae. First vesicles were added to the water with PBS concentrations that are non-toxic to fish (25 % tested in previous experiments). As with this method no obvious toxic effect was observed, vesicles were also injected into the blood island to mimic a systemic exposure. Here as well, no larvae showed any sign of abnormal development, advancing the biocompatibility of the vesicles. However, if ciprofloxacin loaded vesicles (see chapter 3.5) were injected, zebrafish larvae developed heart edema with an

inflated pericardium. These incidences occurred nevertheless with higher probability of 17 % with free ciprofloxacin compared to 5 % and 7 % for SB-OMVs and RO-EVs, respectively. Accordingly, it could be that, due to a beneficial distribution of the vesicles, fewer systemic side effects from vesicle encapsulated ciprofloxacin than from the non-encapsulated antibiotic itself were generated.

Based on endotoxin quantification, cytokine release studies and toxicity testing in zebrafish larvae, there is strong evidence that the vesicles are highly biocompatible and non-toxic. To the best of my knowledge, these are the first results to intensively evaluate the biocompatibility of myxobacterial OMVs and RO-cell derived EVs.

3.4. Uptake

To study the uptake of vesicles in bacteria and cells, vesicles were labelled with a fluorescent membrane dye, DiI. Bacteria and cells were stained with counter-dyes such as SYTO 9 for bacteria, phalloidin-FITC for the cellular cytoskeleton and DAPI for the nucleus. Throughout all experiments, the fluorescence intensity and gain especially for DiI labeled vesicles was matched to controls with no vesicle exposure, to prevent the detection of false positive bacteria or cells. The co-localization of Cbv-OMVs and SB-OMVs was investigated using *E.coli* DH5-alpha, with which the antibacterial activity was also tested later on. A co-localization of vesicles with bacteria could be observed after a 24 h incubation period, suggesting cellular uptake.

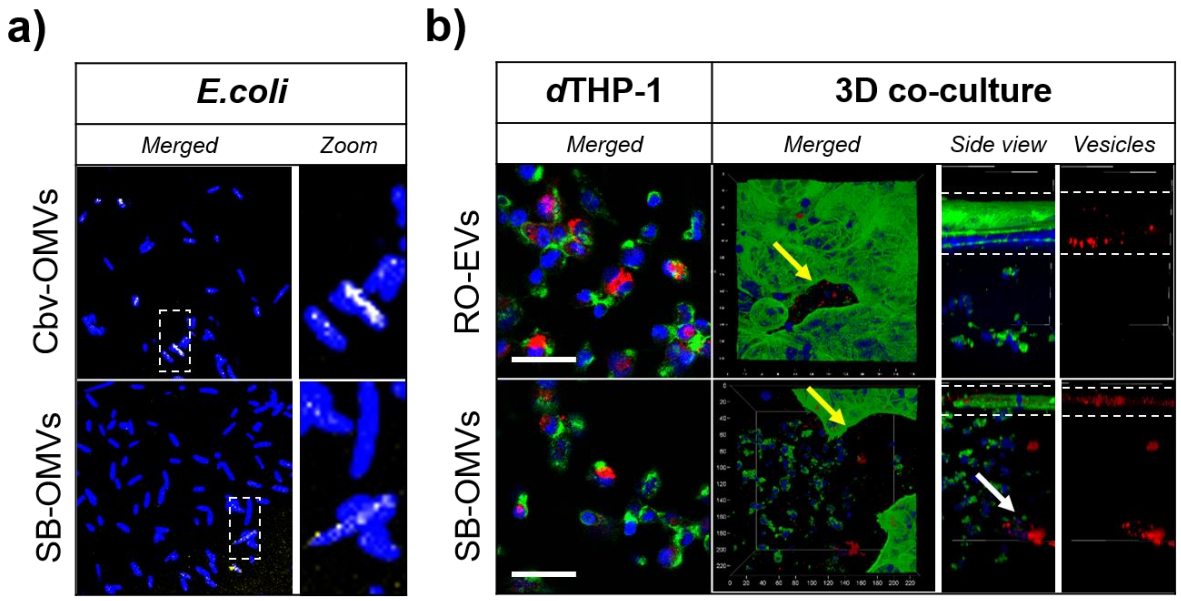

Figure 15 Confocal microscopy images of vesicles incubated with bacteria, immune cells or a 3D co-culture. *a) Uptake of OMVs (yellow) in E.coli (blue) b) Uptake of vesicles (red) in macrophage like dTHP-1 cells (cytoskeleton green, nucleus blue) on a cover slide and*

uptake of vesicles in a three-dimensional co-culture model with an epithelial cell layer (in between dashed lines) and in collagen embedded immune cells.

The interaction of vesicles with cells was first observed in macrophage like *d*THP-1, with a distinct co-localization of cells and labeled vesicles. To further assess the uptake behavior in a more complex setting, with different interconnected cell lines, a three-dimensional gastrointestinal co-culture model was applied. This model consisted of an epithelial layer (CaCo-2) on top of two different immune cells (*d*THP-1 and MUTZ-3) embedded in collagen. Here, vesicles predominantly accumulated in the epithelial cell layer. However, when a slightly modified version of the model with a leaky epithelial barrier was used (yellow arrow in **Figure 15b**), vesicle positive immune cells were occasionally seen. (white arrow in **Figure 15b**).

By analyzing the uptake behavior of OMVs and EVs, their potential as anti-infective drug delivery systems can be recognized. As discussed in chapter 1.1. Challenges in treating bacterial infections, cellular uptake of nanoantibiotics is essential for combating antimicrobial resistance. When uptake in bacteria or infected cells follows, high doses of compound will be released within the target, saturating efflux pumps or stressing degrading enzymes with the aim to finally eliminate the pathogen (28). Moreover, intracellular pathogens can be reached, where poorly bioavailable antibiotics cannot penetrate (212). In conclusion, it has been shown that vesicles are capable of being taken up into cells and bacteria, which may be beneficial towards preventing the development of resistances.

3.5. Antimicrobial Activity

Myxobacteria are producers of a diverse variety of secondary metabolites, including antibacterial agents to pray on competitive bacteria (72, 213). It was postulated that OMVs contain these antimicrobial compounds to aid in nutrient acquisition. Indeed, it has already been shown that OMVs derived from *Myxococcus xanthus*, one of the best known and widely studied strains of the myxobacterial family, are able to inhibit the growth of *Escherichia coli* (214). The inhibitory effect of Cbv- and SB-OMVs was tested on *E.coli* DH5-alpha. Due to the encapsulation of cytobactamid 919-1, a topoisomerase inhibitor produced by Cbv034 myxobacteria and hence associated with their vesicles, the Cbv-OMVs were able to inhibit the growth of *E.coli* in a dose depended manner (**Figure 16a,b**). Since SB-OMVs did not exhibit antibacterial activity, the option of loading them with a model antibiotic was perused. Therefore, different loading techniques were assessed to encapsulate ciprofloxacin (CPX) into the vesicles. As RO-EVs showed inherently good biocompatibility, a small size and expectable yield, these techniques were as well applied to RO-EVs to further be used as drug delivery systems. After initial difficulties to find the right stock concentration and method to remove free

CPX, it was demonstrated that all applied methods led to a more or less efficient encapsulation of CPX. The passive incubation method was the most successful for RO_{CPX}EVs with CPX concentrations up to 70 ng/vesicles × 10^{-12}. The combination of saponin-assisted and passive incubation was the most effective for SB_{CPX}OMVs with 50 ng/vesicle × 10^{-12} CPX. Both vesicles, loaded with different methods were able to inhibit the growth of GI-pathogens *Shigella flexneri* and *Salmonella enterica* (**Figure 16c,d**). Overall, the differently loaded vesicles were able to reduce the CFU count of *Shigella* down to 5.61 log units on average, decreasing the percentage bacterial number to 62 %. Since the growth inhibitory effect of the vesicles on *Salmonella* was not as prominent, further experiments were conducted only on *Shigella*.

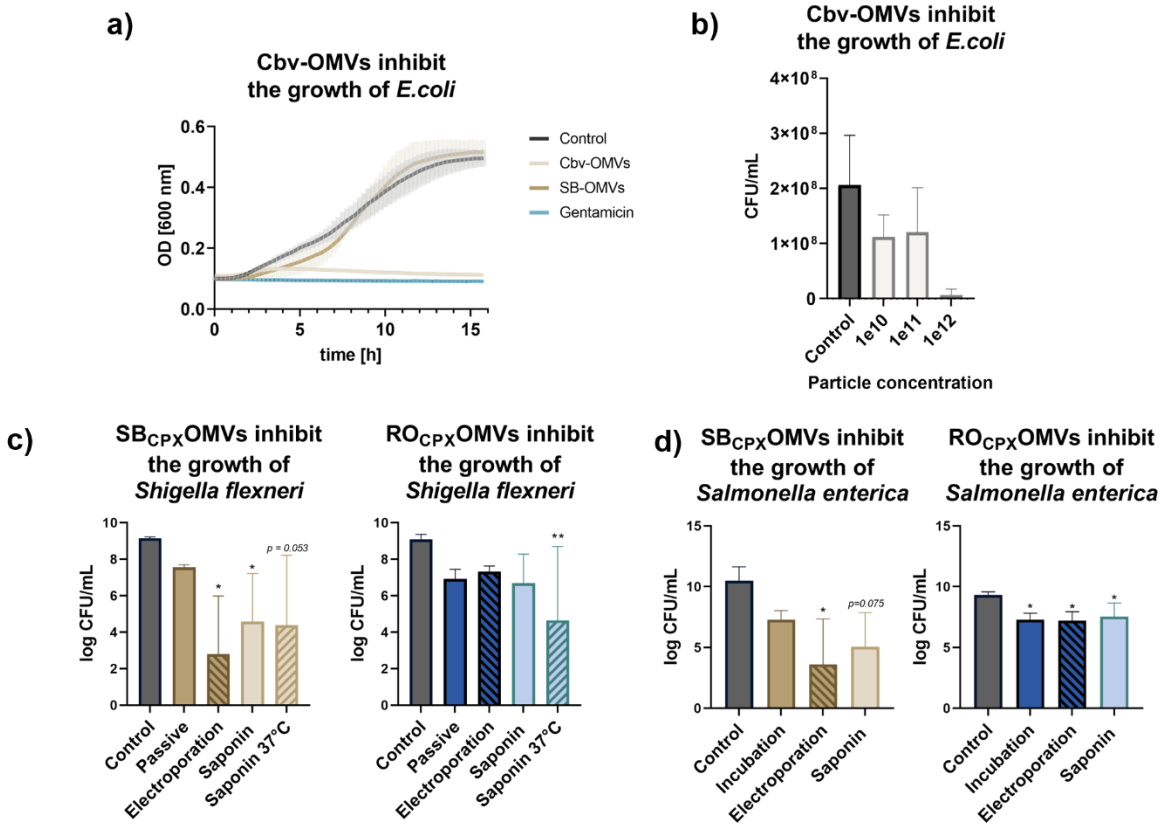

Figure 16 Antimicrobial activity of Cbv-OMVs, SB_{CPX}OMVs and RO_{CPX}EVs. *a) inherent antimicrobial activity of Cbv-OMVs against E.coli b) Cbv-OMVs inhibit the growth of E.coli in a dose depended manner c) SB_{CPX}OMVs and RO_{CPX}EVs were loaded with ciprofloxacin and were able to inhibit the growth of Shigella flexneri and d) Salmonella enterica*

To evaluate the antimicrobial effect of the loaded vesicles *in vivo*, a *Shigella flexneri* GFP zebrafish larvae model was established. These infection models in zebrafish can mimic the pathological pattern of a human infections adequately, as their innate immune system is similar to that of humans (173). A recent study showed, that *Shigella* even invaded immune cells, escaped vacuole digestion and proliferated within the fish until an ultimate lethal concentration was accomplished (215). Although the establishment of the *Shigella* model was successful, the curative effect of CPX loaded vesicles could not be demonstrated. The infection was

severe, whereby only CPX concentrations of 1,000 × minimal inhibitory concentration values showed the desired eradication of the pathogen.

The discovery of inherent antimicrobial OMVs is beneficial towards a facilitated development of an anti-infective drug delivery system. The poorly soluble cytobactamid was naturally encapsulated within the OMVs, which abolished the time-consuming and cost-generating establishment of a loading technique. Nevertheless, it was important to introduce the possibility to load non-inherently active OMVs and EVs, with an antibacterial agent, to take advantage of their natural beneficial characteristics described in the previous chapters. In addition, it is also possible to load various drugs into the vesicles.

4. Conclusion and Outlook

In this work, the foundation for developing a vesicle-based therapy against bacterial infections was established. A new type of OMVs derived from two myxobacterial strains and EVs derived from immune cells were investigated. Both, EVs and OMVs were evaluated towards their characterization, stability, biocompatibility, uptake behavior and antimicrobial activity.

The vesicles exhibited promising characteristics towards their size and stability at different temperatures. Since the lyophilization of the OMVs showed adequate storage stability, the use of cryoprotenctants should be investigated respectively to even enhance their it. The advanced biocompatibility studies underlined the non-toxic effect of the vesicles with RO-EVs being tolerated best. An in depth understanding of the exact mechanisms of cytokine release and studying the activation of Toll-like receptors might give more information on the actual mode of cytokine release. In addition, a profound analysis of the composition of myxobacteria derived OMVs could quantify the definite concentration of endotoxin and might explain their exceedingly low toxicity.

As vesicle uptake in macrophages was observed, the applicability of vesicles in other intracellular, macrophage invading infections might be possible. *Pseudomonas aeruginosa* and *Mycobacterium tuberculosis*, for example invade macrophages in the lung, causing pneumonia or tuberculosis (216, 217). As a broad spectrum antibiotic was used to load the vesicles and cystobactamid 919-1 is effective against several gram-negative and gram-positive pathogens, various therapeutic applications are possible. Further, it would also be beneficial to investigate to what extent the vesicles are able to penetrate mucus. Mucus is present in both the lungs and the GI-tract, protecting the underlying cell layer. This represents an obstacle not only for pathogens, but also for drugs, which are then often unable to reach their target. Since it has been shown that nanoparticles can, to some extend penetrate this network of mucin, it would be interesting to find out whether vesicles share these properties or are even more effective (218). Another barrier that must be overcome is the biofilm, a complex structure of different bacterial colonies and single cells embedded in an extracellular polymer substance. This matrix provides mechanical, as well as chemical protection and facilitates the communication among pathogens. Of particular concern is, that antibiotics are often unable to penetrate the biofilm, promoting the development of resistances (219). Accordingly, it should be investigated whether vesicles are able to overcome this hydrated matrix in order to introduce antibiotics in an advanced targeting manner.

Finally, we were able to establish a pathophysiological relevant *in vivo* model of *Shigella* in zebrafish larvae, with high lethality. With concentrations of 200 µg/mL ciprofloxacin (1000 × MIC), we succeeded in eliminating the *Shigella* infection and secured the survival of the fish.

However, as the bacterial spreading was particularly pronounced and persistent, ciprofloxacin-loaded vesicles failed to contain the infection. In this context, it would be beneficial to use a different infection model with lower lethality and higher susceptibility to antibiotics to demonstrate the therapeutic effect of the vesicles in a realistic setting.

5. References

Illustrations were created with BioRender.com.

1. Brown ED, Wright GD. Antibacterial drug discovery in the resistance era. Nature. 2016;529(7586):336-43.
2. Prevention CfDca. Antibiotic Resistance Threats in the United States 2013 [Available from: https://www.cdc.gov/drugresistance/threat-report-2013/.
3. Fleming A. Penicillin. Nobel Lecture: Alexander Fleming; 1945.
4. Théry C, Witwer KW, Aikawa E, Alcaraz MJ, Anderson JD, Andriantsitohaina R, et al. Minimal information for studies of extracellular vesicles 2018 (MISEV2018): a position statement of the International Society for Extracellular Vesicles and update of the MISEV2014 guidelines. Journal of Extracellular Vesicles. 2018;7(1):1535750.
5. O'Neill J. Tackling drug resistant infections globally: final report and recommendations. 2016.
6. C Davies S, Fowler T, Watson J, Livermore D, Walker D. Annual Report of the Chief Medical Officer: Infection and the rise of antimicrobial resistance2013.
7. Cassini A, Högberg LD, Plachouras D, Quattrocchi A, Hoxha A, Simonsen GS, et al. Attributable deaths and disability-adjusted life-years caused by infections with antibiotic-resistant bacteria in the EU and the European Economic Area in 2015: a population-level modelling analysis. The Lancet Infectious Diseases. 2019;19(1):56-66.
8. Institut RK. Neue Zahlen zu Krankheits-last und Todes-fällen durch antibiotika-resistente Erreger in Europa 2018 [Available from: https://www.rki.de/DE/Content/Infekt/Antibiotikaresistenz/Uebersichtsbeitraege/AMR_Europa.html#:~:text=33.000%20Menschen%20pro%20Jahr%20daran,2.400%20Menschen%20sterben%20daran.
9. Antibiotic resistance threats in the United States, 2019. 2019.
10. Blair JMA, Webber MA, Baylay AJ, Ogbolu DO, Piddock LJV. Molecular mechanisms of antibiotic resistance. Nature Reviews Microbiology. 2014;13:42.
11. Li X-Z, Nikaido H. Efflux-mediated drug resistance in bacteria: an update. Drugs. 2009;69(12):1555-623.
12. Munita JM, Arias CA. Mechanisms of Antibiotic Resistance. Microbiology spectrum. 2016;4(2):10.1128/microbiolspec.VMBF-0016-2015.
13. Richter MF, Drown BS, Riley AP, Garcia A, Shirai T, Svec RL, et al. Predictive rules for compound accumulation yield a broad-spectrum antibiotic. Nature. 2017;545(7654):299-304.
14. Khalid A, Lubián AF, Ma L, Lin RCY, Iredell JR. Characterizing the role of porin mutations in susceptibility of beta lactamase producing Klebsiella pneumoniae isolates to ceftaroline and ceftaroline-avibactam. International Journal of Infectious Diseases. 2020;93:252-7.
15. Grimsey EM, Weston N, Ricci V, Stone JW, Piddock LJV. Overexpression of RamA, Which Regulates Production of the Multidrug Resistance Efflux Pump AcrAB-TolC, Increases Mutation Rate and Influences Drug Resistance Phenotype. Antimicrob Agents Chemother. 2020;64(4):e02460-19.
16. Ernst CM, Slavetinsky CJ, Kuhn S, Hauser JN, Nega M, Mishra NN, et al. Gain-of-Function Mutations in the Phospholipid Flippase MprF Confer Specific Daptomycin Resistance. mBio. 2018;9(6):e01659-18.
17. Yong D, Toleman MA, Giske CG, Cho HS, Sundman K, Lee K, et al. Characterization of a new metallo-beta-lactamase gene, bla(NDM-1), and a novel erythromycin esterase gene carried on a unique genetic structure in Klebsiella pneumoniae sequence type 14 from India. Antimicrob Agents Chemother. 2009;53(12):5046-54.

18. Arunasri K, Mohan SV. Chapter 2.3 - Biofilms: Microbial Life on the Electrode Surface. In: Mohan SV, Varjani S, Pandey A, editors. Microbial Electrochemical Technology: Elsevier; 2019. p. 295-313.
19. Pelgrift RY, Friedman AJ. Nanotechnology as a therapeutic tool to combat microbial resistance. Advanced Drug Delivery Reviews. 2013;65(13–14):1803-15.
20. Gopal Rao G. Risk Factors for the Spread of Antibiotic-Resistant Bacteria. Drugs. 1998;55(3):323-30.
21. GmbH H-IfI. Weltantibiotikawoche 2019 2019 [cited 2020. Available from: https://www.helmholtz-hzi.de/de/aktuelles/thema/weltantibiotikawoche-2019/.
22. Christian Baars OL. Pharmaceutical companies pulling out of antibiotic research: NDR investigation; 2019 [Available from: https://www.tagesschau.de/investigativ/ndr/antibiotika-pharmakonzerne-163.html.
23. Taylor PW, Stapleton PD, Paul Luzio J. New ways to treat bacterial infections. Drug Discovery Today. 2002;7(21):1086-91.
24. Allaker RP, Ren G. Potential impact of nanotechnology on the control of infectious diseases. Transactions of The Royal Society of Tropical Medicine and Hygiene. 2008;102(1):1-2.
25. Huh AJ, Kwon YJ. "Nanoantibiotics": A new paradigm for treating infectious diseases using nanomaterials in the antibiotics resistant era. Journal of Controlled Release. 2011;156(2):128-45.
26. Azzopardi EA, Ferguson EL, Thomas DW. The enhanced permeability retention effect: a new paradigm for drug targeting in infection. Journal of Antimicrobial Chemotherapy. 2012;68(2):257-74.
27. Chen H, Jin Y, Wang J, Wang Y, Jiang W, Dai H, et al. Design of smart targeted and responsive drug delivery systems with enhanced antibacterial properties. Nanoscale. 2018;10(45):20946-62.
28. Singh S, Hussain A, Shakeel F, Ahsan MJ, Alshehri S, Webster TJ, et al. Recent insights on nanomedicine for augmented infection control. International journal of nanomedicine. 2019;14:2301-25.
29. Kamaruzzaman NF, Kendall S, Good L. Targeting the hard to reach: challenges and novel strategies in the treatment of intracellular bacterial infections. Br J Pharmacol. 2017;174(14):2225-36.
30. Menina S, Labouta HI, Geyer R, Krause T, Gordon S, Dersch P, et al. Invasin-functionalized liposome nanocarriers improve the intracellular delivery of anti-infective drugs. RSC Advances. 2016;6(47):41622-9.
31. Majumdar S, Flasher D, Friend DS, Nassos P, Yajko D, Hadley WK, et al. Efficacies of liposome-encapsulated streptomycin and ciprofloxacin against Mycobacterium avium-M. intracellulare complex infections in human peripheral blood monocyte/macrophages. Antimicrob Agents Chemother. 1992;36(12):2808-15.
32. Ho D-K, Costa A, De Rossi C, de Souza Carvalho-Wodarz C, Loretz B, Lehr C-M. Polysaccharide Submicrocarrier for Improved Pulmonary Delivery of Poorly Soluble Anti-infective Ciprofloxacin: Preparation, Characterization, and Influence of Size on Cellular Uptake. Molecular Pharmaceutics. 2018;15(3):1081-96.
33. Cavalli R, Gasco MR, Chetoni P, Burgalassi S, Saettone MF. Solid lipid nanoparticles (SLN) as ocular delivery system for tobramycin. International Journal of Pharmaceutics. 2002;238(1):241-5.
34. Kisich KO, Gelperina S, Higgins MP, Wilson S, Shipulo E, Oganesyan E, et al. Encapsulation of moxifloxacin within poly(butyl cyanoacrylate) nanoparticles enhances efficacy against intracellular Mycobacterium tuberculosis. International Journal of Pharmaceutics. 2007;345(1):154-62.
35. Schumacher I, Margalit R. Liposome-Encapsulated Ampicillin: Physicochemical and Antibacterial Properties. Journal of Pharmaceutical Sciences. 1997;86(5):635-41.

36. Onyeji C, D C, Marangos M. Enhanced killing of methicillin-resistant Staphylococcus aureus in human macrophages by liposome-entrapped vancomycin and teicoplanin. Infection. 1994;22:338-42.
37. Gao F, Xu L, Yang B, Fan F, Yang L. Kill the Real with the Fake: Eliminate Intracellular Staphylococcus aureus Using Nanoparticle Coated with Its Extracellular Vesicle Membrane as Active-Targeting Drug Carrier. ACS Infectious Diseases. 2019;5(2):218-27.
38. Grumezescu V, Holban AM, Iordache F, Socol G, Mogoşanu GD, Grumezescu AM, et al. MAPLE fabricated magnetite@eugenol and (3-hidroxybutyric acid-co-3-hidroxyvaleric acid)–polyvinyl alcohol microspheres coated surfaces with anti-microbial properties. Applied Surface Science. 2014;306:16-22.
39. Anversa Dimer F, de Souza Carvalho-Wodarz C, Goes A, Cirnski K, Herrmann J, Schmitt V, et al. PLGA nanocapsules improve the delivery of clarithromycin to kill intracellular Staphylococcus aureus and Mycobacterium abscessus. Nanomedicine : nanotechnology, biology, and medicine. 2019.
40. Zaki N, Hafez M. Enhanced Antibacterial Effect of Ceftriaxone Sodium-Loaded Chitosan Nanoparticles Against Intracellular Salmonella typhimurium. AAPS PharmSciTech. 2012;13:411-21.
41. Magallanes M, Dijkstra J, Fierer J. Liposome-incorporated ciprofloxacin in treatment of murine salmonellosis. Antimicrob Agents Chemother. 1993;37(11):2293-7.
42. Stone NRH, Bicanic T, Salim R, Hope W. Liposomal Amphotericin B (AmBisome(®)): A Review of the Pharmacokinetics, Pharmacodynamics, Clinical Experience and Future Directions. Drugs. 2016;76(4):485-500.
43. Biopharma M. Potentially the first oral formulation of a potent gram-negative antibiotic 2020 [Available from: https://www.matinasbiopharma.com/lnc-technology/mat2501.
44. Ivask A, Juganson K, Bondarenko O, Mortimer M, Aruoja V, Kasemets K, et al. Mechanisms of toxic action of Ag, ZnO and CuO nanoparticles to selected ecotoxicological test organisms and mammalian cells in vitro: A comparative review. Nanotoxicology. 2014;8(sup1):57-71.
45. Karavolos M, Holban A. Nanosized Drug Delivery Systems in Gastrointestinal Targeting: Interactions with Microbiota. Pharmaceuticals (Basel, Switzerland). 2016;9(4):62.
46. Sil S, Dagur RS, Liao K, Peeples ES, Hu G, Periyasamy P, et al. Strategies for the use of Extracellular Vesicles for the Delivery of Therapeutics. 2019.
47. Nasiri Kenari A, Cheng L, Hill AF. Methods for loading therapeutics into extracellular vesicles and generating extracellular vesicles mimetic-nanovesicles. Methods. 2020.
48. György B, Hung ME, Breakefield XO, Leonard JN. Therapeutic Applications of Extracellular Vesicles: Clinical Promise and Open Questions. Annual review of pharmacology and toxicology. 2015;55:439-64.
49. Caruso S, Poon IKH. Apoptotic Cell-Derived Extracellular Vesicles: More Than Just Debris. Frontiers in Immunology. 2018;9(1486).
50. Armstrong D, Wildman DE. Extracellular Vesicles and the Promise of Continuous Liquid Biopsies. J Pathol Transl Med. 2018;52(1):1-8.
51. Fuhrmann G, Herrmann IK, Stevens MM. Cell-derived vesicles for drug therapy and diagnostics: Opportunities and challenges. Nano Today. 2015;10(3):397-409.
52. El Andaloussi S, Mager I, Breakefield XO, Wood MJA. Extracellular vesicles: biology and emerging therapeutic opportunities. Nat Rev Drug Discov. 2013;12(5):347-57.
53. Yáñez-Mó M, Siljander PRM, Andreu Z, Bedina Zavec A, Borràs FE, Buzas EI, et al. Biological properties of extracellular vesicles and their physiological functions. J Extracell Vesicles. 2015;4(1):27066.

54. Latifkar A, Hur YH, Sanchez JC, Cerione RA, Antonyak MA. New insights into extracellular vesicle biogenesis and function. Journal of Cell Science. 2019;132(13):jcs222406.
55. van Niel G, D'Angelo G, Raposo G. Shedding light on the cell biology of extracellular vesicles. Nature Reviews Molecular Cell Biology. 2018;19(4):213-28.
56. Yáñez-Mó M, Siljander P, Andreu Z, Bedina Zavec A, Borràs F, Buzás E, et al. Biological properties of extracellular vesicles and their physiological functions. Journal of Extracellular Vesicles. 2015;4.
57. Mulcahy LA, Pink RC, Carter DRF. Routes and mechanisms of extracellular vesicle uptake. Journal of extracellular vesicles. 2014;3:10.3402/jev.v3.24641.
58. Mathieu M, Martin-Jaular L, Lavieu G, Théry C. Specificities of secretion and uptake of exosomes and other extracellular vesicles for cell-to-cell communication. Nature Cell Biology. 2019;21(1):9-17.
59. Chivet M, Javalet C, Laulagnier K, Blot B, Hemming FJ, Sadoul R. Exosomes secreted by cortical neurons upon glutamatergic synapse activation specifically interact with neurons. Journal of extracellular vesicles. 2014;3:24722-.
60. Soares AR, Martins-Marques T, Ribeiro-Rodrigues T, Ferreira JV, Catarino S, Pinho MJ, et al. Gap junctional protein Cx43 is involved in the communication between extracellular vesicles and mammalian cells. Scientific Reports. 2015;5(1):13243.
61. Roier S, Zingl FG, Cakar F, Durakovic S, Kohl P, Eichmann TO, et al. A novel mechanism for the biogenesis of outer membrane vesicles in Gram-negative bacteria. Nature Communications. 2016;7(1):10515.
62. Kuehn AJMaMJ. Outer Membrane Vesicles. 2005.
63. Dutta S, Iida K-i, Takade A, Meno Y, Nair GB, Yoshida S-i. Release of Shiga Toxin by Membrane Vesicles in Shigella dysenteriae Serotype 1 Strains and In Vitro Effects of Antimicrobials on Toxin Production and Release. Microbiology and Immunology. 2004;48(12):965-9.
64. Horstman AL, Kuehn MJ. Enterotoxigenic Escherichia coli secretes active heat-labile enterotoxin via outer membrane vesicles. The Journal of biological chemistry. 2000;275(17):12489-96.
65. Kadurugamuwa JL, Beveridge TJ. Bacteriolytic effect of membrane vesicles from Pseudomonas aeruginosa on other bacteria including pathogens: conceptually new antibiotics. Journal of Bacteriology. 1996;178(10):2767-74.
66. Rumbo C, Fernández-Moreira E, Merino M, Poza M, Mendez JA, Soares NC, et al. Horizontal transfer of the OXA-24 carbapenemase gene via outer membrane vesicles: a new mechanism of dissemination of carbapenem resistance genes in Acinetobacter baumannii. Antimicrob Agents Chemother. 2011;55(7):3084-90.
67. Schwechheimer C, Kuehn MJ. Outer-membrane vesicles from Gram-negative bacteria: biogenesis and functions. Nature Reviews Microbiology. 2015;13:605.
68. O'Donoghue EJ, Krachler AM. Mechanisms of outer membrane vesicle entry into host cells. Cellular microbiology. 2016;18(11):1508-17.
69. Berleman J, Auer M. The role of bacterial outer membrane vesicles for intra- and interspecies delivery. Environmental Microbiology. 2013;15(2):347-54.
70. Schertzer JW, Schertzer JW, Whiteley M. Bacterial Outer Membrane Vesicles in Trafficking, Communication and the Host-Pathogen Interaction. Journal of Molecular Microbiology and Biotechnology. 2013;23(1-2):118-30.
71. Evans AGL, Davey HM, Cookson A, Currinn H, Cooke-Fox G, Stanczyk PJ, et al. Predatory activity of Myxococcus xanthus outer-membrane vesicles and properties of their hydrolase cargo. Microbiology. 2012;158(11):2742-52.
72. Keane R, Berleman J. The predatory life cycle of Myxococcus xanthus. Microbiology. 2016;162(1):1-11.

73. Berleman JE, Kirby JR. Deciphering the hunting strategy of a bacterial wolfpack. FEMS Microbiology Reviews. 2009;33(5):942-57.
74. Müller KJWaaR. Myxobacterial secondary metabolites: bioactivities and modes-of-action. Nat Prod Rep. 2010.
75. Berleman J, Allen S, Danielewicz M, Remis J, Gorur A, Cunha J, et al. The Lethal Cargo of Myxococcus xanthus Outer Membrane Vesicles. Frontiers in microbiology. 2014;5:474.
76. li Z, ye X, Liu M, Xia C, Zhang L, Luo X, et al. A novel outer membrane β-1,6-glucanase is deployed in the predation of fungi by myxobacteria. The ISME Journal. 2019;13:1-13.
77. Palsdottir H, Remis JP, Schaudinn C, O'Toole E, Lux R, Shi W, et al. Three-Dimensional Macromolecular Organization of Cryofixed Myxococcus xanthus Biofilms as Revealed by Electron Microscopic Tomography. Journal of Bacteriology. 2009;191(7):2077-82.
78. Pasquali L, Svedbom A, Srivastava A, Rosén E, Lindqvist U, Ståhle M, et al. Circulating microRNAs in extracellular vesicles as potential biomarkers for psoriatic arthritis in patients with psoriasis. Journal of the European Academy of Dermatology and Venereology. 2020;n/a(n/a).
79. Takeuchi T, Mori K, Sunayama H, Takano E, Kitayama Y, Shimizu T, et al. Antibody-Conjugated Signaling Nanocavities Fabricated by Dynamic Molding for Detecting Cancers Using Small Extracellular Vesicle Markers from Tears. Journal of the American Chemical Society. 2020;142(14):6617-24.
80. Mehaffy C, Kruh-Garcia NA, Graham B, Jarlsberg LG, Willyerd CE, Borisov A, et al. Identification of Mycobacterium tuberculosis peptides in serum extracellular vesicles from persons with latent tuberculosis infection. Journal of Clinical Microbiology. 2020:JCM.00393-20.
81. Dissanayake K, Nõmm M, Lättekivi F, Ressaissi Y, Godakumara K, Lavrits A, et al. Individually cultured bovine embryos produce extracellular vesicles that have the potential to be used as non-invasive embryo quality markers. Theriogenology. 2020;149:104-16.
82. Levine L, Habertheuer A, Ram C, Korutla L, Schwartz N, Hu RW, et al. Syncytiotrophoblast extracellular microvesicle profiles in maternal circulation for noninvasive diagnosis of preeclampsia. Scientific Reports. 2020;10(1):6398.
83. Murphy DE, de Jong OG, Brouwer M, Wood MJ, Lavieu G, Schiffelers RM, et al. Extracellular vesicle-based therapeutics: natural versus engineered targeting and trafficking. Experimental & Molecular Medicine. 2019;51(3):1-12.
84. Zhu Y-z, Hu X, Zhang J, Wang Z-h, Wu S, Yi Y-y. Extracellular Vesicles Derived From Human Adipose-Derived Stem Cell Prevent the Formation of Hypertrophic Scar in a Rabbit Model. Annals of Plastic Surgery. 2020;84(5).
85. Giunti D, Marini C, Parodi B, Usai C, Milanese M, Bonanno G, et al. Exosome-shuttled miRNAs contribute to the modulation of the neuroinflammatory microglia phenotype by mesenchymal stem cells. Implication for amyotrophic lateral sclerosis2019.
86. Medalla M, Chang W, Calderazzo SM, Go V, Tsolias A, Goodliffe JW, et al. Treatment with mesenchymal-derived extracellular vesicles reduces injury-related pathology in pyramidal neurons of monkey perilesional ventral premotor cortex EVs reduce injury-related pathology in vPMC. The Journal of Neuroscience. 2020:JN-RM-2226-19.
87. Hu G, Xia Y, Zhang J, Chen Y, Yuan J, Niu X, et al. ESC-sEVs Rejuvenate Senescent Hippocampal NSCs by Activating Lysosomes to Improve Cognitive Dysfunction in Vascular Dementia. Advanced Science. 2020;n/a(n/a):1903330.
88. Timár CI, Lőrincz ÁM, Csépányi-Kömi R, Vályi-Nagy A, Nagy G, Buzás EI, et al. Antibacterial effect of microvesicles released from human neutrophilic granulocytes. Blood. 2013;121(3):510-8.

89. Jiang Z, Liu Y-m, Niu X, Yin J-y, Hu B, Guo S-C, et al. Exosomes secreted by human urine-derived stem cells could prevent kidney complications from type I diabetes in rats. Stem Cell Research & Therapy. 2016;7.
90. Pisano C, Galley J, Elbahrawy M, Wang Y, Farrell A, Brigstock D, et al. Human Breast Milk-Derived Extracellular Vesicles in the Protection Against Experimental Necrotizing Enterocolitis. Journal of Pediatric Surgery. 2020;55(1):54-8.
91. Kadurugamuwa JL, Beveridge TJ. Delivery of the Non-Membrane-Permeative Antibiotic Gentamicin into Mammalian Cells by Using Shigella flexneri Membrane Vesicles. Antimicrob Agents Chemother. 1998;42(6):1476-83.
92. Huang W, Zhang Q, Li W, Yuan M, Zhou J, Hua L, et al. Development of novel nanoantibiotics using an outer membrane vesicle-based drug efflux mechanism. Journal of Controlled Release. 2020;317:1-22.
93. Fuhrmann G, Serio A, Mazo M, Nair R, Stevens MM. Active loading into extracellular vesicles significantly improves the cellular uptake and photodynamic effect of porphyrins. Journal of Controlled Release. 2015;205:35-44.
94. Garofalo M, Saari H, Somersalo P, Crescenti D, Kuryk L, Aksela L, et al. Antitumor effect of oncolytic virus and paclitaxel encapsulated in extracellular vesicles for lung cancer treatment. Journal of Controlled Release. 2018;283:223-34.
95. Pascucci L, Coccè V, Bonomi A, Ami D, Ceccarelli P, Ciusani E, et al. Paclitaxel is incorporated by mesenchymal stromal cells and released in exosomes that inhibit in vitro tumor growth: A new approach for drug delivery. Journal of Controlled Release. 2014;192:262-70.
96. Ye Z, Zhang T, He W, Jin H, Liu C, Yang Z, et al. Methotrexate-Loaded Extracellular Vesicles Functionalized with Therapeutic and Targeted Peptides for the Treatment of Glioblastoma Multiforme. ACS Applied Materials & Interfaces. 2018;10(15):12341-50.
97. Tian Y, Li S, Song J, Ji T, Zhu M, Anderson GJ, et al. A doxorubicin delivery platform using engineered natural membrane vesicle exosomes for targeted tumor therapy. Biomaterials. 2014;35(7):2383-90.
98. Sun D, Zhuang X, Xiang X, Liu Y, Zhang S, Liu C, et al. A Novel Nanoparticle Drug Delivery System: The Anti-inflammatory Activity of Curcumin Is Enhanced When Encapsulated in Exosomes. Molecular Therapy. 2010;18(9):1606-14.
99. Carobolante G, Mantaj J, Ferrari E, Vllasaliu D. Cow Milk and Intestinal Epithelial Cell-Derived Extracellular Vesicles as Systems for Enhancing Oral Drug Delivery. Pharmaceutics. 2020;12(3):226.
100. Yang X, Shi G, Guo J, Wang C, He Y. Exosome-encapsulated antibiotic against intracellular infections of methicillin-resistant Staphylococcus aureus. International journal of nanomedicine. 2018;13:8095-104.
101. Haney MJ, Klyachko NL, Zhao Y, Gupta R, Plotnikova EG, He Z, et al. Exosomes as drug delivery vehicles for Parkinson's disease therapy. Journal of Controlled Release. 2015;207:18-30.
102. Altanerova U, Babincova M, Babinec P, Benejova K, Jakubechova J, Altanerova V, et al. Human mesenchymal stem cell-derived iron oxide exosomes allow targeted ablation of tumor cells via magnetic hyperthermia. International journal of nanomedicine. 2017;12:7923-36.
103. Wang Y YJ, Cai L, Liu T, Wang X, Zhang Y, Zhou Z, Li T, Liu M, Lai R, Xiangning Liu. Bone-targeted extracellular vesicles from mesenchymal stem cells for osteoporosis therapy. Journal of nanobiotechnology. 2020.
104. Yang X, Xie B, Peng H, Shi G, Sreenivas B, Guo J, et al. Eradicating intracellular MRSA via targeted delivery of lysostaphin and vancomycin with mannose-modified exosomes. J Control Release. 2020;329:454-67.
105. Kooijmans SAA, Fliervoet LAL, van der Meel R, Fens M, Heijnen HFG, van Bergen En Henegouwen PMP, et al. PEGylated and targeted extracellular vesicles display enhanced cell specificity and circulation time. J Control Release. 2016;224:77-85.

106. Lener T, Gimona M, Aigner L, Börger V, Buzas E, Camussi G, et al. Applying extracellular vesicles based therapeutics in clinical trials – an ISEV position paper. Journal of Extracellular Vesicles. 2015;4:10.3402/jev.v4.30087.
107. Alam NH, Ashraf H. Treatment of Infectious Diarrhea in Children. Pediatric Drugs. 2003;5(3):151-65.
108. Hamer DH, Gill CJ, Chilengi R. Intestinal Infections: Overview. In: Quah SR, editor. International Encyclopedia of Public Health (Second Edition). Oxford: Academic Press; 2017. p. 322-35.
109. Cohen D, Muhsen K. Vaccines for enteric diseases. Human Vaccines & Immunotherapeutics. 2019;15(6):1205-14.
110. Kotloff KL, Blackwelder WC, Nasrin D, Nataro JP, Farag TH, van Eijk A, et al. The Global Enteric Multicenter Study (GEMS) of diarrheal disease in infants and young children in developing countries: epidemiologic and clinical methods of the case/control study. Clinical infectious diseases : an official publication of the Infectious Diseases Society of America. 2012;55 Suppl 4(Suppl 4):S232-S45.
111. Liu J, Platts-Mills JA, Juma J, Kabir F, Nkeze J, Okoi C, et al. Use of quantitative molecular diagnostic methods to identify causes of diarrhoea in children: a reanalysis of the GEMS case-control study. The Lancet. 2016;388(10051):1291-301.
112. Mani S, Wierzba T, Walker RI. Status of vaccine research and development for Shigella. Vaccine. 2016;34(26):2887-94.
113. Kim YJ, Park KH, Park DA, Park J, Bang BW, Lee SS, et al. Guideline for the Antibiotic Use in Acute Gastroenteritis. Infection & chemotherapy. 2019;51(2):217-43.
114. Doron S, Snydman DR. Risk and safety of probiotics. Clinical infectious diseases : an official publication of the Infectious Diseases Society of America. 2015;60 Suppl 2(Suppl 2):S129-S34.
115. Guandalini S. Probiotics for Prevention and Treatment of Diarrhea. Journal of Clinical Gastroenterology. 2011;45:S149-S53.
116. DuPont HL, Levine MM, Hornick RB, Formal SB. Inoculum Size in Shigellosis and Implications for Expected Mode of Transmission. The Journal of Infectious Diseases. 1989;159(6):1126-8.
117. Kotloff KL, Riddle MS, Platts-Mills JA, Pavlinac P, Zaidi AKM. Shigellosis. The Lancet. 2018;391(10122):801-12.
118. Philpott D, Edgeworth J, Sansonetti P. The pathogenesis of Shigella flexneri infection: Lessons from in vitro and in vivo studies. Philosophical transactions of the Royal Society of London Series B, Biological sciences. 2000;355:575-86.
119. Dekker JP, Frank KM. Salmonella, Shigella, and yersinia. Clinics in laboratory medicine. 2015;35(2):225-46.
120. Small P, Blankenhorn D, Welty D, Zinser E, Slonczewski JL. Acid and base resistance in Escherichia coli and Shigella flexneri: role of rpoS and growth pH. Journal of bacteriology. 1994;176(6):1729-37.
121. Nikfar R, Shamsizadeh A, Darbor M, Khaghani S, Moghaddam M. A Study of prevalence of Shigella species and antimicrobial resistance patterns in paediatric medical center, Ahvaz, Iran. Iranian journal of microbiology. 2017;9(5):277-83.
122. Ashida H, Mimuro H, Sasakawa C. Shigella manipulates host immune responses by delivering effector proteins with specific roles. Frontiers in immunology. 2015;6:219-.
123. Mattock E, Blocker AJ. How Do the Virulence Factors of Shigella Work Together to Cause Disease? Frontiers in Cellular and Infection Microbiology. 2017;7(64).
124. High N, Mounier J, Prévost MC, Sansonetti PJ. IpaB of Shigella flexneri causes entry into epithelial cells and escape from the phagocytic vacuole. The EMBO journal. 1992;11(5):1991-9.

125. Southwick FS, Purich DL. Listeria and Shigella actin-based motility in host cells. Transactions of the American Clinical and Climatological Association. 1998;109:160-73.
126. Raqib R, Mia SMS, Qadri F, Alam TI, Alam NH, Chowdhury AK, et al. Innate Immune Responses in Children and Adults with Shigellosis. Infection and Immunity. 2000;68(6):3620-9.
127. Jennison AV, Verma NK. Shigella flexneri infection: pathogenesis and vaccine development. FEMS Microbiology Reviews. 2004;28(1):43-58.
128. Stefan Hagel H-JE, Gerhard E. Feurle, Winfried V. Kern, Petra Lynen Jansen, Peter Malfertheiner, Thomas Marth, Elisabeth Meyer, Martin Mielke,Verena Moos, Lutz von Müller, Jacob Nattermann, Monika Nothacker, Christian Pox, Emil Reisinger, Bernd Salzberger, Helmut J. F. Salzer, Marko Weber, Thomas Weinke, Sebastian Suerbaum, Ansgar W. Lohse, Andreas Stallmach, Tilo Andus, Christoph Berg, Hendrik Bläker, Rainer Duchmann, Stefan Ebensberger, Torsten Feldt, Antje Flieger, Thomas Frieling, Walter Heise, Marina Höhne, Daniel Jaspersen, André Jefremow, Björn Jensen, Irmtraut Koop, Bernhard Lembcke, Christoph Loddenkemper, Christoph Lübbert, Harald Matthes, Markus Menges, Joachim Richter, Christoph Spinner, Hinrich Sudeck, Roger Vogelmann, Peter Walger. S2k-Leitlinie Gastrointestinale Infektionen und Morbus Whipple. Arbeitsgemeinschaft der Wissenschaftlichen Medizinischen Fachgesellschaften eV. 2015.
129. Gu B, Cao Y, Pan S, Zhuang L, Yu R, Peng Z, et al. Comparison of the prevalence and changing resistance to nalidixic acid and ciprofloxacin of Shigella between Europe–America and Asia–Africa from 1998 to 2009. International Journal of Antimicrobial Agents. 2012;40(1):9-17.
130. Azmi IJ, Khajanchi BK, Akter F, Hasan TN, Shahnaij M, Akter M, et al. Fluoroquinolone Resistance Mechanisms of Shigella flexneri Isolated in Bangladesh. PLoS One. 2014;9(7):e102533.
131. Bardsley M, Jenkins C, Mitchell HD, Mikhail AFW, Baker KS, Foster K, et al. Persistent Transmission of Shigellosis in England Is Associated with a Recently Emerged Multidrug-Resistant Strain of <span class="named-content genus-species" id="named-content-1">Shigella sonnei</span&gt. Journal of Clinical Microbiology. 2020;58(4):e01692-19.
132. Phoebe Williams JAB. Dysentery (Shigellosis) current WHO guidelines and the WHO essential medicine list for children. 2016.
133. Camacho AI, Irache JM, de Souza J, Sánchez-Gómez S, Gamazo C. Nanoparticle-based vaccine for mucosal protection against Shigella flexneri in mice. Vaccine. 2013;31(32):3288-94.
134. Mukherjee R, Dutta D, Patra M, Chatterjee B, Basu T. Nanonized tetracycline cures deadly diarrheal disease ‘shigellosis’ in mice, caused by multidrug-resistant Shigella flexneri 2a bacterial infection. Nanomedicine: Nanotechnology, Biology and Medicine. 2019;18:402-13.
135. Susewind J, de Souza Carvalho-Wodarz C, Repnik U, Collnot E-M, Schneider-Daum N, Griffiths GW, et al. A 3D co-culture of three human cell lines to model the inflamed intestinal mucosa for safety testing of nanomaterials. Nanotoxicology. 2016;10(1):53-62.
136. Leonard F, Collnot E-M, Lehr C-M. A Three-Dimensional Coculture of Enterocytes, Monocytes and Dendritic Cells To Model Inflamed Intestinal Mucosa in Vitro. Molecular Pharmaceutics. 2010;7(6):2103-19.
137. Bouwmeester H, Poortman J, Peters RJ, Wijma E, Kramer E, Makama S, et al. Characterization of Translocation of Silver Nanoparticles and Effects on Whole-Genome Gene Expression Using an In Vitro Intestinal Epithelium Coculture Model. ACS Nano. 2011;5(5):4091-103.

138. Alzheimer M, Svensson SL, König F, Schweinlin M, Metzger M, Walles H, et al. A three-dimensional intestinal tissue model reveals factors and small regulatory RNAs important for colonization with Campylobacter jejuni. PLOS Pathogens. 2020;16(2):e1008304.
139. Lindén SK, Driessen KM, McGuckin MA. Improved In vitro Model Systems for Gastrointestinal Infection by Choice of Cell Line, pH, Microaerobic Conditions, and Optimization of Culture Conditions. Helicobacter. 2007;12(4):341-53.
140. Hua S. Orally administered liposomal formulations for colon targeted drug delivery. Frontiers in Pharmacology. 2014;5(138).
141. Lundquist P, Artursson P. Oral absorption of peptides and nanoparticles across the human intestine: Opportunities, limitations and studies in human tissues. Advanced Drug Delivery Reviews. 2016;106:256-76.
142. Thamphiwatana S, Fu V, Zhu J, Lu D, Gao W, Zhang L. Nanoparticle-stabilized liposomes for pH-responsive gastric drug delivery. Langmuir : the ACS journal of surfaces and colloids. 2013;29(39):12228-33.
143. Huck BC, Hartwig O, Biehl A, Schwarzkopf K, Wagner C, Loretz B, et al. Macro- and Microrheological Properties of Mucus Surrogates in Comparison to Native Intestinal and Pulmonary Mucus. Biomacromolecules. 2019;20(9):3504-12.
144. Maisel K, Ensign L, Reddy M, Cone R, Hanes J. Effect of surface chemistry on nanoparticle interaction with gastrointestinal mucus and distribution in the gastrointestinal tract following oral and rectal administration in the mouse. Journal of controlled release : official journal of the Controlled Release Society. 2015;197:48-57.
145. Bellmann S, David C, Fasano A, Momcilovic D, Scimeca J, Waldman W, et al. Mammalian gastrointestinal tract parameters modulating the integrity, surface properties, and absorption of food-relevant nanomaterials. Wiley Interdisciplinary Reviews: Nanomedicine and Nanobiotechnology. 2015;7.
146. Hasani S, Pellequer Y, Lamprecht A. Selective Adhesion of Nanoparticles to Inflamed Tissue in Gastric Ulcers. Pharmaceutical Research. 2009;26(5):1149-54.
147. Maruyama K. Intracellular targeting delivery of liposomal drugs to solid tumors based on EPR effects. Advanced Drug Delivery Reviews. 2011;63(3):161-9.
148. Leonard F, Ali, H., Collnot, E.-M., Crielaard, B., Lammers, T., Storm, G. and Lehr, C.-M. Screening of budesonide nanoformulations for treatment of inflammatory bowel disease in an inflamed 3D cell-culture model. ALTEX - Alternatives to animal experimentation. 2012;29 (3):275-85.
149. Laroui H, Wilson DS, Dalmasso G, Salaita K, Murthy N, Sitaraman SV, et al. Nanomedicine in GI. American journal of physiology Gastrointestinal and liver physiology. 2011;300(3):G371-G83.
150. Rubio APD, Martínez J, Palavecino M, Fuentes F, López CMS, Marcilla A, et al. Transcytosis of Bacillus subtilis extracellular vesicles through an in vitro intestinal epithelial cell model. Scientific Reports. 2020;10(1):3120.
151. Ren G, Hu D, Cheng EWC, Vargas-Reus MA, Reip P, Allaker RP. Characterisation of copper oxide nanoparticles for antimicrobial applications. International Journal of Antimicrobial Agents. 2009;33(6):587-90.
152. Trucillo P, Ferrari PF, Campardelli R, Reverchon E, Perego P. A Supercritical Assisted Process for the Production of Amoxicillin Loaded Liposomes for Anti-microbial Applications. The Journal of Supercritical Fluids. 2020:104842.
153. Behera S, Patra JK, Pramanik K, Panda N, Thatoi H. Characterization and Evaluation of Antibacterial Activities of Chemically Synthesized Iron Oxide Nanoparticles. World Journal of Nano Science and Engineering. 2012;2:196-200.
154. Nnamani P, Ugwu A, Ibezim E, Onoja S, Odo A, Windbergs M, et al. Preparation, characterisation and in vitro antibacterial property of ciprofloxacin-loaded nanostructured lipid carrier for treatment of Bacillus subtilis infection. Journal of Microencapsulation. 2019;36(1):32-42.

155. Menina S, Eisenbeis J, Kamal MAM, Koch M, Bischoff M, Gordon S, et al. Bioinspired Liposomes for Oral Delivery of Colistin to Combat Intracellular Infections by Salmonella enterica. Advanced Healthcare Materials.0(0):1900564.
156. Webb MS, Boman NL, Wiseman DJ, Saxon D, Sutton K, Wong KF, et al. Antibacterial Efficacy against an In Vivo Salmonella typhimurium Infection Model and Pharmacokinetics of a Liposomal Ciprofloxacin Formulation. Antimicrob Agents Chemother. 1998;42(1):45-52.
157. Desiderio JV, Campbell SG. Intraphagocytic Killing of Salmonella typhimurium by Liposome-Encapsulated Cephalothin. The Journal of Infectious Diseases. 1983;148(3):563-70.
158. Lutwyche P, Cordeiro C, Wiseman DJ, St-Louis M, Uh M, Hope MJ, et al. Intracellular Delivery and Antibacterial Activity of Gentamicin Encapsulated in pH-Sensitive Liposomes. Antimicrob Agents Chemother. 1998;42(10):2511.
159. Seong M, Lee DG. Silver Nanoparticles Against Salmonella enterica Serotype Typhimurium: Role of Inner Membrane Dysfunction. Current Microbiology. 2017;74(6):661-70.
160. Luo M, Jia Y-Y, Jing Z-W, Li C, Zhou S-Y, Mei Q-B, et al. Construction and optimization of pH-sensitive nanoparticle delivery system containing PLGA and UCCs-2 for targeted treatment of Helicobacter pylori. Colloids and Surfaces B: Biointerfaces. 2018;164:11-9.
161. Thamphiwatana S, Gao W, Obonyo M, Zhang L. In vivo treatment of Helicobacter pylori infection with liposomal linolenic acid reduces colonization and ameliorates inflammation. Proceedings of the National Academy of Sciences. 2014;111(49):17600.
162. Angsantikul P, Thamphiwatana S, Zhang Q, Spiekermann K, Zhuang J, Fang RH, et al. Coating nanoparticles with gastric epithelial cell membrane for targeted antibiotic delivery against Helicobacter pylori infection. Advanced therapeutics. 2018;1(2):1800016.
163. li C, Zhang Y, Su T, Feng L, Long Y, Chen Z. Silica-coated flexible liposomes as a nanohybrid delivery system for enhanced oral bioavailability of curcumin. International journal of nanomedicine. 2012;7:5995-6002.
164. Taipaleenmäki E, Christensen G, Brodszkij E, Mouritzen SA, Gal N, Madsen S, et al. Mucopenetrating polymer – Lipid hybrid nanovesicles as subunits in alginate beads as an oral formulation. Journal of Controlled Release. 2020.
165. Pati R, Shevtsov M, Sonawane A. Nanoparticle Vaccines Against Infectious Diseases. Frontiers in immunology. 2018;9:2224-.
166. Lasic DD. Novel applications of liposomes. Trends in Biotechnology. 1998;16(7):307-21.
167. Haider Hussain N, Shahlaa MS, Abdulwahid BA-S. Protective Humoral Immunity Induced by Lipopolysaccharide Incorporated Liposome in Mice Against Shigella flexneri Infection. Al-Nahrain Journal of Science. 2018;16(3).
168. Desiderio JV, Campbell SG. Immunization against experimental murine salmonellosis with liposome-associated O-antigen. Infection and Immunity. 1985;48(3):658.
169. Zhao W, Wu W, Xu X. Oral vaccination with liposome-encapsulated recombinant fusion peptide of urease B epitope and cholera toxin B subunit affords prophylactic and therapeutic effects against H. pylori infection in BALB/c mice. Vaccine. 2007;25(44):7664-73.
170. Lieschke GJ, Currie PD. Animal models of human disease: zebrafish swim into view. Nature Reviews Genetics. 2007;8(5):353-67.
171. Amsterdam A, Hopkins N. Mutagenesis strategies in zebrafish for identifying genes involved in development and disease. Trends in genetics : TIG. 2006;22:473-8.
172. Consortium TGR. [Available from: https://www.ncbi.nlm.nih.gov/grc.

173. Gomes MC, Mostowy S. The Case for Modeling Human Infection in Zebrafish. Trends in Microbiology. 2019.
174. Kimmel CB, Ballard WW, Kimmel SR, Ullmann B, Schilling TF. Stages of embryonic development of the zebrafish. Dev Dyn. 1995;203(3):253-310.
175. Goldsmith J, Jobin C. Think Small: Zebrafish as a Model System of Human Pathology. Journal of biomedicine & biotechnology. 2012;2012:817341.
176. Novoa B, Figueras A. Zebrafish: Model for the Study of Inflammation and the Innate Immune Response to Infectious Diseases. In: Lambris JD, Hajishengallis G, editors. Current Topics in Innate Immunity II. New York, NY: Springer New York; 2012. p. 253-75.
177. Sullivan C, Kim CH. Zebrafish as a model for infectious disease and immune function. Fish & Shellfish Immunology. 2008;25(4):341-50.
178. Herbomel P, Thisse B, Thisse C. Ontogeny and behaviour of early macrophages in the zebrafish embryo. Development. 1999;126(17):3735.
179. Clatworthy AE, Lee JS-W, Leibman M, Kostun Z, Davidson AJ, Hung DT. Pseudomonas aeruginosa infection of zebrafish involves both host and pathogen determinants. Infection and immunity. 2009;77(4):1293-303.
180. Prajsnar TK, Cunliffe VT, Foster SJ, Renshaw SA. A novel vertebrate model of Staphylococcus aureus infection reveals phagocyte-dependent resistance of zebrafish to non-host specialized pathogens. Cellular Microbiology. 2008;10(11):2312-25.
181. Boldock E, Surewaard BGJ, Shamarina D, Na M, Fei Y, Ali A, et al. Human skin commensals augment Staphylococcus aureus pathogenesis. Nature Microbiology. 2018;3(8):881-90.
182. Duggan GM, Mostowy S. Use of zebrafish to study Shigella infection. 2018;11(2):dmm032151.
183. Mazon-Moya MJ, Willis AR, Torraca V, Boucontet L, Shenoy AR, Colucci-Guyon E, et al. Septins restrict inflammation and protect zebrafish larvae from Shigella infection. PLoS pathogens. 2017;13(6):e1006467-e.
184. Willis AR, Moore C, Mazon-Moya M, Krokowski S, Lambert C, Till R, et al. Injections of Predatory Bacteria Work Alongside Host Immune Cells to Treat Shigella Infection in Zebrafish Larvae. Current biology : CB. 2016;26(24):3343-51.
185. Sieber S, Grossen P, Detampel P, Siegfried S, Witzigmann D, Huwyler J. Zebrafish as an early stage screening tool to study the systemic circulation of nanoparticulate drug delivery systems in vivo. Journal of Controlled Release. 2017;264:180-91.
186. van Pomeren M, Brun NR, Peijnenburg WJGM, Vijver MG. Exploring uptake and biodistribution of polystyrene (nano)particles in zebrafish embryos at different developmental stages. Aquatic Toxicology. 2017;190:40-5.
187. Miao X, Li Y, Wang X, Lee SM-Y, Zheng Y. Transport Mechanism of Coumarin 6 Nanocrystals with Two Particle Sizes in MDCKII Monolayer and Larval Zebrafish. ACS Applied Materials & Interfaces. 2016;8(20):12620-30.
188. Lu Y, Zhang Y, Deng Y, Jiang W, Zhao Y, Geng J, et al. Uptake and Accumulation of Polystyrene Microplastics in Zebrafish (Danio rerio) and Toxic Effects in Liver. Environmental Science & Technology. 2016;50(7):4054-60.
189. Fenaroli F, Westmoreland D, Benjaminsen J, Kolstad T, Skjeldal FM, Meijer AH, et al. Nanoparticles as Drug Delivery System against Tuberculosis in Zebrafish Embryos: Direct Visualization and Treatment. ACS Nano. 2014;8(7):7014-26.
190. Ulanova LS, Pinheiro M, Vibe C, Nunes C, Misaghian D, Wilson S, et al. Treatment of Francisella infections via PLGA- and lipid-based nanoparticle delivery of antibiotics in a zebrafish model. Diseases of Aquatic Organisms. 2017;125(1):19-29.
191. Zhang X, Song J, Klymov A, Zhang Y, de Boer L, Jansen JA, et al. Monitoring local delivery of vancomycin from gelatin nanospheres in zebrafish larvae. International journal of nanomedicine. 2018;13:5377-94.

192. Lotha R, Sundaramoorthy NS, Shamprasad BR, Nagarajan S, Sivasubramanian A. Plant nutraceuticals (Quercetrin and Afzelin) capped silver nanoparticles exert potent antibiofilm effect against food borne pathogen Salmonella enterica serovar Typhi and curtail planktonic growth in zebrafish infection model. Microbial Pathogenesis. 2018;120:109-18.
193. Bowman CR, Bailey FC, Elrod-Erickson M, Neigh AM, Otter RR. Effects of silver nanoparticles on zebrafish (Danio rerio) and Escherichia coli (ATCC 25922): A comparison of toxicity based on total surface area versus mass concentration of particles in a model eukaryotic and prokaryotic system. Environmental Toxicology and Chemistry. 2012;31(8):1793-800.
194. Batalha IL, Bernut A, Schiebler M, Ouberai MM, Passemar C, Klapholz C, et al. Polymeric nanobiotics as a novel treatment for mycobacterial infections. Journal of Controlled Release. 2019;314:116-24.
195. Mary B, Ghoroghi S, Hyenne V, Goetz JG. Live tracking of extracellular vesicles in larval zebrafish. Methods in Enzymology: Academic Press; 2020.
196. Scott A, Ballesteros LS, Bradshaw M, Power A, Lorriman J, Love J, et al. In vivo characterisation of endogenous cardiovascular extracellular vesicles in larval and adult zebrafish. bioRxiv. 2020:742692.
197. Kobayashi-Sun J, Yamamori S, Kondo M, Kuroda J, Ikegame M, Suzuki N, et al. Uptake of osteoblast-derived extracellular vesicles promotes the differentiation of osteoclasts in the zebrafish scale. Communications Biology. 2020;3(1):190.
198. Matsuda A, Moirangthem A, Angom RS, Ishiguro K, Driscoll J, Yan IK, et al. Safety of bovine milk derived extracellular vesicles used for delivery of RNA therapeutics in zebrafish and mice. Journal of Applied Toxicology. 2020;40(5):706-18.
199. Vader P, Mol EA, Pasterkamp G, Schiffelers RM. Extracellular vesicles for drug delivery. Advanced Drug Delivery Reviews. 2016;106:148-56.
200. van der Meel R, Fens MHAM, Vader P, van Solinge WW, Eniola-Adefeso O, Schiffelers RM. Extracellular vesicles as drug delivery systems: Lessons from the liposome field. Journal of Controlled Release. 2014;195:72-85.
201. Lehrich BM, Liang Y, Fiandaca MS. Foetal bovine serum influence on in vitro extracellular vesicle analyses. Journal of Extracellular Vesicles. 2021;10(3):e12061.
202. Salouti M, Ahangari A. Nanoparticle based Drug Delivery Systems for Treatment of Infectious Diseases. In: Sezer AD, editor. Application of Nanotechnology in Drug Delivery. Rijeka: InTech; 2014. p. Ch. 05.
203. Nguyen TL, Nguyen TH, Nguyen DH. Development and In Vitro Evaluation of Liposomes Using Soy Lecithin to Encapsulate Paclitaxel. International Journal of Biomaterials. 2017;2017:8234712.
204. He C, Hu Y, Yin L, Tang C, Yin C. Effects of particle size and surface charge on cellular uptake and biodistribution of polymeric nanoparticles. Biomaterials. 2010;31(13):3657-66.
205. Witwer KW, Buzás EI, Bemis LT, Bora A, Lässer C, Lötvall J, et al. Standardization of sample collection, isolation and analysis methods in extracellular vesicle research. 2013. 2013.
206. Gimona M, Pachler K, Laner-Plamberger S, Schallmoser K, Rohde E. Manufacturing of Human Extracellular Vesicle-Based Therapeutics for Clinical Use. International Journal of Molecular Sciences. 2017;18(6):1190.
207. Frank J, Richter M, de Rossi C, Lehr C-M, Fuhrmann K, Fuhrmann G. Extracellular vesicles protect glucuronidase model enzymes during freeze-drying. Scientific Reports. 2018;8(1):12377.
208. Williams DF. On the mechanisms of biocompatibility. Biomaterials. 2008;29(20):2941-53.
209. McCullough KZ. Endotoxins. American Pharmaceutical Review. 2017.

210. Kleiveland CR. Peripheral Blood Mononuclear Cells. In: Verhoeckx K, Cotter P, López-Expósito I, Kleiveland C, Lea T, Mackie A, et al., editors. The Impact of Food Bioactives on Health: in vitro and ex vivo models. Cham: Springer International Publishing; 2015. p. 161-7.
211. Ozato K, Tsujimura H, Tamura T. Toll-like receptor signaling and regulation of cytokine gene expression in the immune system. Biotechniques. 2002;Suppl:66-8, 70, 2 passim.
212. Couvreur P, Fattal E, Andremont A. Liposomes and Nanoparticles in the Treatment of Intracellular Bacterial Infections. Pharmaceutical Research. 1991;8(9):1079-86.
213. Baumann S, Herrmann J, Raju R, Steinmetz H, Mohr KI, Hüttel S, et al. Cystobactamids: Myxobacterial Topoisomerase Inhibitors Exhibiting Potent Antibacterial Activity. Angewandte Chemie International Edition. 2014;53(52):14605-9.
214. Berleman JE, Allen S, Danielewicz MA, Remis JP, Gorur A, Cunha J, et al. The lethal cargo of Myxococcus xanthus outer membrane vesicles. Frontiers in Microbiology. 2014;5(474).
215. Mostowy S, Boucontet L, Mazon Moya MJ, Sirianni A, Boudinot P, Hollinshead M, et al. The Zebrafish as a New Model for the In Vivo Study of Shigella flexneri Interaction with Phagocytes and Bacterial Autophagy. PLOS Pathogens. 2013;9(9):e1003588.
216. Del Porto P, Cifani N, Guarnieri S, Di Domenico EG, Mariggiò MA, Spadaro F, et al. Dysfunctional CFTR alters the bactericidal activity of human macrophages against Pseudomonas aeruginosa. PLoS One. 2011;6(5):e19970-e.
217. Weiss G, Schaible UE. Macrophage defense mechanisms against intracellular bacteria. Immunol Rev. 2015;264(1):182-203.
218. Ho D-K, Frisch S, Biehl A, Terriac E, De Rossi C, Schwarzkopf K, et al. Farnesylated Glycol Chitosan as a Platform for Drug Delivery: Synthesis, Characterization, and Investigation of Mucus–Particle Interactions. Biomacromolecules. 2018;19(8):3489-501.
219. Stewart PS, William Costerton J. Antibiotic resistance of bacteria in biofilms. The Lancet. 2001;358(9276):135-8.
220. K. Koenig 1 aHS, 3. Laser-Induced Autofluorescence for Medical Diagnosis. Journal of Fluorescence. 1994;Vol. 4.

6. List of publications, oral and poster presentations

Articles published in international peer-reviewed journals

Schulz E, Goes A, Garcia R, Panter F, Koch M, Müller R, Fuhrmann K, Fuhrmann G. Biocompatible bacteria-derived vesicles show inherent antimicrobial activity. Journal of Controlled Release. 2018;290:46-55

Schulz E, Karagianni A, Koch M, Fuhrmann G. Hot EVs – How temperature affects extracellular vesicles. European Journal of Pharmaceutics and Biopharmaceutics. 2020;146:55-63.

Goes A, Lapuhs P, Kuhn T, **Schulz E**, Richter R, Panter F, Dahlem C, Garica R, Kiemer AK, Müller R, Fuhrmann G. Myxobacteria-Derived Outer Membrane Vesicles: Potential Applicability Against Intracellular Infections. Cells. 2020;9(220):194.

Manuscripts under preparation

Heinrich E, Hartwig O, Walt C, Koch M, Kiemer A.K, Loretz B, Lehr CM, Müller R, Fuhrmann G. A biocompatible carrier system against GI infections: Ciprofloxacin loaded Extracellular Vesicles inhibit the growth of *Shigella flexneri*

Trenkenschuh E, Richter M, **Heinrich E**, Koch M, Fuhrmann G, Friess W. Formulation development of lyophilized extracellular vesicles with long-term stability. Submitted to Advanced Healthcare Materials.

Oral and poster presentations

Talk at 12th International Symposium on Biological Barriers 2018, Saarbrücken

Talk at Controlled Release Society - Local Chapter Germany 2019, Leipzig

(*Award for the best presentation*)

Talk at Controlled Release Society - Oral Focus Group, 2020, virtual

(*Award for second best presentation*)

Talk at Controlled Release Society Annual Meeting & Exposition, 2020, virtual

Poster presentation at HIPS Symposium, 2018, Saarbrücken

Poster presentation, at Doktorandentag der Universität des Saarlandes, 2018, Saarbrücken

7. Scientific Output

7.1. Biocompatible bacteria-derived vesicles show inherent antimicrobial activity

Eilien Schulz, Adriely Goes, Ronald Garcia, Fabian Panter, Marcus Koch, Rolf Müller, Kathrin Fuhrmann, Gregor Fuhrmann

Journal of Controlled Release. 2018, 290, 46-55

DOI: 10.1016/j.jconrel.2018.09.030

Journal of Controlled Release 290 (2018) 46–55

Contents lists available at ScienceDirect

Journal of Controlled Release

journal homepage: www.elsevier.com/locate/jconrel

Special issue contribution ESCDD 2018

Biocompatible bacteria-derived vesicles show inherent antimicrobial activity

Eilien Schulz[1,2], Adriely Goes[1,2], Ronald Garcia[3,4], Fabian Panter[3], Marcus Koch[5], Rolf Müller[2,3,4], Kathrin Fuhrmann[1] and Gregor Fuhrmann[1,2]*

[1]Helmholtz Institute for Pharmaceutical Research Saarland (HIPS), Helmholtz Centre for Infection Research (HZI), Biogenic Nanotherapeutics group (BION), Campus E8.1, 66123 Saarbrücken

[2]Department of Pharmacy, Saarland University, Campus E8.1, 66123 Saarbrücken, Germany

[3]Helmholtz Institute for Pharmaceutical Research Saarland (HIPS), Helmholtz Centre for Infection Research (HZI), Department of Microbial Natural Products (MINS), Campus E8.1, 66123 Saarbrücken

[4]German Center for Infection Research (DZIF), Partner site Hannover-Braunschweig 38124, Germany

[5]INM – Leibniz Institute for New Materials, Campus D2 2, 66123, Saarbrücken, Germany

***Corresponding author**, phone: +49 68198806 1500, email: gregor.fuhrmann@helmholtz-hzi.de

ORCID IDs: Eilien Schulz: 0000-0002-9769-8980, Adriely Goes: 0000-0003-2629-6068; Fabian Panter: 0000-0002-1783-6803; Rolf Müller: 0000-0002-1042-5665; Kathrin Fuhrmann: 0000-0002-5599-9718; Gregor Fuhrmann: 0000-0002-6688-5126

Keywords: outer membrane vesicles; extracellular vesicles; biogenic drug carriers; nanoantibiotics; myxobacteria; electron cryomicroscopy

Abstract

Up to 25,000 people die each year from resistant infections in Europe alone, with increasing incidence. It is estimated that a continued rise in bacterial resistance by 2050 would lead up to 10 million annual deaths worldwide, exceeding the incidence of cancer deaths. Although the design of new antibiotics is still one way to tackle the problem, pharmaceutical companies investigate far less into new drugs than 30 years ago. Incorporation of antibiotics into nanoparticle drug carriers ("nanoantibiotics") is currently investigated as a promising strategy to make existing antibiotics regain antimicrobial strength and overcome certain types of microbial drug resistance. Many of these synthetic systems enhance the antimicrobial effect of drugs by protecting antibiotics from degradation and reducing their side effects. Nevertheless, they often cannot selectively target pathogenic bacteria and – due to their synthetic origin – may induce side-effects themselves.

In this work, we present the characterisation of naturally derived outer membrane vesicles (OMVs) as biocompatible and inherently antibiotic drug carriers. We isolated OMVs from two representative strains of myxobacteria, *Cystobacter velatus* Cbv34 and Sorangiineae species strain SBSr073, a bacterial order with the ability of lysing other bacterial strains and currently investigated as sources of new secondary metabolites. We investigated the myxobacterias' inherent antibacterial properties after isolation by differential centrifugation and purification by size-exclusion chromatography. OMVs have an average size range of 145-194 nm. We characterised their morphology by electron cryomicroscopy and found that OMVs are biocompatible with epithelial cells and differentiated macrophages. They showed a low endotoxin activity comparable to those of control samples, indicating a low acute inflammatory potential. In addition, OMVs showed inherent stability under different storage conditions, including 4 °C, -20 °C, -80 °C and freeze-drying. OMV uptake in Gram-negative model bacterium *Escherichia coli* (*E. coli*) showed similar to better incorporation than liposome controls, indicating the OMVs may interact with model bacteria *via* membrane fusion. Bacterial uptake correlated with antimicrobial activity of OMVs as measured by growth inhibition of *E. coli.* OMVs from Cbv34 inhibited growth of *E. coli* to a comparable extent as the clinically established antibiotic gentamicin. Liquid-chromatography coupled mass spectrometry analyses revealed the presence of cystobactamids in OMVs, inhibitors of bacterial topoisomerase currently studied to treat different Gram-negative and Gram-positive pathogens. This work, may serve as an important basis for further evaluation of OMVs derived from myxobacteria as novel therapeutic delivery systems against bacterial infections.

Introduction

Over the last decades bacterial resistance to antibiotics is rapidly rising, largely as a result of their wide availability, overuse and misuse [1]. As a result, antibiotic-resistant bacteria that are difficult to treat such as methicillin-resistant *Staphylococcus aureus* (*S. aureus*) [2] become highly common and are causing a serious global health problem [3]. In Europe alone up to 25,000 patients die each year as a result of those infections which is costing the European Union €1.5 billion annually [2]; and these numbers are seriously on the rise. One way of addressing the challenging question of how to deal with drug-resistant bacteria is still the discovery of novel antibiotic compounds [4]. However due to the risk of spontaneous resistance development, pharmaceutical companies investigate far less into the cost-intensive development process for new antibiotics than 30 years ago [1, 3]. Another viable strategy to bypass bacterial resistance is to encapsulate known antibiotics into nanoparticulate drug delivery systems ("nanoantibiotics") [5, 6]. Nanoparticles are among the promising avenues to improve drug transport to the site of infection [7, 8]. Loading of antibiotics polymyxin B and ampicillin into liposomes was shown to significantly increase the antibiotic activity, even against difficult pathogens such as *P. aeruginosa* and *S. aureus* [9]. Moreover, encapsulation into nanoparticles can reduce adverse side-effects such as acute kidney injury induced by aminoglycosides [10, 11]. However, the ability of certain nanoantibiotics to exclusively target pathogenic bacteria leaving commensal bacteria of the natural microflora unaffected is often suboptimal [9] and they may potentially induce immunogenicity due to their synthetic origin [9, 10], both problems manifest upon repeated administration which is necessary during long-term antibiotic therapy. Biogenic approaches, such as cell-derived vesicles [12], are found in nature or based on natural processes and they represent a promising alternative to artificial systems as they can potentially bypass immune activation and are inherently biocompatible [13, 14]. Such avenues offer a unique opportunity to learn from their physiological role and tissue interaction paving the way to develop new bioinspired drug carriers [15].

Extracellular vesicles (EVs) are small phospholipid based nanoparticles decorated with membrane and surface proteins and they are thought to be involved in cell-to-cell transfer of information [16, 17]. EVs are currently explored for potential therapy of different applications ranging from cancer therapy [18], inflammation [19], gene delivery [20] and to fighting infections [21] because of their natural composition and inherent targeting properties [22]. Nevertheless, ongoing limitations of EVs include issues of upscale production in a biotechnologically controllable manner and post-processing regarding loading and modification for targeted tissue interaction [23] which may overall compromise their applicability in clinical trials. In this work, we investigate a non-toxic and biocompatible type of EVs, namely outer membrane vesicles (OMVs) isolated from non-pathogenic soil-bacteria called myxobacteria. Since myxobacteria

are inexpensive to ferment, their OMVs may thus be biotechnologically easily accessible and on top of that we show that they are inherently loaded with a recently discovered class of antibiotics effective against Gram-negative bacteria.

Outer membrane vesicles (OMVs) are spherical nanoparticles produced by Gram-negative bacteria [24, 25]. They originate from budding of the bacterial outer membrane and have been shown to hold manifold functions, including communication among bacteria themselves [26], involvement in procurement of nutrients, biofilm formation [27], transfer of virulence factors [28] or immunomodulation of the host [29]. OMVs are studied in detail for vaccination applications [30] with candidates now tested in clinical studies. OMVs have also been engineered for cancer therapy applications [31] but not in detail for delivery of antimicrobial compounds. Interestingly, OMVs can naturally carry bacteriolytic secondary metabolites, using them as weapons during the competition for environmental niches [32]. There are examples of inherently bacteriolytic OMVs derived from pathogens such as *Pseudomonas aeruginosa* [33]. It has been shown that some OMVs derived from other strains, e.g. *Enterobacter* or *Citrobacter* are able to kill other bacteria by transporting peptidoglycan hydrolases into their prey [34]. Although an interesting property, it remains doubtful whether such potentially strong immunogenic particles may be used in humans. To bypass these biocompatibility issues, we employed myxobacteria as producers of OMVs [35]. Myxobacteria are a class of δ-proteobacteria, which are predominantly found in soil. They are producers of versatile secondary metabolites, which offer new effective mechanisms of action and, among other effects, have antibacterial activity [36]. Most importantly, myxobacteria are non-pathogenic to humans but they show a predatory lifestyle and prey on other bacterial competitors [37]. Myxobacteria prey on Gram-negative and Gram-positive bacteria as nutrient source [38] and they are not able to synthesise three branched chain amino acids such as leucine, valine and isoleucine [39]. It was previously shown that *Myxococcus xanthus* produce hydrolase containing OMVs to kill competing bacteria [40]. Such unspecific enzyme induced antimicrobial effect may not be selective enough to kill prokaryotic cells while leaving human tissue unaffected.

Here, we thus aimed at identifying new candidates of myxobacterial OMVs that physiologically contain antibiotic compounds for a selective and efficient treatment of bacterial infection. We further investigated the natural properties of myxobacteria OMVs including their inherent antimicrobial potential against Gram-negative model bacteria *E. coli* and their compatibility with human cells. We characterised OMVs from two myxobacterial strains, namely *Cystobacter velatus* strain Cbv34 and the unclassified Sorangiineae species strain SBSr073 and show that they are biocompatible and stable at different storage conditions. OMVs possess an inherent antimicrobial effect against model pathogens which was

comparable to the clinically used antibiotic gentamicin. Our results create an important basis for an advanced development of bacterial OMVs as alternative antimicrobial drug carriers.

Materials and Methods

Microbial culture

Strain SBSr073 of the Sorangiineae suborder was cultivated in 2SWT medium **(**Bacto tryptone 0.3%**,** Soytone 0.1%**,** Glucose 0.2%**,** Soluble starch 0.2%**,** Maltose monohydrate 0.1%**,** Cellobiose 0.2%**,** $CaCl_2$ $2H_2O$ 0.05%**,** $MgSO_4$ $7H_2O$ 0.1%**,** HEPES 10mM**,** pH 7.0 adjusted with KOH**)**. *Cystobacter velatus* (Cbv34), a member of the Cystobacterineae suborder, was cultivated in M-medium (1.0% bacto peptone, 1.0% maltose, 0.2% $CaCl_2$, 0.1% $MgSO_4$, 50 mM HEPES pH 7.2 and 8 mg/L Fe-EDTA) at 30 °C and maintained at 180 rpm. *Escherichia coli* (*E. coli*) DH5-alpha bacteria (DSM 6897) were incubated at 37 °C and 180 rpm in lysogeny broth medium. All cultures were split after reaching stationary phase (**Figure S1**). SBSr073 forms aggregates and therefore the measured optical density at 600 nm (OD600) was inconclusive. Hence, the culture was split after 8 days of incubation of a 1% (v/v) inoculum. A growth curve of Cbv34 was established by measuring the OD600 twice a day with a cell density meter model 40 (Fischer Scientific, USA) with semi-micro cuvettes using medium as blank. Cbv34 bacterial culture was started at an OD600 of 0.1 and the stationary phase was reached after 4 days at an OD600 of 3.8. A cryogenic culture of all strains was established in 25% (v/v) glycerol.

Isolation and purification of OMVs

For optimal OMV isolation from conditioned media, myxobacteria needed to be cultured for at least four passages when they reached their stationary phase. Conditioned media from all strains were collected in 50 mL falcon tubes and their OMVs isolated using our previously established protocol [41]. In brief, they were centrifuged at 9500 x *g* for 10 min at 4 °C, 40 mL of the supernatant was then carefully transferred by pipetting into new falcon tubes and centrifuged at 9500 x g for 15 min at 4 °C. Afterwards, 30 mL of this supernatant was filled into ultracentrifugation tubes and pelleted at 100,000 x g and 4 °C for 2 hours (rotor SW 32 Ti, Beckman Coulter). The supernatant was removed carefully and the pellet was re-suspended with 400 µL filtered phosphate buffered saline (PBS, Gibco PBS tablets without calcium, magnesium and phenol red). To check if the isolation successfully removed living bacteria, 100 µL of this pellet were spread on agar plates, containing all nutrients from each media plus 1.5% (w/v) agar and incubated at 30 °C for 8 days.

For further purification, the pellet was applied on a size exclusion chromatography (SEC) column filled with sepharose CL-2B (GE Life Science, United Kingdom) to separate

vesicles from proteins that may have as well been pelleted during ultracentrifugation. The pellet to gel ratio was approximately 1 in 100 parts. Fractions of 0.5 to 1 mL were collected into polypropylene (PP) tubes (Axygen) (**Figure S2**) and stored at 4 °C for up to one week before further characterisation.

Characterisation of OMVs

Size distribution and yield of OMVs were assessed using Nanoparticles Tracking Analysis (NTA LM-10, Malvern, United Kingdom). To ensure equivalent results, samples were diluted up to 1:1000 in order to have a concentration of 20 to 120 particles per frame. 100 µL of sample were applied onto the chamber equipped with a green laser. A video was recorded with a camera level varying between 13 and 15 using NanoSight 3.1. Each sample was recorded three times for 30 seconds and calculated with a detection threshold of approximately 5 to ensure results are comparable amongst each other.

To determine the protein concentration of the fractions collected from SEC, a bicinchoninic assay kit (Sigma Aldrich) was used, according to manufacturer's specification. All samples were analysed in duplicates against an albumin standard with concentrations of 0.5, 5, 10, 20 and 30 µg/mL. Polydispersity index (PDI) and zeta potential of OMVs was measured on a Malvern Zetasizer.

Electron microscopy of OMVs

For electron cryomicroscopy (cryo-EM), OMVs were purified as described above and dispersions with a concentration of ~10^{11} particles/mL were used for analysis. For sample preparation a 3 µL droplet was placed onto a holey carbon film (type S147-4, Plano) before plotting for 2 sec using a Gatan cryoplunger model CP3 (Pleasanton) and plunging into liquid ethane at T=108 K. The frozen samples were transferred under liquid nitrogen to a Gatan model 914 cryo-TEM sample holder and investigated by bright-field TEM imaging at T=100 K and 15 pA/cm^2 (JEM-2100 LaB6, Jeol).

Biocompatibility of OMVs

A ToxinSensor™ Chromogenic LAL Endotoxin assay kit (GenScript), which is an enzyme based chromogenic test, was used to determine the endotoxin concentration of OMVs. It is an alternative to the gel-clot and turbidimetric tests for lipopolysaccharide (LPS) quantification. According to the manufacturer's specification all samples were examined within either 24h after isolation or stored at -20 °C before analysis. After mixing the sample with a limulus amebocyte lysate, the proteolytic activity of factor C was activated by endotoxins. The protease then catalysed the cleavage of p-nitroaniline (pNA) of a synthetic peptide (Ac-Ile-Glu-

Ala-Arg-pNA). After diazo-coupling of pNA the absorbance was read at 545 nm using a polystyrene 96 well plate. All samples were measured in technical duplicates.

Biocompatibility of OMVs was studied by assessing viability and cytotoxicity two cell types, namely epithelial lung carcinoma cells (A549) and acute monocytic leukemia monocytes (THP-1) which were activated to macrophages. These cell lines were chosen to simulate interactions of OMVs with epithelial barriers and immune cells present at sites of infections. A549 cells were seeded into 96-well plates at densities of 10,000 to 20,000 cells/well and left to grow for 48 h. THP-1 cells were seeded into 96-well plates at densities of 100,000 cells/well, subsequently differentiated to adherent macrophages (dTHP-1) with 30 ng/mL of phorbol 12-myristate 13-acetate (PMA) and left to grow for 48 h. Then, the old cell culture medium was replaced with fresh serum free and phenol red free RPMI 1640 medium (Thermo Fisher) and the cells were incubated with 10, 100, 1,000 and 10,000 purified OMVs/cell, and PBS as negative control and Triton X 1% (w/v) as positive control for 24 h. 100 µL of cell-free supernatant were transferred to a fresh 96-well plate for subsequent lactate dehydrogenase assay (LDH assay, see below). To assess cell viability, cells were washed and mixed with 100 µL fresh medium and 100 µL 10% PrestoBlue Cell Viability Reagent (Thermo Fisher) in medium. Cells were incubated at 37 °C for 10 min to 2 h, bottom fluorescence was read (excitation 560 nm and emission 590 nm) and viability calculated in comparison to PBS controls. For LDH detection in supernatants, a kit (Cytotoxicity Detection Kit, Merck) was used per supplier's instructions by incubating with the reaction mixture and an absorbance measurement at 490 nm.

Storage stability of OMVs

Each OMV sample was stored in PBS and at 4 °C, -20 °C, -80 °C and freeze dried to evaluate their stability [42]. Aliquots of 100 µL of each sample were kept in MaxyClear microtubes (Axygen) to avoid vesicles absorption to the plastic surface of the tubes. After determining particle concentration and size by NTA (correspond to 100%), the samples were stored for 7 to 75 days. For freeze-drying (lyophilisation), samples were snap frozen with liquid nitrogen and then dried overnight for at least 16 h using a LypoCube (Christ) freeze dryer.

Liposome controls

Liposomes were prepared using a mixture of 1,2-dimyristoyl-sn-glycero-3-phosphorylcholine (DMPC) and dipalmitoyl phosphatidylcholine (DPPC) at a ratio of 2:3 (mol%) and a concentration of 5 mM in a final volume of 1 mL. They were prepared using thin-film hydration as described previously [43]. In brief, lipids were suspended in filtered PBS at 42 °C, and extruded 21 times through a 200 nm polycarbonate membrane (all material from Avanti Lipids).

Uptake assessment and antibiotic activity of OMVs

Liposomes and OMVs were labelled and their cellular uptake was assessed in *E. coli* DH5-alpha model bacterium grown to an OD600 of 0.15. Liposomes and OMVs of SBSr073 and Cbv34 were incubated with 1 µL DiI (Vybrant DiI Cell-labelling solution) for 30 minutes. Non-incorporated dye was removed by SEC. The fluorescence intensity of each fraction was measured and the two most concentrated OMV fractions were used for further evaluation. After incubating *E. coli* with OMVs and liposomes for 1 h, 8 h and 24 h the bacteria were labelled with 1.5 µL SYTO 9 Green fluorescent nucleic acid stain and incubated at 37 °C for 10 min. After centrifugation at 9500 x *g* for 5 min, bacteria were fixed with 4% paraformaldehyde for 10-15 min at 37 °C. Before applying 10 µL of sample on a coverslip with a drop of mounting medium all samples were washed with PBS. Images were taken using a Leica TCS SB8 confocal microscope with a 64x magnification lens. A laser with an excitation wavelength of 561 nm (digital gain: 82%, pinhole: 111.5 µm, filter: 566- 673 nm, laser intensity: 2.0%) was set up to visualise DiI labelled vesicles and liposomes. Another laser with a wavelength of 488 nm (digital gain: 11%, pinhole: 111.5 µm, filter: 493-554 nm, laser intensity: 2.0%) was used to visualise SYTO 9 stained bacteria. All images were taken with the same set up, averaging and speed to allow sample comparison; and analysed using the Zen 2012 SP1 (black edition) software.

The antimicrobial effect of vesicles on *E. coli* DH5-alpha was analysed by incubating 100 µL of bacteria suspension (OD600 of 0.1) with 100 µL OMVs in a 96 PS well plate. Sterile PBS was used as a negative control and antibiotic gentamicin (16 µg/mL) was applied as positive control. To prevent evaporation, the outer wells of the microplate were filled with water. The plate was incubated at 37 °C in a Tecan infinite 200 Pro plate reader, measuring the absorbance at 600 nm every 15 min for at least 16 h. OMVs were also diluted 1:5, 1:10, 1:50 or 1:100 with sterile PBS in order to calculate a dose response curve. Colony-forming units (CFU) were measured by incubating OMVs with *E. coli.* For this, *E. coli* DH5-alpha was cultivated in lysogeny broth at 37 °C and 180 rpm until log phase was reached. The bacterial culture was diluted to 10^8 CFU/ml and incubated overnight with different concentrations of purified OMVs (10^{10}, 10^{11} and 10^{12} vesicles/mL). Serial dilutions of the samples were prepared, inoculated on lysogeny broth agar plates and incubated overnight at 37 °C. Afterwards CFUs/mL were counted and quantified.

Liquid-chromatography coupled mass spectrometry

To assess the active principle within myxobacterial OMVs, they were analysed by liquid-chromatography coupled mass spectrometry (LC-MS). First, 1 mL of purified OMV sample was mixed with 1 mL of methanol to achieve complete solubilisation of EVs. After

solvent evaporation the residue was taken up in 150 µL of methanol and centrifuged at 21500 x *g* for 5 min to remove debris and insoluble salts. 1 mL of this sample was subsequently analysed by UHPLS-HRMS on a Dionex Ultimate 3000 RSLC system using a Waters BEH C18 column (50 x 2.1 mm, 1.7 µm) connected to a Waters VanGuard BEH C18 1.7 µm guard column. Separation of 1 µl sample was achieved by a linear gradient from (A) H_2O + 0.1 % FA to (B) ACN + 0.1 % FA at a flow rate of 600 µL/min and 45 °C column temperature. Gradient conditions were as follows: 0 – 0.5 min, 5% B; 0.5 – 18.5 min, 5 – 95% B; 18.5 – 20.5 min, 95% B; 20.5 – 21 min, 95 – 5% B; 21-22.5 min, 5% B. UV spectra were recorded by a diode-array detector in the range from 200 to 600 nm. The LC flow was split to 75 µL/min before entering the Bruker Daltonics maXis 4G hr-qToF mass spectrometer using the Apollo II ESI source. Mass spectra were acquired in centroid mode ranging from 150 – 2500 m/z at a 2 Hz full scan rate and data were annotated using the in house myxobacterial metabolome *MXbase Database,* established at the Helmholtz Institute for Pharmaceutical Research Saarland (HIPS), by automated comparison of retention time, exact mass and isotope pattern accuracy using Bruker Daltonics Target analysis 1.3. A detailed description of spectra annotation can be found in the supplementary information.

Statistical analysis

All data are displayed as mean ± standard deviation (SD), indicating the number of *n* independent experiment in each figure. All measurements were at least made in independent triplicates. Results were analysed statistically with Sigma Plot using One-way ANOVA followed by Tukey *post-hoc* test to compare the mean values between individual groups. Significant p-values were illustrated as * for $p< 0.05$ and ** $p< 0.005$.

Results and Discussion

OMVs are efficiently isolated from bacterial culture and they show promising storage stability

In this work, we compared two strains of myxobacteria from representative suborders as source for OMVs, namely SBSr073 (Sorangiineae suborder) and Cbv34 (*Cystobacterineae* suborder). According to our growth curves strain Cbv34 showed a doubling time of tD_{Cbv34}= 4.7 h ± 1.0, reaching stationary phase after 50 h (**Figure S1a**). To obtain the maximum amount of OMVs while avoiding artefacts of dead cells or presence of protein aggregates, we decided to use conditioned medium after 80 h (stationary phase) for their isolation (**Figure S1b**). It is important to mention, that both strains require at least four full passages after starting the culture from cryogenic stocks to achieve optimal bacterial growth (**Figure S1c**). Strain SBSr073 formed aggregates when in liquid medium, which made OD600 measurements

inconclusive (**Figure S1d**). When dispersing clumps with glass beads and under vortexing, aggregates would form again within 2 days of culture. Thus samples of conditioned medium were generally taken after 8 days of growth and with bacterial morphology not altered. Bright field microscopy of both bacterial strains revealed typical rod shape of myxobacteria and similar culture conditions were used throughout the entire study to ensure reproducible OMV properties. For strain Cbv34, we obtained best OMV results when the culture medium reached a viscous constitution. We were able to keep these myxobacteria in constant culture for more than 3 months without loss of phenotype or major alterations of morphology as observed by light microscopy.

OMVs were subsequently isolated from conditioned culture medium using differential ultracentrifugation [43]. Bacteria were removed by centrifuging the culture at 9500 x *g* for 10 minutes and 15 min. After the ultracentrifugation at 100,000 x *g*, 100 µL of in PBS re-suspended pellet were plated on agar plates and incubated for 8 days to verify that all bacteria had been removed during centrifugation and the final pellet contained only OMVs (**Figure S1e**). Re-suspended OMV pellets were purified by SEC to separate protein aggregates from vesicles. This technique is effective for separating molecules and particles according to their size. The successful purification of the OMVs from soluble proteins is shown in **Figure S2**, suggesting that OMVs mainly eluted at 6-8 mL for SBSr073 and 7-9 mL for Cbv34 with free protein aggregates eluting at fractions 15 and later. We subsequently pooled the highest concentrated fractions to assess the OMVs using cryo-EM (**Figure 1a**). This method was mainly applied to study morphology and shape of vesicles derived from both bacterial strains [44]. The lipid-bilayer is clearly visible which indicates that OMVs were not all destroyed during isolation and purification. These images also show that the combination of ultracentrifugation with SEC to purify OMVs was reproducible without inducing artefacts from membrane fusion or disruption. In few images we observed multi-lamellar vesicles which may be a type of the recently described outer-inner membrane vesicles [45]. These particles were reported to occur in only up to 1.2% of OMV preparations from selected strains, which is consistent with our observations in cryo-EM images. To verify these findings, the particle concentration and size of all collected fractions was analysed by NTA (**Figure 1b**). In all subsequent experiments, OMV quantification was only based on NTA measurements. The most abundant fractions contained concentrations of 10^{10}-10^{11}particles/mL which is 10-100fold more than vesicle concentrations reported for mammalian cells [43]. Indeed, low EV amount is one of the major challenges when developing these biogenic carriers for drug therapy [23]. However, microbial culture is already an established biotechnological process with the possibility to upscale which is a big asset to produce these nanodelivery systems. The average hydrodynamic radius of OMVs measured by NTA was 145 nm for Cbv34, and 194 nm for SBSr073 OMVs. When further assessing the physio-chemical properties of purified OMVs, we observed a relatively

small PDI of 0.14 and 0.22 for SBSr073 and Cbv34 (**Table S1**), respectively, which may suggest that with these sizes OMVs can be filtered to sterility [46]. Despite OMVs are derived from cells, their size distribution is rather narrow and it suggests that the majority of the particles have a homogenous distribution.

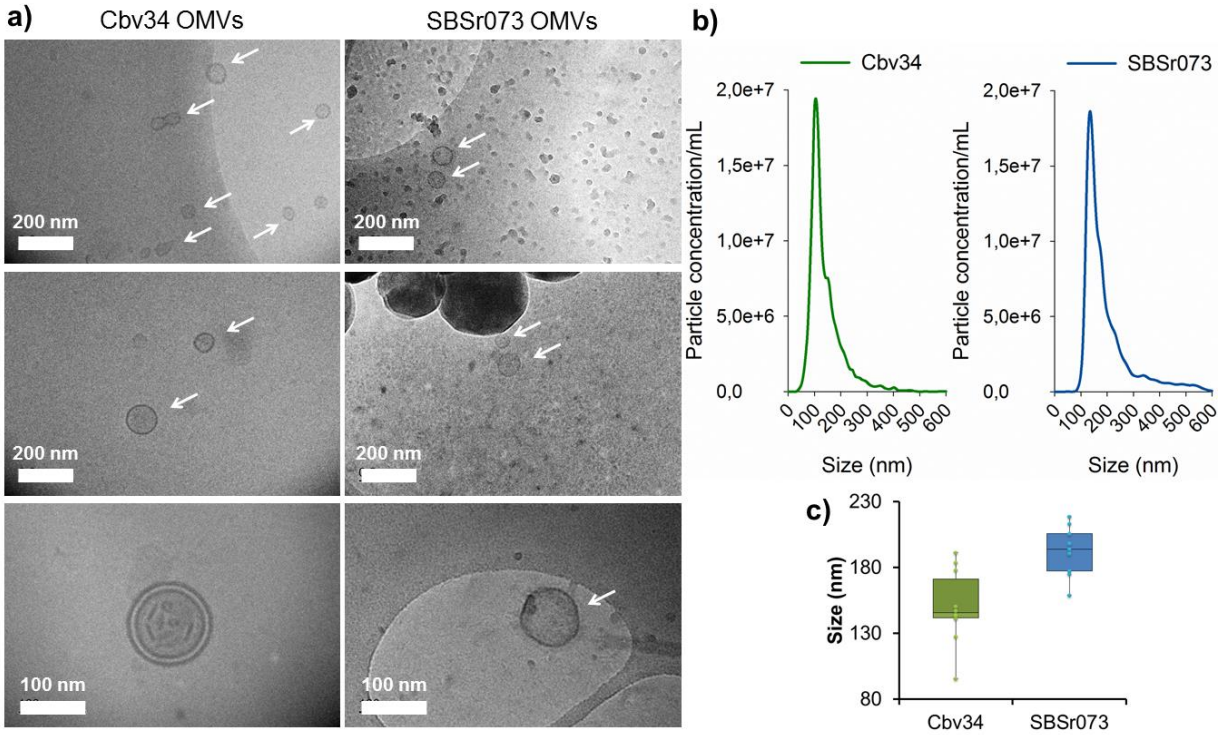

Figure 1. Electron cryomicroscopy characterisation and size distribution of myxobacterial OMVs. a) OMVs were analysed by cryo-EM at different magnifications and are marked with arrows. Bright areas in the images indicate regions of lower transmission, small and big black spots in the SBSr073 samples are ice crystals as identified by their shape. **b)** Averaged spectra of size distribution of OMVs from Cbv34 and SBSr073 measured by nanoparticle tracking analysis after size exclusion chromatography purification and **c)** corresponding boxplot of average OMV sizes, Mean ± SD, *n* = 10.

Due to their cellular origin, the zeta potential of OMVs was slightly negative which is often associated with low stability and tendency to aggregate. We thus investigated the stability of these vesicles by storing samples at 4 °C, -20 °C, -80 °C and upon lyophilisation (freeze-drying) (**Figure 2**). After 7 and 75 days, size and particle concentration was measured and compared to day zero (set to 100%). A reduction in particle concentration was seen at all conditions after 7 days but was less pronounced for Cbv34 OMVs with a decrease to 70% when freeze-dried and 40% when stored at -80 °C (**Figure 2a**). Such loss may be due to unspecific agglomeration or disintegration of vesicles. After 75 days only 14% of OMVs were recovered when stored at -20 °C but 40% remained when samples were lyophilized. SBSr073 OMVs were most stable during lyophilisation, even after 75 days (**Figure 2c**). Interestingly, a

major size drift was observed when storing these OMVs at 4 °C (**Figure 2d**). Until now, there are very little reports on a standardized and preferred method for storing OMVs and EVs yet although it is essential for advanced studies [42, 47] and storage of vesicles at -80 °C is recommended [48]. Our results indicate that freeze-drying is a valid alternative for storing OMVs as it was also shown in literature [42, 49]. Based on our stability data we decided to use OMVs within 3 days after purification. In all subsequent evaluations, OMVs and liposomes of 148 nm size were used at similar concentrations for appropriate comparison (**Figure S3a**).

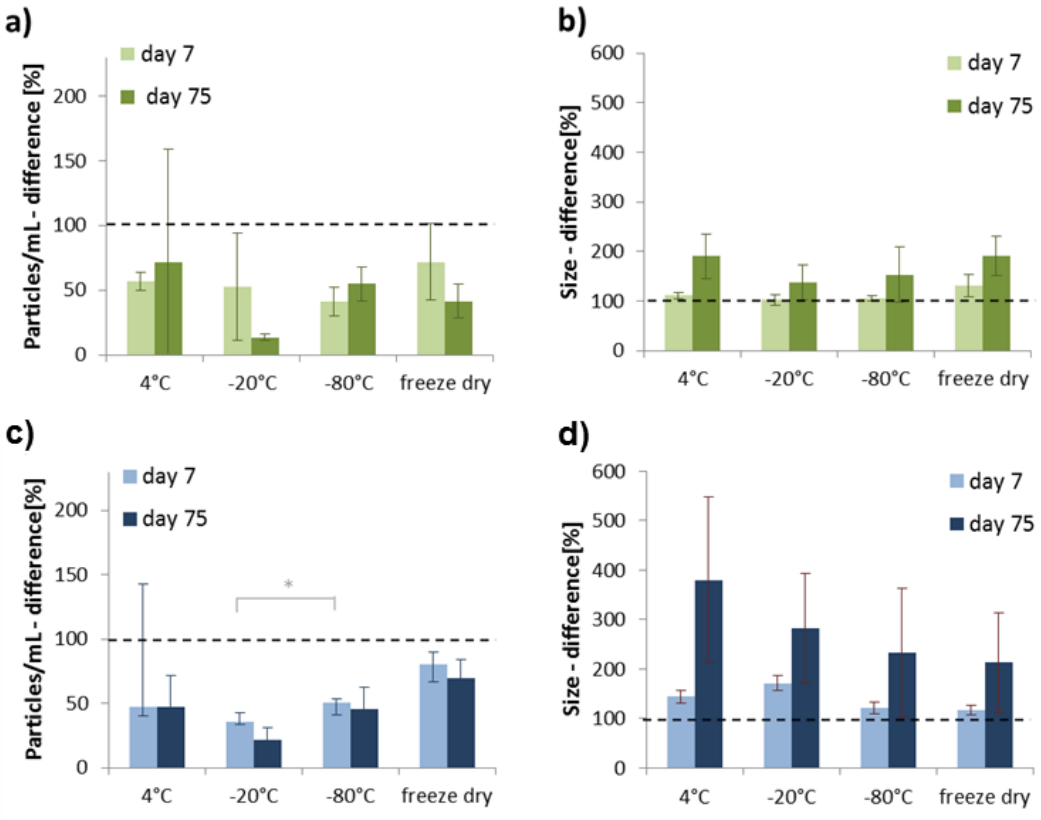

Figure 2. Stability of myxobacterial OMVs upon different storage conditions. OMVs from Cbv34 and SBSr073 were isolated, purified, and stored for 7 and 75 days in PBS and under different conditions (4 °C, -20 °C, -80 °C, and after freeze-drying and at RT). **a)** Particle concentration of Cbv34 OMVs and **b)** evolution in size of Cbv34 OMVs, **c)** Particle concentration of SBSr073 OMVs, **d)** evolution in size of SBSr073 OMVs. Mean ± SD, *n* = 3, **p*<0.05 (ANOVA followed by Tukey *post-hoc* test).

OMVs show very good biocompatibility and only little endotoxin activity

Biocompatibility of myxobacterial OMVs was evaluated using epithelial A549 cells and differentiated dTHP-1 macrophages to assess cell viability and cytotoxicity (**Figure 3**). A549 cells were used as normal epithelial control cells while dTHP-1 cells were stimulated with concentrations of PMA (30 ng/mL) to stimulate differentiation to macrophages and mimic

inflammatory processes that are often associated with bacterial infections [50]. When incubating OMVs with A549 and dTHP-1 cells at different vesicle-to-cell ratios, no impact on general cell viability was observed for any of the cells compared to PBS controls (**Figure 3a and b**). We further evaluated whether any underlying cytotoxicity was present by applying a lactate-dehydrogenase test which measures cellular toxicity and cytolysis. Interestingly, even at very high concentrations of 10,000 OMVs/cell no cytotoxic effects were observed which indicated no immanent toxicity in our *in vitro* cell models (**Figure 3c and d**). Differentiated dTHP-1 cells are macrophage cells with a high phagocytosis rate and are potentially sensitive towards external stimuli but in our hands we did not see signs of distress or alterations in cell morphology when dTHP-1 cells were incubated at high OMV concentrations (**Figure 3e**) and in comparison to positive controls using cytotoxic Triton X. In dTHP-1 cells we see a small increase in cell viability upon addition of very large quantities of OMVs which may be induced by a nutrient bolus of lipids due to the high OMV concentration. No toxic effects were observed for control liposomes used at the same concentrations as OMVs (**Figure S3b and c**).

To analyse the potential of OMVs to induce immune reactions during application in a therapeutic setting, a chromogenic limulus amoebocyte lysate endotoxin assay was performed. Such endotoxin assay allows an estimation on the biocompatibility of a material as it gives information if samples contain immuno-stimulatory lipopolysaccharides. As OMVs could not be prepared under sterile conditions, we used the PBS wash from the SEC column as negative control. We observed that the endotoxin concentration of OMVs was not increased compared to the PBS negative control (**Figure 3f**). As another control, the endotoxin activity of strain Cbv34 and *E. coli* bacteria were measured when reaching the same OD600 of 3.5. Interestingly, although the bacterial density was comparable, *E. coli* showed a higher concentration of endotoxins (1.60 EU/mL), while strain Cbv34 exhibited low levels of endotoxins comparable to their OMVs (0.75 EU/mL) and to PBS controls. Our results suggest a lower endotoxin activity of myxobacterial OMVs compared to other Gram-negative microbial materials in general. It has been shown that some myxobacteria have a lack of LPS as a component of their outer membrane [51]. Ruiz *et al.* found an altered immune response of myxospores in sheep compared to other Gram-negative spores [52], which may be due to a partial modification of polysaccharides [53]. Our results suggest inherent biocompatibility of bacterial OMVs from myxobacteria, which may aid for their applicability in therapeutic settings.

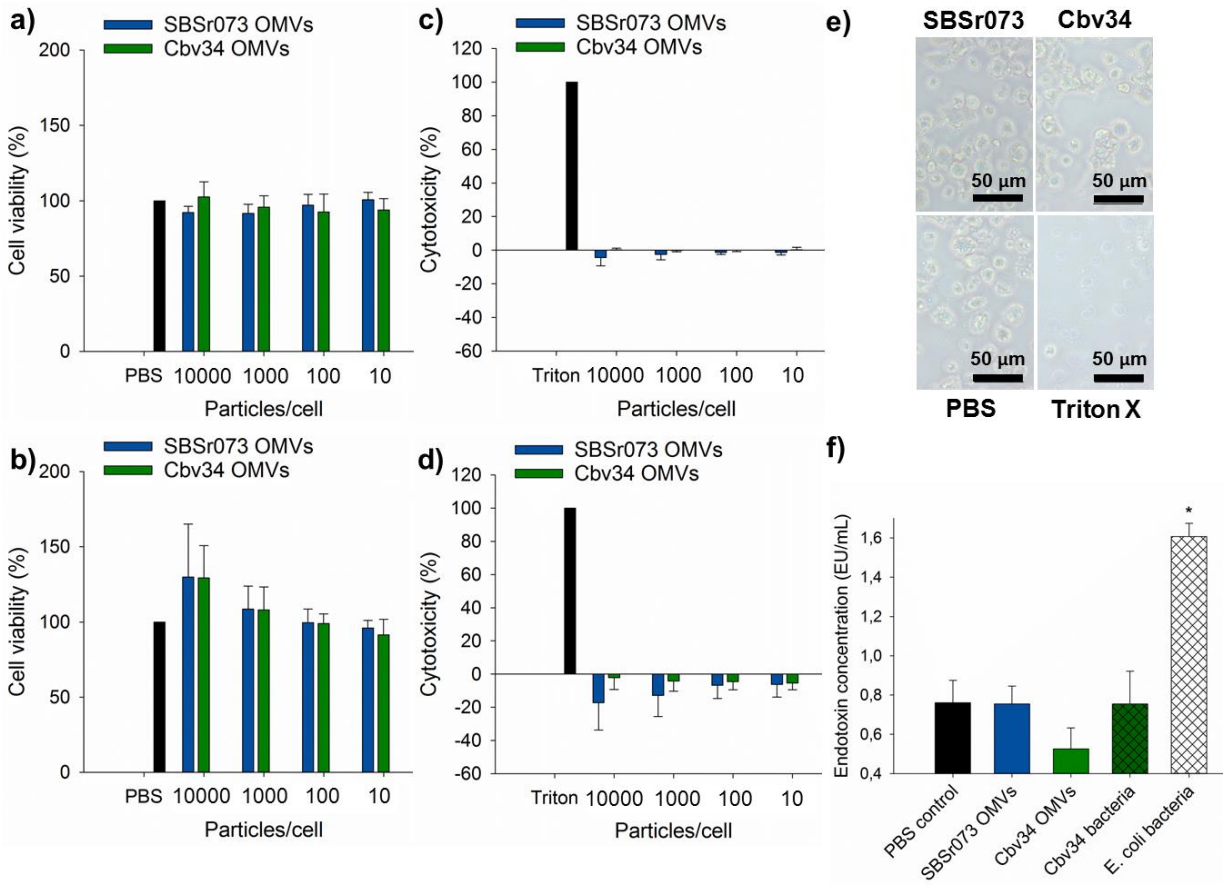

Figure 3. Biocompatibility and endotoxin assessment of myxobacterial OMVs. Cell viability of Cbv34 and SBSr073 OMVs when incubated for 24 h with **a)** A549 epithelial cells and **b)** dTHP-1 macrophage cells, and lactate-dehydrogenase cytotoxicity assay of OMVs incubated for 24 h with **c)** A549 and **d)** dTHP-1 cells. Mean ± SD, *n* = 4–6. **e)** Representative light microscopy images of dTHP-1 cells incubated for 24 h with Cbv34 OMVs, PBS (negative control) or Triton X (1%, positive control). **f)** Endotoxin activity of OMVs compared to control PBS collected from the SEC column under similar conditions. Cbv34 bacteria showed a lower concentration of endotoxins compared to *E. coli* when culturing samples with similar cell densities. Mean ± SD, *n* = 3, **p*<0.05 (ANOVA followed by Tukey *post-hoc* test)

The co-localisation of OMVs with model bacteria is comparable to standard liposomes

E. coli DH5-alpha were incubated with DiI labelled OMVs or liposomes for 1, 8, and 24 h in order to visualize interaction of OMVs with target model bacteria. The dyes were excited with two different lasers, for DiI at 561 nm and for detection of SYTO 9 labelled bacteria at 488 nm. SYTO 9 was used for visualisation of all live and dead bacteria during microscopy. After 1 h (**Figure S4**) and 8 h of incubation with *E. coli*, very little to no co-localisation was detected for both types of OMVs and for liposomes. As seen in **Figure 4** after 24 h incubation, we observed co-localisation of SYTO 9 labelled bacteria with DiI labelled OMVs (zoom in **Figure 4b** and arrows in **Figure S4**). Control samples incubating *E. coli* with DiI dye alone and in the

absence of OMVs did not show co-localised fluorescence (**Figure S5b**). After 24 h of incubation with DiI labelled liposomes, we qualitatively observed less co-localisation. Liposomes may have accumulated in the extracellular matrix of the bacteria as indicated by a diffuse bright halo around the *E. coli*. For all experiments, comparable labelling efficiency of OMVs versus liposomes was employed (**Figure S5a**). We further studied *z*-stack images of *E. coli* incubated for 20 h with Cbv34 OMVs (final concentration 10^{12} OMVs/mL) which were washed before imaging (**Figure S6**). For some bacteria we observed co-localisation (indicated by arrows) but we also saw unspecific accumulation of OMVs in bacterial proximity. Overall, our results suggest that OMVs are co-localising with *E. coli* similarly to synthetic liposomes. There are three possible scenarios for OMVs to interact with cells, whether they belong to their own or competing other species: i) releasing cargo nearby cells, ii) physical fusion with the target outer membrane, or iii) by interaction with mammalian cell membranes *via* receptors. For OMV uptake into mammalian cells, different mechanisms ranging from direct fusion to endocytic uptake are currently discussed [54]. Evans *et al.* observed an increased fusion effect of OMVs when Glyceraldehyde 3-phosphate dehydrogenase (GDPH) was added to *E. coli* [40]. The GDPH is an enzyme involved in eukaryotic membrane fusion, which may indicate that OMVs are eventually taken up through direct membrane fusion. We qualitatively observed a comparable co-localisation of natural *vs*. synthetic lipid carriers (i.e., OMVs *vs*. liposomes) in *E. coli* which may relate to the fluidity of the nanoparticle membrane in bacterial uptake as shown previously [55]. For other OMVs fusion with target bacteria was proposed [35], but upcoming assessments will need to indicate whether OMVs from Cbv34 and SBSr073 also follow this mechanism. Our findings nevertheless give a first insight into how interaction of OMVs compares to synthetic carriers which may serve as a point of reference to the creation of semi-synthetic OMV-mimetics with enhanced bacterial interaction.

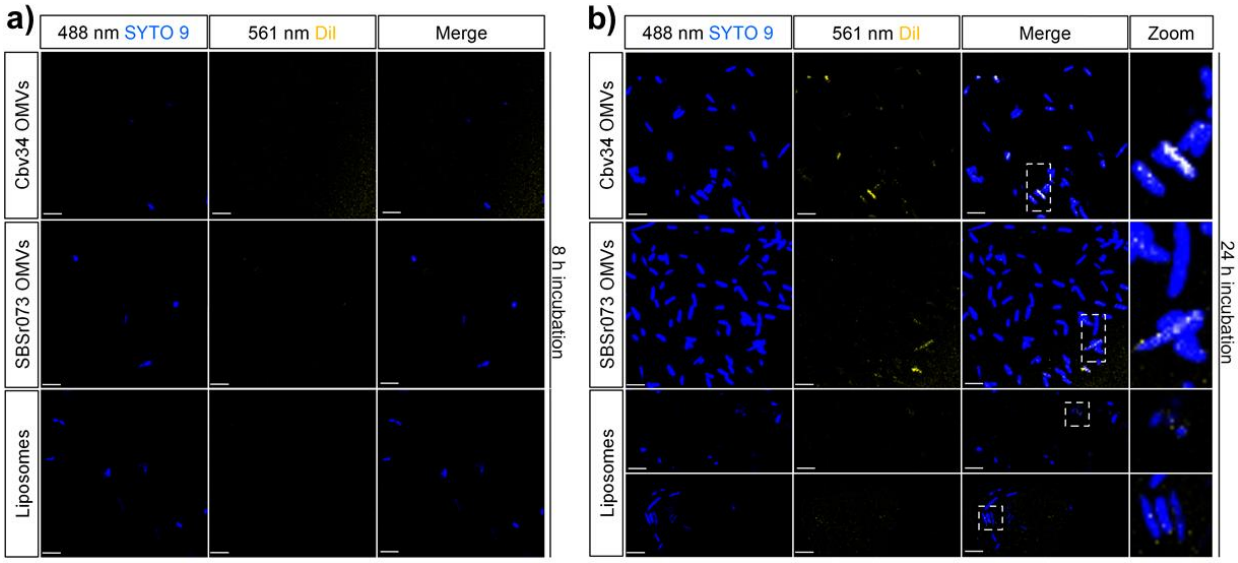

Figure 4. Representative confocal fluorescence images of *E. coli* incubated with OMVs. *E. coli* DH5-alpha incubated with fluorescently (DiI)-labelled Cbv34 OMVs (10^{11}/mL), SBSr073 (10^{10}/mL) OMVs, and Liposomes (10^{11}/mL) for **a)** 8 h and **b)** 24 h. Images were taken using the same laser settings at 561 nm and 488 nm. Scale bars represent 5 µm. Zoomed-in images displayed show co-localisation of fluorescently labelled OMVs with magnified bacteria. Measurement settings and image analysis is similar for all images; false colouring was set to blue and yellow to better visualise co-localisation in the merged images.

OMVs are intrinsically loaded with antimicrobial drugs and show a growth inhibition using model bacteria

Following the promising results during uptake experiments in *E. coli* model bacteria, we investigated the antibacterial effect of OMVs. To do so, they were incubated with *E.coli* in a 96 well plate, screening the OD600 every 15 minutes. This simple real-time detection method showed that OMVs from Cbv34 had a strong inhibitory effect on *E.coli* growth when incubated at concentrations of 10^{12} vesicles/mL (**Figure 5a**). As control, concentrations of 10^{12} OMVs/mL did not influence our OD600-based measurements in absence of bacteria. The OMV-induced inhibitory effect was comparable to a standard aminoglycoside antibiotic, gentamicin, at concentrations of 16 µg/mL. To elucidate whether this inhibitory effect of OMVs was bacteriostatic or bactericidal we performed counting of CFUs after incubation with *E. coli* (**Figure 5b**). It was shown that Cbv34 OMVs completely inhibited bacterial growth when incubated at concentrations of 10^{12} vesicles/mL. Indeed, CFU counting confirmed our previously seen growth inhibition and the OMVs' effect was proven to be bacteriolytic because very small amounts of living colonies were observed upon plating. We calculated that 16 µg/mL gentamicin correspond to approximately 4×10^{15} drug molecules to inhibit bacterial growth, while 2×10^{11} OMVs induced a comparable effect. To further investigate this effect, we

incubated *E. coli* with varying concentrations of OMVs which revealed a typical sigmoidal dose-response curve (**Figure 5c**). In this OD600-based assay, OMV concentrations between 10^{11} and 10^{12} vesicles/mL were necessary to obtain the growth inhibition effect, which also matched our CFU data. Concentrations of 10^{11} to 10^{12} vesicles/mL corresponded in our assay to an antimicrobial activity range of 140-2500 OMVs/CFU. We did not observe any impact on *E. coli* growth when incubating bacteria with comparable concentrations of control liposomes (**Figure S3c**). When further studying the OMV producers, we observed that Cbv34 bacteria were able to predate and lyse *E. coli* within 48 h of cultivation on agar (**Figure S7**), while SBSr073 bacteria were slowly swarming and showed weak predation. In consistency with these results, we only observed a small influence of SBSr073 OMVs on the growth rate of *E. coli* DH5-alpha. As seen in **Figure 5a**, SBSr073 OMVs appeared to induce a small bacteriostatic effect until 4-6 h of incubation with model bacteria which was not maintained during the entire incubation period of 16 h. Nevertheless, given their biocompatibility profile, SBSr073 OMVs may in the future be loaded with common antibiotics to assess their delivery potential in an infection setting.

Myxobacteria are promising producers of various antibacterial compounds, as it was shown in literature [36]. We thus investigated the Cbv34 OMVs' active principle. In doing so, OMV samples were extracted using methanol as solvent and analysed by LC-MS. We identified a cystobactamid in the vesicle samples derived from Cbv34, eluting at a retention time of approximately 9 min and with an extracted ion chromatogram at 920.309 ± 0.02 Da (**Figure S8**). An scheduled precursor list based targeted MS^2 experiment was applied to this main chromatographic peak in order to rule out mass-spectrometric artefacts and to confirm our finding. When comparing the OMV peak with a cystobactamid 919-1 standard we observed very good agreement in MS^2 spectral fingerprint and displaying the subsequent losses of the derivatised p-aminobenzoic acid moieties from the cystobactamid backbone (**Figure S9**) which confirmed presence of the compound within Cbv34 OMVs. Unfortunately, it was not possible to quantify the amount of cystobactamid within acceptable error margins because of the limit of quantification and potential ion suppression effects induced by the OMV background signal. We further aimed at better analysing the antimicrobial effect of OMVs by determining the minimal inhibitory concentration of free cystobactamid 919-1 to be 32 µg/mL using *E. coli* DH5-alpha model bacteria while Cbv34 OMVs showed a minimal inhibitory concentration of 10^{12} particles/mL. We also performed CFU counting of various cystobactamid and OMV concentrations **(Figure S10)**. Mass spectrometry control experiments additionally revealed that cystobactamid is not contained in SBSr073 OMVs, pointing towards a role as active principle of Cbv34 OMVs. Cystobactamids are an important new class of antimicrobials which inhibit the bacterial type IIa topoisomerases and are effective against *E.coli* as well as several problem pathogens [56, 57]. Thus intrinsically loaded biocompatible vesicles, as we showed

here, alleviates drug carrier development in many ways: method validation for drug encapsulation is not needed, therefore the risk of modulating the vesicle membrane and its properties during post-processing is low. These naturally-equipped OMVs from strain Cbv34 may be an important step towards using EV-based therapies in the near future.

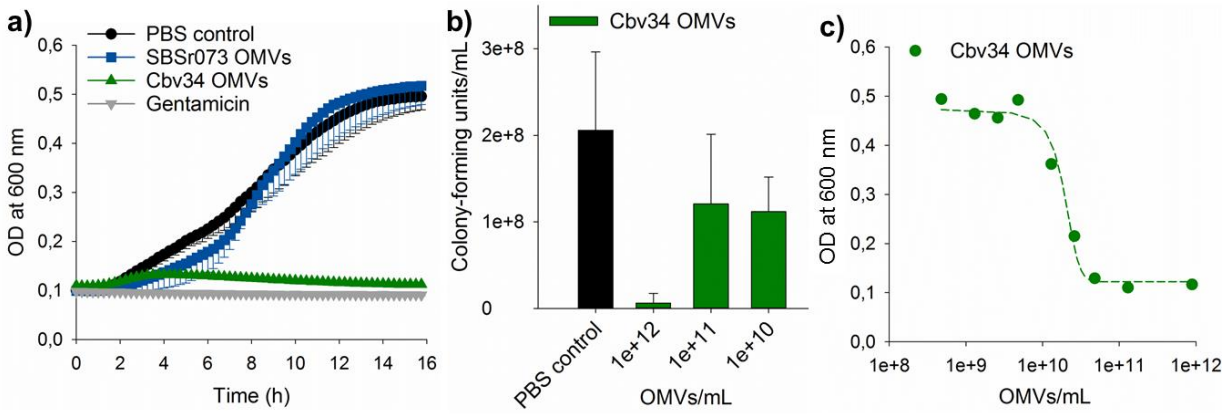

Figure 5. Inherent antibiotic effect of OMVs when incubated with *E. coli.* a) Incubation of Cbv34 OMVs (concentration 10^{11}/mL) and SBSr073 OMVs (concentration 10^{10}/mL) with *E. coli* and in comparison to free gentamicin (16 µg/mL). Mean ± SD, *n* = 3. **b)** Counting of colony-forming units of *E. coli* DH5-alpha incubated with different concentrations of Cbv34 OMVs. Mean ± SD, *n* = 3. **c)** Dose response curve of Cbv34 OMVs by incubating increasing concentrations of OMVs with *E. coli*.

Conclusions

In this work, we present a new type of OMVs derived from myxobacteria that shows intrinsic antibiotic activity. These OMVs exhibit promising properties regarding size distribution and stability upon storage. Bacteria as sources for EVs are ideal as their high-yield cultivation on industrial scale is widely practiced which aides in the clinical translation of the current approach. Uptake studies indicated that OMVs are interacting with Gram-negative bacterial strains in a similarly manner than liposomes but further evaluations of these processes are required. Furthermore, advanced biocompatibility studies, such as an incubation of OMVs in complex *in vitro* models, and additional investigations regarding immunogenicity on other human cell lines or in small animal models are necessary. Regarding the OMV activity profile, it would be important to study other model bacteria or bacterial biofilms, which are an important barrier to successful antibiotic therapy at the moment [58]. Likewise, bacterial loading of cystobactamids into OMVs may be controllable through varying culture conditions. Indeed, lower potency of Cbv34 OMVs was observed when bacteria were used at lower passage numbers after inoculation from cryogenic stock indicating that culture periods may have an influence on antimicrobial activity (**Figure S11**).

The ability of these OMVs to target infected tissue would need to be studied using suitable *in vivo* models [6]. As their antimicrobial cargo compounds are naturally packed into OMVs, they are potentially protected from destruction by degrading enzymes which may reduce probability of new resistances [5]. OMVs may be bioengineered to possess small moieties enabling optimised targeting to pathogens while concurrently reducing accumulation in healthy mammalian cells as it was shown for other EVs [59]. These OMVs finally present a water-soluble version of poorly water-soluble cystobactamid which is relevant when developing this promising drug for other application routes, such as oral or lung delivery [60]. Ultimately, our findings provide an important step towards further developing OMVs from myxobacteria as promising antimicrobial drug carriers.

Acknowledgements

This work was supported by the NanoMatFutur Junior Research programme from the Federal Ministry of Education and Research, Germany (grant number 13XP5029A, BEVA). We thank Jennifer Herrmann for providing cystobactamid 919-1 standards.

Author contributions

E.S. conducted all experiments on OMVs isolation and characterisation, prepared figures and analysed experiments; A.G. assessed antimicrobial activity of OMVs together with E.S.; R.G. set-up the myxobacterial cultures and assisted in their maintenance; F.P. executed LC-MS analyses; M.K. collected electron cryomicroscopy images; R.M. provided myxobacterial strains and helped with the study design; K.F. executed biocompatibility analyses and supervised the work. G.F. conceived the study, supervised the project and wrote the main manuscript text together with E.S. All authors analysed data and reviewed the manuscript.

Additional information

The authors declare no competing financial interests.

References

[1] H.R. Meredith, J.K. Srimani, A.J. Lee, A.J. Lopatkin, L. You, Collective antibiotic tolerance: mechanisms, dynamics and intervention, Nat Chem Biol, 11 (2015) 182-188.

[2] J.M.A. Blair, M.A. Webber, A.J. Baylay, D.O. Ogbolu, L.J.V. Piddock, Molecular mechanisms of antibiotic resistance, Nat Rev Micro, 13 (2015) 42-51.

[3] M. Perros, A sustainable model for antibiotics, Science, 347 (2015) 1062-1064.

[4] R. Sommer, S. Wagner, K. Rox, A. Varrot, D. Hauck, E.-C. Wamhoff, J. Schreiber, T. Ryckmans, T. Brunner, C. Rademacher, R.W. Hartmann, M. Brönstrup, A. Imberty, A. Titz, Glycomimetic, Orally Bioavailable LecB Inhibitors Block Biofilm Formation of Pseudomonas aeruginosa, J. Am. Chem. Soc., 140 (2018) 2537-2545.

[5] H. Zazo, C.I. Colino, J.M. Lanao, Current applications of nanoparticles in infectious diseases, J. Control. Release, 224 (2016) 86-102.

[6] R.S. Santos, C. Figueiredo, N.F. Azevedo, K. Braeckmans, S.C. De Smedt, Nanomaterials and molecular transporters to overcome the bacterial envelope barrier: Towards advanced delivery of antibiotics, Adv. Drug Deliv. Rev., (2017).

[7] P. Meers, M. Neville, V. Malinin, A.W. Scotto, G. Sardaryan, R. Kurumunda, C. Mackinson, G. James, S. Fisher, W.R. Perkins, Biofilm penetration, triggered release and in vivo activity of inhaled liposomal amikacin in chronic Pseudomonas aeruginosa lung infections, J. Antimicrob. Chemother., 61 (2008) 859-868.

[8] C.-M. Huang, C.-H. Chen, D. Pornpattananangkul, L. Zhang, M. Chan, M.-F. Hsieh, L. Zhang, Eradication of drug resistant Staphylococcus aureus by liposomal oleic acids, Biomaterials, 32 (2011) 214-221.

[9] A.J. Huh, Y.J. Kwon, “Nanoantibiotics”: A new paradigm for treating infectious diseases using nanomaterials in the antibiotics resistant era, J. Control. Release, 156 (2011) 128-145.

[10] R.Y. Pelgrift, A.J. Friedman, Nanotechnology as a therapeutic tool to combat microbial resistance, Adv. Drug Deliv. Rev., 65 (2013) 1803-1815.

[11] R. Schiffelers, G. Storm, I. Bakker-Woudenberg, Liposome-encapsulated aminoglycosides in pre-clinical and clinical studies, J. Antimicrob. Chemother., 48 (2001) 333-344.

[12] P. García-Manrique, M. Matos, G. Gutiérrez, C. Pazos, M.C. Blanco-López, Therapeutic biomaterials based on extracellular vesicles: classification of bio-engineering and mimetic preparation routes, J Extracell Vesicles, 7 (2018) 1422676.

[13] A. Parodi, R. Molinaro, M. Sushnitha, M. Evangelopoulos, J.O. Martinez, N. Arrighetti, C. Corbo, E. Tasciotti, Bio-inspired engineering of cell- and virus-like nanoparticles for drug delivery, Biomaterials, 147 (2017) 155-168.

[14] A. Goes, G. Fuhrmann, Biogenic and biomimetic carriers as versatile transporters to treat infections, ACS Infectious Diseases, 4 (2018) 881-892.

[15] J.-W. Yoo, D.J. Irvine, D.E. Discher, S. Mitragotri, Bio-inspired, bioengineered and biomimetic drug delivery carriers, Nat Rev Drug Discov, 10 (2011) 521-535.

[16] H. Zhang, D. Freitas, H.S. Kim, K. Fabijanic, Z. Li, H. Chen, M.T. Mark, H. Molina, A.B. Martin, L. Bojmar, J. Fang, S. Rampersaud, A. Hoshino, I. Matei, C.M. Kenific, M. Nakajima, A.P. Mutvei, P. Sansone, W. Buehring, H. Wang, J.P. Jimenez, L. Cohen-

Gould, N. Paknejad, M. Brendel, K. Manova-Todorova, A. Magalhães, J.A. Ferreira, H. Osório, A.M. Silva, A. Massey, J.R. Cubillos-Ruiz, G. Galletti, P. Giannakakou, A.M. Cuervo, J. Blenis, R. Schwartz, M.S. Brady, H. Peinado, J. Bromberg, H. Matsui, C.A. Reis, D. Lyden, Identification of distinct nanoparticles and subsets of extracellular vesicles by asymmetric flow field-flow fractionation, Nat. Cell Biol., 20 (2018) 332-343.

[17] J.P.K. Armstrong, M.N. Holme, M.M. Stevens, Re-Engineering Extracellular Vesicles as Smart Nanoscale Therapeutics, ACS Nano, 11 (2017) 69-83.

[18] H. Zhang, T. Deng, R. Liu, M. Bai, L. Zhou, X. Wang, S. Li, X. Wang, H. Yang, J. Li, T. Ning, D. Huang, H. Li, L. Zhang, G. Ying, Y. Ba, Exosome-delivered EGFR regulates liver microenvironment to promote gastric cancer liver metastasis, Nature Communications, 8 (2017) 15016.

[19] D. Yuan, Y. Zhao, W.A. Banks, K.M. Bullock, M. Haney, E. Batrakova, A.V. Kabanov, Macrophage exosomes as natural nanocarriers for protein delivery to inflamed brain, Biomaterials, 142 (2017) 1-12.

[20] D.S. Sutaria, J. Jiang, O.A. Elgamal, S.M. Pomeroy, M. Badawi, X. Zhu, R. Pavlovicz, A.C.P. Azevedo-Pouly, J. Chalmers, C. Li, M.A. Phelps, T.D. Schmittgen, Low active loading of cargo into engineered extracellular vesicles results in inefficient miRNA mimic delivery, J Extracell Vesicles, 6 (2017) 1333882.

[21] G. Fuhrmann, A.L. Neuer, I.K. Herrmann, Extracellular vesicles – A promising avenue for the detection and treatment of infectious diseases?, Eur. J. Pharm. Biopharm., 118 (2017) 56-61.

[22] G. Fuhrmann, I. Herrmann, M.M. Stevens, Cell-derived vesicles for drug therapy and diagnostics: opportunities and challenges, Nano Today, 10 (2015) 397-409.

[23] M.I. Ramirez, M.G. Amorim, C. Gadelha, I. Milic, J.A. Welsh, V.M. Freitas, M. Nawaz, N. Akbar, Y. Couch, L. Makin, F. Cooke, A.L. Vettore, P.X. Batista, R. Freezor, J.A. Pezuk, L. Rosa-Fernandes, A.C.O. Carreira, A. Devitt, L. Jacobs, I.T. Silva, G. Coakley, D.N. Nunes, D. Carter, G. Palmisano, E. Dias-Neto, Technical challenges of working with extracellular vesicles, Nanoscale, 10 (2018) 881-906.

[24] L. Brown, J.M. Wolf, R. Prados-Rosales, A. Casadevall, Through the wall: extracellular vesicles in Gram-positive bacteria, mycobacteria and fungi, Nat Rev Micro, advance online publication (2015).

[25] A. Kulp, M.J. Kuehn, Biological Functions and Biogenesis of Secreted Bacterial Outer Membrane Vesicles, Annu. Rev. Microbiol., 64 (2010) 163-184.

[26] J. Berleman, M. Auer, The role of bacterial outer membrane vesicles for intra- and interspecies delivery, Environ. Microbiol., 15 (2013) 347-354.

[27] H. Yonezawa, T. Osaki, S. Kurata, M. Fukuda, H. Kawakami, K. Ochiai, T. Hanawa, S. Kamiya, Outer Membrane Vesicles of Helicobacter pylori TK1402 are Involved in Biofilm Formation, BMC Microbiol., 9 (2009) 197.

[28] L.M. Mashburn, M. Whiteley, Membrane vesicles traffic signals and facilitate group activities in a prokaryote, Nature, 437 (2005) 422-425.

[29] M. Kaparakis-Liaskos, R.L. Ferrero, Immune modulation by bacterial outer membrane vesicles, Nat Rev Immunol, 15 (2015) 375-387.

[30] K. Watanabe, Bacterial membrane vesicles (MVs): novel tools as nature- and nano-carriers for immunogenic antigen, enzyme support, and drug delivery, Appl. Microbiol. Biotechnol., 100 (2016) 9837-9843.

[31] V. Gujrati, S. Kim, S.H. Kim, J.J. Min, H.E. Choy, S.C. Kim, S. Jon, Bioengineered Bacterial Outer Membrane Vesicles as Cell-Specific Drug-Delivery Vehicles for Cancer Therapy, ACS Nano, 8 (2014) 1525-1537.

[32] I. Olsen, A. Amano, Outer membrane vesicles – offensive weapons or good Samaritans?, Journal of Oral Microbiology, 7 (2015) 10.3402/jom.v3407.27468.

[33] J.L. Kadurugamuwa, T.J. Beveridge, Bacteriolytic effect of membrane vesicles from Pseudomonas aeruginosa on other bacteria including pathogens, J. Bacteriol., 178 (1996) 2767-2774.

[34] Z. Li, A.J. Clarke, T.J. Beveridge, Gram-Negative Bacteria Produce Membrane Vesicles Which Are Capable of Killing Other Bacteria, J. Bacteriol., 180 (1998) 5478-5483.

[35] D.E. Whitworth, Chapter 1 - Myxobacterial Vesicles: Death at a Distance?, in: S.S. Allen I. Laskin, M.G. Geoffrey (Eds.) Adv. Appl. Microbiol., Academic Press, 2011, pp. 1-31.

[36] T. Hoffmann, D. Krug, N. Bozkurt, S. Duddela, R. Jansen, R. Garcia, K. Gerth, H. Steinmetz, R. Müller, Correlating chemical diversity with taxonomic distance for discovery of natural products in myxobacteria, Nature Communications, 9 (2018) 803.

[37] J.E. Berleman, J.R. Kirby, Deciphering the hunting strategy of a bacterial wolfpack, FEMS Microbiol. Rev., 33 (2009) 942-957.

[38] B. Norén, K.B. Raper, Antibiotic activity of Myxobacteria in relation to their bacteriolytic capacity, J. Bacteriol., 84 (1962) 157-162.

[39] B.S. Goldman, W.C. Nierman, D. Kaiser, S.C. Slater, A.S. Durkin, J.A. Eisen, C.M. Ronning, W.B. Barbazuk, M. Blanchard, C. Field, C. Halling, G. Hinkle, O. Iartchuk, H.S. Kim, C. Mackenzie, R. Madupu, N. Miller, A. Shvartsbeyn, S.A. Sullivan, M. Vaudin, R. Wiegand, H.B. Kaplan, Evolution of sensory complexity recorded in a myxobacterial genome, Proceedings of the National Academy of Sciences, 103 (2006) 15200-15205.

[40] A.G.L. Evans, H.M. Davey, A. Cookson, H. Currinn, G. Cooke-Fox, P.J. Stanczyk, D.E. Whitworth, Predatory activity of Myxococcus xanthus outer-membrane vesicles and properties of their hydrolase cargo, Microbiology, 158 (2012) 2742-2752.

[41] G. Fuhrmann, R. Chandrawati, P.A. Pamar, T.J. Keane, S.A. Maynard, S. Bertazzo, M.M. Stevens, Engineering extracellular vesicles with the tools of enzyme prodrug therapy, Advanced Materials, 30 (2018) 1706616.

[42] J. Frank, M. Richter, C. De Rossi, C.-M. Lehr, K. Fuhrmann, G. Fuhrmann, Extracellular vesicles protect glucuronidase model enzymes during freeze-drying, Scientific Reports, 8 (2018) 12377.

[43] G. Fuhrmann, A. Serio, M. Mazo, R. Nair, M.M. Stevens, Active loading into extracellular vesicles significantly improves the cellular uptake and photodynamic effect of porphyrins, J. Control. Release, 205 (2015) 35-44.

[44] D. Danino, Cryo-TEM of soft molecular assemblies, Curr Opin Colloid Interface Sci, 17 (2012) 316-329.

[45] C. Pérez-Cruz, L. Delgado, C. López-Iglesias, E. Mercade, Outer-Inner Membrane Vesicles Naturally Secreted by Gram-Negative Pathogenic Bacteria, PLOS ONE, 10 (2015) e0116896.

[46] L. Zhang, Z. Cao, Y. Li, J.-R. Ella-Menye, T. Bai, S. Jiang, Softer Zwitterionic Nanogels for Longer Circulation and Lower Splenic Accumulation, ACS Nano, 6 (2012) 6681-6686.

[47] Á.M. Lőrincz, C.I. Timár, K.A. Marosvári, D.S. Veres, L. Otrokocsi, Á. Kittel, E. Ligeti, Effect of storage on physical and functional properties of extracellular vesicles derived from neutrophilic granulocytes, J Extracell Vesicles, 3 (2014) 25465.

[48] K.W. Witwer, E.I. Buzás, L.T. Bemis, A. Bora, C. Lässer, J. Lötvall, E.N. Nolte-'t Hoen, M.G. Piper, S. Sivaraman, J. Skog, C. Théry, M.H. Wauben, F. Hochberg, Standardization of sample collection, isolation and analysis methods in extracellular vesicle research, J Extracell Vesicles, 2 (2013) 20360.

[49] C. Arigita, W. Jiskoot, J. Westdijk, C. van Ingen, W.E. Hennink, D.J.A. Crommelin, G.F.A. Kersten, Stability of mono- and trivalent meningococcal outer membrane vesicle vaccines, Vaccine, 22 (2004) 629-642.

[50] E.K. Park, H.S. Jung, H.I. Yang, M.C. Yoo, C. Kim, K.S. Kim, Optimized THP-1 differentiation is required for the detection of responses to weak stimuli, Inflammation Res., 56 (2007) 45-50.

[51] M. Keck, N. Gisch, H. Moll, F.-J. Vorhölter, K. Gerth, U. Kahmann, M. Lissel, B. Lindner, K. Niehaus, O. Holst, Unusual Outer Membrane Lipid Composition of the Gram-negative, Lipopolysaccharide-lacking Myxobacterium Sorangium cellulosum So ce56, J. Biol. Chem., 286 (2011) 12850-12859.

[52] C. Ruiz, A. Ruiz-Bravo, G.A. De Cienfuegos, A. Ramos-Cormenzana, Immunomodulation by Myxospores of Myxococcus xanthus, Microbiology, 131 (1985) 2035-2039.

[53] C. Ruiz, A. Ruiz-Bravo, A. Ramos-Cormenzana, Endotoxin-like activities inMyxococcus xanthus, Curr. Microbiol., 15 (1987) 343-345.

[54] E.J. O'Donoghue, A.M. Krachler, Mechanisms of outer membrane vesicle entry into host cells, Cell. Microbiol., 18 (2016) 1508-1517.

[55] K. Forier, K. Raemdonck, S.C. De Smedt, J. Demeester, T. Coenye, K. Braeckmans, Lipid and polymer nanoparticles for drug delivery to bacterial biofilms, J. Control. Release, 190 (2014) 607-623.

[56] S. Baumann, J. Herrmann, R. Raju, H. Steinmetz, K.I. Mohr, S. Hüttel, K. Harmrolfs, M. Stadler, R. Müller, Cystobactamids: Myxobacterial Topoisomerase Inhibitors Exhibiting Potent Antibacterial Activity, Angewandte Chemie International Edition, 53 (2014) 14605-14609.

[57] S. Hüttel, G. Testolin, J. Herrmann, T. Planke, F. Gille, M. Moreno, M. Stadler, M. Brönstrup, A. Kirschning, R. Müller, Discovery and Total Synthesis of Natural Cystobactamid Derivatives with Superior Activity against Gram-Negative Pathogens, Angewandte Chemie International Edition, 56 (2017) 12760-12764.

[58] T. Bjarnsholt, O. Ciofu, S. Molin, M. Givskov, N. Hoiby, Applying insights from biofilm biology to drug development - can a new approach be developed?, Nat Rev Drug Discov, 12 (2013) 791-808.

[59] S.A.A. Kooijmans, L.A.L. Fliervoet, R. van der Meel, M.H.A.M. Fens, H.F.G. Heijnen, P.M.P. van Bergen en Henegouwen, P. Vader, R.M. Schiffelers, PEGylated and targeted extracellular vesicles display enhanced cell specificity and circulation time, J. Control. Release, 224 (2016) 77-85.

[60] K. Fuhrmann, G. Fuhrmann, Recent advances in oral delivery of macromolecular drugs and benefits of polymer conjugation, Curr Opin Colloid Interface Sci, 31 (2017) 67-74.

Supplementary Information

Biocompatible bacteria-derived vesicles show inherent antimicrobial activity

Eilien Schulz, Adriely Goes, Ronald Garcia, Fabian Panter, Marcus Koch, Rolf Müller, Kathrin Fuhrmann and Gregor Fuhrmann*

Figure S1. Growth curve and cell morphology of myxobacteria.
Figure S2. Protein and particle concentration of collected fractions from SEC.
Table S1. Physico-chemical characteristics of myxobacterial OMVs.
Figure S3. Complementary liposome control experiments.
Figure S4. Complementary confocal fluorescence images of OMVs incubated with *E. coli*.
Figure S5. Mean fluorescence of labelled OMVs and liposomes used for *in vitro* imaging and control confocal fluorescence microscopy images.
Figure S6. Complementary z-stack confocal fluorescence images of OMVs incubated with *E. coli*.
Figure S7. Predatory behaviour of Cbv34 myxobacteria on *E. coli.*
Figure S8. Liquid chromatography-mass spectrometry based identification of Cystobactamid 919-1 in the methanolic crude extract of Cbv34 OMVs.
Figure S9. Comparison of the MS^2 spectrum of Cystobactamid 919-1 from Cbv34 OMVs to the MS^2 spectrum of Cystobactamid 919-1 reference standard.
Figure S10. Antimicrobial activity of Cbv34 OMVs compared to free cystobactamid.
Figure S11. Dose response of Cbv34 OMVs obtained from lower passage numbers.

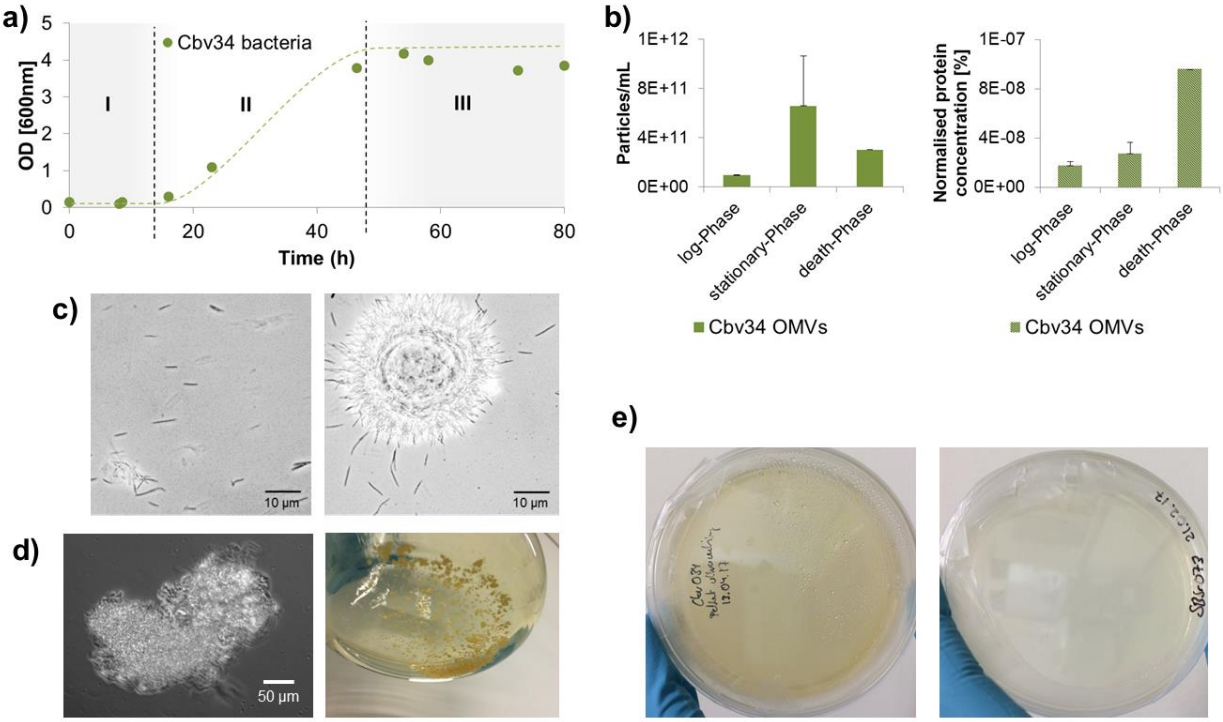

Figure S1. Growth curve and cell morphology of myxobacteria. **a)** Growth curve of Cbv34 bacteria during (I) lag-phase, (II) log-phase and (III) stationary-phase. Cbv34 grow in high density and with a doubling time of tD_{Cbv34}= 4.7 h ± 1.0; Mean, *n* = 3-4. Cbv34 bacteria were grown in M medium (1.0% bacto peptone, 1.0% maltose, 0.2% CaCl2, 0.1% MgSO4, 50 mM HEPES pH 7.2 and 8 mg/L Fe-EDTA) at 30 °C and maintained at 180 rpm. A growth curve of SBSr073 bacteria could not be taken as this culture formed aggregates and the OD could not be measured. SBSr073 bacteria were cultured in 2SWT medium (Bacto tryptone 0.3%, Soytone 0.1%, Glucose 0.2%, Soluble starch 0.2%, Maltose monohydrate 0.1%, Cellobiose 0.2%, $CaCl_2$ $2H_2O$ 0.05%, $MgSO_4$ $7H_2O$ 0.1%, HEPES 10mM, pH 7.0 adjusted with KOH) **b)** Cbv34 OMV characteristics during different growth phases: particle concentration and protein concentration normalised by particle concentration. *n* = 3. **c)** Bright field microscopy images of Cbv34 in culture and after inoculation from a cryo stock. **d)** Bright field microscopy images of myxobacteria SBSr073 and photograph of clumpy bacteria containing flask. **e)** When plating 100 µL of EV-pellet isolated from SBSr073 and Cbv34 for 8 days on 1.5% (w/v) agar no bacterial growth was detected. Agar plates were prepared using the liquid culture media of each bacterium.

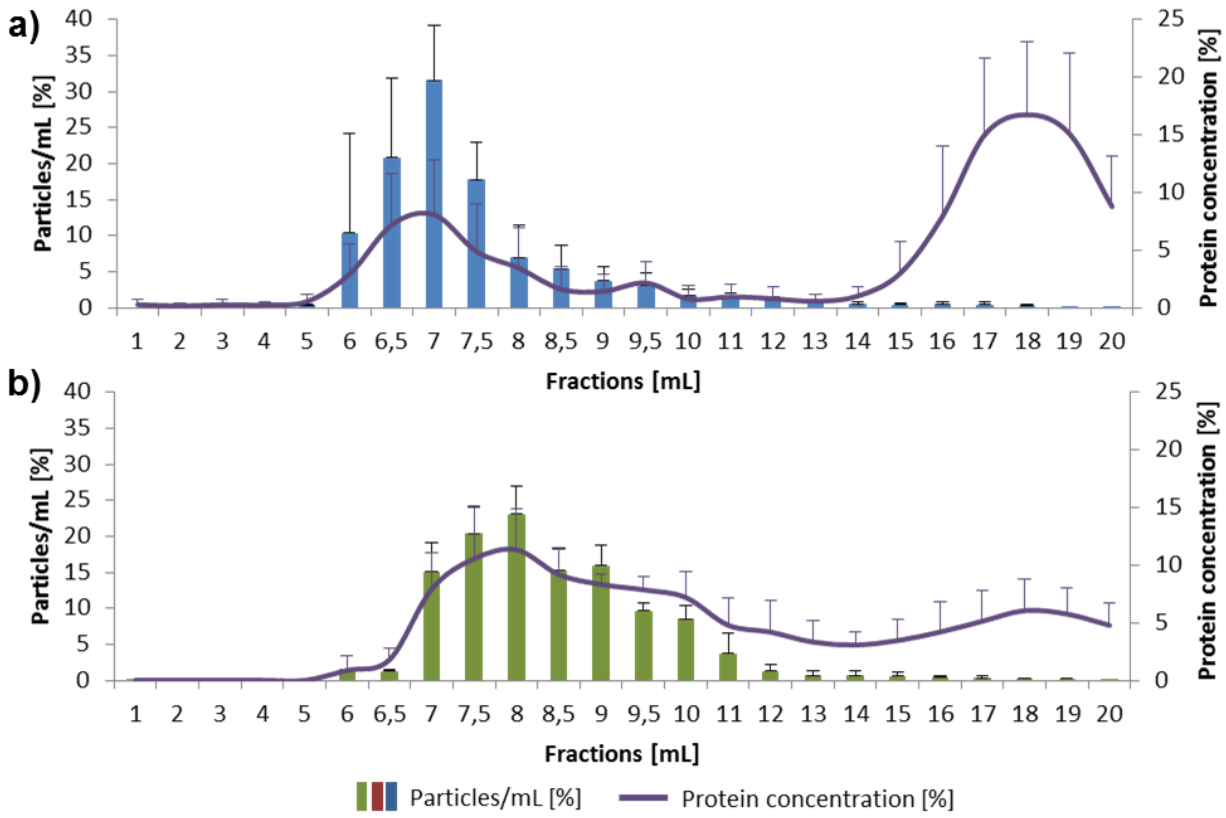

Figure S2. Protein and particle concentration of collected fractions from SEC. a) SBSr073 OMVs, **b)** Cbv34 OMVs; the sum of all values corresponds to 100%. Each fraction corresponds to the percentage of the total concentration (particles or proteins). Mean ± SD, *n* = 3-7

Table S1. Physico-chemical characteristics of myxobacterial OMVs.

OMV source	Particle size ± SD measured by NTA (n = 16-27)	PDI (n = 3)	Total protein concentration OMVs [µg/mL] (n = 4-7)	ξ-potential (n = 3)
SBSr073	194 ± 18 nm	0.143 ± 0.01	8.0 ± 4.0 µg/mL	-6.81 ± 0.61 mV
Cbv34	145 ± 27 nm	0.222 ± 0.06	84.8 ± 71.7 µg/mL	-4.76 ± 0.65 mV

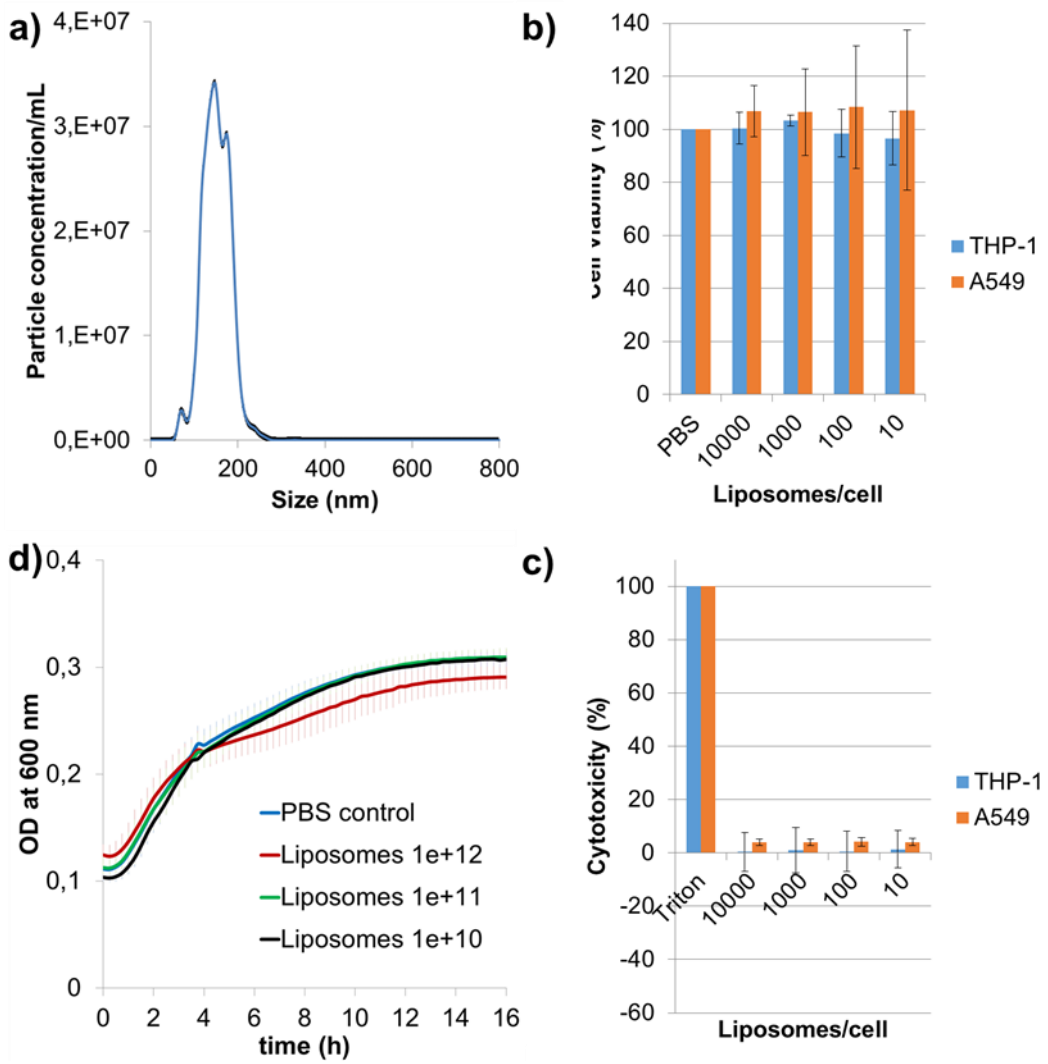

Figure S3. Complementary liposome control experiments. a) Size distribution of liposomes (1,2-dimyristoyl-sn-glycero-3-phosphorylcholine (DMPC) and dipalmitoyl phosphatidylcholine (DPPC) at a ratio of 2:3 mol%) measured by NTA (representative sample). **b)** Cell viability of liposomes when incubated for 24 h with stimulated dTHP-1-1 macrophage cells and A549 epithelial cells, and **c)** lactate-dehydrogenase cytotoxicity assay of liposomes incubated for 24 h with dTHP-1-1 and A549 cells. Mean ± SD, *n* = 3–4. **c**) Growth curve of *E. coli* DH5-alpha incubated with different concentration of liposomes or PBS (control). Mean ± SD, *n* = 3

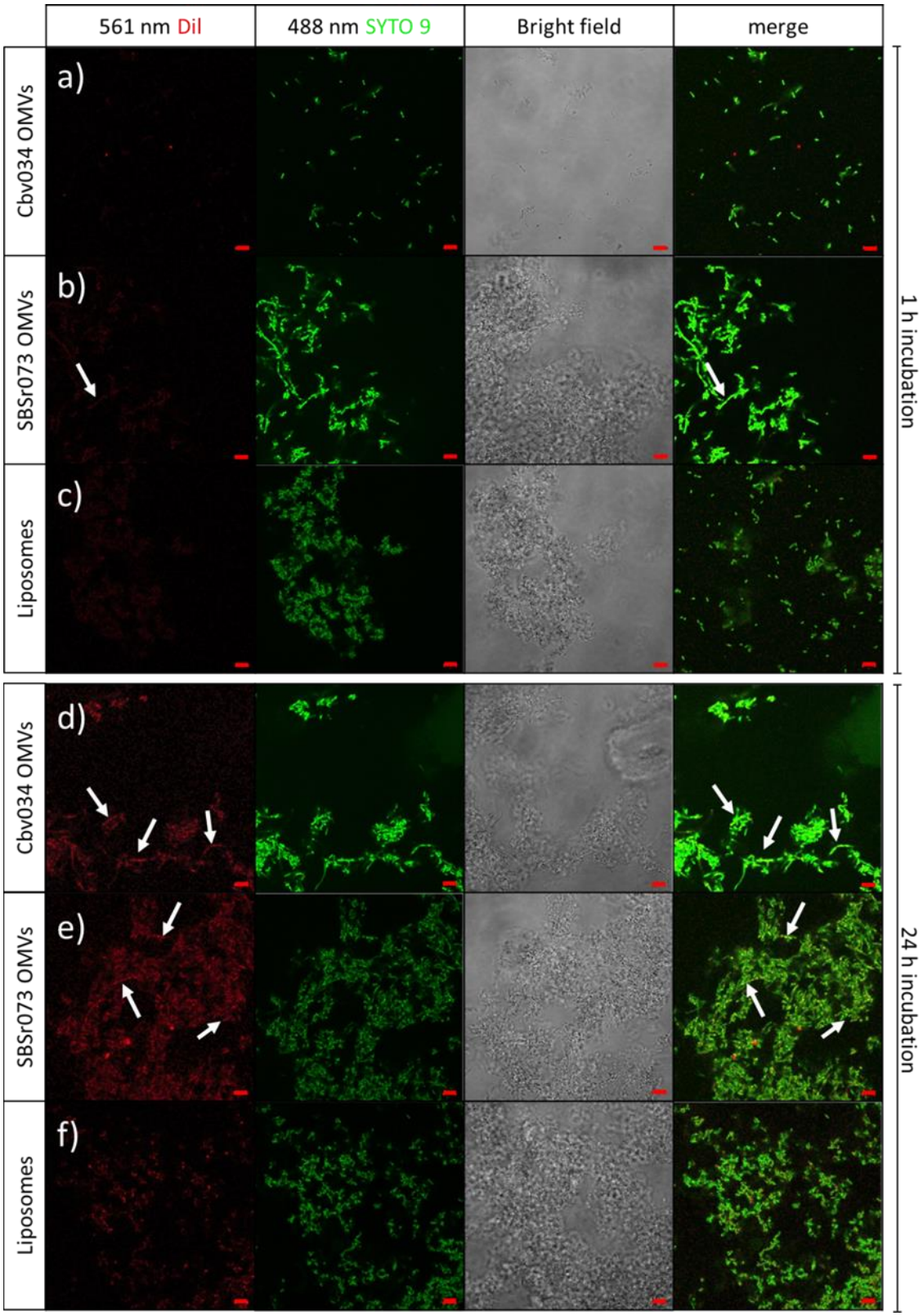

Figure S4. Complementary confocal fluorescence images of *E. coli* incubated with OMVs. 1 h incubation of *E. coli* DH5-alpha with **a)** fluorescently-labelled Cbv34 OMVs, **b)** SBSr073 OMVs, and **c)** liposomes. 24 h incubation of *E. coli* DH5-alpha with **d)** fluorescently-labelled Cbv34 OMVs, **e)** SBSr073 OMVs, and **f)** liposomes. Images were taken using the same settings at 561 nm laser (red colour) and 488 nm laser (green colour). For visualisation,

bacteria were stained with SYTO 9. Scale bars are 5 µm. Measurement settings and image analysis is similar for all images.

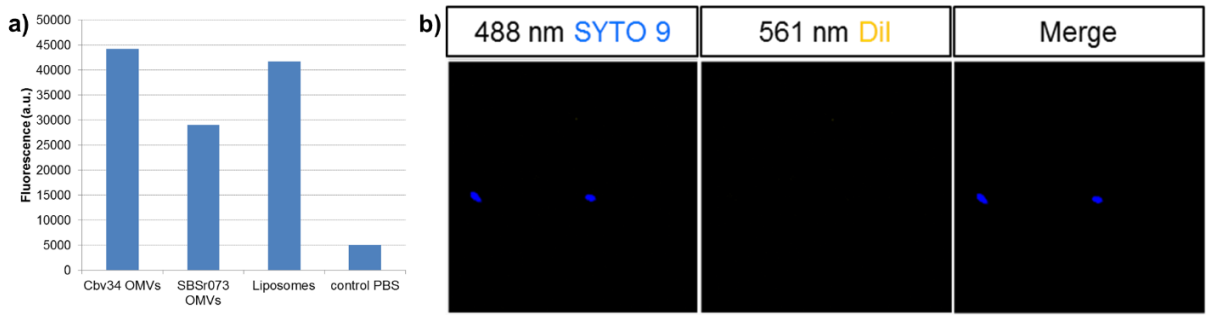

Figure S5. Mean fluorescence of labelled OMVs and liposomes used for *in vitro* imaging and control confocal fluorescence microscopy images. a) Detection of fluorescence upon DiI labelling (ex 490nm/em 570 nm) in the most abundant SEC fractions of Cbv34 OMVs (10^{11} particles/mL)**,** SBSr073 OMVs (10^{10} particles/mL), and liposomes (10^{11} particles/mL). Representative measurement using PBS as control. **b**) Representative confocal fluorescence images of *E. coli* incubated for 24 h with DiI dye alone and in absence of OMVs. All measurement and image analysis settings are similar to those in the main **Figure 3**.

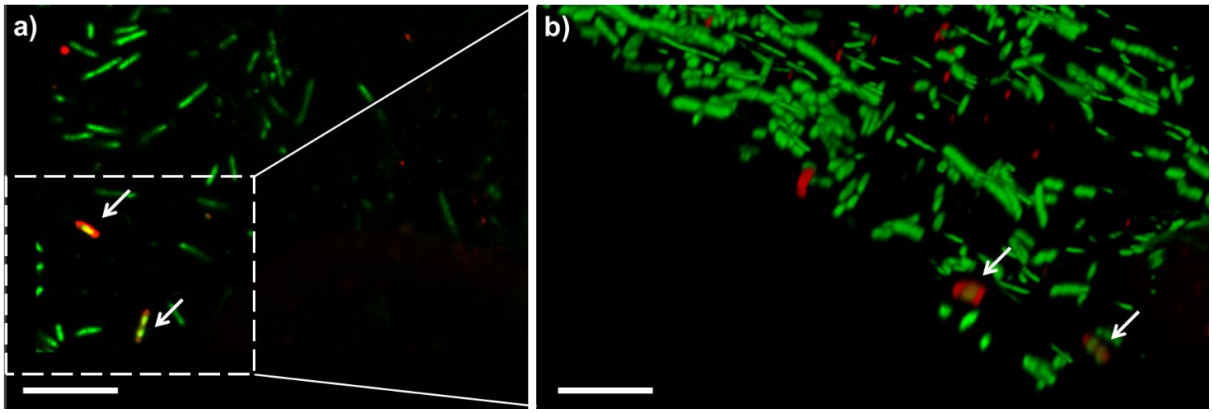

Figure S6. Complementary z-stack confocal fluorescence images of *E. coli* incubated with OMVs*.* 24 h incubation of *E. coli* DH5-alpha with DiI-labelled Cbv34 OMVs (red). **a**) Top view confocal image, **b**) 3D-image of marked rectangle in a) using z-stack mode. Images were taken using the same settings at 561 nm laser (red colour) and 488 nm laser (green colour). For visualisation, bacteria were stained with SYTO 9 (in green).

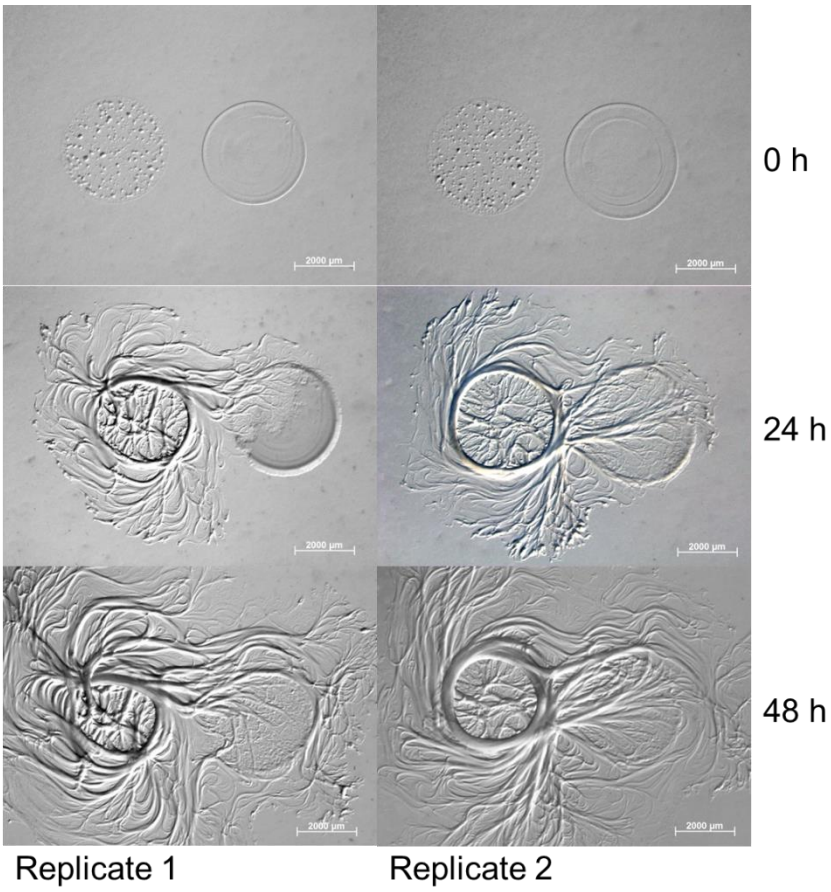

Figure S7. Predatory behaviour of Cbv34 myxobacteria on *E. coli.* Myxobacteria (left) and *E. coli* (right, DSM 1116) were seeded on VY/2 agar and both incubated for up to 48 h at 30 °C. VY/2 agar contains baker's yeast 5.00 g, CaCl2 x 2 H2O 1.36 g, Vitamin B12 0.50 mg, Agar 15.00 g and distilled water 1000.0 mL (DSMZ recipe).

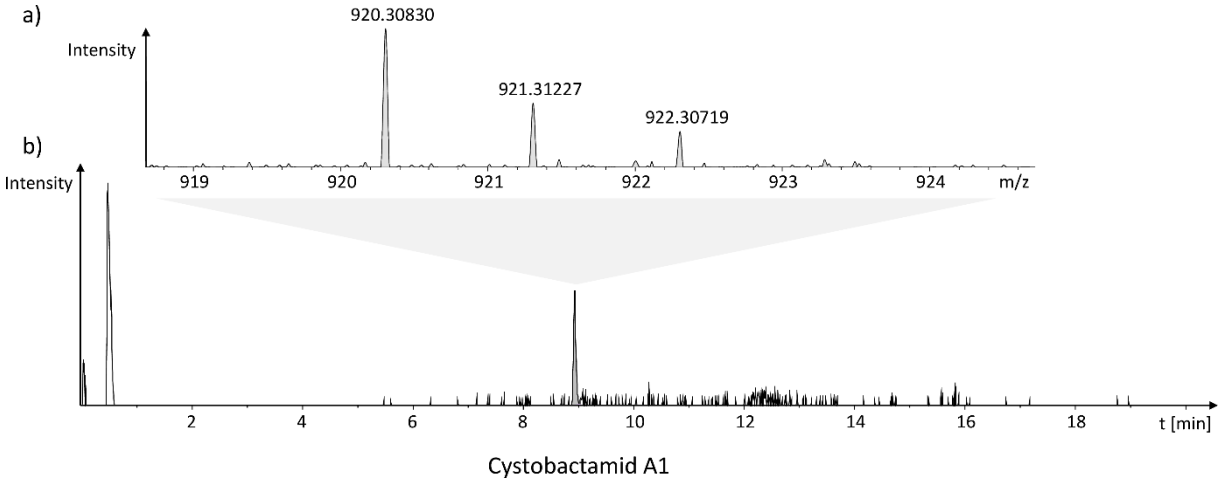

Figure S8. LC-MS based identification of Cystobactamid 919-1 in the methanolic crude extract of Cbv34 OMVs. UHPLC-HRMS chromatogram acquired on the Dionex Ultimate 3000 RSLC coupled to a Bruker maXis 4G qTOF mass spectrometer. 1 mL of methanolic OMV extract is separated, **b)** depicts the EIC at 920.309 ± 0.02 Da across the chromatogram visualising the Cystobactamid 919-1 peak, **a)** depicts the magnified mass spectrum at maximum intensity for the Cystobactamid 919-1 peak.

Mass spectra were acquired in centroid mode ranging from 150 – 2500 m/z at a 2 Hz full scan rate. Mass spectrometry source parameters were set to 500V as end plate offset; 4000V as capillary voltage; nebuliser gas pressure 1 bar; dry gas flow of 5 l/min and a dry temperature of 200 °C. Ion transfer and quadrupole settings are set to Funnel RF 350 Vpp; Multipole RF 400 Vpp as transfer settings and Ion energy of 5eV as well as a low mass cut of 300 m/z as Quadrupole settings. Collision cell was set to 5.0 eV and pre pulse storage time is set to 5 µs. Spectra acquisition rate was set to 2Hz. Calibration is done automatically before every LC-MS run by injection of sodium formiate and calibration on the sodium formiate clusters forming in the ESI source. All MS analyses were acquired in the presence of the lock masses $C_{12}H_{19}F_{12}N_3O_6P_3$; $C_{18}H_{19}O_6N_3P_3F_2$ and $C_{24}H_{19}F_{36}N_3O_6P_3$ which generate the $[M+H]^+$ ions of 622.028960; 922.009798 and 1221.990638. LCMS data are annotated using the in-house *MXbase* myxobacterial metabolome data at Helmholtz Institute for Pharmaceutical Research Saarland by automated comparison of retention time, exact mass and isotope pattern accuracy using Bruker Daltonics Target analysis 1.3.

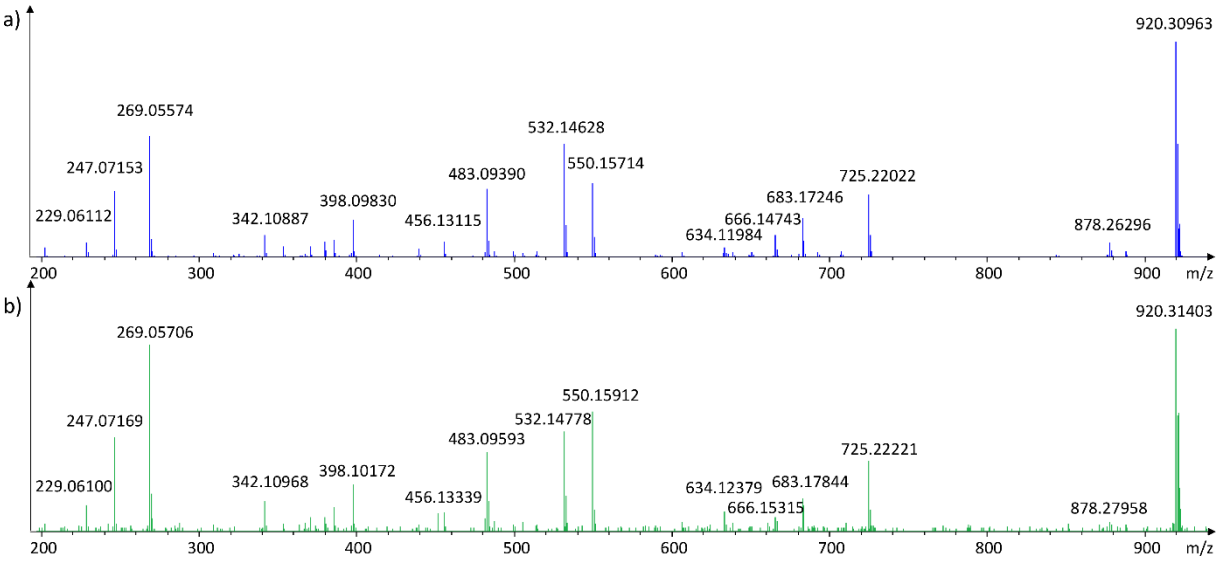

Figure S9. Comparison of the MS² spectrum of Cystobactamid 919-1 from Cbv34 OMVs to the MS² spectrum of Cystobactamid 919-1 reference standard. HRMS² spectrum of **a)** cystobactamid 919-1 standard and **b)** cystobactamid 919-1 in Cbv34 OMVs on the Bruker maXis 4G qTOF spectrometer to verify the identified peak as cystobactamid 919-1. Identified fragments show excellent agreement to the reference substance. LC and MS conditions for scheduled precursor list (SPL) guided MS² data acquisitions were kept constant according to section standardised UHPLC-MS conditions. MS² data acquisition parameters were set to exclusively fragment SPL entries. SPL entries were edited manually to selectively target the precursor mass of cystobactamid 919-1. SPL tolerance parameters for precursor ion selection were set to 0.2 minutes and 0.05 m/z in the SPL MS/MS method. CID Energy is ramped from 35 eV for 500 m/z to 45 eV for 1000 m/z and 60 eV for 2000 m/z. MS full scan acquisition rate was set to 2Hz and MS/MS spectra acquisition rates were ramped from 1 to 4 Hz for precursor ion intensities of 10 kcts to 1000 kcts.

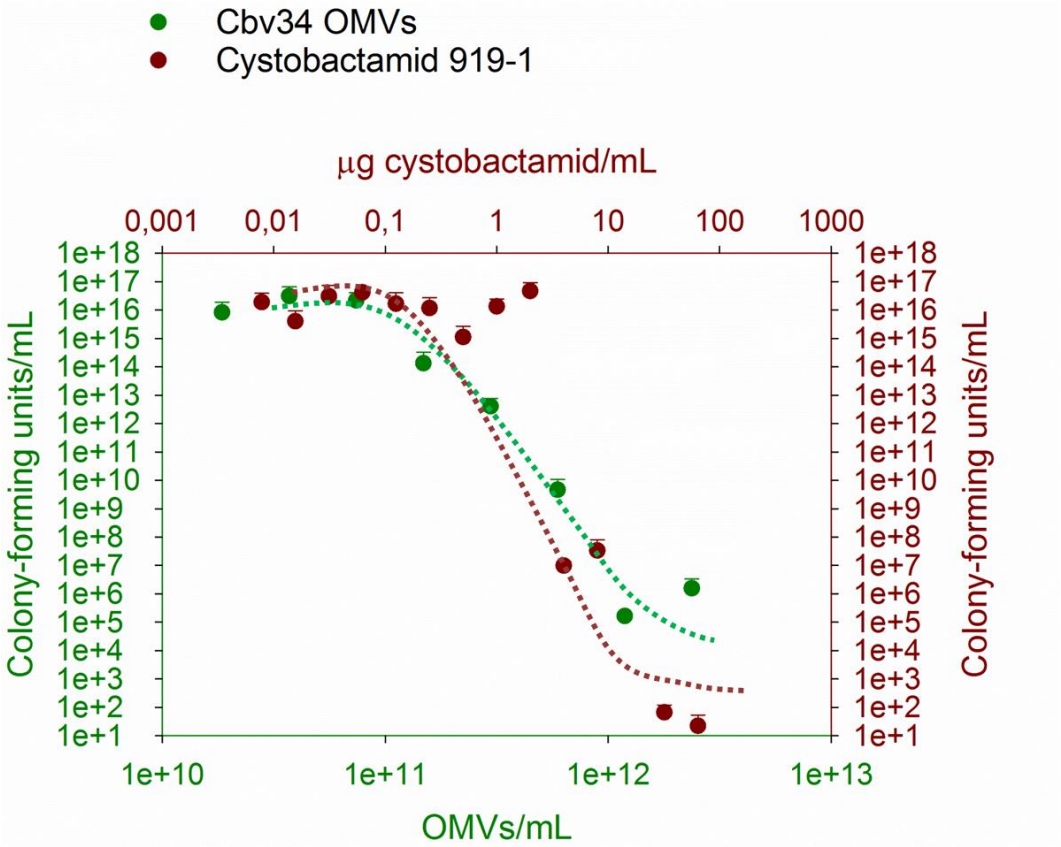

Figure S10. Antimicrobial activity of Cbv34 OMVs compared to free cystobactamid. OMVs from Cbv34 and cystobactamid 919-1 were incubated with *E. coli* at different concentrations. Colony-forming units were counted for both samples. Mean ± SD, *n* = 3.

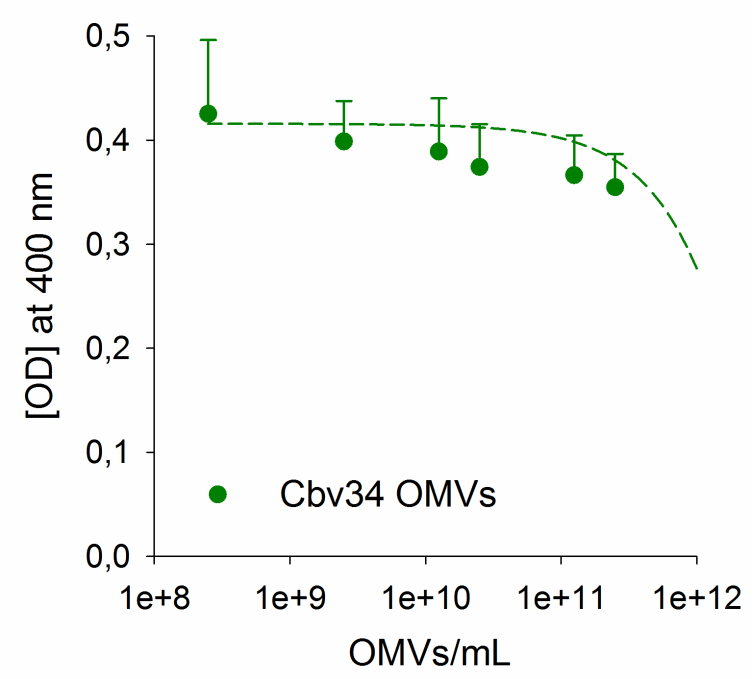

Figure S11. Dose response of Cbv34 OMVs obtained from lower passage numbers. Cbv34 myxobacteria were brought into culture from cryo stock and used during passages 1-4. During these lower passage numbers, OMVs isolated from culture supernatant showed a lower antimicrobial activity as seen from the dose response curve. The curve was obtained by incubating increasing concentrations of low passage Cbv34 OMVs with *E. coli*. Mean, *n* = 3.

7.2. Hot EVs - How temperature affects extracellular vesicles

Eilien Schulz, Anna Karagianni, Marcus Koch, Gregor Fuhrmann

European Journal of Pharmaceutics and Biopharmaceutics. 2020, 146, 55-63

DOI: 10.1016/j.ejpb.2019.11.010

European Journal of Pharmaceutics and Biopharmaceutics 146 (2020) 55–63

Contents lists available at ScienceDirect

European Journal of Pharmaceutics and Biopharmaceutics

journal homepage: www.elsevier.com/locate/ejpb

Hot EVs – how temperature affects extracellular vesicles

Eilien Schulz [1,2], Anna Karagianni [1], Marcus Koch [3], Gregor Fuhrmann [1,2]*

[1] Biogenic Nanotherapeutics Group (BION), Helmholtz Centre for Infection Research (HZI), Helmholtz Institute for Pharmaceutical Research Saarland (HIPS), Campus E8.1, Saarbrücken 66123, Germany

[2] Department of Pharmacy, Saarland University, Campus E8.1, Saarbrücken 66123, Germany

[3] INM – Leibniz Institute for New Materials, Campus D2.2, Saarbrücken 66123, Germany

*__Corresponding author__, phone: +49 68198806 1500, Email: gregor.fuhrmann@helmholtz-hzi.de

ORCID IDs: Eilien Schulz: 0000-0002-9769-8980, Anna Karagianni: 0000-0002-0831-1247, Gregor Fuhrmann: 0000-0002-6688-5126

Keywords: extracellular vesicles, outer membrane vesicles, lymphoblastoid cells, myxobacteria, drug carriers, flow cytometry, heat stability, autoclaving

Abstract

In recent years, extracellular vesicles (EVs) and outer membrane vesicles (OMVs) have become an extensive and diverse field of research. They hold potential as diagnostic markers, therapeutics and for fundamental biological understanding. Despite ongoing studies, numerous information regarding function, content and stability of EVs remains unclear. If EVs and OMVs ought to be used as therapeutics and in clinical environments, their stability is one of the most important factors to be considered. Especially for formulation development, EVs and OMVs need to be stable at higher temperatures. To the best of our knowledge, very little work has been published regarding heat stability of neither EVs nor OMVs. In the present study, we investigated B lymphoblastoid cell-derived EVs and OMVs derived from myxobacterial species *Sorangiineae* as model vesicles. We exposed the vesicles to 37 °C, 50 °C, 70 °C and 100 °C for 1 h, 6 h and 24 h, and also autoclaved them. Physico-chemical analysis such as size, particle concentration and protein concentration showed interestingly minor alterations, particularly at 37 °C. Flow cytometry analysis emphasised these results suggesting that after heat impact, EVs and OMVs were still able to be taken up by macrophage-like dTHP-1 cells. These data indicate that both mammalian and bacterial vesicles show intrinsic stability at physiological temperature. Our findings are important to consider for vesicle formulation and for advanced bioengineering approaches.

1. Introduction

Outer membrane vesicles (OMVs) were first mentioned 50 years ago in 1967, as Chatterjee et al detected particles in proximity to *Vibrio cholera* membranes in electron microscopy images (1). A few years later, in 1983 Pan et al. were the first ones to observe extracellular vesicles (EVs), while they monitored a transferrin receptor in sheep (2). Since then, this area of research has expanded extensively. Both, EVs and OMVs are nano-sized phospholipid bilayered assemblies and serve as transport vehicles for cell-cell communication (3). Their structure and surface is, in most cases, comparable to their cellular origin and consists of receptors, proteins or for OMVs lipopolysaccharides (4, 5). Contents may vary, but generally imply nucleic acid, proteins and secondary metabolites, such as toxins or compounds that are often unique to their origin (4-6). EVs have been isolated from a large variety of cells derived from the immune system, different tissues or the nervous system (3). OMVs, on the other hand have been isolated from almost all known gram-negative bacteria (7). Both, EVs and OMVs hold potential for the development of new therapeutics. They have already been applied in tissue repair, neurodegenerative disorders and cancer therapy (8). For example, EVs derived from mesenchymal stem cells have previously reached clinical trials as novel therapeutics for functional recovery after ischemic strokes (9). OMVs, on the other hand have been studied for vaccination, as drug delivery systems against cancer (10) or infections (11). Different routes of EV application have been established, either as intravenous suspensions or incorporated into hydrogels, for example for enzyme prodrug therapy (12, 13). Although many protocols have been established concerning vesicle isolation, the temperature stability of EVs and OMVs has not been studied comprehensively. Some publications analysed storage conditions for EV suspensions, while we and others have recently introduced a freeze-drying method using cryo-protectants (14-16). To our knowledge, very little is known to date concerning the stability of EVs and OMVs at increasing temperatures. Lee et al. studied the stability of EVs from Kaposi's sarcoma-associated herpesvirus-infected human endothelial cells and found that even after 4 days the particle concentration of samples incubated at 37 °C did not alter (17). Moreover, Cheng et al determined the particle concentration of EVs at 37 °C and at 60 °C, resulting only in minor physical changes (18). However, it is essential to estimate the heat stability of EVs and OMVs in a more comprehensive manner, as it will help to evaluate their clinical and pharmaceutical applicability. In terms of pharmaceutical applicability, heat will also play a role during spray drying (19) or in the chemical modification to attach targeting moieties (20). In addition, to understand the biological role of EVs, higher temperatures could be necessary. As extracellular vesicles are often comprised of phospholipids, such as phosphatidylcholine, sphingomyelin and phosphatidylserine, they are similar in structure compared to liposomes (21). Heat-induced fusion of EVs with liposomes may also be beneficial to form new biocompatible nanocarriers (22). For intravenous injection, EVs need to be sterile as an aseptic

production is not always possible. Sterilisation methods such as filtration may result in a loss of sample, leading to concentration issues (23). Pressurised saturated steam sterilisation, autoclaving may be convenient and quick, but potentially harsh method to obtain sterile vesicles for clinical applications.

Here, we used EVs derived from B lymphoblastoid cells (RO cells). They are a well-defined and commercially available cell line obtained from a patient with severe combined immunodeficiency, not expressing MHC class II complexes (24, 25). Thus, RO cell derived EVs may be low in immunogenicity. The cells can be grown in suspension and, therefore can be easily cultivated even in large quantities. We also established a method to cultivate RO cells in a low space consuming manner. As a second model vesicle we studied OMVs derived from the myxobacterial strain SBSr073. Myxobacteria are gram-negative, soil living bacteria, that are producer of a large variety of secondary metabolites (26). We recently showed that SBSr073 OMVs are non-toxic to human cells and have the potential to be further developed as a drug carrier system (11). As myxobacteria are found in various environments including deserts (27), we hypothesised that the OMVs they produce may be more resistant to high temperatures compared to human EVs, which are adapted to a body temperature of 37 °C.

2. Materials and Methods

2.1. Cell culture

B lymphoblastoid cells (RO cells) (DSMZ, ACC 452, Braunschweig, Germany) were cultured in T75 flasks with an initial seeding density of $0.75*10^6$ cells/mL. After thawing cells, they were grown in RPMI (Gibco) with 15% (v/v) foetal calve serum (FCS) (25). Before EV isolation, RPMI with 10% (v/v) insulin-transferrin-selenium-ethanolamine (Thermo Fischer) was used. Cultures started with a volume of 45 mL in an upright position. After 3 days, 25 mL supernatant was removed and replaced with 50 mL fresh medium. Another subsequent 4 days later, 50 mL supernatant was removed for EV isolation. Supernatants were stored at -80 °C up to 2 months. Cells were used until passage 40. THP-1 cells were cultivated in RPMI with 10 % (v/v) FCS. Alternating, cells were seeded with an initial density of 2 or 3 million cells and cultivated for 3 or 4 days.

2.2. Microbial culture

SBSr073 myxobacteria (kindly provided by Rolf Müller, Department of Microbial Natural Products, Helmholtz Institute for Pharmaceutical Research, Saarbrücken) were cultivated as described previously (11), in 2SWT medium (0.3% (m/v) bacto tryptone, 0.1% (m/v) soytone, 0.2% (m/v) glucose, 0.2% (m/v) soluble starch, 0.1% (m/v) maltose monohydrate, 0.2% (m/v) cellobiose, 0.05% (m/v) $CaCl_2*2H_2O$, 0.1% (m/v) $MgSO_4*7H_2O$ and 10mM HEPES, pH 7.0 adjusted with KOH). The bacterial suspension was cultivated at 30 °C and shaken at 180 rpm (Ecotron, Infors HT, Bottmingen, Switzerland) for one week until OMV isolation. As this strain forms aggregates, it was not possible to determine a growth curve based neither on optical density measurements, nor on colony forming unit counting (11). OMVs were isolated from cultures cultivated until passage 6.

2.3. Isolation and purification of EVs and OMVs

Fifty millilitres of RO supernatant were first centrifuged at 300 × g for 8 min to remove cells. Forty millilitre were then transferred to a new tube and centrifuged at 9,500 × g for 15 min. SBSr073 supernatant was first centrifuged at 9,500 × g for 10 min to remove bacteria (28). Forty millilitre of this supernatant were centrifuged, at 9,500 × g for 15 min. Both samples were then ultracentrifuged at 100,000 × g for 2 h at 4 °C (Rotor SW 32 Ti, Beckman Coulter, Brea, USA) (29). Pellets were resuspended in either 400 µL phosphate buffered saline (PBS, Gibco PBS tablets without calcium, magnesium and phenol red) or, in case of RO EVs, in 500 µL cell culture supernatant. Vesicles were purified by size exclusion chromatography, using a 30 mL (SBSr073 OMVs) or a 10 mL (RO EVs) sepharose CL-2B (GE Life Science, United Kingdom) column, collecting 1 mL fractions with PBS as elution buffer.

2.4. Physico-chemical characterisation of EVs and OMVs

Nanoparticle Tracking Analysis (NTA LM-10, Malvern, Malvern, United Kingdom) was used to determine particle concentrations and their hydrodynamic diameter (30). Samples were diluted up to 1000 fold in order to have a concentration of 10 to 100 particles per frame. A 30 s video at a camera level of 14 to 15 was recorded 3 times before the particle concentration was calculated by NanoSight 3.3 software with a detection threshold of 5. A bicinchoninic assay kit (Sigma Aldrich) was used to quantify protein concentrations of each sample in duplicates, according to the manufacturer's specifications before and after heat treatment. To quantify the total protein content in vesicles, 25 µL of RIPA buffer (50 mM Tric-HCl, 150 mM NaCl, 0,5%

deoxycholic acid, 1% NP-40, 0,1% sodium-dodecyl-sulfate) were incubated with 75 µL of sample for 5 min before another bicinchoninic assay was performed.

2.5. Heat testing

The two SEC fractions with the highest particle concentration were pooled (final volume 2 mL), transferred to glass containers, airtight sealed with caps and used for heat experiments. Samples were incubated in an incubator (Memmert UN 75, Schwabach, Germany) with a constant temperature of 37 °C, 50 °C, 70 °C or 100 °C. After 1 h, 6 h and 24 h evaporated water was measured by weight difference, replaced and samples were used for further experiments. To autoclave vesicles, they were injected into brown glass containers with rubber plugs and sealed with metal caps (Zscheile & Klinger GmbH, Hamburg, Germany) and heated up to 121 °C for 20 min at 2 bar. The temperature of a water control with the same volume was used. According to the European Pharmacopoeia, this method is one of the recommended methods for sterilisation (31). To test sterility, 100 µL of autoclaved samples were incubated on lysogeny broth agar plates (Sigma Aldrich) for 4 days at 37 °C.

2.6. Electron microscopy

To perform cryogen electron cryomicroscopy, vesicles were concentrated using centrifugal filters (Ultracel YM – 30) until one-hundredth of volume was left. Three microliters of this solution was placed onto a holey carbon film (type S147-4, Plano, Wetzlar, Germany) and plotted for 2s with a Gatan ((Pleasanton, CA, US) cryoplunger model CP3, before plunging into liquid ethane at T = 108 K. Under liquid nitrogen, vesicles were transferred to a Gatan model 914 cryo-TEM sample holder. At T = 100 K samples were imaged via bright field TEM (JEM-2100 LaB6, Jeol, Akishima, Tokio, Japan) under low-dose conditions.

2.7. FACS analysis of THP-1 with vesicles

OMVs and EVs were stained with 2 µL of DiI (Vybrant DiI Cell-labelling solution 1 mM) for 15 min at 37 °C. A size exclusion chromatography with sepharose CL-2B was performed to remove non-incorporated dye. Fluorescence intensity (λ_{Ex}/ λ_{Em} 490/570 nm) was measured for each sample. The fraction with the highest intensity was used for further experiments. It is important to mention, that autoclaved samples had to be centrifuged for 2.5 min at 9,500 × g in order to remove dye aggregates induced by heat and pressure. THP-1 (DSMZ, ACC16, Braunschweig, Germany) were seeded into 48 well plates with a density of 200,000 cells per well. THP-1 were stimulated with 7.5 ng/mL phorbol 12-myristate 13-acetate (PMA) (Sigma

Aldrich) for 24 h, to stimulate the differentiation to macrophage like dTHP-1. Afterwards cells were incubated with 100 µL of each vesicle sample for 24 h, resulting in a ratio 2.5×10^5 RO EVs and 1×10^6 SBSr073 OMVs per cell. Two washing steps with PBS were carried out before cells were incubated with accutase solution (Sigma Aldrich) for 20 min at RT to detach the cells. Four wells were pooled to perform one flow cytometry (FACS) (LSRFortessa X-20, BD) analysis. Cells incubated with 100 µL PBS served as control. A red laser at 561 nm (PE phycoerythrin) was used to detect DiI labelling. Ten thousand events per sample acquired by BD FACSDiva 8.0.2, were analysed with FlowJo software version 7.6.5.

2.8. Confocal imaging

Stimulated THP-1 (see 2.8.) with a density of 200,000 cells per well, were incubated with 100 µL of each DiI labelled EV or OMV sample in an 8 well chamber plate (SPL Life Science) for 24 h. After removing the supernatant, cells were stained with fluorescein labelled wheat germ agglutinin (Vector laboratories) for 15 min at 37 °C. Subsequently, cells were fixed with 3.7 % (v/v) paraformaldehyde for 20 min at room temperature (RT). Nucleus staining was performed using a 1 µg/mL 4′,6-Diamidino-2-phenylindole dihydrochloride (DAPI) (Sigma Aldrich) solution (32). For confocal imaging (Leica TCS SB8) a 488 nm laser was used to visualise fluorescein, a 405 nm laser for DAPI and a 561 nm laser for DiI. Leica Application Suite X software was used to process the images.

2.9. Statistical analysis

All data is reported in mean (x) and standard deviation (SD), where *n* indicates the number of independent experiments. Statistical analysis was performed by SigmaPlot 14.0 using One-way ANOVA , followed by a Tukey *post-hoc* test, to compare the different groups. Significant *p*-values were stated as * for $p < 0.05$, ** for $p < 0.01$ or with the exact *p*-value.

3. Results and Discussion

3.1. Heat-induced physico-chemical alteration of vesicles

In this work, we analysed the heat stability of two different types of vesicles, EVs derived from B lymphoblastoid RO cells and OMVs derived from the myxobacterial strain SBSr073. For this, the vesicles were isolated, purified and incubated at 37 °C, 50 °C, 70 °C and 100 °C for 1 h, 6 h and 24 h. The size of EVs and OMVs remained constant at 37 °C, even after 24 h. Yet, at

higher temperatures of 50°C, 70 °C and 100 °C small changes were detected (**Fig. 1 a,d**). The particle concentration of RO EVs decreased the higher and longer the samples were incubated. The most drastically change was detected at 100 °C, when particle concentrations decreased almost tenfold (**Fig. 1 b**). SBSr073 OMVs also showed a strong particle concentration decrease after 24 h at 100 °C with a remaining 36% (**Fig. 1 e**). Contributing to this, the size distribution of vesicles treated at 37 °C for 24 h showed similar trends compared to their controls (**Fig. 2 a,c**), whereas the 100 °C samples showed stronger variations (**Fig. 2 b, d**). If one looks at the protein concentration, here again, high temperatures und longer incubations times resulted in physico-chemical alteration. Especially RO EVs showed an increase of ca. 140 % of protein concentration after 24 h at 100 °C (**Fig. 1 c**). In contrast, the protein concentration of SBSr073 samples remained relatively constant, even at high temperatures. We hypothesise, that the decrease of the particle concentration is due to a disruption of the vesicles themselves, leading to a release of encapsulated proteins and thus an increase of protein concentration. The higher the temperature, the less stable the vesicles were and the leakier these nanostructures became. Nevertheless, for both, particle and protein concentration, RO EVs altered more drastically compared to SBSr073 OMVs, suggesting a higher physico-chemical stability of bacteria derived vesicles. Contributing to this effect is the common environment both types of vesicles can be found in. As the origin of RO EVs is the human body, which is maintained at 37 °C, they are more likely stable at 37 °C. SBSr073 OMVs, however, are derived from myxobacteria, a gram-negative population that has been adapted to various environments, from the south pole and tropical rainforests to deserts (27). In order to survive, one of their communication tools, their OMVs need to be stable in those harsh conditions. It is therefore likely, that the OMVs are more stable than the EVs.

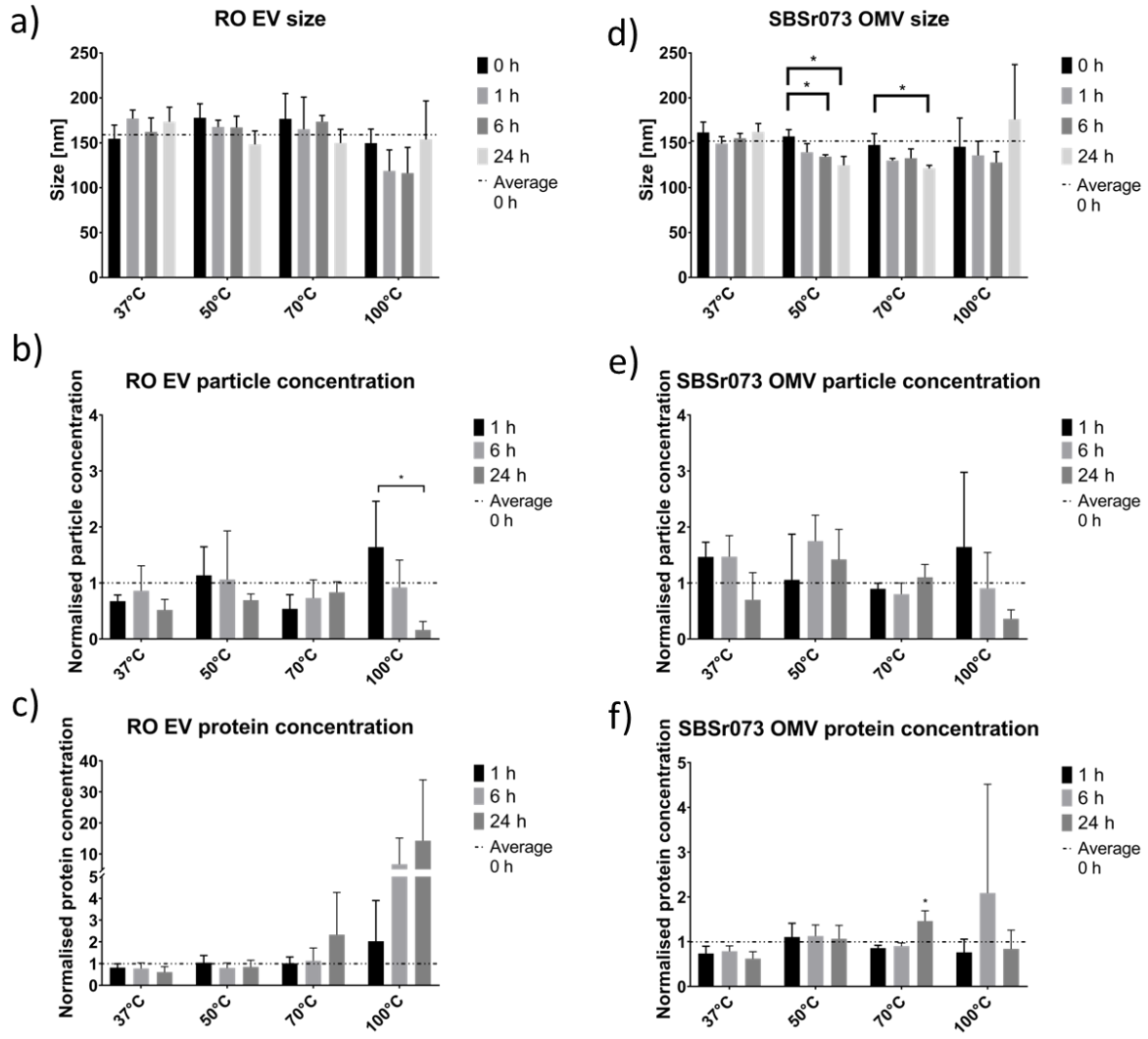

Fig 1 Physico-chemical alteration after incubation at 37 °C, 50 °C, 70 °C, 100 °C for 1 h, 6 h and 24 h. a) RO EV size distribution before and after 24 h at 37 °C b) RO EV size distribution before and after 24 h at 100 °C c) RO EV normalised particle concentration measured by NTA d) RO EV normalised protein concentration determined via BCA e) SBSr073 OMV distribution before and after 24 h at 37 °C f) SBSr073 OMV size distribution before and after 24 h at 100 °C g) SBSr073 OMV normalised particle concentration h) SBSr073 OMV normalised protein concentration. Mean ± SD, n = 3, *p < 0.05 (ANOVA followed by Tukey *post-hoc* test). Samples were normalised to particle and protein concentrations before the heat treatment. The dashed line indicates the average value of all samples at time point 0 h.

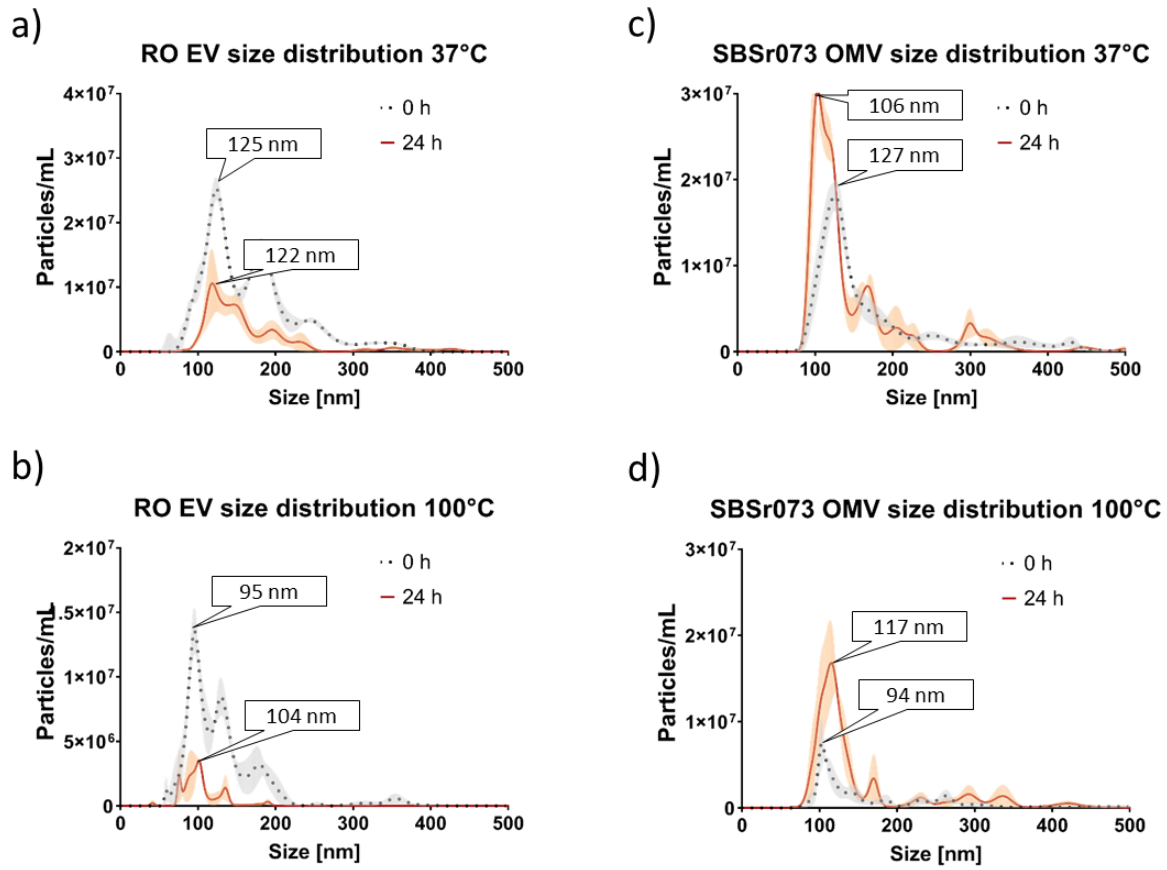

Fig 2 Representative size distribution before and after incubation at 37 °C, 100 °C for 24 h. a) RO EV size distribution after 24 h at 37 °C b) RO EV size distribution after 24 h at 100 °C c) SBSr073 OMV size distribution after 24 h 37 °C d) SBSr073 OMV size distribution after 24 h at 100 °C.

3.2. Impact of autoclaving on vesicles

Autoclaved samples showed comparable results to samples incubated at 100 °C. As seen in **Figure 3**, particle concentrations decreased while protein concentrations increased. The mean size increased slightly, and the size distribution became broader (**Fig. 3 a, b**). However, here again, the release of proteins of OMV samples was not as strong as the protein release of EVs (**Fig. 3 c, f**).

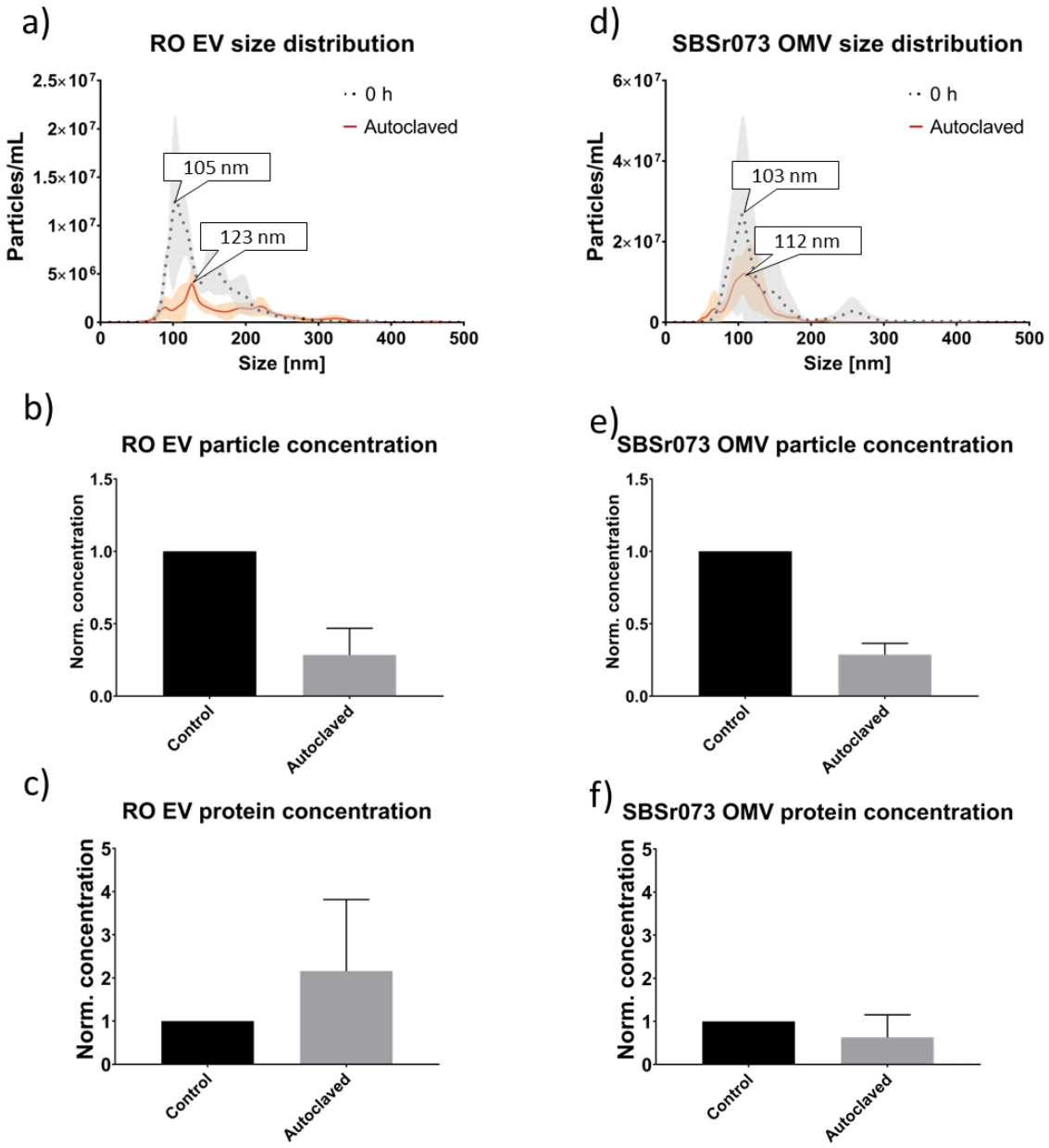

Fig 3 Physico-chemical alteration of RO EVs and SBSr073 OMVs after autoclaving. a) RO EV size distribution b) RO EV normalised particle concentration c) RO EV normalised protein concentration d) SBSr073 size distribution e) SBSr073 OMV normalised particle concentration f) SBSr073 OMV normalised protein concentration. Samples were normalised to particle and protein concentrations before autoclaving. Mean ± SD, n = 3

The alteration of the morphology of the vesicles due to the physico-chemical changes were also investigated by cryogenic electron microscopy (cryo-EM). By using cryo-EM we also wanted to verify the bulk size measurements determined by NTA. As shown in **Figure 4** the lipid bilayer of the vesicles was clearly visible and intact (white arrows). Sizes determined by cryo-EM indicated smaller diameters compared to data collected by NTA. Indeed, NTA utilises Brownian motion to calculate the hydrodynamic diameter of particles and has a detection limit

of 10 nm with low sensitivity (33). This may lead to enlarged particle sizes compared to cryo-EM imaging, where samples are most likely visualised in their native state. As purifying with a size exclusion step diluted samples, we concentrated them using centrifugal filters and compared them with resuspended pellets after ultracentrifugation. We noticed that sufficient concentrations of vesicles are crucial in order to visualise them and that results conducted by NTA often leads to an overestimation of sample concentration (33, 34). Unpurified vesicles showed debris and other artefacts that were also co-precipitated (**Fig. 3 a, f**). Subsequently, size exclusion chromatography was applied to obtain vesicles, which were then analysed by cryo-EM. With cryo-EM imaging techniques we were able to analyse single vesicles and showed that they were intact, do not form aggregates and no artefacts during the heat-treatment were formed (**Fig. 4 c,d and h, i**).

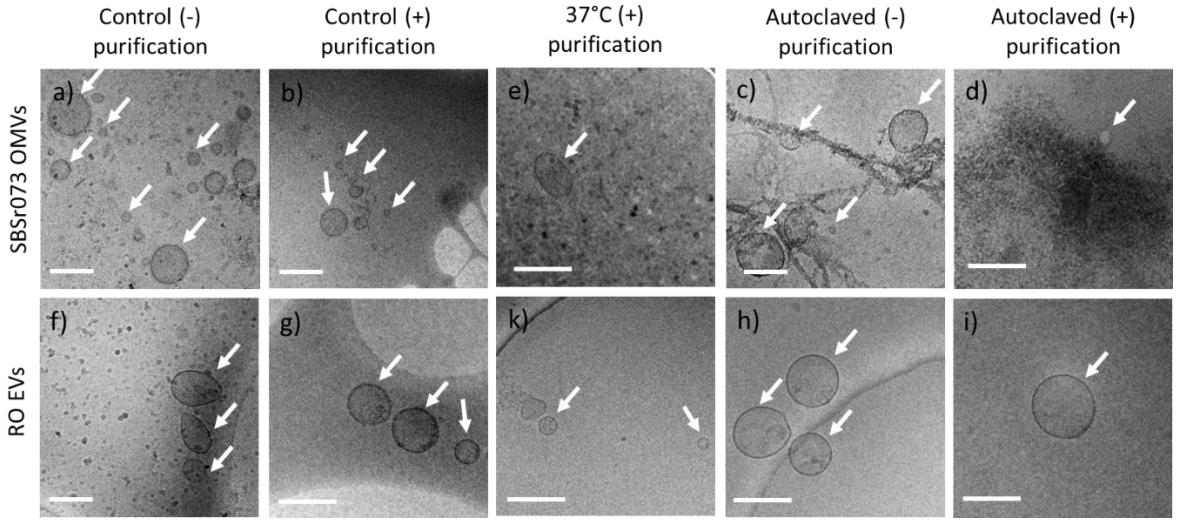

Fig 4 Cryo electron microscopy images of control and heat-treated SBSr073 OMVs and RO EVs. a) and b) SBSr073 OMVs without and with purification via SEC c) and d) respectively autoclaved SBSr073 OMVs without and with purification e) SBSr073 OMVs incubated at 37 °C for 24 h and purified f) and g) RO EV without and with purification via SEC h) and i) respectively autoclaved RO EVs without and with purification k) RO EVs incubation at 37 °C for 24 h and purified. Representative micrographs; arrows indicate presence of EVs and OMVs; scale bars are 0.2 µm.

3.3. Uptake of heat-treated vesicles in cells analysed by FACS and confocal microscopy

Next, we assessed, whether the observed physico-chemical alterations also influenced the biological behaviour of vesicles. We incubated heat-treated vesicles with stimulated macrophage-like dTHP-1 for 24 h and studied their uptake. An incubation period of 24 h was necessary to ensure vesicles had adequate time to interact with the cells. After this incubation period, fluorescence positive cells were analysed by flow cytometry (**Fig. 5**). A co-localization

of labelled vesicles and cells lead to a shift to higher signal intensities of the red phycoerythrin (PE) (λem 561 nm) laser compared to dTHP-1 cells alone, indicating vesicle uptake (**Fig. 5 a, b**). When samples were incubated at 37 °C for 24 h, interaction with dTHP-1 cells was comparable to non-heat-treated controls. Interestingly, autoclaved EVs were still substantially taken up by macrophages with at least 50 % of DiI positive THP-1 cells, whereas autoclaved OMVs resulted in even 70% of positive cells (**Fig. 5 c, d**). Control experiments using DiI in PBS and purification by SEC did not show any positive signal during FACS measurements (**Fig. S4 a, b**). Our results show that cellular uptake of vesicles does not only depend on the particle concentration itself. Additionally, we suggest that the heat treatment did not significantly interfere with the amount of vesicles taken up. As we did not normalise the samples after the heat treatment in terms of particle concentration, still a high amount of vesicles was interacting with the macrophages even though the particle concentration decreased after autoclaving (**Fig. 2 b, e and Fig. 5 c,d**).

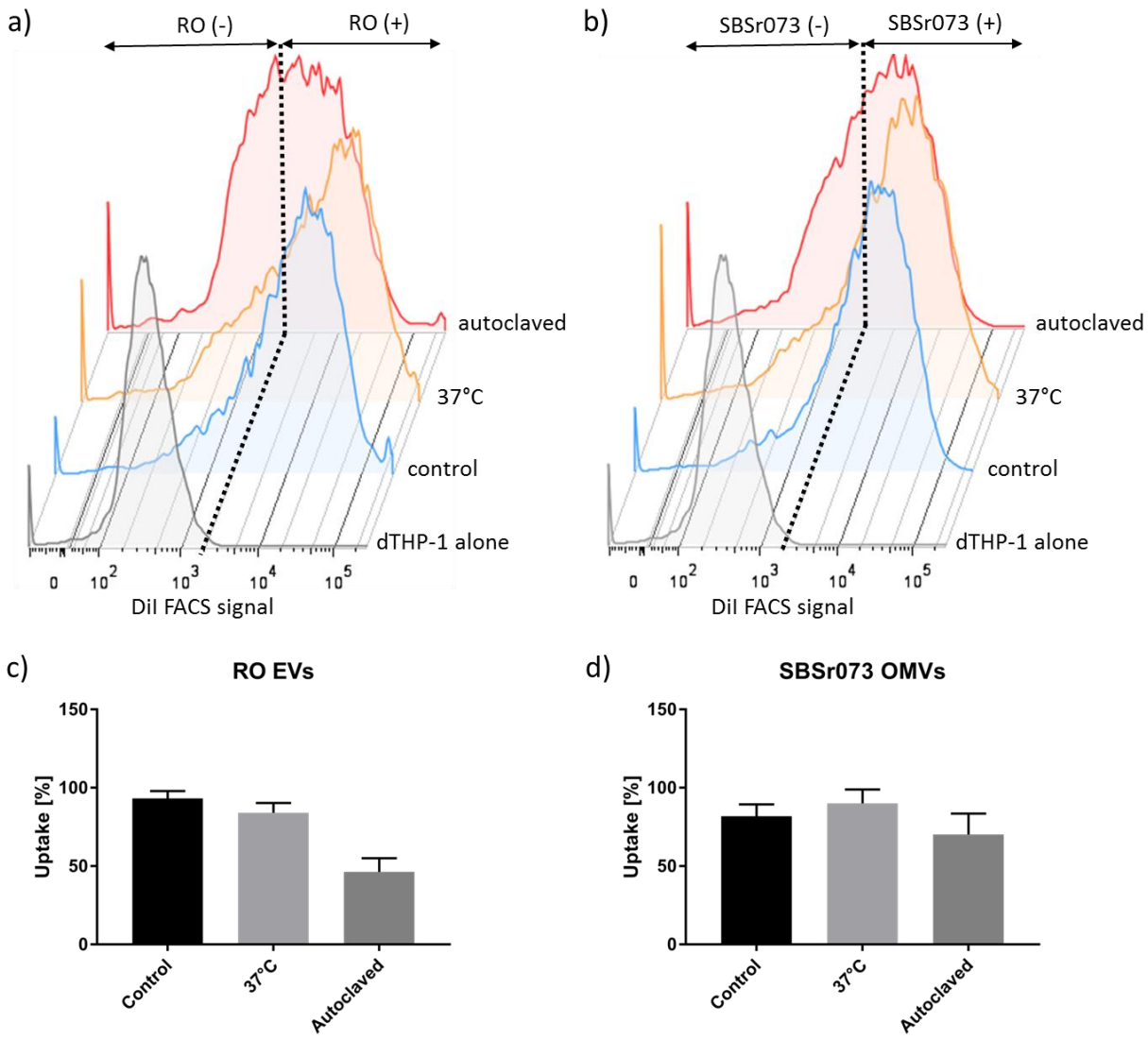

Fig 5 Interaction of RO EVs and SBSr073 OMVs with dTHP-1 upon heat treatment at 37 °C for 24 h and autoclaving and analysed by FACS a) Representative signal shift of dTHP-1 without (-) or with (+) RO EV treatment (non-treated RO EVs: blue line, RO EVs incubated at 37 °C for 24 h: orange line, RO EVs autoclaved: red line) b) Representative signal shift of dTHP-1 without (-) or with (+)SBSr073 OMV treatment (non-treated SBSr073 OMVs: blue line, SBSr073 OMVs incubated at 37 °C for 24 h: orange line, SBSr073 OMVs autoclaved: red line) c) Uptake in percentage induced by different heat-treated RO EVs in dTHP-1 measured via FACS. Mean ± SD, n = 3 - 4 d) Uptake in percentage induced by different heat-treated SBSr073 OMVs in dTHP-1 measured via FACS. Mean ± SD, n = 3 -4.

Confocal microscopy was further used to better understand vesicle interaction with dTHP-1 cells and to show individual cell uptake. We wanted to visualise the vesicle-cell interaction of single cells and obtain complementary information to the FACS data by assessing differences between heat-treated and non-heat-treated EVs and OMVs in presence of macrophages.

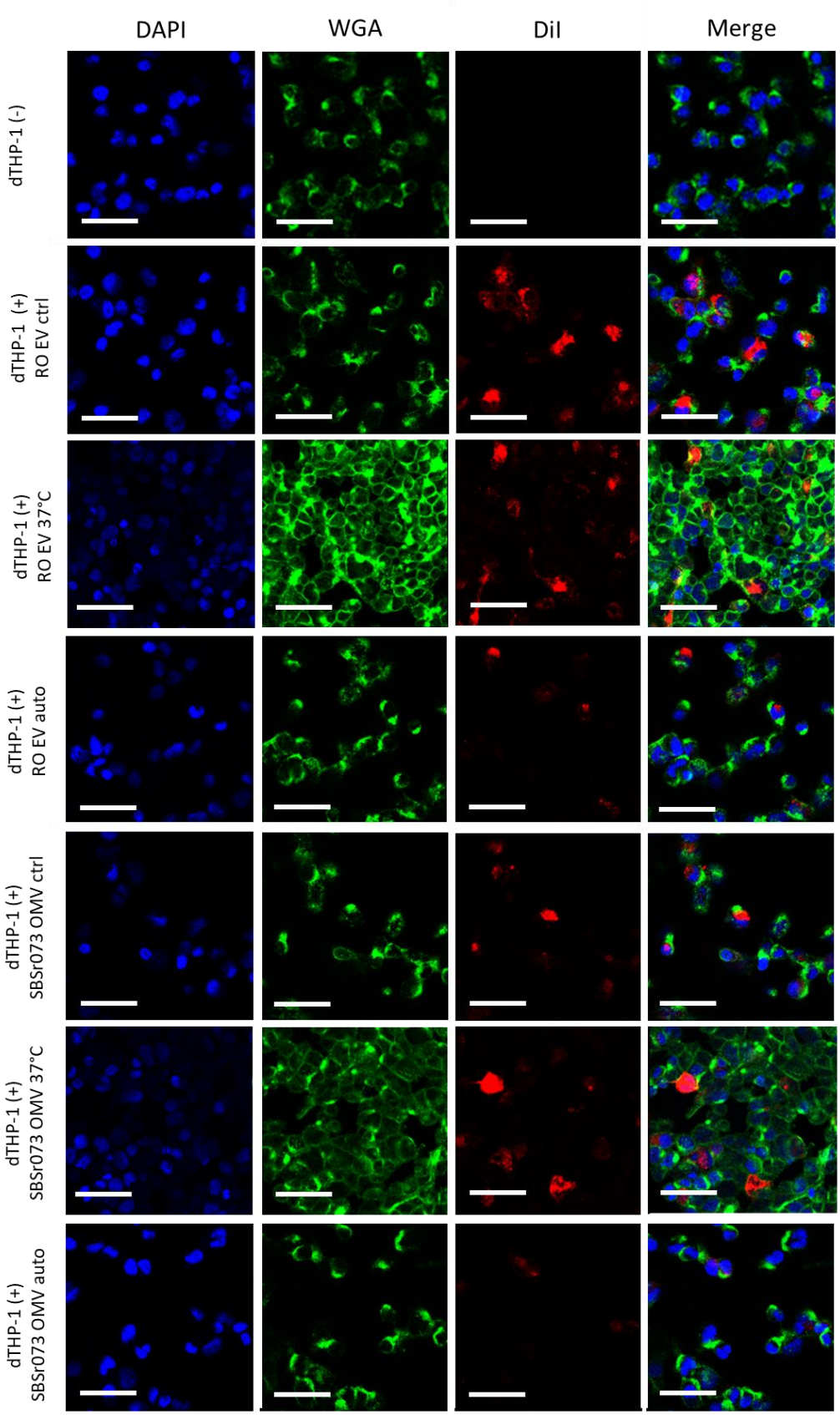

Fig 6 Confocal imaging of dTHP-1 incubated with RO EVs and SBSr073 OMVs. Cells were incubated with DiI (red) labeled EVs or OMVs for 24 h. Nuclei were stained with DAPI (blue),

while whole cell staining was undertaken using fluorescein labelled wheat germ agglutinin (green). dTHP-1 cells treated with PBS were used as negative controls. DAPI was excited using a 405 nm laser, a 488 nm laser for WGA and a 561 nm laser for DiI. Representative micrographs; scale bar represents 50 µm.

As seen in **Figure 6**, cells treated only with PBS did not show any positive signal at 561 nm emission (*i.e*., laser used for DiI detection). Controls and vesicles incubated at 37 °C showed, comparably to FACS data, similar DiI fluorescence intensities within the dTHP-1. On the contrary, cells treated with autoclaved vesicles showed a lower signal in individual cells. In contrast to FACS data, here the reduction of the particle concentration after autoclaving also resulted in a lower fluorescence intensity. Here, quantitative differences were visualised by confocal microscopy, whereas FACS was not able to detect these differences, as only DiI positive cells were measured. Overall, our data showed a surprisingly inherent stability of EVs and OMVs even when treated at higher temperatures. Nevertheless, it is still important to assess thermal stability of each vesicle type individually, using different techniques and methods.

4. Conclusion

In this work, we investigated the impact of heat on the stability of model EVs and OMVs derived from human cells and non-pathogenic bacteria. We could show that these vesicles were physico-chemically at stable at 37 °C for 24 h. Surprisingly, vesicles derived from non-pathogenic bacteria also show higher tolerance to hot temperatures, even up to 100 °C compared to cell derived vesicles. Cryo-EM imaging additionally revealed the vesicles' morphology after heat impact and revealed no differences or artefacts. FACS and confocal analysis furthermore emphasises these results, indicating a high amount of uptake of control vesicles as well as low temperature treated vesicles.

Our results create a sound basis for advanced evaluation of EVs, for example, heat stability of drug loaded vesicles and the possible protection of thermally instable compounds encapsulated into vesicles, such as proteins. Such evaluation would be important for an EV formulation by spray drying or functionalisation for oral delivery (15). Additional information regarding cytotoxicity and impact on cell viability of possible heat induced by-products would be interesting to further understand the heat stability of EVs and OMVs.

Acknowledgements

This work was supported by the NanoMatFutur Junior Research programme form the Federal Ministry of Education and Research, Germany (grant number 13XP6039A). We thank Olga Hartwig with helping to establish a FACS method and Annette Boese for her support with confocal microscopy.

Author contributions

A.K. conducted all experiments on physico-chemical stability of OMVs and EVs. E.S. cultured RO cells and SBSr073 bacteria, conducted all functional experiments by FACS and confocal microscopy and wrote the manuscript text together with G.F. M.K. recorded cryo-electron microscopy images. G.F. conceived the study and supervised the project. All authors analysed the data and reviewed the manuscript.

References

1. Chatterjee SN, Das J. Electron Microscopic Observations on the Excretion of Cell-wall Material by Vibrio cholerae. Microbiology. 1967;49(1):1-11.
2. Pan B-T, Johnstone RM. Fate of the transferrin receptor during maturation of sheep reticulocytes in vitro: Selective externalization of the receptor. Cell. 1983;33(3):967-78.
3. Mathieu M, Martin-Jaular L, Lavieu G, Théry C. Specificities of secretion and uptake of exosomes and other extracellular vesicles for cell-to-cell communication. Nature Cell Biology. 2019;21(1):9-17.
4. Fuhrmann G, Herrmann IK, Stevens MM. Cell-derived vesicles for drug therapy and diagnostics: Opportunities and challenges. Nano Today. 2015;10(3):397-409.
5. Yu Y-j, Wang X-h, Fan G-C. Versatile effects of bacterium-released membrane vesicles on mammalian cells and infectious/inflammatory diseases. Acta Pharmacologica Sinica. 2017;39:514.
6. Schwechheimer C, Kuehn MJ. Outer-membrane vesicles from Gram-negative bacteria: biogenesis and functions. Nature Reviews Microbiology. 2015;13:605.
7. Kuehn AJMaMJ. Outer Membrane Vesicles. 2005.
8. Lener T, Gimona M, Aigner L, Börger V, Buzas E, Camussi G, et al. Applying extracellular vesicles based therapeutics in clinical trials – an ISEV position paper. Journal of Extracellular Vesicles. 2015;4:10.3402/jev.v4.30087.
9. clinicaltrail.gov. Allogenic Mesenchymal Stem Cell Derived Exosome in Patients With Acute Ischemic Stroke [Clinical Trail]. [updated 31.12.18. Available from: https://clinicaltrials.gov/ct2/show/NCT03384433.
10. Gujrati V, Kim S, Kim S-H, Min JJ, Choy HE, Kim SC, et al. Bioengineered Bacterial Outer Membrane Vesicles as Cell-Specific Drug-Delivery Vehicles for Cancer Therapy. ACS Nano. 2014;8(2):1525-37.
11. Schulz E, Goes A, Garcia R, Panter F, Koch M, Müller R, et al. Biocompatible bacteria-derived vesicles show inherent antimicrobial activity. Journal of Controlled Release. 2018;290:46-55.

12. Pinheiro A, Silva AM, Teixeira JH, Gonçalves RM, Almeida MI, Barbosa MA, et al. Extracellular vesicles: intelligent delivery strategies for therapeutic applications. Journal of Controlled Release. 2018;289:56-69.
13. Fuhrmann G, Chandrawati R, Parmar PA, Keane TJ, Maynard SA, Bertazzo S, et al. Engineering Extracellular Vesicles with the Tools of Enzyme Prodrug Therapy. Advanced materials (Deerfield Beach, Fla). 2018;30(15):e1706616-e.
14. Lőrincz ÁM, Timár CI, Marosvári KA, Veres DS, Otrokocsi L, Kittel Á, et al. Effect of storage on physical and functional properties of extracellular vesicles derived from neutrophilic granulocytes. Journal of Extracellular Vesicles. 2014;3(1):25465.
15. Frank J, Richter M, de Rossi C, Lehr C-M, Fuhrmann K, Fuhrmann G. Extracellular vesicles protect glucuronidase model enzymes during freeze-drying. Scientific Reports. 2018;8(1):12377.
16. Charoenviriyakul C, Takahashi Y, Nishikawa M, Takakura Y. Preservation of exosomes at room temperature using lyophilization. International Journal of Pharmaceutics. 2018;553(1):1-7.
17. Park SJ, Jeon H, Yoo S-M, Lee M-S. The effect of storage temperature on the biological activity of extracellular vesicles for the complement system. In Vitro Cellular & Developmental Biology - Animal. 2018;54(6):423-9.
18. Cheng Y, Zeng Q, Han Q, Xia W. Effect of pH, temperature and freezing-thawing on quantity changes and cellular uptake of exosomes. Protein & Cell. 2019;10(4):295-9.
19. Goldbach P, Brochart H, Stamm, A. Spray-Drying of liposomes for a Pulmonary Administration. I. Chemical Stability of Phospholipids. Drug Development and Industrial Pharmacy. 1993;19(19):2611-22.
20. Bamberger D, Hobernik D, Konhäuser M, Bros M, Wich PR. Surface Modification of Polysaccharide-Based Nanoparticles with PEG and Dextran and the Effects on Immune Cell Binding and Stimulatory Characteristics. Molecular Pharmaceutics. 2017;14(12):4403-16.
21. Skotland T, Sandvig K, Llorente A. Lipids in exosomes: Current knowledge and the way forward. Progress in Lipid Research. 2017;66:30-41.
22. Ruigrok RWH, Martin SR, Wharton SA, Skehel JJ, Bayley PM, Wiley DC. Conformational changes in the hemagglutinin of influenza virus which accompany heat-induced fusion of virus with liposomes. Virology. 1986;155(2):484-97.
23. Vergauwen G, Dhondt B, Van Deun J, De Smedt E, Berx G, Timmerman E, et al. Confounding factors of ultrafiltration and protein analysis in extracellular vesicle research. Scientific Reports. 2017;7(1):2704.
24. Martin R. Hadam RD, Gerd Dammer, Claudia Derau, Dietrich Niethammer. Expression of MHC-Antigens in MHC-Class-II-Deficiency. Jaak Vossen CG, editor1986. 89-96 p.
25. Préval Cd, Hadam MR, Mach B. Regulation of Genes for HLA Class II Antigens in Cell Lines from Patients with Severe Combined Immunodeficiency. New England Journal of Medicine. 1988;318(20):1295-300.
26. Müller KJWaaR. Myxobacterial secondary metabolites: bioactivities and modes-of-action. Nat Prod Rep. 2010.
27. Reichenbach H. The ecology of the myxobacteria. Environmental Microbiology. 1999;1(1):15-21.
28. Fuhrmann G, Serio A, Mazo M, Nair R, Stevens MM. Active loading into extracellular vesicles significantly improves the cellular uptake and photodynamic effect of porphyrins. Journal of Controlled Release. 2015;205:35-44.
29. Shao H, Im H, Castro CM, Breakefield X, Weissleder R, Lee H. New Technologies for Analysis of Extracellular Vesicles. Chemical Reviews. 2018;118(4):1917-50.
30. Gardiner C, Ferreira YJ, Dragovic RA, Redman CWG, Sargent IL. Extracellular vesicle sizing and enumeration by nanoparticle tracking analysis. Journal of Extracellular Vesicles. 2013;2:10.3402/jev.v2i0.19671.
31. Agency EM. Guideline on the sterilisation of the medicinal product, active substance, excipient and primary container. 2019.

32. Menina S, Eisenbeis J, Kamal MAM, Koch M, Bischoff M, Gordon S, et al. Bioinspired Liposomes for Oral Delivery of Colistin to Combat Intracellular Infections by Salmonella enterica. Advanced Healthcare Materials.0(0):1900564.
33. Bachurski D, Schuldner M, Nguyen P-H, Malz A, Reiners KS, Grenzi PC, et al. Extracellular vesicle measurements with nanoparticle tracking analysis - An accuracy and repeatability comparison between NanoSight NS300 and ZetaView. Journal of extracellular vesicles. 2019;8(1):1596016-.
34. Arraud N, Linares R, Tan S, Gounou C, Pasquet J-M, Mornet S, et al. Extracellular vesicles from blood plasma: determination of their morphology, size, phenotype and concentration. Journal of Thrombosis and Haemostasis. 2014;12(5):614-27.

Supplementary Information

Hot EVs – how temperature affects extracellular vesicles

Eilien Schulz, Anna Karagianni, Marcus Koch, Gregor Fuhrmann*

Figure S1 Physico-chemical alteration upon incubation at 37 °C, 50 °C, 70 °C, 100 °C for 1 h, 6 h and 24 h

Figure S2 Total protein concentration of heat-treated vesicles

Figure S3 Representative size exclusion chromatography of RO EVs and SBSr73 OMVs

Figure S4 FACS signals of control samples

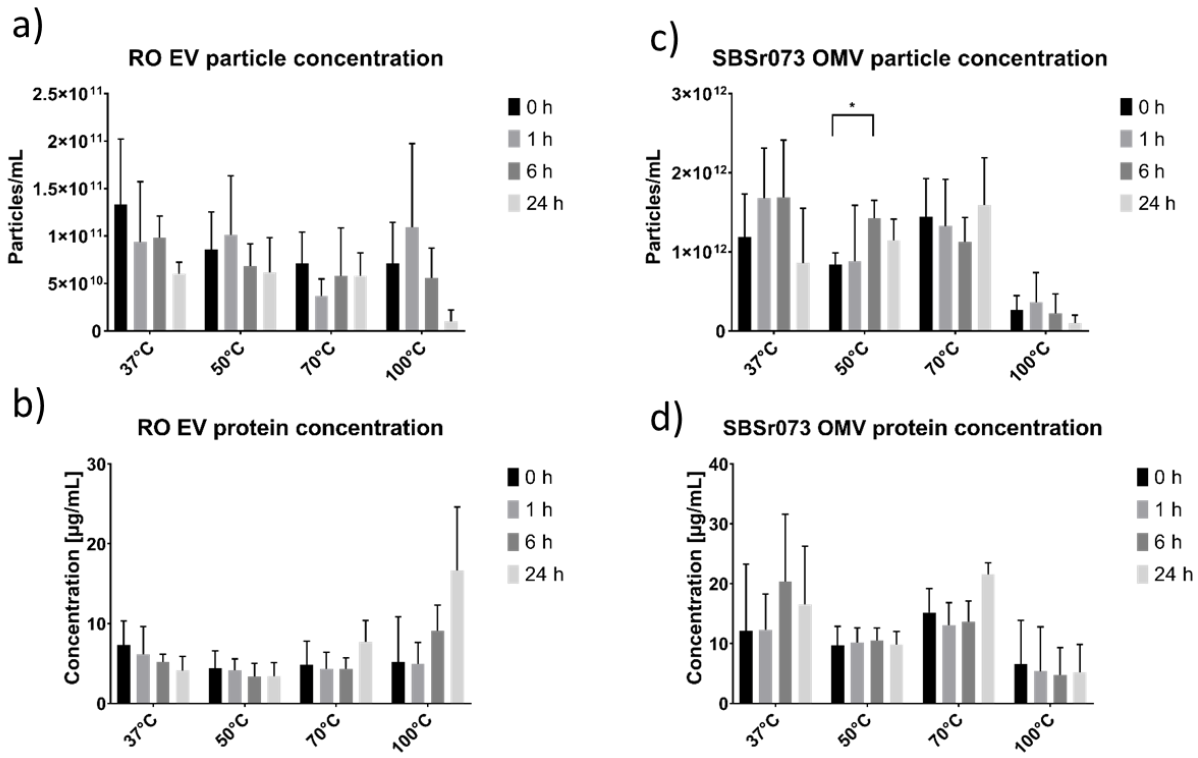

Figure S1 Physico-chemical alteration upon incubation at 37 °C, 50 °C, 70 °C, 100 °C for 1 h, 6 h and 24 h. a) RO EV particle concentration measured by NTA b) RO EV protein concentration determined by BCA c) SBSr073 OMV particle concentration d) SBSr073 OMV protein concentration. Mean ± SD, n = 3, *p < 0.05 (ANOVA followed by Tukey *post-hoc* test).

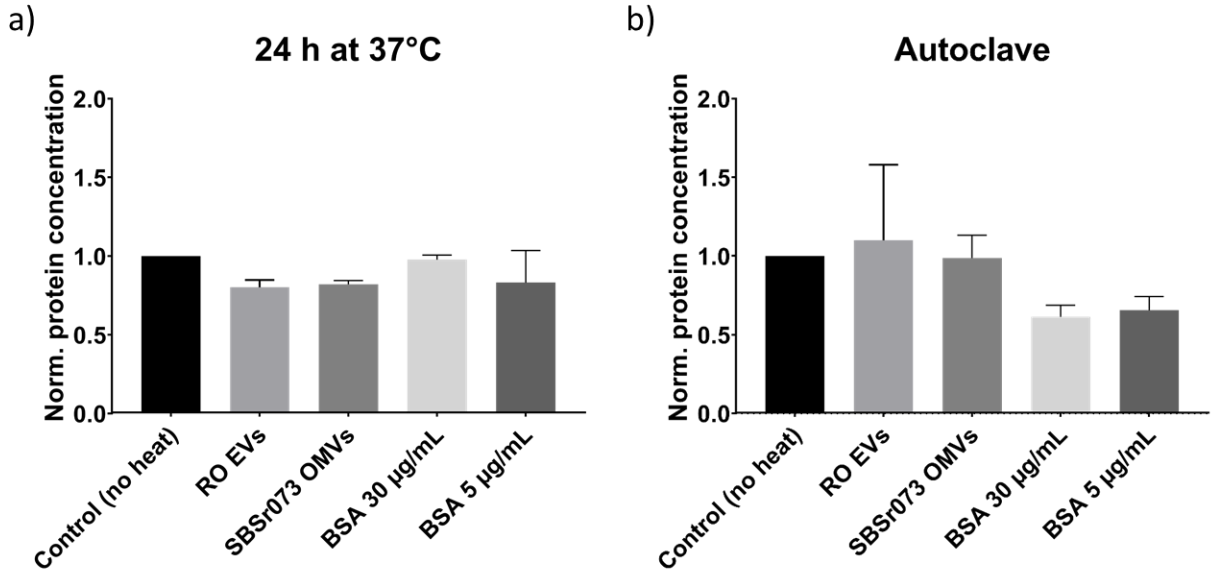

Figure S2 Total protein concentration of a) EVs and OMVs incubated at 37°C for 24 h b) autoclaved EVs and OMVs. Vesicles were heat-treated and afterwards lysed with RIPA

buffer, a strong detergent, for 5 min, and the total protein concentration was determined by a bicinchoninic assay. As control and for data normalisation, non-heat-treated and RIPA buffer lysed vesicles were used. As an additional control, two different concentrations of bovine serum albumin (BSA) were treated at similar conditions. Mean ± SD, n = 3

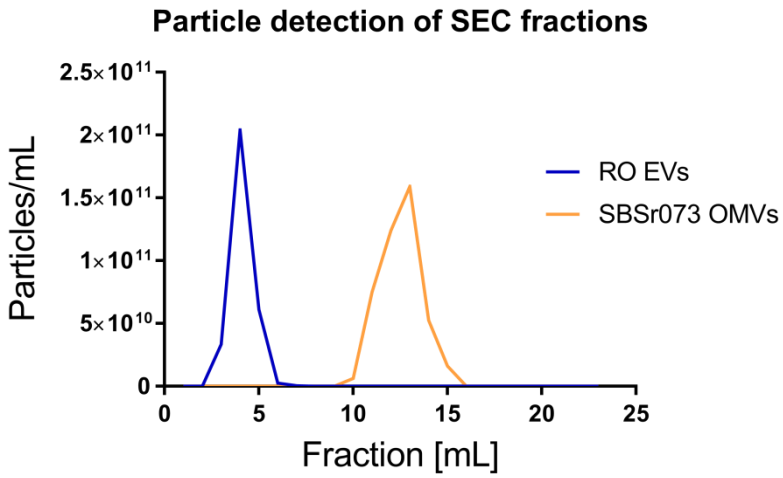

Figure S3 Representative size exclusion chromatography of RO EVs and SBSr073 OMVs. As the yield of RO EVs is considerably lower compared to bacterial OMVs from SBSr073, a 10 mL column was sufficient to separate purified vesicles from external proteins while minimising the dilution of the vesicles. SBSr073 were purified using a 35 mL column, to ensure adequate purification of vesicles. RO EVs typically eluted after 3-6 mL, SBSr073 after 10-15 mL.

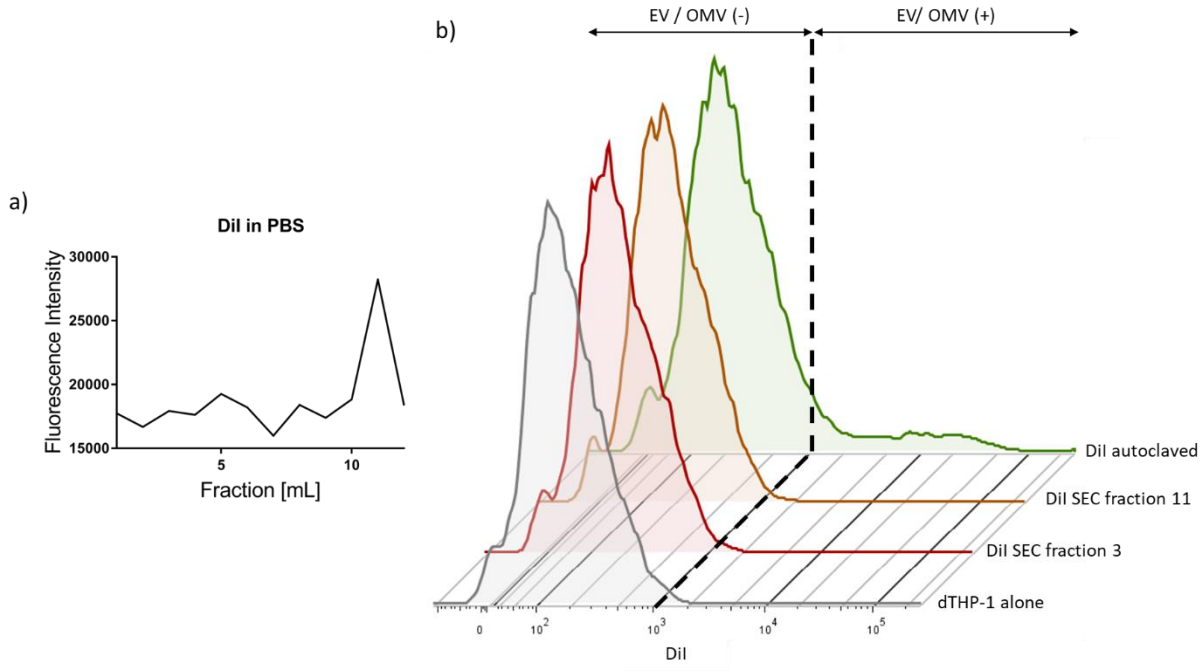

Figure S4 FACS signals of control samples a) 2 µL DiI were incubated with 1 mL PBS and loaded on to a 10 mL sepharose column. Fluorescence of each fraction was measured. b) Histogram plot of DiI positive dTHP-1 cells with DiI signal intensity (PE laser – x-axis). Different fractions (3 and 11) of DiI eluting from the SEC were also incubated with dTHP-1 and did not show a positive signal during FACS analysis.

7.3. Myxobacteria-Derived Outer Membrane Vesicles: Potential Applicability Against Intracellular Infections

Adriely Goes, Philipp Lapuhs, Thomas Kuhn, Eilien Schulz, Robert Richter, Fabian Panter, Charlotte Dahlem, Marcus Koch, Ronald Garcia, Alexandra K. Kiemer, Rolf Müller and Gregor Fuhrmann

Cells, 2020, 9, 194

DOI: 10.3390/cells9010194

cells

MDPI

Article

Myxobacteria-Derived Outer Membrane Vesicles: Potential Applicability Against Intracellular Infections

Adriely Goes [1,2], Philipp Lapuhs [1,2], Thomas Kuhn [1,2], Eilien Schulz [1,2], Robert Richter [2,3], Fabian Panter [4], Charlotte Dahlem [5], Marcus Koch [6], Ronald Garcia [4], Alexandra K. Kiemer [5], Rolf Müller [2,4,7] and Gregor Fuhrmann [1,2,*]

[1] Helmholtz Centre for Infection Research (HZI), Biogenic Nanotherapeutics Group (BION), Helmholtz Institute for Pharmaceutical Research Saarland (HIPS), Campus E8.1, Saarbrücken 66123, Germany; adriely.goes@helmholtz-hips.de (A.G.); philipp.lapuhs@gmail.com (P.L.); thomas.kuhn@helmholtz-hips.de (T.K.); eilien.schulz@helmholtz-hips.de (E.S.)

[2] Department of Pharmacy, Saarland University, Campus Building E8.1, Saarbrücken 66123, Germany;

[3] Helmholtz Centre for Infection Research (HZI), Department of Drug Delivery (DDEL), Helmholtz Institute for Pharmaceutical Research Saarland (HIPS), Campus E8.1, Saarbrücken 66123, Germany; robert.richter@helmholtz-hips.de (R.R.)

[4] Helmholtz Centre for Infection Research (HZI), Department of Microbial Natural Products (MINS), Helmholtz Institute for Pharmaceutical Research Saarland (HIPS), Campus E8.1, Saarbrücken 66123, Germany; fabian.panter@helmholtz-hips.de (F.P.); ronald.garcia@helmholtz-hips.de (R.G.) ; rolf.mueller@helmholtz-hips.de (R.M.)

[5] Department of Pharmacy, Pharmaceutical Biology, Saarland University, Saarbrücken 66123, Germany; charlotte.dahlem@uni-saarland.de (C.D.); pharm.bio.kiemer@mx.uni-saarland.de (A.K.K.)

[6] INM-Leibniz Institute for New Materials, Campus D2 2, Saarbrücken 66123, Germany; marcus.koch@leibniz-inm.de

[7] German Center for Infection Research (DZIF), Braunschweig 38124, Germany

* Correspondence: gregor.fuhrmann@helmholtz-hips.de; Tel.: +49-68-198-806 (ext. 1500.)

Received: 06 December 2019; Accepted: 08 January 2020; Published: 09 January 2020

Abstract: In 2019, it was estimated that 2.5 million people die from lower tract respiratory infections annually. One of the main causes of these infections is *Staphylococcus aureus*, a bacterium that can invade and survive within mammalian cells. *S. aureus* intracellular infections are difficult to treat because several classes of antibiotics are unable to permeate through the cell wall and reach the pathogen. This condition increases the need for new therapeutic avenues, able to deliver antibiotics efficiently. In this work, we obtained outer membrane vesicles (OMVs) derived from the myxobacteria *Cystobacter velatus* strain Cbv34 and *Cystobacter ferrugineus* strain Cbfe23, that are naturally antimicrobial, to target intracellular infections, and investigated how they can affect the viability of epithelial and macrophage cell lines. We evaluated by cytometric bead array whether they induce the expression of proinflammatory cytokines in blood immune cells. Using confocal laser scanning microscopy and flow cytometry, we also investigated their interaction and uptake into mammalian cells. Finally, we studied the effect of OMVs on planktonic and intracellular *S. aureus*. We found that while Cbv34 OMVs were not cytotoxic to cells at any concentration tested, Cbfe23 OMVs affected the viability of macrophages, leading to a 50% decrease at a concentration of 125,000 OMVs/cell. We observed only little to moderate stimulation of release of TNF-alpha, IL-8, IL-6 and IL-1beta by both OMVs. Cbfe23 OMVs have better interaction with the cells than Cbv34 OMVs, being taken up faster by them, but both seem to remain mostly on the cell surface after 24 h of incubation. This, however, did not impair their bacteriostatic activity against intracellular *S. aureus*. In this study, we provide an important basis for implementing OMVs in the treatment of intracellular infections.

Keywords: extracellular vesicles; antimicrobial resistance; *Staphylococcus aureus*; intracellular infection; outer membrane vesicles; biogenic drug carriers

1. Introduction

Pulmonary infections represent a serious health risk for today's society. The Global Burden of Disease Study 2016 has estimated that lower respiratory infections are one of the leading causes of death worldwide, especially in children aged five years and younger [1,2]. Lung infection is also a frequent complication for patients with cystic fibrosis (CF), an inherited, systemic disorder caused by a mutation in the cystic fibrosis trans-membrane regulator channel [3,4]. CF lung disease is characterized by the accumulation of a thick mucus in the airway, which favors lung inflammation and persistent, chronic bacterial infection. One of the main pathogens causing lung infections in CF patients is *Staphylococcus aureus* (*S. aureus*) [5,6]. Besides being able to form biofilms, it is known that *S. aureus* can also invade

professional and non-professional phagocytes and is able to survive intracellularly by escaping the endosomal pathway into the cytoplasm [7–10].

The antibiotics currently available on the market are not optimal for treating intracellular infections, as most of them need higher concentrations and a longer therapy time to induce a positive effect [11]. Generally, free antibiotics (e.g., aminoglycosides) are unable to eradicate intracellular infections due to their hydrophilic characteristics and high polarity, which prevent their permeation into mammalian cells [12–17]. To address this problem, increased efforts have been made towards improved drug delivery using nanotechnology, surface modification, biomimetic and biogenic carriers to overcome this barrier [18–21]. Carriers such as liposomes have been successful at delivering antibiotics to biofilms and eradicating them [22].

Myxobacteria are a group of Gram-negative bacteria that are abundant in soil. Many of these bacteria show predatory behavior [23], and interact, move and prey by forming coordinated swarms [24]. They belong to the class Delta Proteobacteria, phylum Proteobacteria. Myxobacteria are potent producers of antimicrobial compounds [25–28] and they are non-pathogenic to humans. Outer membrane vesicles (OMVs) are nanoparticles shed from the outer membrane of Gram-negative bacteria [29–31]. OMVs derived from myxobacteria have been shown to be involved in intercolony communication but also as predatory weapons against other bacteria [32]. We recently reported on myxobacterial OMVs with inherent antimicrobial properties due to their cystobactamid cargo [33]. Cystobactmids are topoisomerase inhibitors that have potent antibacterial activity [34]. However, the antimicrobial activity of myxobacterial OMVs has only been shown against the planktonic model bacterium (*Escherichia coli* strain DH5-alpha), which is not clinically relevant. Here, we expand the evaluation of these OMVs to clinically important *S. aureus* pathogens. For potential OMV translation, it is necessary to biotechnologically obtain them at large amounts. Myxobacterial cultures are suitable for this purpose, because they can be increased to several liters, which facilitates the large-scale isolation of their OMVs [34].

In this study, we explore the myxobacterial strains *Cystobacter velatus* Cbv34 and *Cystobacter ferrugineus* Cbfe23 for the production of natural antibacterial OMVs and analyze their potential for uptake by mammalian cells and the eradication of intracellular *S. aureus*. Our results show that both Cbv34 and Cbfe23 OMVs are efficiently taken up into macrophages and epithelial cells without affecting their viability. Importantly, they presented an antibacterial effect against intracellular *S. aureus*.

2. Materials and Methods

2.1. Myxobacterial Culture

The myxobacterial strains Cbv34 (*Cystobacter velatus*) and Cbfe23 (*Cystobacter ferrugineus*) were cultured in 100 mL M-Medium (*w*/*v*, 1.0% phytone, 1.0% maltose, 0.1% $CaCl_2$, 0.1% $MgSO_4$, 50 mM HEPES, pH adjusted to 7.2 with KOH) at 30 °C and 180 rpm. Upon reaching the stationary phase at 6–7 days, 50 mL of the culture was removed for OMV isolation. The remaining volume was used as an inoculum for the next passage of the myxobacterial culture. Growth curves of the cultures were established as described in a previous study [33].

2.2. Isolation and Purification of Outer Membrane Vesicles

In order to obtain potent OMVs with a high yield, the myxobacteria were cultured for at least three passages prior to performing the isolation. Fifty milliliters of the cultures were used and centrifuged at 9500 × *g* for 10 min at 4 °C. The supernatant was transferred to a new falcon tube and centrifuged once again at 9500 × *g*, for 15 min at 4 °C. Thirty milliliters of the resulting supernatant was added into an ultracentrifugation tube and pelleted at 100,000 × *g* for 2 h at 4 °C using a rotor type SW 32 Ti (Beckman Coulter). The supernatant was removed, and the pellet was dispersed in 300 µL phosphate buffered saline (PBS, Gibco PBS tablets without calcium, magnesium and phenol red) (Sigma-Aldrich; Co., St. Louis, MO, USA) filtered with 0.2 µm mixed cellulose ester filters (Whatman, GE Healthcare UK Limited, Little Chalfont, UK). In order to remove the free protein present in the pellet, a size exclusion chromatography (SEC) was performed. The pellet was added to a 60 mL column filled with 35–40 mL of Sepharose CL-2B (GE Healthcare Bio-Sciences AB, Uppsala, Sweden) in PBS. One milliliter fractions of OMVs in PBS were collected into polypropylene (PP) tubes (Axygen, Corning Incorporated, Reynosa, Mexico) next to a Bunsen burner, to obtain aseptic conditions. The fractions were kept at 4 °C for up to one month. Prior to infection, experiments and measurements of particle parameters, the fractions were filtered with Puredisc 25 AS (GE Healthcare UK Limited, Little Chalfont, UK) to assure sterility.

2.3. Liquid-Chromatography Coupled Mass Spectrometry

2.3.1. OMV Preparation

OMV pellets were resuspended in 500 µL of particle-free PBS and lyophilized for 16 h. The dried pellet was mixed with 300 µL of MeOH and vortexed for 1–2 min. The OMV extract was centrifuged to remove debris. Then, the supernatant was transferred to a vial for LC-MS analysis.

2.3.2. UHPLC MS Conditions

UPLC-hrMS analysis was performed on a Dionex (Germering, Germany) Ultimate 3000 RSLC system using a Waters (Eschborn, Germany) BEH C18 column (50 × 2.1 mm, 1.7 µm) equipped with a Waters VanGuard BEH C18 1.7 µm guard column. Separation of 1 µl sample was achieved by a linear gradient from (A) H_2O + 0.1% FA to (B) ACN + 0.1% FA at a flow rate of 600 µL/min and a column temperature of 45 °C. Gradient conditions were as follows: 0–0.5 min, 5% B; 0.5–18.5 min, 5%–95% B; 18.5–20.5 min, 95% B; 20.5–21 min, 95%–5% B; 21–22.5 min, 5% B. UV spectra were recorded by a DAD in the range 200–600 nm. The LC flow was split to 75 µL/min before entering the Bruker Daltonics maXis 4G hrToF mass spectrometer (Bremen, Germany) using the Apollo II ESI source. Mass spectra were acquired in centroid mode ranging from 150–2500 *m*/*z* (mass/charge) at a 2 Hz full scan rate. Mass spectrometry source parameters are set to 500 V as end plate offset; 4000 V as capillary voltage; nebulizer gas pressure 1 bar; dry gas flow of 5 L/min and a dry temperature of 200 °C. Ion transfer and quadrupole settings are set to Funnel RF 350 Vpp; Multipole RF 400 Vpp as transfer settings and Ion energy of 5 eV as well as a low mass cut of 300 *m*/*z* as Quadrupole settings. Collision cell is set to 5.0 eV and pre pulse storage time is set to 5 µs. Spectra acquisition rate is set to 2 Hz. Calibration is done automatically before every LC-MS run by the injection of sodium formate and calibration on the sodium formate clusters forming in the ESI source. All MS analyses are acquired in the presence of the lock masses $C_{12}H_{19}F_{12}N_3O_6P_3$; $C_{18}H_{19}O_6N_3P_3F_2$ and $C_{24}H_{19}F_{36}N_3O_6P_3$, which generate the $[M + H]^+$ ions of 622.03; 922.01 and 1221.10.

2.3.3. LC-MS Data Bucketing and Annotation Using Metaboscape Software

Acquired LC-MS data are bucketed by Bruker Metaboscape 4.0 SR1 using the qTOF data optimized TReX 3D algorithm. Bucketed analyses are checked for library hits against our in-house database of myxobacterial natural products called myxobase. Library hits are retained if they show a retention time deviation under the described parameters of less than 0.2 min, *m*/*z* value deviation of less than 5 ppm and isotope pattern ratio congruence lower than 30 milliSigma.

2.3.4. Conditions for MS^2 Analysis

LC and MS conditions for automatic precursor selection MS^2 data acquisitions remain as described in section-standardized UHPLC-MS conditions. CID Energy is ramped from 35 eV for 500 *m*/*z* to 45 eV for 1000 *m*/*z* and 60 eV for 2000 *m*/*z*. MS full scan acquisition rate was set to 2 Hz and MS/MS spectra acquisition rates were ramped from 1 to 4 Hz for precursor ion intensities of 10 to 1000 kcts.

2.3.5. GNPS Clustering Parameters

MS^2 data of the vesicle extracts were uploaded to the Global Natural Product Social Molecular Networking (GNPS) server at University of California San Diego [35]. A molecular network was created, using a parent mass tolerance of 0.05 Da and a fragment ion tolerance of 0.1 Da. Cosine score of edges considered to network was set to extend 0.7 and the minimum matched fragment peaks were set to 5. The clustered dataset was visualized using Cytoscape 3.7.2 (Cytoscape Consortium, UCSD San Diego, USA).

2.4. Cryogenic Electron Microscopy

Cryogenic transmission electron microscopy (cryo-TEM) was performed on OMVs pellets after ultracentrifugation and purified fractions as previously described [33]. Three to four microliters of the sample were dropped onto a holey carbon grid (type S147-4, Plano, Wetzlar, Germany) and plotted for 2 s before plunging into liquid ethane at T= −165 °C using a Gatan (Pleasanton, CA, USA) CP3 cryo plunger. The sample was transferred under liquid nitrogen to a Gatan model 914 cryo-TEM sample holder and analyzed at T = −173 °C by low-dose TEM bright-field imaging using a JEOL (Tokyo, Japan) JEM-2100 LaB6 at 200 kV accelerating voltage. Images with 1024 × 1024 pixels were acquired using a Gatan Orius SC1000 CCD camera at 2 s binning and 4 s imaging time.

2.5. Cell Culture

The murine macrophage cell line RAW 264.7 was obtained from the European Collection of Authenticated Cell Cultures (ECACC) and cultured in Dulbecco's Modified Eagle Medium (DMEM) (1X) (Life Technologies Limited, Paisley, UK) supplemented with 10% (*v*/*v*) fetal bovine serum (FBS) (Life Technologies Limited, Paisley, UK). The adenocarcinomic human alveolar basal epithelial cell line (A549) and the human acute leukemia monocyte cell line (THP-1) were both purchased from the German Collection of Microorganisms and Cell Cultures (DSMZ) and cultured in RPMI 1640 (Life Technologies Limited, Paisley, UK) supplemented with 10% (*v*/*v*) FBS. RAW264.7 and A549 cells were split once a week, starting with 0.2×10^6 cells/13 mL for RAW and A549. THP-1 cells were split twice a week to a seeding density of $2–3 \times 10^6$ cells/13 mL. Mycoplasma tests were conducted regularly.

2.6. Cell Viability and Cytotoxicity

To assess the viability and cytotoxicity of cells upon treatment, the cells were seeded into 96-well plates at a density of 20,000 cells/well (RAW 264.7 and A549) and 100,000 cells/well (THP-1). To stimulate the THP-1 cells into macrophages, they were incubated with 30 ng/mL of phorbol 12-myristate 13-acetate (PMA). All cells were grown for 48 h. Within every set of experiments, a live-control, using cells treated with PBS (100 µL cell medium plus 100 µL

PBS), which did not show any change in cell viability or morphology, and a dead-control, using cells treated with 1% (*v*/*v*) Triton-X 100 (Sigma-Aldrich; Co., St. Louis, MO, USA) were included. During the assays, cells were cultured in FCS-free medium to prevent falsified results caused by traces of lactate dehydrogenase (LDH) contained in the medium. Cells were incubated with 100 µL of OMV suspension in PBS at different concentrations (1×10^{12}, 1×10^{11} and 1×10^{10} OMVs/mL) and 100 µL of cell medium for 24 h. For cytotoxicity evaluation, after an incubation time of 24 h, 100 µL of medium were removed to be analyzed by LDH-assay, which detects the amount of LDH released into the medium upon cell death after plasma membrane damage, and mixed with 100 µL of LDH-reagent (Roche Diagnostics GmbH, Mannheim, Germany), prepared according to the supplier's protocol. After an incubation time of 5 min at room temperature (RT), the absorbance of the solution was measured at 492 nm. For viability, PrestoBlue (Thermo Fisher Scientific, Waltham, MA, USA) reagent, which detects metabolically active cells, was diluted by 1 in 10 with the respective medium of the cells. The remaining medium in the wells was removed and 100 µL of the diluted PrestoBlue reagent was added. After 20 min of incubation at 37 °C, fluorescence of the emerging dye was measured at an excitation of 560 nm and emission of 590 nm with a Tecan Infinity Pro 200 (Tecan, Männedorf, Switzerland).plate reader

2.7. Cytokine Detection of OMV-Treated PBMCs

Peripheral blood mononuclear cells (PBMCs) were isolated by centrifugation from buffy coats, derived from three different donors obtained from the Blood Donation Center, Saarbrücken, Germany, authorized by the local ethics committee (State Medical Board of Registration, Saarland, Germany; permission no. 173/18). The cells were cultured in a 96-well plate with 100,000 cells per well in RPMI 1640 (Sigma Aldrich, St. Louis, MO, USA). Pellets of OMVs were isolated by ultracentrifugation as described above. One-hundred microliters of sterile PBS was used to resuspend the pellets. The particle concentration was determined via nanoparticle tracking analysis and the samples were diluted with PBMC medium to a final concentration of 5×10^6 and 5×10^5 particles per cell. After 4 h of incubation at 37 °C, cell supernatants were collected and stored at −80 °C for further analysis. A BD cytometric bead array human inflammatory cytokines kit was used according to manufacturer's specification to quantify the concentrations of IL-8, IL-10, Il-6, Il-1 beta, TNF alpha and IL-12p70.

2.8. Antimicrobial Effect upon Storage

The stability of the OMVs' antimicrobial effect was tested by maintaining the purified fractions at 4 °C for up to four weeks before testing them against *E. coli* DH5-alpha. After treating *E. coli* with different dilutions of OMVs for 18 h at 37 °C, the optical density was measured at 600 nm with a plate reader.

2.9. Bacteriomimetic Liposome Preparation

Bacteriomimetic liposomes were prepared by thin film hydration, as previously reported, with minor modifications [36]. A 6% (*w*/*v*) phospholipid solution was prepared by dissolving 1-hexadecanoyl-2-(9Z-octadecenoyl)-sn-glycero-3-phosphoethanolamine (POPE), 1-hexadecanoyl-2-(9Z-octadecenoyl)-sn-glycero-3-phospho-(1′-rac-glycerol) (sodium salt) (POPG) and 1,1′,2,2′-tetra-(9Z-octadecenoyl) cardiolipin (sodium salt) (CL) (Avanti Polar Lipids Inc., Alabaster, AL, USA) (weight ratio 70:20:10) in 5 mL of a chloroform-methanol blend (2:1) in a 250 mL round bottom flask. A Rotavapor R-205 (BÜCHI Labortechnik GmbH, Essen, Germany) was employed to remove the solvent under low pressure (60 min, 200 mbar, 135 rpm, 80 °C; 30 min, 40 mbar, 135 rpm, 80 °C). The remaining lipid film was rehydrated by adding 5 mL PBS (pH 7.4) containing 10% (*v*/*v*) ethanol and rotating for 60 min (70 °C, 135 rpm, atmospheric pressure). The obtained liposomes were sonicated for 60 min followed by 10 extrusion cycles at 70 °C, employing a Liposofast L-50 extruder (Avestin Europe GmbH, Mannheim, Germany).

2.10. Flow Cytometry and Confocal Laser Scanning Microscopy to Assess OMV Uptake into Mammalian Cells

Purified fractions of OMVs and a suspension of the bacteriomimetic liposome control were incubated with 2 µL of 1,1′-dioctadecyl-3,3,3′,3′-tetramethylindocarbocyanine perchlorate (DiI) (Molecular Probes Inc., Eugene, OR, USA) for 30 min at 37 °C. Afterwards, the suspensions were purified with a 10 mL column filled with Sepharose CL-2B (GE Life Science, UK) in PBS to remove any unbound dye. The fluorescence of the fractions was measured with a plate reader and the fractions with the highest concentrations were used. The DiI-stained particles were diluted 1:5 in cell culture medium with 1% penicillin and streptomycin (*v*/*v*) (Life Technologies Corporation, Grand Island, NY, USA) and incubated with cells at different time points.

For flow cytometry experiments, A549 and RAW 264.7 cells were seeded in 24-well plates with a density of 2×10^5 cells per well and incubated for 48 h at 37 °C and 5% CO_2.

Prior to flow cytometry (LSRFortessa, BD Bioscience, San Jose, CA, USA) analysis, the cells were washed with PBS and detached by using trypsin/EDTA (Life Technologies Limited, Paisley, UK) (A549) or a cell scraper (RAW 264.7). The cells were diluted with 2% (*v*/*v*) FCS in PBS and then added into FACS tubes for uptake analysis. Cells treated with PBS diluted in mammalian cell culture medium (1:5 dilution) were used as a negative control to set up the Phycoerythrin (PE) channel gate. A 10,000 live cells threshold was set to be analyzed from forward versus side scatter (FSC vs. SSC) gating. Single cells were determined by forward height versus forward area scatter (FCS-H vs. FCS-A) gating. The percentage of positive cells and the mean fluorescence intensity (MFI), which can be used to evaluate the amount of

fluorescent particles taken up by the cells, were determined by analysis with the FlowJo 10.6.1 software (FlowJo LLC, Ashland, OR, USA) using the Phycoerythrin area channel (PE-A).

For confocal laser scanning microscopy (CLSM), the cells were seeded in 8-well chambers (SPL Life Sciences, Pocheon-si, Gyeonggi-do, Korea) with 4×10^4 cells per well. After the incubation time points, the cells seeded in the 8-well chambers were washed with PBS and fixed with 3.7% (*v*/*v*) paraformaldehyde in PBS. The cells were stained with Alexa Fluor 488 Phalloidin (Life Technologies Coorporation, Eugene, OR, USA) for 1 h and DAPI (4′,6-Diamidino-2-phenylindole dihydrochloride) (Sigma-Aldrich Co., St. Louis, USA) for 30 min, washing the cells with PBS between the staining steps. The chambers were disassembled and mounted on a coverslip prior to CLSM analysis (Leica TCS SP8, Leica Microsystems, Wetzlar, Germany). The captured images were processed with the LAS X software (LAS X 1.8.013370, Leica Microsystems, Wetzlar, Germany).

2.11. Bacterial Culture

Staphylococcus aureus strain Newman and *Escherichia coli* strain DH5-alpha were obtained from the DSMZ (German Collection of Microorganisms and Cell Culture). Overnight cultures were prepared using 20 mL of brain heart infusion (BHI) broth (Becton; Dickinson and Company, Sparks, MD, USA) for *S. aureus* and Luria broth (LB) (Sigma-Aldrich; Co., St. Louis, MO, USA) for *E. coli* inoculated with a single colony. Cultures were incubated at 37 °C and 180 rpm.

2.12. Intracellular Infection

A549 cells were seeded (2×10^4 cells/well) into 96-well plates and incubated for 48 h. Ten milliliters of the bacterial overnight culture was pelleted at 2000 × *g*, 4 °C, for 5 min and resuspended in PBS. The bacterial suspension in PBS was then diluted to approximately 2×10^6 colony forming units per mL (CFU/mL) in mammalian cell medium. The cells were infected for 2 h (approximately multiplicity of infection (MOI) = 100), following washing with PBS and treatment with 50 µg/mL gentamicin for 30 min. After an additional washing step, cells were treated for 24 h with different concentrations of OMVs and controls, each diluted in cell culture medium. After 24 h incubation, the cells were lysed with HBSS (Hanks Buffered Saline Solution) (Life Technologies Limited, Paisley, UK) supplemented with 0.1% bovine serum albumin (Sigma-Aldrich Co., St. Louis, MO, USA) (*w*/*v*) and 0.1% Triton-X 100 (Sigma-Aldrich; Co., St. Louis, MO, USA) (*v*/*v*). Serial dilutions were prepared in a PBS solution containing 0.05% Tween-20 (Sigma-Aldrich, Co., St. Louis, MO, USA) (*v*/*v*) and inoculated on BHI agar plates (Becton; Dickinson and Company, Sparks, MD, USA), which were then incubated at 37 °C overnight. Afterwards, the single colonies were counted and the CFU/mL values calculated.

2.13. Statistical Analysis

The data is displayed as mean ± standard error of the mean (SEM). The number of independent experiments (*n*) is shown in each figure. The experiments and measurements were conducted at least in triplicates. The results were analyzed by GraphPad Prism 8.3 (GraphPad Software, San Diego, CA, USA), using Kruskal-Wallis test by ranks, followed by Dunn's multiple comparisons test. Significant *P*-values were illustrated as * $p < 0.05$, ** $p < 0.005$, *** $p < 0.0005$ and **** $p < 0.0001$.

3. Results

3.1. OMVs are Successfully Isolated by Ultracentrifugation and SEC

The OMVs were isolated from the myxobacterial cultures (Figure S1) and successfully separated from free proteins remaining in the pellet by SEC (Figure S2), using our standardized protocol [33]. The Cbfe23 OMVs were round-shaped and electron-dense, with a well delimited membrane, shown in the cryo-TEM micrographs (Figure 1). The main fractions of OMVs were about 120–150 nm in size (Figure S3). Cbfe23 OMVs had a zeta potential of −5.3 ± 0.7 mV while Cbv34 OMVs showed a zeta potential of −4.7 ± 0.6 mV, as recently reported by our group [33]. The liposomes used as a control for the uptake studies had a zeta potential of −24.5 ± 1.2 mV.

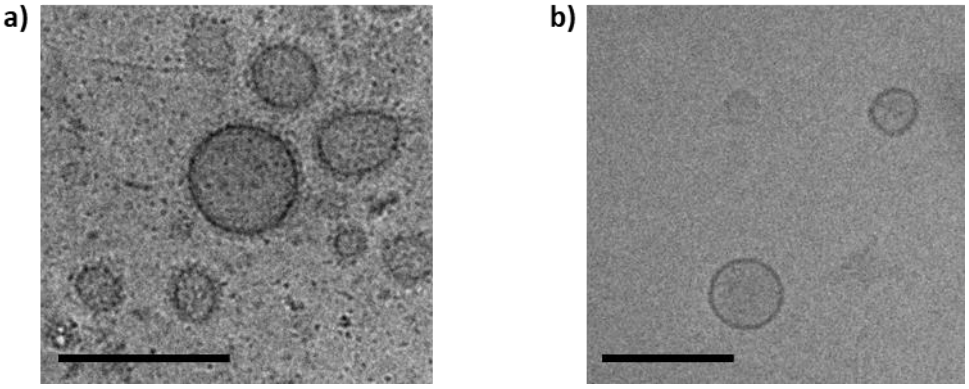

Figure 1. Cryo-TEM micrographs of (**a**) Cbfe23 outer membrane vesicles (OMVs) and (**b**) Cbv34 OMVs. Both OMVs are spherical and about 150 nm in size. Scale bars = 200 nm.

3.2. Myxobacterial OMVs Neither Affect Viability of Mammalian Cells nor Induce Cytotoxicity

The viability of alveolar epithelial cells A549, the macrophage cell line RAW 264.7 and differentiated THP-1 were investigated upon 24 h of incubation with different OMV concentrations (Figure 2). Cbv34 OMVs did not impact the viability of the cells at any concentration tested. The Cbfe23 OMVs were well tolerated until concentrations of 125,000

OMVs/cell. Very high amounts of OMVs (i.e., 125,000 OMVs/cell) decreased the macrophage cell line viability by 50% (Figure 2c and e), and by around 60% when incubated with A549 cells (Figure 2a). A comparable effect was observed for serial dilutions of cystobactamid, the natural compound previously identified in Cbv34 OMVs (Figure 2g) [33]. Cbv34 OMVs increased viability above 100% when incubated with dTHP-1 cells. We had previously observed this effect, which may be due to the nutrient bolus of lipids provided by high amounts of OMVs [33]. To further evaluate this effect, the cytotoxicity was assessed by LDH assay. As seen in Figure 2b,d,f, we did not detect any underlying cytotoxicity in all concentrations of OMVs tested and a similar result was obtained from different concentrations of cystobactamid (Figure 2h).

3.3. Proinflammatory Cytokine Detection by Flow Cytometry

To better understand the effect that OMVs may have on primary immune cells, we isolated peripheral blood mononuclear cells and incubated them with different concentrations of myxobacterial OMVs. As seen in Figure 3, in comparison to the positive control lipopolysaccharide, we only observed a tendency for the stimulation of release of TNF-alpha, IL-8, IL-6 and IL-1beta. Only at concentrations of 1×10^{13} particles/mL of Cbv34 OMVs, an increase in production of IL-1beta was found. The treatment with high concentrations of OMVs (1×10^{13} particles/mL) seemed to affect the viability of PBMCs, as seen by light microscopy (Figure S5).

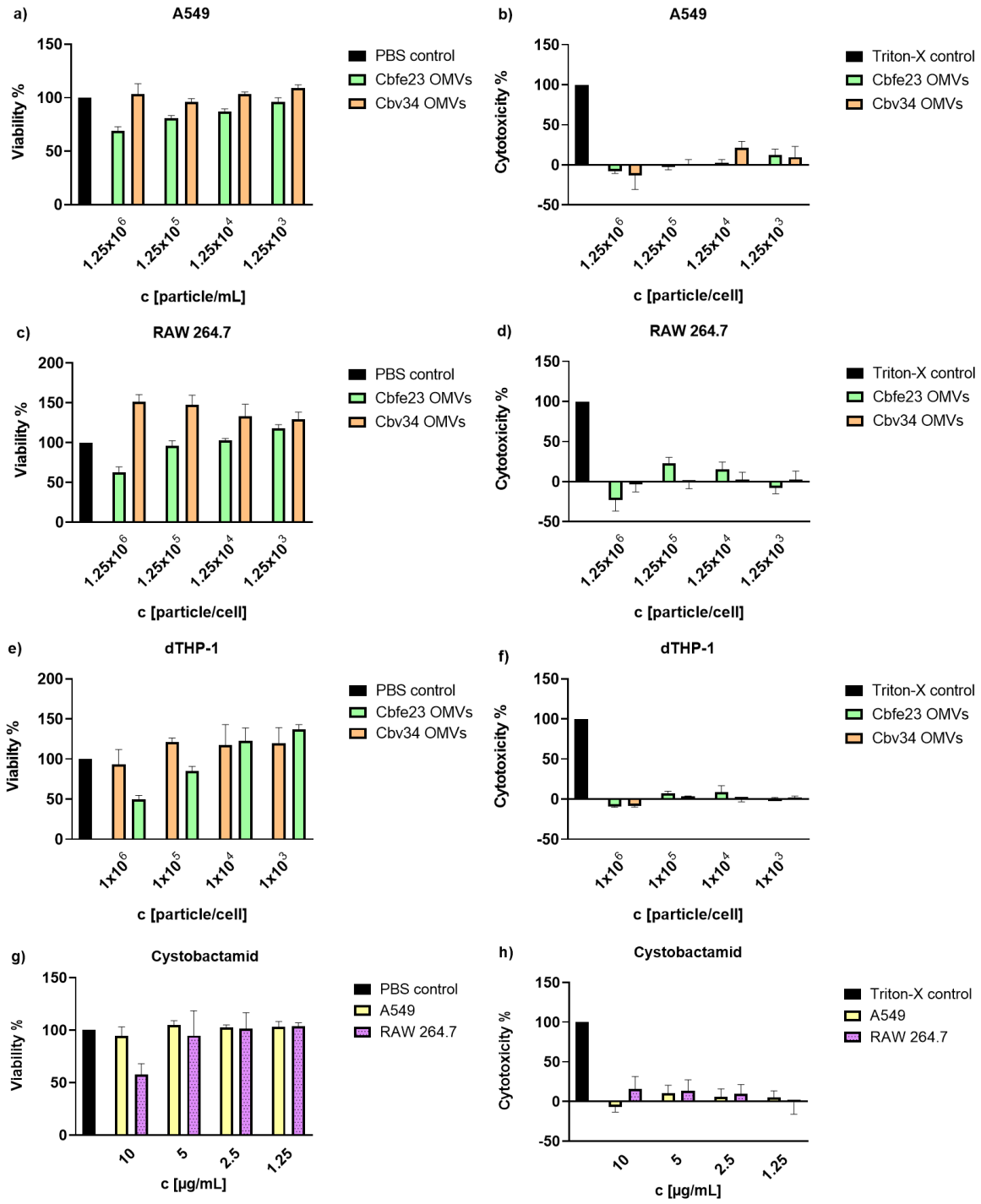

Figure 2. Cell viability and cytotoxicity of Cbv34 OMVs and Cbfe23 OMVs upon 24 h of treatment. Viability of (**a**) A549, (**c**) RAW 264.7 and (**e**) differentiated THP-1 cells, and lactate-dehydrogenase cytotoxicity of OMVs incubated with (**b**) A549, (**d**) RAW 264.7 and (**f**) differentiated THP-1 cells. Effect of cystobactamid on the (**g**) viability and (**h**) cytotoxicity of A549 and RAW 264.7 cells. Mean ± SEM, *n* = 3. No statistically significant differences were observed for any sample.

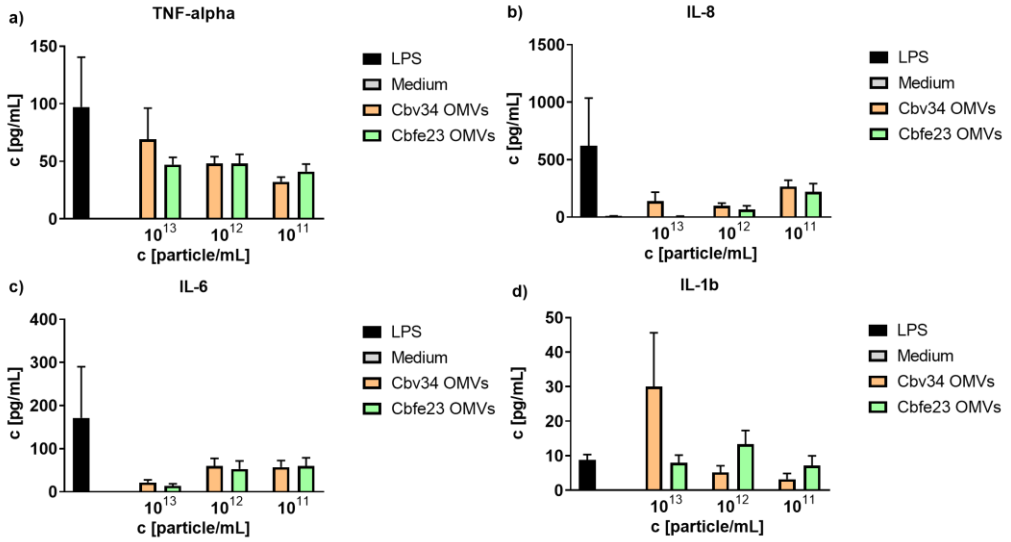

Figure 3. Cytokine detection of OMV-treated peripheral blood mononuclear cells (PBMCs). OMV-induced release of (**a**) TNF-alpha, (**b**) IL-8), (**c**) IL-6 and (**d**) IL 1-b at different concentrations. Mean ± SEM, *n* = 3.

3.4. Myxobacterial OMVs Are Able to Kill Planktonic S. aureus

OMVs had a killing effect at concentrations of approximately 1×10^{12} particles/mL. This correlates to a ratio of 3×10^{3} particles per CFU of *S. aureus* (Figure 4). We credit this effect to the cystobactamid compounds found in the OMV pellets (Figure S6). We were further interested to see if the antibacterial effect of myxobacterial OMVs is preserved during storage. For this, we tested whether Cbv34 OMVs are active against *E. coli* DH5-alpha after storage at 4 °C for up to 28 days based on our recent protocol [33]. Under these conditions, the antimicrobial activity of the OMVs remained potent and dose-dependent over time (Figure 5).

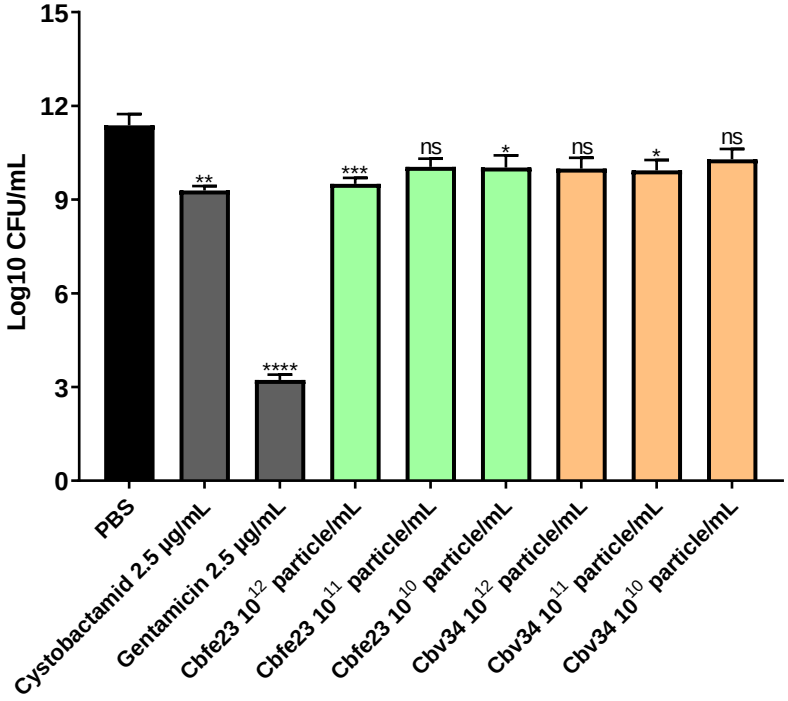

Figure 4. Antibacterial activity of Cbfe23 and Cbv34 OMVs against *S. aureus* strain Newman after 4 h of incubation at 37 °C. Mean ± SEM, $n = 3$. Significance was defined in comparison to the PBS control (black column) as * p-value < 0.05, *** $p < 0.0005$, **** p-value < 0.0001 and ns = not significant.

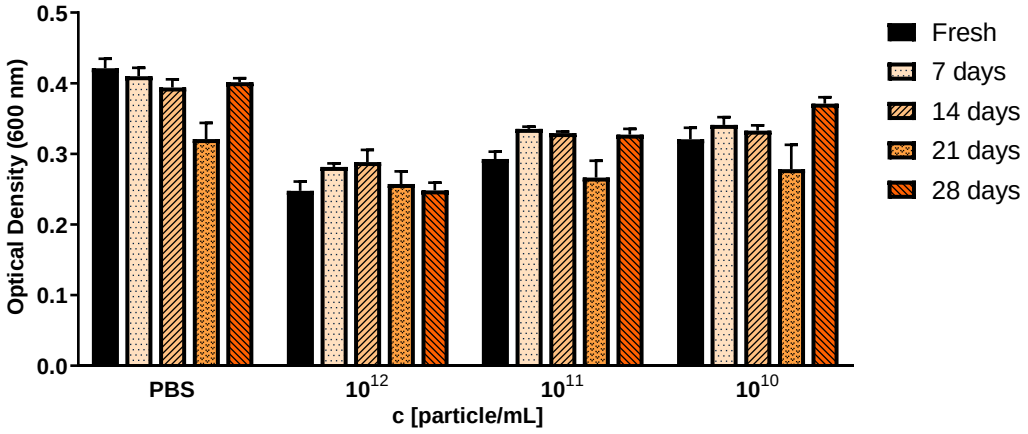

Figure 5. Antibacterial activity of Cbv34 OMVs against *E. coli* DH5-alpha right after isolation (fresh), and upon storage at 4 °C for 7, 14, 21 and 28 days. The treatment was done for 18 h at 37 °C. Mean ± SEM, $n = 3$.

3.5. OMVs Are Taken Up by Mammalian Cells

The interaction with and uptake of the OMVs in A549 epithelial cells and RAW 264.7 immune cells were assessed by flow cytometry (Figures 6 and 7) and CLSM (Figure 8). In

comparison to liposomes prepared from bacterial phospholipids, we observed a significantly slower uptake of OMVs in A549 cells at 4 and 24 h of incubation (Figure 6a,d). The MFI of the liposomes was significantly higher when compared to the OMVs at the 4 h time point with A549 cells (Figure 6b). The MFI difference remained high between Cbv34 OMVs and liposomes at 24 h, but it was not significant when Cbfe23 OMVs and liposomes were compared (Figure 6e). As for the uptake into RAW 264.7 cells, Cbfe23 OMVs and bacterial liposomes did not show any significant difference in terms of percentage of positive cells and MFI (Figure 7), both having a percentage of positive cells of nearly 90% at 4 h incubation time (Figure 7a). However, Cbv34 OMVs had a significantly lower percentage of positive cells when compared to the bacterial liposomes at 4 h (Figure 7a) and lower MFI at 24 h (Figure 7e). At the 24 h time point, all particles led to 100% of fluorescent cells with RAW 264.7 cells (Figure 7d). MFI remained comparable between all the samples at the 4 h time point (Figure 7b). The representative histograms of the uptake of DiI-stained particles in A549 cells (Figure 6c,f) and RAW 264.7 cells (Figure 7c,f) show the shift in the histograms of the samples compared to the untreated control (red).

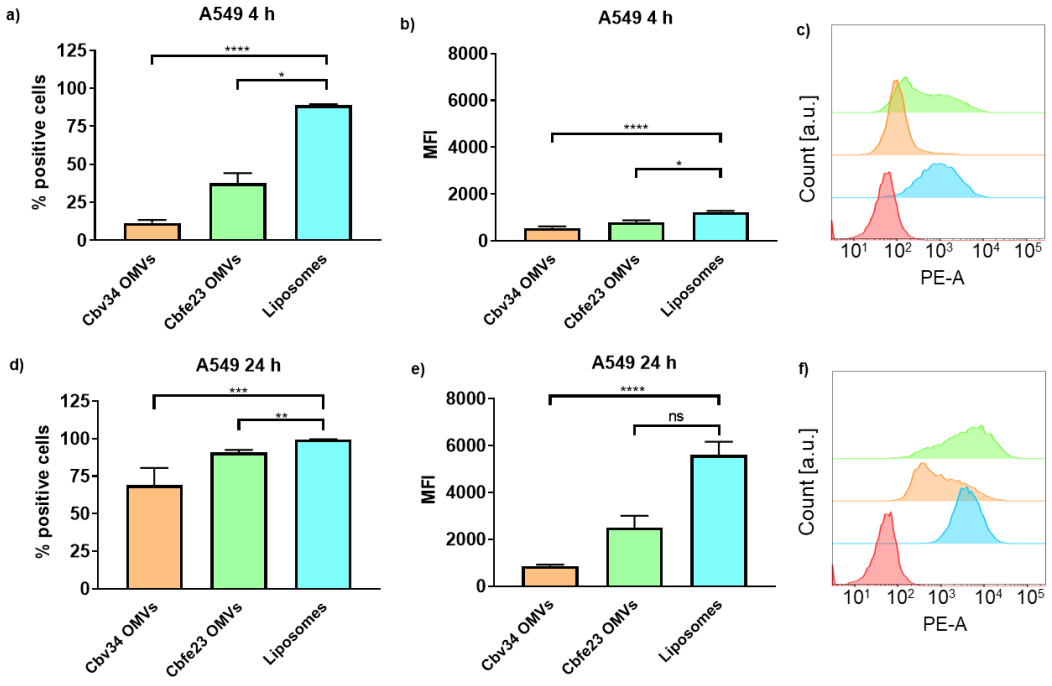

Figure 6. Interaction and uptake of OMVs and liposomes after incubation with A549 cells. The percentage of positive cells (which interacted with DiI-labelled OMVs) after (**a**) 4 h and (**d**) 24 h of incubation. The MFI after (**b**) 4 h and (**e**) 24 h of incubation. Representative histograms of Cbfe23 OMVs (green), Cbv34 OMVs (orange), liposomes (blue) and untreated control (red) after (**c**) 4 h and (**f**) 24 h of incubation. Mean ± SEM, $n = 3$. * $p < 0.05$, ** $p < 0.005$, *** $p < 0.0005$ and **** $p < 0.0001$.

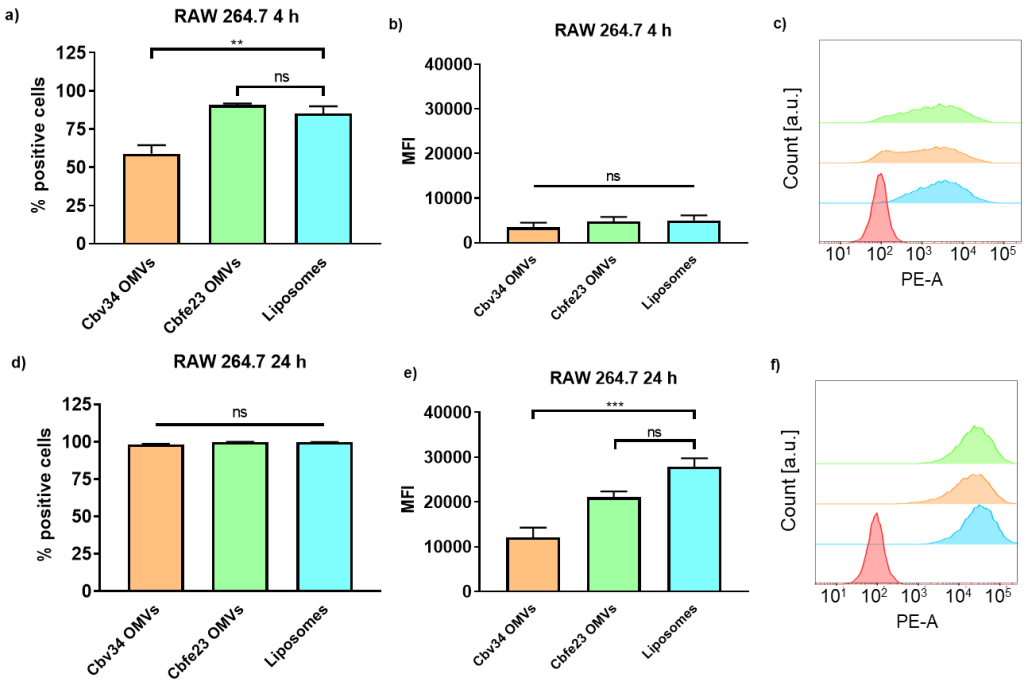

Figure 7. Interaction and uptake of OMVs and liposomes after incubation with RAW 264.7 cells. The percentage of positive cells (which interacted with DiI-labelled OMVs) after (**a**) 4 h and (**d**) 24 h of incubation. The MFI after b) 4 h and e) 24 h of incubation. Representative histograms of Cbfe23 OMVs (green), Cbv34 OMVs (orange), liposomes (blue) and untreated control (red) after (**c**) 4 h and (**f**) 24 h of incubation. Mean ± SEM, $n = 3$. ** $p < 0.005$, *** $p < 0.0005$ and ns = not significant.

As for the localization of the particles within the cells, we observed little fluorescence signal coming from the particles after 4 h of incubation with A549 (Figure S7), and a higher fluorescence of Cbfe23 OMVs when incubated with RAW 264.7 cells for 4 h (Figure S8), when compared to the Cbv34 OMVs. Even though we saw DiI-stained Cbv34 and Cbfe23 OMVs within the cells, we did not observe colocalization with the cytoskeleton at any investigated time point (Figure 8). We noticed a removal of OMVs by PBS washing during the staining process, which may indicate that they are mostly bound onto the cell surface. When the cells were washed once with PBS and fixed, we observed a high number of fluorescent particles in A549 cells (Figures S9 and S10).

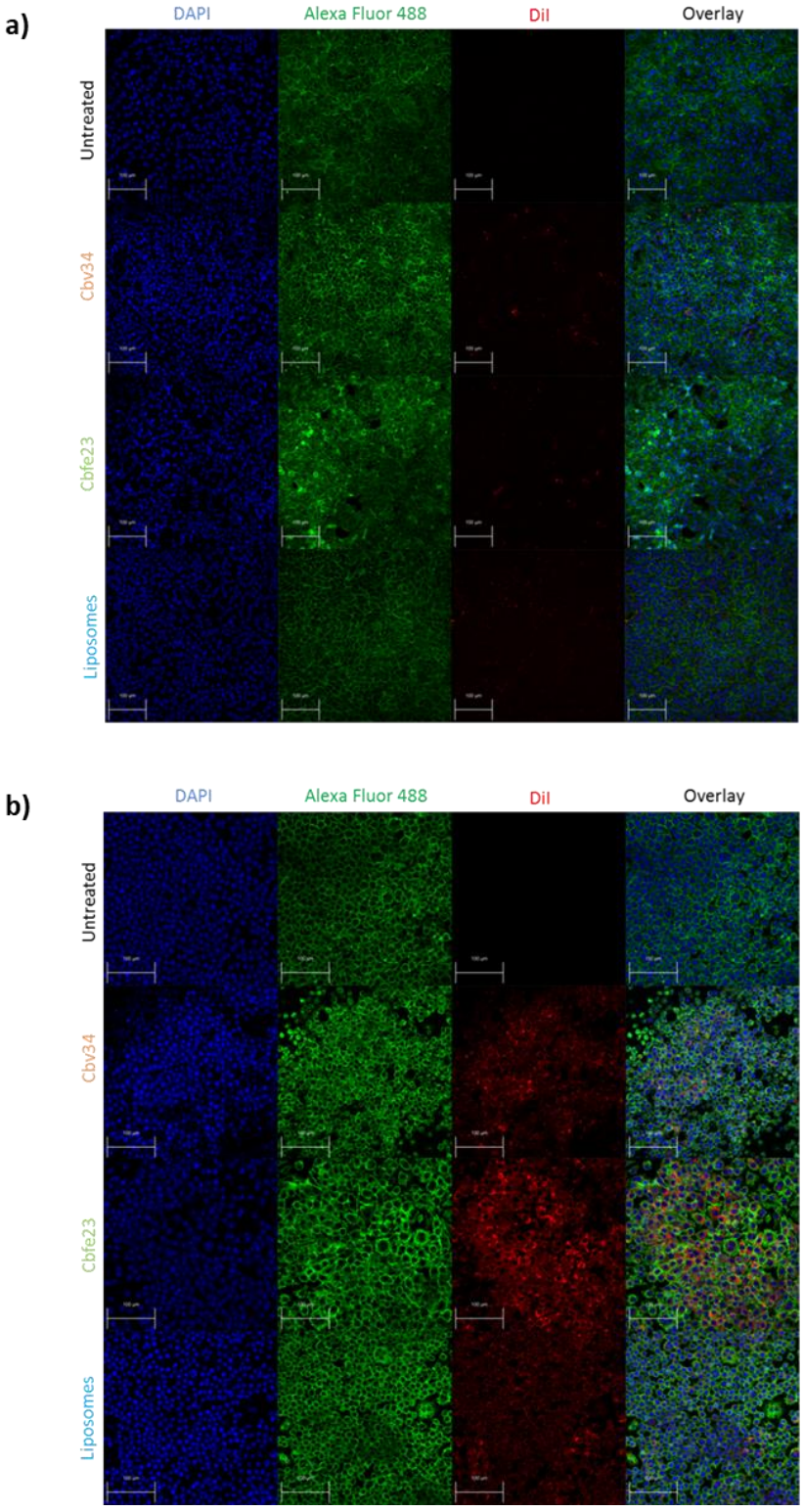

Figure 8. Uptake of fluorescent particles investigated by confocal laser scanning microscopy (CLSM) after 24 h of incubation with (**a**) A549 and (**b**) RAW 264.7 cells. The cells nuclei are stained with DAPI (blue), while the F-actin is labelled with Alexa Fluor 488 Phalloidin (green). OMVs and bacterial liposomes are stained with DiI (red). Scale bar = 100 µm.

3.6. OMVs Are Able to Kill Intracellular Pathogens

We investigated the ability of myxobacterial OMVs to treat intracellular infections caused by *S. aureus* in A549 cells. The most active concentrations were 10^8 OMVs/mL and 10^{11} OMVs/mL for Cbfe23 and Cbv34 OMVs, respectively (Figure 9). The highest concentrations of Cbfe23 OMVs were not tested, because they negatively influenced the viability of the cells, as shown in Figure 2a. Gentamicin is soluble in water, while cystobactamid is dissolved in DMSO (dimethyl sulfoxide), so we included DMSO as a solvent control. The DMSO might contribute to the antibacterial effect of the free cystobactamid, as we observed a tendency of lower CFU amounts in the DMSO sample alone. Both free gentamicin and cystobactamid, together with the solvent control DMSO, were not significantly different when compared among themselves. Our OMVs, which are in aqueous suspension, showed a more pronounced reduction in bacterial growth compared to free antibiotics. By comparing this with the number of bacteria present in the cells after 2 h of uptake (time zero), we see that the effect of the OMVs against *S. aureus* is bacteriostatic. This effect was also confirmed by the statistical analysis, which did not show a significant difference in bacterial growth between the most effective OMV concentrations and the time zero control (blue dashed line in Figure 9).

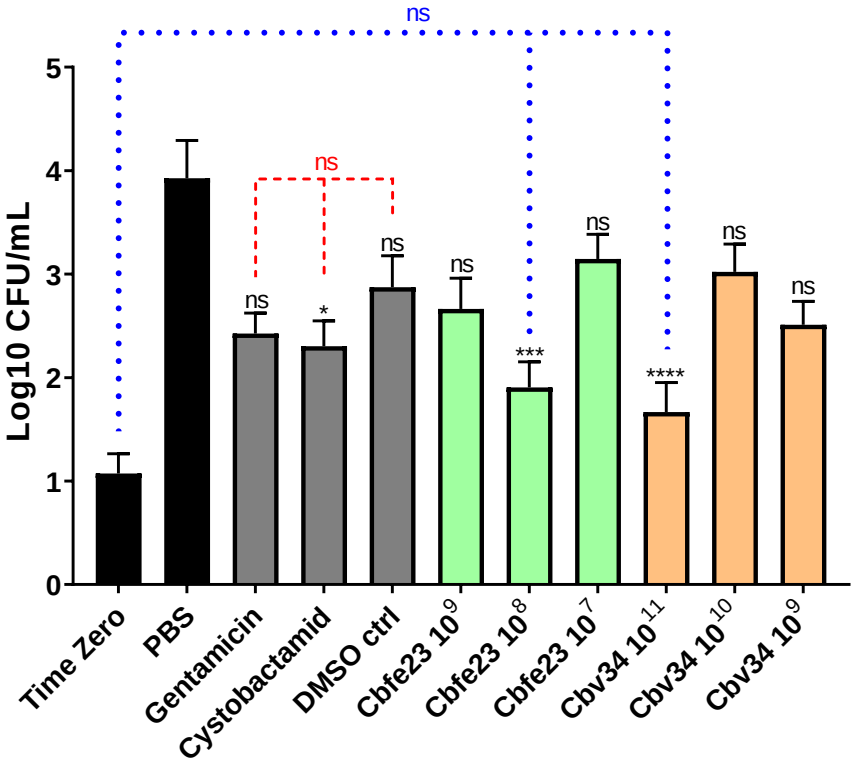

Figure 9. Antibacterial effect of OMVs against intracellular *S. aureus* after 24 h of treatment. Mean ± SEM, *n* = 3–4 independent experiments. Significance was defined in relation to the PBS control as ns = not significant, * *p*-value < 0.05, *** *p*-value < 0.0005 and **** *p*-value < 0.0001. Red dashed lines represent the comparison

between gentamicin 10 µg/mL, cystobactamid 10 µg/mL and the DMSO control = not significant. Blue dotted lines represent the comparison between the time zero (2 h bacterial uptake), Cbfe23 10^8 particles/mL and Cbv34 10^{11} particles/mL.

4. Discussion

Cbv34 and Cbfe23 OMVs were successfully isolated by differential centrifugation and SEC, presenting a size of approximately 120–150 nm, which is an advantageous size for interaction with target cells and accumulation in inflamed infectious tissue [37]. The Cryo-TEM images showed spherical forms for Cbv34 OMVs, but for Cbfe23 OMVs, rod-shaped particles were also seen (Figure S4). We suspect that these particles might be fragments of outer membrane tubes (OMTs), which are known to be produced by some myxobacterial strains [38].

As for the viability and cytotoxicity, we showed low to absent toxicity for Cbv34 OMVs, as also reported in literature [33]. Cbfe23 OMVs, which were studied here for the first time, reduced the viability of the cells only at a concentration of 125,000 OMVs/cell. This might be caused by a higher load of antibiotic in comparison to Cbv34 OMVs, since we could see that a concentration of 10 µg/mL cystobactamid also had a similar negative effect on cell viability. No dramatic cytotoxicity was detected at any concentrations tested for either OMV. We have tested whether our OMVs induce the production of proinflammatory cytokines to better understand the potential immunogenicity of our carriers. IL-6, which is a multifunctional cytokine, and TNF, are released in response to inflammation and mediate reactions to its effects, such as fever [39,40]. IL-8 and IL-1b induce chemotaxis and play a key role in inflammation, recruiting neutrophils to the site of infection [41–43]. Our OMVs promoted a mild release of proinflammatory cytokines compared to the LPS control. As an exception, the concentration of 10^{13} Cbfe23 OMVs/mL stimulated a high production of IL-1beta, but possibly induced cell death, as observed by light microscopy (Figure S5). IL-1beta is known to be negatively influenced in production by the use of molecules that induce autophagy [44], which contributes to cell survival. This result might also lead to a clue about the mechanisms of how Cbfe23 OMVs induce cell death at high concentrations.

Even though high concentrations of OMVs were needed to inhibit the growth of planktonic bacteria, concentrations of 10^{12} OMVs/mL and higher did not seem to be required for an antibacterial effect against intracellular pathogens. When intracellular CFUs were assessed to investigate the OMVs' activity against *S. aureus*, a bacterial growth inhibition was identified, especially from Cbfe23 OMVs. In literature, the Cbfe23 strain has not been reported to produce

cystobactamids [45]. Here, we modified the composition of the bacterial culture medium by using phytone as a carbon source, instead of the previously reported skimmed milk and soy flour [45]. Due to this modification, we were able to identify cystobactamids 919-1 and 920-1 [46–48] as the active compounds in the OMV extract (Figure S6). For the potential application of OMVs as an antibacterial therapy in the clinic, their formulations must be stable for a certain period, preferably without any special storage conditions, such as deep freezing at −80 °C and the use of cryoprotectants. Since we have already showed an antibacterial effect of Cbv34 OMVs against *E. coli* [26] and the easy handling of this bacterium, we investigated OMV storage stability at 4 °C with this model pathogen. We found that the dose-dependent antibacterial activity of Cbv34 OMVs was conserved during 28 days of storage. This result matches recent findings that show extracellular vesicles' inherent stability under different storage conditions [49,50].

Compared to bacteriomimetic liposomes, OMVs showed different uptake kinetics with immune and epithelial cells. While liposomes are rapidly taken up in all cell types at high amounts, OMVs seemed to have a preferentially better uptake in immune cells than in epithelial cells. Surface charge may play a role in this mechanism, but surface proteins of OMVs are also important for this effect, as was shown for mammalian vesicles [51]. As we show, OMVs have an antibacterial effect against internalized *S. aureus* in A549 cells. Both Cbfe23 and Cbv34 OMVs showed a higher antibacterial effect, when compared to the untreated control, than the free gentamicin and cystobactamid. Free antibiotics generally have a low permeation through mammalian cell membranes and thus favor intracellular infections, which may become persistent and difficult to treat. The use of myxobacterial OMVs as nanocarriers could possibly overcome the cellular barrier and successfully deliver the antibacterial compound to the lungs, potentially being administered locally as an aerosol.

The next steps to further evaluate myxobacterial OMVs as drug carriers are to rule out their immunogenicity in complex in vitro models of inflammation [52], and the evaluation of their antibacterial activity in an infected animal model.

5. Conclusions

OMVs from Cbv34 and Cbfe23 are not only low in toxicity in different cell lines, but also in primary immune cells. They are able to mediate killing of one of the most important Gram-positive problem pathogens, *S. aureus*. These OMVs are able to be taken up into infected cells and showed efficient bacteriostatic effect against intracellular *S. aureus* infections.

Supplementary Materials: The following are available online at www.mdpi.com/xxx/s1. Figure S1: Morphology of Cbfe23 (passage 3, 5 days in culture) and Cbv34 (passage 9, 7 days in culture), Figure S2: Particle size measured by dynamic light scattering and protein concentration of Cbfe23 size exclusion chromatography fractions (1 mL each) were measured

by BCA (bicinchoninic acid) assay (Sigma-Aldrich Co., St. Louis, MO, USA), Figure S3: Representative graphs of size distributions measured by nanoparticle tracking analysis of a) Cbv34 and b) Cbfe23 OMVs, Figure S4: Cryo-TEM micrographs of Cbfe23 pellets after ultracentrifugation, Figure S5: Light microscopy images showing the morphology of peripheral blood mononuclear cells (PBMCs) after 4 h treatment with OMVs and controls, Figure S6: a) LC-MS Base peak chromatogram of the OMV extract (black) highlighting the two major cystobactamids: cystobactamid 919-1 (A, red, m/z 920.31 ± 0.05 Da) and cystobactamid 920-1 (B, blue, m/z 921.30 ± 0.05 Da) as extracted ion chromatograms, Figure S7: Uptake/interaction of OMVs and liposomes with A549 cells after 4 h incubation measured by confocal laser scanning microscopy, Figure S8: Uptake/interaction of OMVs and liposomes with RAW 264.7 cells after 4 h of incubation measured by confocal laser scanning microscopy, Figure S9: Uptake/interaction imaging of OMVs and liposomes after 4 h incubation with A549, following one single wash with PBS and fixation by confocal laser scanning microscopy, Figure S10: Uptake/interaction imaging of OMVs and liposomes after 24 h incubation with A549, following one single wash with PBS and fixation by confocal laser scanning microscopy.

Author Contributions: A.G. performed all bacterial and mammalian cell culture, OMVs isolation, particle measurements, antibacterial assays, infection assays, confocal laser scanning microscopy, flow cytometry, data analysis and wrote the main manuscript draft. P.L. performed particle characterization and staining together with A.G. T.K. performed viability and cytotoxicity assays. E.S. and C.D. isolated PBMCs. E.S. performed cytokine detection. R.R. prepared and characterized the bacteriomimetic liposomal formulation. F.P. performed mass spectrometry measurements. M.K. obtained cryo-TEM images. A.K.K. supervised and revised cytokine detection experiments. R.G. and R.M. kindly provided myxobacterial strains and advised on their culture conditions. G.F. conceived the project, supervised the work and wrote the manuscript together with A.G. All authors contributed to the writing of the manuscript.

Funding: This work was supported by a Junior Research grant from the Federal Ministry of Research and Education (NanoMatFutur programme, grant number 13XP5029A). This work was supported, in part, by the Deutsche Forschungsgemeinschaft (DFG, to A.K.K., KI702).

Acknowledgments: We would like to thank Jana Westhues and Petra König for their help with the mammalian cell culture.

Conflicts of Interest: The authors declare no conflict of interest.

References

1. Troeger, C.; Blacker, B.; Khalil, I.A.; Rao, P.C.; Cao, J.; Zimsen, S.R.M.; Albertson, S.B.; Deshpande, A.; Farag, T.; Abebe, Z.; et al. Estimates of the global, regional, and national morbidity, mortality, and aetiologies of lower respiratory infections in 195 countries, 1990–2016: A systematic analysis for the Global Burden of Disease Study 2016. *Lancet Infect. Dis.* **2018**, *18*, 1191–1210.
2. Naghavi, M.; Abajobir, A.A.; Abbafati, C.; Abbas, K.M.; Abd-Allah, F.; Abera, S.F.; Aboyans, V.; Adetokunboh, O.; Ärnlöv, J.; Afshin, A.; et al. Global, regional, and national age-sex specific mortality for 264 causes of death, 1980–2016: A systematic analysis for the Global Burden of Disease Study 2016. *Lancet* **2017**, *390*, 1151–1210.
3. Sherrard, L.J.; Tunney, M.M.; Elborn, J.S. Infections in chronic lung diseases 2 Antimicrobial resistance in the respiratory microbiota of people with cystic fi brosis. *Lancet* **2014**, *384*, 703–713.
4. Lommatzsch, S.T.; Aris, R. Genetics of cystic fibrosis. *Semin. Respir. Crit. Care Med.* **2009**, *30*, 531–538.
5. Ahmed, M.I.; Mukherjee, S. Treatment for chronic methicillin-sensitive Staphylococcus aureus pulmonary infection in people with cystic fibrosis. *Cochrane Database Syst. Rev.* **2018**, *3*, CD011581.
6. Ulrich, M.; Herbert, S.; Berger, J.; Bellon, G.; Louis, D.; Münker, G.; Döring, G. Localization of Staphylococcus aureus in Infected Airways of Patients with Cystic Fibrosis and in a Cell Culture Model of S. aureus Adherence. *Am. J. Respir. Cell Mol. Biol.* **1998**, *19*, 83–91.
7. Tranchemontagne, Z.R.; Camire, R.B.; O'Donnell, V.J.; Baugh, J.; Burkholder, K.M. Staphylococcus aureus Strain USA300 Perturbs Acquisition of Lysosomal Enzymes and Requires Phagosomal Acidification for Survival inside Macrophages. *Infect. Immun.* **2016**, *84*, 241–253.
8. Flannagan, R.S.; Heit, B.; Heinrichs, D.E. Intracellular replication of Staphylococcus aureus in mature phagolysosomes in macrophages precedes host cell death, and bacterial escape and dissemination. *Cell. Microbiol.* **2016**, *18*, 514–535.
9. Fraunholz, M.; Sinha, B. Intracellular staphylococcus aureus: Live-in and let die. *Front. Cell. Infect. Microbiol.* **2012**, *2*, 1–10.
10. Löffler, B.; Tuchscherr, L.; Niemann, S.; Peters, G. Staphylococcus aureus persistence in non-professional phagocytes. *Int. J. Med. Microbiol.* **2014**, *304*, 170–176.
11. Barcia-Macay, M.; Seral, C.; Mingeot-Leclercq, M.-P.; Tulkens, P.M.; Van Bambeke, F. Pharmacodynamic evaluation of the intracellular activities of antibiotics against Staphylococcus aureus in a model of THP-1 macrophages. *Antimicrob. Agents Chemother.* **2006**, *50*, 841–851.

12. Vaudaux, P.; Waldvogel, F.A. Gentamicin antibacterial activity in the presence of human polymorphonuclear leukocytes. *Antimicrob. Agents Chemother.* **1979**, *16*, 743–749.
13. Carlier, M.-B.; Zenebergh, A.; Tulkens, P.M. Cellular uptake and subcellular distribution of roxithromycin and erythromycin in phagocytic cells. *J. Antimicrob. Chemother.* **1987**, *20*, 47–56.
14. Jacobs, R.F.; Wilson, C.B. Activity of Antibiotics in Chronic Granulomatous Disease Leukocytes. *Pediatr. Res.* **1983**, *17*, 916–919.
15. Jacobs, R.F.; Wilson, C.B. Intracellular penetration and antimicrobial activity of antibiotics. *J. Antimicrob. Chemother.* **1983**, *12*, 13–20.
16. Bongers, S.; Hellebrekers, P.; Leenen, L.P.H.; Koenderman, L.; Hietbrink, F. Intracellular Penetration and Effects of Antibiotics on Staphylococcus aureus Inside Human Neutrophils: A Comprehensive Review. *Antibiotics* **2019**, *8*, 54.
17. Anversa Dimer, F.; de Souza Carvalho-Wodarz, C.; Goes, A.; Cirnski, K.; Herrmann, J.; Schmitt, V.; Pätzold, L.; Abed, N.; De Rossi, C.; Bischoff, M.; et al. PLGA nanocapsules improve the delivery of clarithromycin to kill intracellular Staphylococcus aureus and Mycobacterium abscessus. *Nanomed. Nanotechnol. Biol. Med.* **2020**, *24*, 102125.
18. Menina, S.; Eisenbeis, J.; Kamal, M.A.M.; Koch, M.; Bischoff, M.; Gordon, S.; Loretz, B.; Lehr, C. Bioinspired Liposomes for Oral Delivery of Colistin to Combat Intracellular Infections by *Salmonella enterica*. *Adv. Healthc. Mater.* **2019**, 1900564.
19. Castoldi, A.; Empting, M.; De Rossi, C.; Mayr, K.; Dersch, P.; Hartmann, R.; Müller, R.; Gordon, S.; Lehr, C.M. Aspherical and Spherical InvA497-Functionalized Nanocarriers for Intracellular Delivery of Anti-Infective Agents. *Pharm. Res.* **2019**, *36*, 1–13.
20. Yang, X.; Shi, G.; Guo, J.; Wang, C.; He, Y. Exosome-encapsulated antibiotic against intracellular infections of methicillin-resistant Staphylococcus aureus. *Int. J. Nanomed.* **2018**, *13*, 8095–8104.
21. Goes, A.; Fuhrmann, G. Biogenic and Biomimetic Carriers as Versatile Transporters to Treat Infections. *ACS Infect. Dis.* **2018**, *4*, 881–892.
22. Forier, K.; Raemdonck, K.; De Smedt, S.C.; Demeester, J.; Coenye, T.; Braeckmans, K. Lipid and polymer nanoparticles for drug delivery to bacterial biofilms. *J. Control. Release* **2014**, *190*, 607–623.
23. Reichenbach, H. The ecology of the myxobacteria. *Environ. Microbiol.* **1999**, *1*, 15–21.
24. Wu, Y.; Jiang, Y.; Kaiser, D.; Alber, M. Social interactions in myxobacterial swarming. *PLoS Comput. Biol.* **2007**, *3*, 2546–2558.
25. Reichenbach, H.; Gerth, K.; Irschik, H.; Kunze, B.; Höfle, G. Myxobacteria: A source of new antibiotics. *Trends Biotechnol.* **1988**, *6*, 115–121.
26. Weissman, K.J.; Müller, R. Myxobacterial secondary metabolites: Bioactivities and modes-of-action. *Nat. Prod. Rep.* **2010**, *27*, 1276.

27. Reichenbach, H. Myxobacteria, producers of novel bioactive substances. *J. Ind. Microbiol. Biotechnol.* **2001**, *27*, 149–156.
28. Hoffmann, T.; Krug, D.; Bozkurt, N.; Duddela, S.; Jansen, R.; Garcia, R.; Gerth, K.; Steinmetz, H.; Müller, R. Correlating chemical diversity with taxonomic distance for discovery of natural products in myxobacteria. *Nat. Commun.* **2018**, *9*, 1–10.
29. Schwechheimer, C.; Kuehn, M.J. Outer-membrane vesicles from Gram-negative bacteria: Biogenesis and functions. *Nat. Rev. Microbiol.* **2015**, *13*, 605–619.
30. Kulp, A.; Kuehn, M.J. Biological Functions and Biogenesis of Secreted Bacterial Outer Membrane Vesicles. *Annu. Rev. Microbiol.* **2010**, *64*, 163–184.
31. Woith, E.; Fuhrmann, G.; Melzig, M.F. Extracellular Vesicles—Connecting Kingdoms. *Int. J. Mol. Sci.* **2019**, *20*, 5695.
32. Evans, A.G.L.; Davey, H.M.; Cookson, A.; Currinn, H.; Cooke-Fox, G.; Stanczyk, P.J.; Whitworth, D.E. Predatory activity of Myxococcus xanthus outer-membrane vesicles and properties of their hydrolase cargo. *Microbiology* **2012**, *158*, 2742–2752.
33. Schulz, E.; Goes, A.; Garcia, R.; Panter, F.; Koch, M.; Müller, R.; Fuhrmann, K.; Fuhrmann, G. Biocompatible bacteria-derived vesicles show inherent antimicrobial activity. *J. Control. Release* **2018**, *290*, 46–55.
34. Baumann, S.; Herrmann, J.; Raju, R.; Steinmetz, H.; Mohr, K.I.; Hüttel, S.; Harmrolfs, K.; Stadler, M.; Müller, R. Cystobactamids: Myxobacterial Topoisomerase Inhibitors Exhibiting Potent Antibacterial Activity. *Angew. Chem. Int. Ed.* **2014**, *53*, 14605–14609.
35. Wang, M.; Carver, J.J.; Phelan, V.V.; Sanchez, L.M.; Garg, N.; Peng, Y.; Nguyen, D.D.; Watrous, J.; Kapono, C.A.; Luzzatto-Knaan, T.; et al. Sharing and community curation of mass spectrometry data with Global Natural Products Social Molecular Networking. *Nat. Biotechnol.* **2016**, *34*, 828–837.
36. Graef, F.; Vukosavljevic, B.; Michel, J.-P.; Wirth, M.; Ries, O.; De Rossi, C.; Windbergs, M.; Rosilio, V.; Ducho, C.; Gordon, S.; et al. The bacterial cell envelope as delimiter of anti-infective bioavailability – An in vitro permeation model of the Gram-negative bacterial inner membrane. *J. Control. Release* **2016**, *243*, 214–224.
37. He, C.; Hu, Y.; Yin, L.; Tang, C.; Yin, C. Effects of particle size and surface charge on cellular uptake and biodistribution of polymeric nanoparticles. *Biomaterials* **2010**, *31*, 3657–3666.
38. Wei, X.; Vassallo, C.N.; Pathak, D.T.; Wall, D. Myxobacteria Produce Outer Membrane-Enclosed Tubes in Unstructured Environments. *J. Bacteriol.* **2014**, *196*, 1807–1814.
39. Banks, W.A.; Kastin, A.J.; Gutierrez, E.G. Penetration of interleukin-6 across the murine blood-brain barrier. *Neurosci. Lett.* **1994**, *179*, 53–56.

40. Coceani, F.; Lees, J.; Mancilla, J.; Belizario, J.; Dinarello, C.A. Interleukin-6 and tumor necrosis factor in cerebrospinal fluid: Changes during pyrogen fever. *Brain Res.* **1993**, *612*, 165–171.
41. Harada, A.; Sekido, N.; Akahoshi, T.; Wada, T.; Mukaida, N.; Matsushima, K. Essential involvement of interleukin-8 (IL-8) in acute inflammation. *J. Leukoc. Biol.* **1994**, *56*, 559–564.
42. Baggiolini, M.; Loetscher, P.; Moser, B. Interleukin-8 and the chemokine family. *Int. J. Immunopharmacol.* **1995**, *17*, 103–108.
43. Sauder, D.N.; Mounessa, N.L.; Katz, S.I.; Dinarello, C.A.; Gallin, J.I. Chemotactic cytokines: The role of leukocytic pyrogen and epidermal cell thymocyte-activating factor in neutrophil chemotaxis. *J. Immunol.* **1984**, *132*, 828–832.
44. Shaw, S.Y.; Tran, K.; Castoreno, A.B.; Peloquin, J.M.; Lassen, K.G.; Khor, B.; Aldrich, L.N.; Tan, P.H.; Graham, D.B.; Kuballa, P.; et al. Selective modulation of autophagy, innate immunity, and adaptive immunity by small molecules. *ACS Chem. Biol.* **2013**, *8*, 2724–2733.
45. Raju, R.; Mohr, K.I.; Bernecker, S.; Herrmann, J.; Müller, R. Cystodienoic acid: A new diterpene isolated from the myxobacterium Cystobacter sp. *J. Antibiot.* **2015**, *68*, 473–475.
46. Baumann, S.; Herrmann, J.; Raju, R.; Steinmetz, H.; Mohr, K.I. Cystobactamids : Myxobacterial topoisomerase inhibitors exhibiting broad spectrum antibacterial activity. *Angew. Chem.* **2014**.
47. Planke, T.; Moreno, M.; Hüttel, S.; Fohrer, J.; Gille, F.; Norris, M.D.; Siebke, M.; Wang, L.; Müller, R.; Kirschning, A. Cystobactamids 920-1 and 920-2: Assignment of the Constitution and Relative Configuration by Total Synthesis. *Org. Lett.* **2019**, *21*, 1359–1363.
48. Cheng, B.; Müller, R.; Trauner, D. Total Syntheses of Cystobactamids and Structural Confirmation of Cystobactamid 919-2. *Angew. Chem. Int. Ed.* **2017**, *56*, 12755–12759.
49. Frank, J.; Richter, M.; de Rossi, C.; Lehr, C.-M.; Fuhrmann, K.; Fuhrmann, G. Extracellular vesicles protect glucuronidase model enzymes during freeze-drying. *Sci. Rep.* **2018**, *8*, 12377.
50. Schulz, E.; Karagianni, A.; Koch, M.; Fuhrmann, G. Hot EVs – how temperature affects extracellular vesicles. *Eur. J. Pharm. Biopharm.* **2019**.
51. Saari, H.; Lázaro-Ibáñez, E.; Viitala, T.; Vuorimaa-Laukkanen, E.; Siljander, P.; Yliperttula, M. Microvesicle- and exosome-mediated drug delivery enhances the cytotoxicity of Paclitaxel in autologous prostate cancer cells. *J. Control. Release* **2015**, *220*, 727–737.
52. Susewind, J.; de Souza Carvalho-Wodarz, C.; Repnik, U.; Collnot, E.-M.; Schneider-Daum, N.; Griffiths, G.W.; Lehr, C.-M. A 3D co-culture of three human cell lines to model

the inflamed intestinal mucosa for safety testing of nanomaterials. *Nanotoxicology* **2015**, *5390*, 1–10.

cells

Supplementary Material

Myxobacteria-derived outer membrane vesicles: potential applicability against intracellular infections

Adriely Goes, Philipp Lapuhs, Thomas Kuhn, Eilien Schulz, Robert Richter, Fabian Panter, Charlotte Dahlem, Marcus Koch, Ronald Garcia, Alexandra K. Kiemer, Rolf Müller and Gregor Fuhrmann

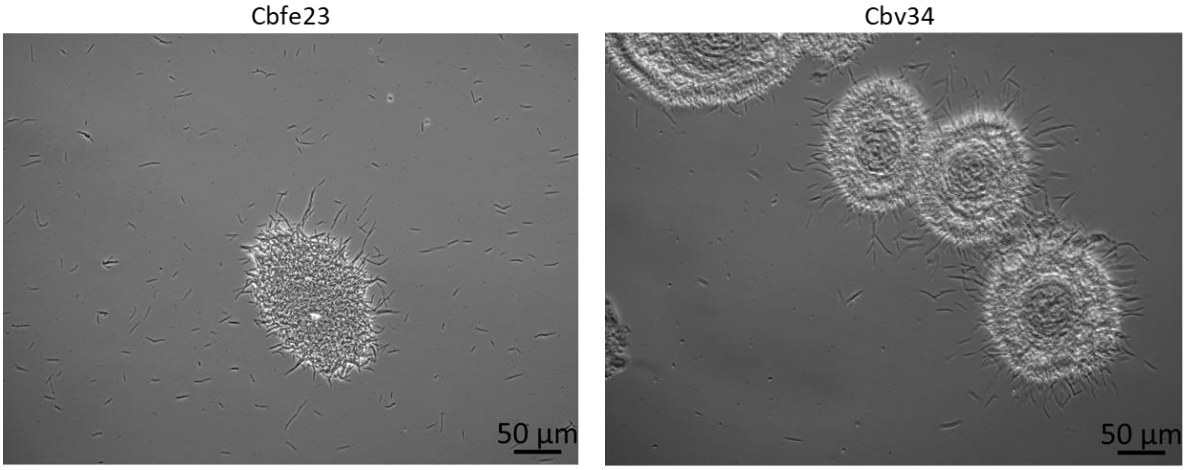

Figure S1: Morphology of Cbfe23 (passage 3, 5 days in culture) and Cbv34 (passage 9, 7 days in culture). Myxobacteria form cell aggregates in liquid culture. Images were taken with a light microscope (Zeiss, Germany). Scale bars = 50 µm.

Protein concentration and particle size of Cbfe23 OMVs

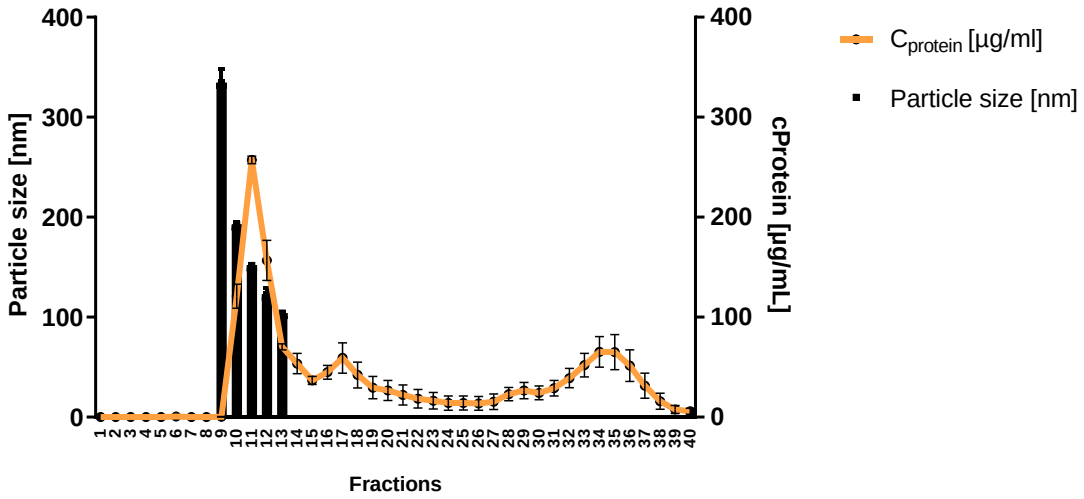

Figure S2: Particle size measured by dynamic light scattering and protein concentration of Cbfe23 size exclusion chromatography fractions (1 mL each) were measured by BCA (bicinchoninic acid) assay (Sigma-Aldrich Co., St. Louis, MO, USA). Mean ± SEM, *n* = 3.

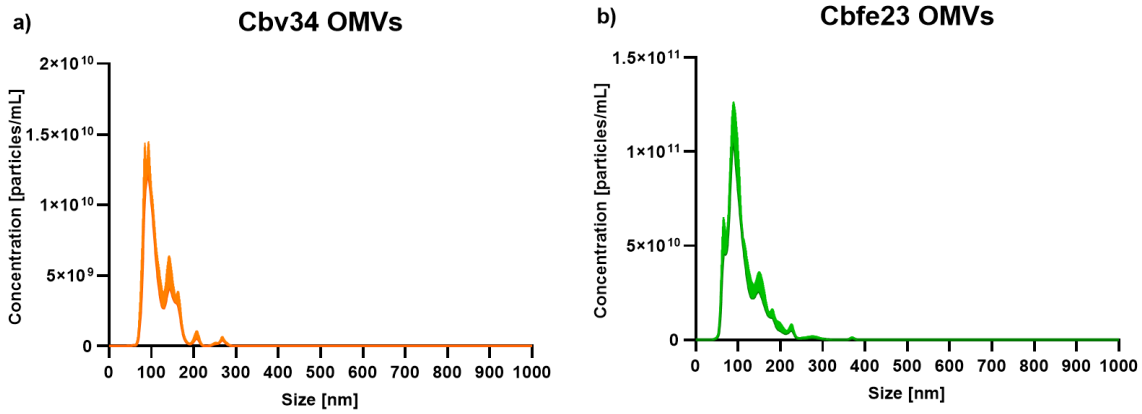

Figure S3: Representative graphs of size distributions measured by nanoparticle tracking analysis of a) Cbv34 and b) Cbfe23 OMVs. Mean + SEM.

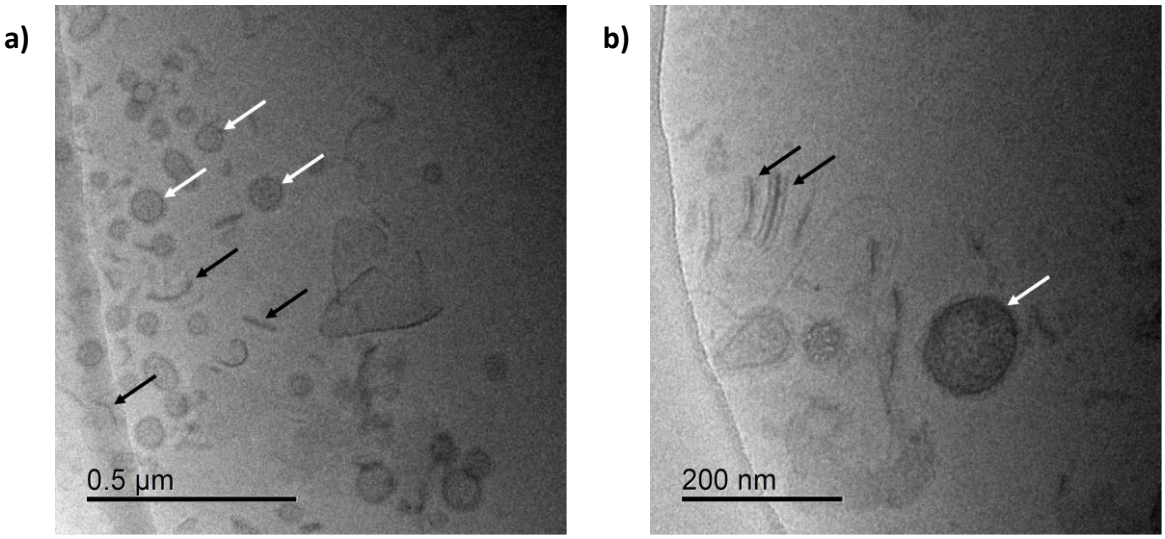

Figure S4: Cryo-TEM micrographs of Cbfe23 pellets after ultracentrifugation. The white arrows indicate OMVs with spherical shape and electron dense cores. The black arrows indicate rod-shaped electron dense particles of similar size as the OMVs.

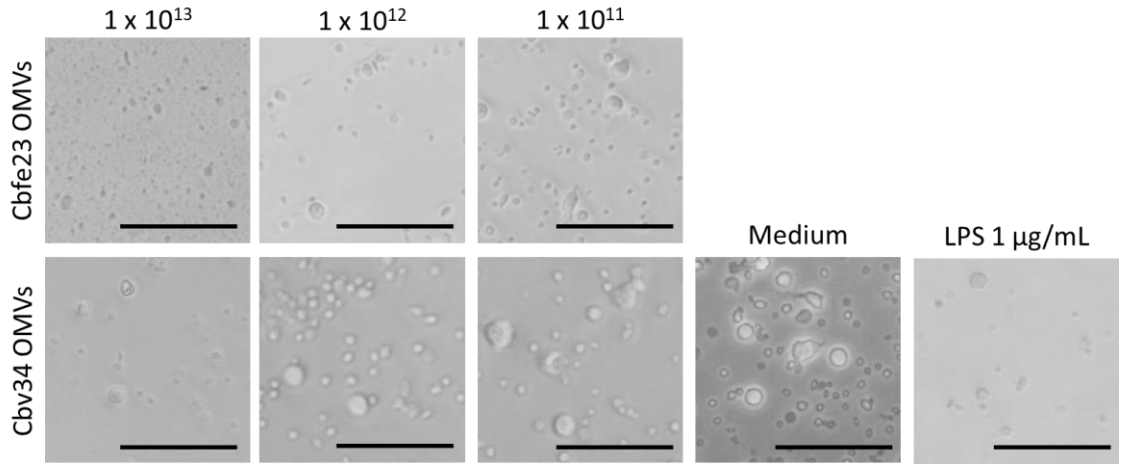

Figure S5: Light microscopy images showing the morphology of peripheral blood mononuclear cells (PBMCs) after 4 h treatment with OMVs and controls. The viability of the cells appeared to be compromised upon treatment with high concentrations of OMVs (1×10^{13} OMVs/mL). Scale bars = 50 µm.

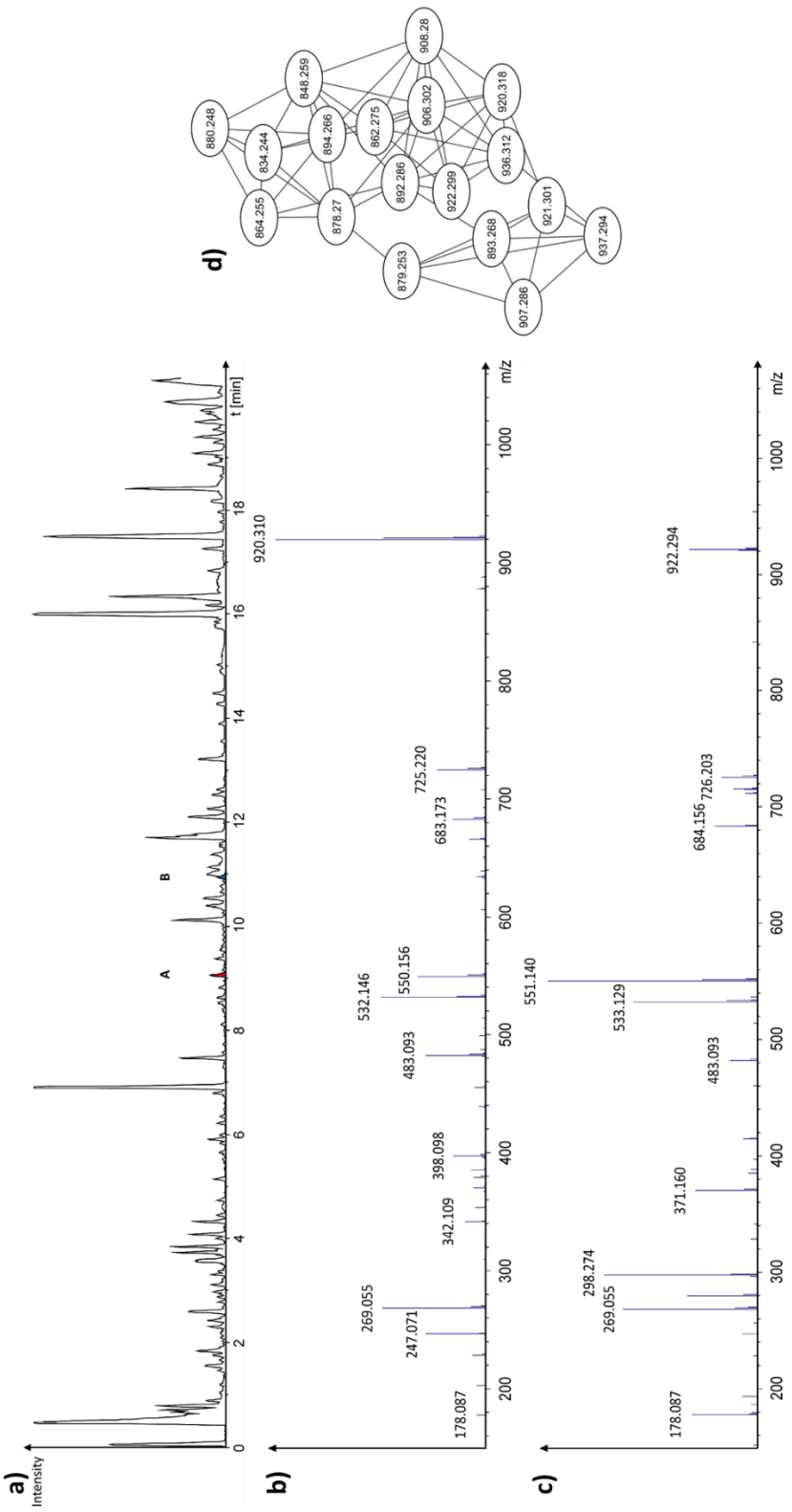

Figure S6: a) LC-MS Base peak chromatogram of the OMV extract (black) highlighting the two major cystobactamids: cystobactamid 919-1 (A, red, m/z 920.31 ± 0.05 Da) and cystobactamid 920-1 (B, blue, m/z 921.30 ± 0.05 Da) as extracted ion chromatograms. b) ESI-CID-MS² spectrum of cystobactamid 919-1 from the OMV samples measured on a maXis 4G qTOF spectrometer c) ESI-CID-MS² spectrum of

cystobactamid 920-1 from the OMV samples measured on a maXis 4G qTOF spectrometer d) Spectral network created by GNPS using the MS^2 data from the OMV extract samples depicting the precursor masses of all cystobactamid derivatives contained in the samples.

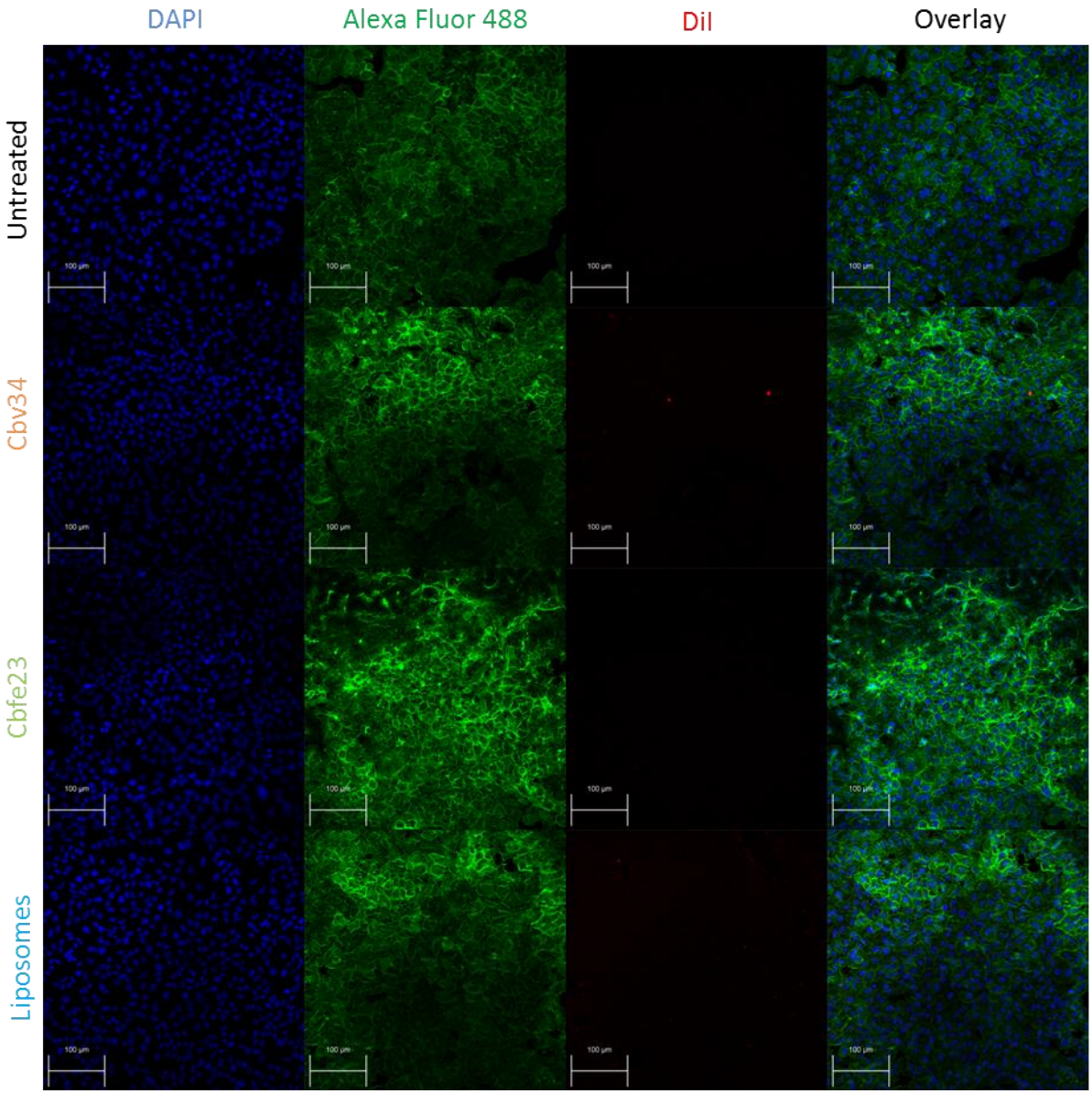

Figure S7: Uptake/interaction of OMVs and liposomes with A549 cells after 4 h incubation measured by confocal laser scanning microscopy. The cells nuclei are stained by DAPI (blue), while the F-actin is labelled by Alexa Fluor® 488 Phalloidin (green). Scale bars = 100 µm.

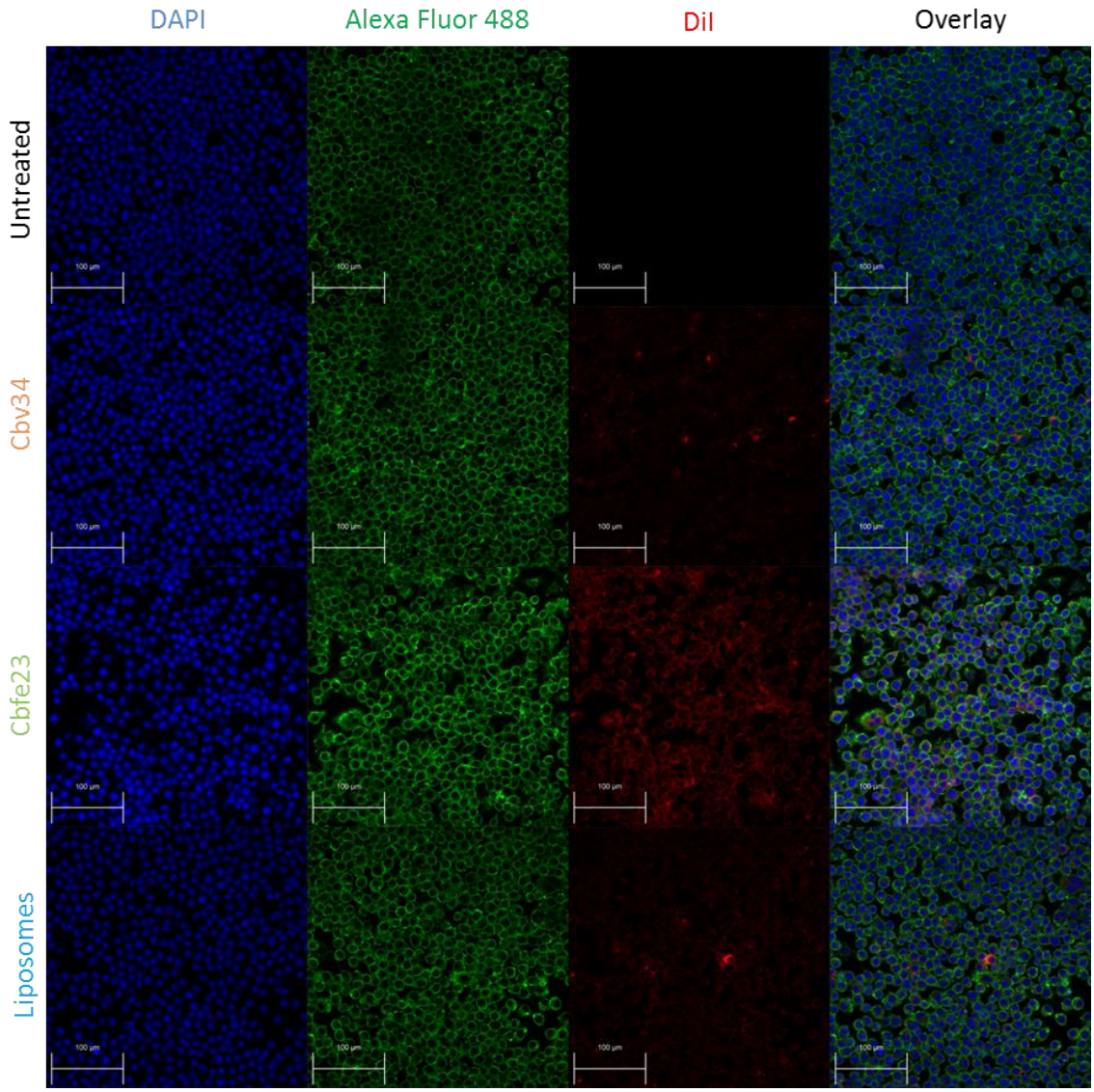

Figure S8: Uptake/interaction of OMVs and liposomes with RAW 264.7 cells after 4 h of incubation measured by confocal laser scanning microscopy. The cells nuclei are stained by DAPI (blue), while the F-actin is labelled by Alexa Fluor® 488 Phalloidin (green). Scale bars = 100 µm.

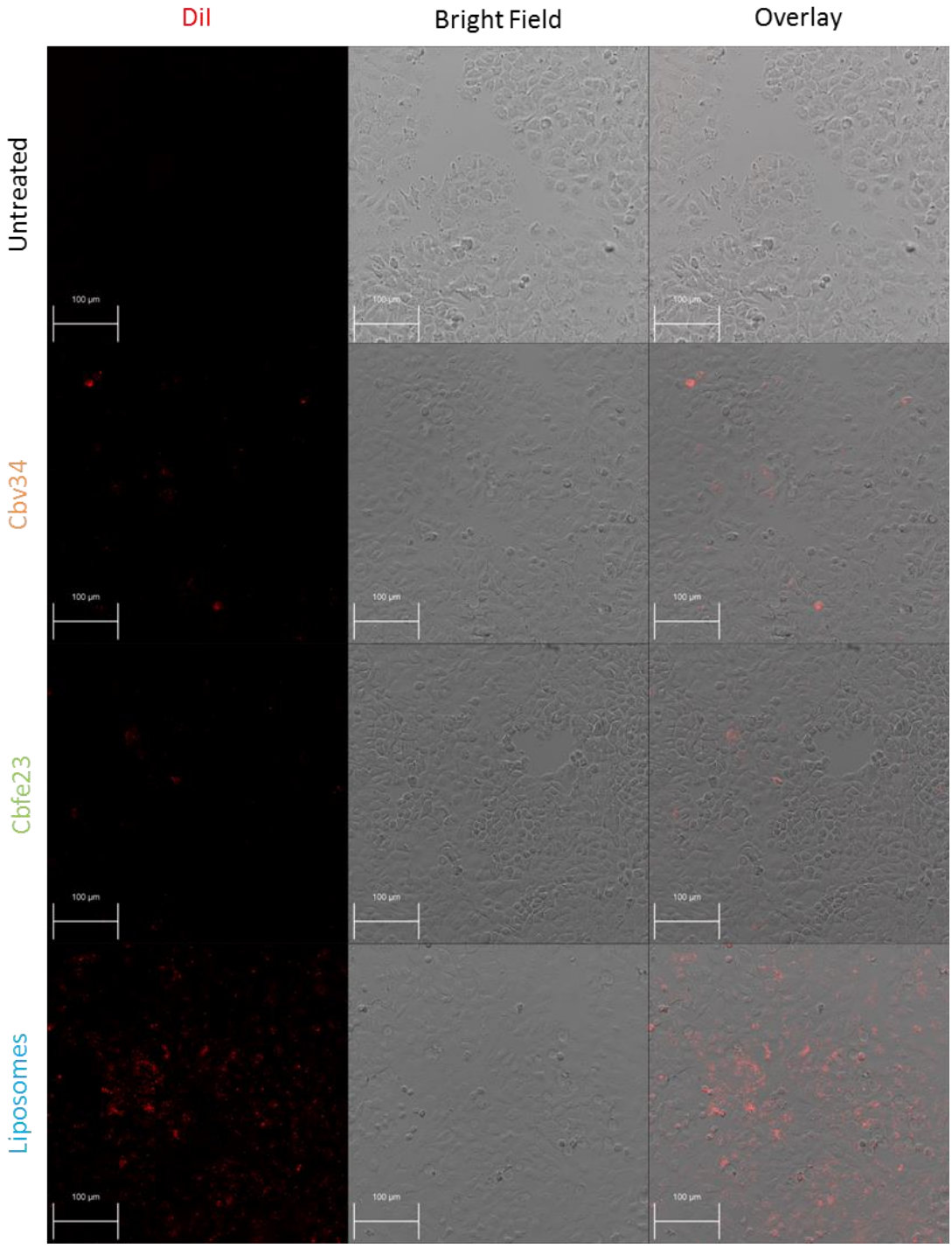

Figure S9: Uptake/interaction imaging of OMVs and liposomes after 4 h incubation with A549, following one single wash with PBS and fixation by confocal laser scanning microscopy. Cells were imaged with bright field and OMVs and liposomes were stained with DiI (red). Scale bars = 100 µm.

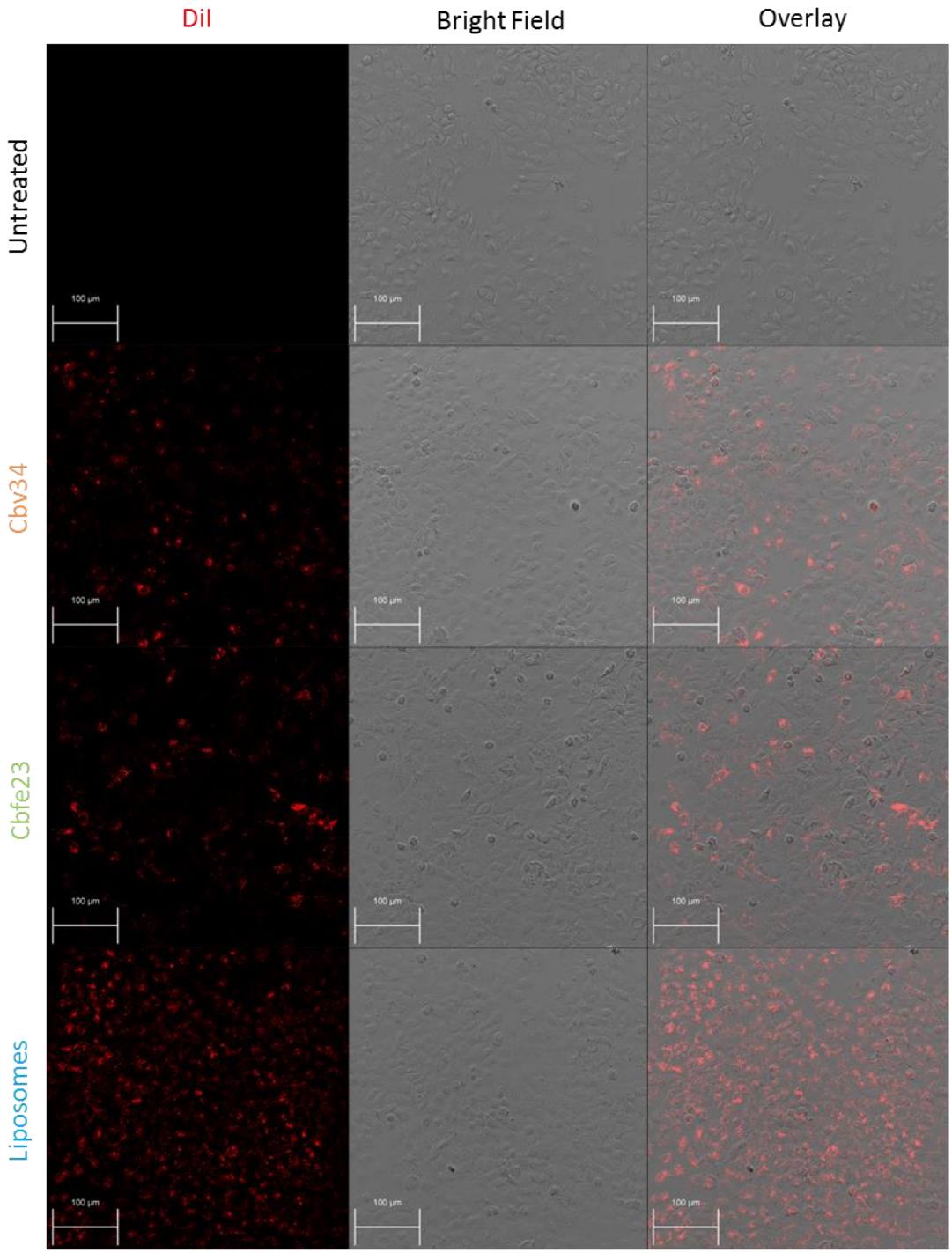

Figure S10: Uptake/interaction imaging of OMVs and liposomes after 24 h incubation with A549, following one single wash with PBS and fixation by confocal laser scanning microscopy. Cells were imaged with bright field and OMVs and liposomes were stained with DiI (red). Scale bars = 100 µm.

7.4. A biocompatible carrier system against GI infections: Ciprofloxacin loaded Extracellular Vesicles inhibit the growth of *Shigella flexneri*

Eilien Heinrich, Olga Hartwig, Christine Walt, Marcus Koch, Alexandra K. Kiemer, Brigitta Loretz, Claus-Michael Lehr, Rolf Müller and Gregor Fuhrmann

The data presented in this chapter is content of a forthcoming manuscript and has not been published yet.

A biocompatible carrier system against GI infections: Ciprofloxacin loaded Extracellular Vesicles inhibit the growth of *Shigella flexneri*

Eilien Heinrich[1,2], Olga Hartwig[2,3], Christine Walt[2,4], Marcus Koch[5], Alexandra K. Kiemer[6], Brigitta Loretz[2,3], Claus-Michael Lehr[2,3], Rolf Müller[2,4] and Gregor Fuhrmann[1,2]*

[1]Helmholtz-Institute for Pharmaceutical Research Saarland (HIPS), Helmholtz-Centre for Infection Research (HZI), Biogenic Nanotherapeutics Group (BION), Campus E8.1, 66123 Saarbrücken

[2]Department of Pharmacy, Saarland University, Campus E8.1, 66123 Saarbrücken, Germany

[3]Helmholtz-Institute for Pharmaceutical Research Saarland (HIPS), Helmholtz-Centre for Infection Research (HZI), Department of Drug Delivery (DDEL), Campus E8.1, 66123 Saarbrücken

[4]Helmholtz-Institute for Pharmaceutical Research Saarland (HIPS), Helmholtz-Centre for Infection Research (HZI), Department of Microbial Natural Products (MINS), Campus E8.1, 66123 Saarbrücken

[5]INM – Leibniz Institute for New Materials, Campus D2 2, 66123, Saarbrücken, Germany

[6]Department of Pharmacy, Pharmaceutical Biology, Saarland University, Campus C2.3, 66123 Saarbrücken, Germany

*__Corresponding author__, phone: +49 68198806 1500, email: gregor.fuhrmann@helmholtz-hzi.de

ORCID IDs: Eilien Heinrich: 0000-0002-9769-8980, Gregor Fuhrmann: 0000-0002-6688-5126

KEYWORDS: *extracellular vesicles, outer membrane vesicles, biogenic drug carrier, Shigella flexneri, zebrafish larvae, infection, ciprofloxacin*

Abstract

Antimicrobial resistance causes 25,000 deaths worldwide annually. Due to misuse in livestock, poor infection control, over-prescription and compliance issues this number is estimated to rise up to 10 million by 2050. Meanwhile, the number of newly approved antibiotics is decreasing, as the development is expensive and mostly unprofitable for pharmaceutical companies. Hence, the need to improve presently existing antibiotics is inevitable. One promising strategy to reuse clinically known drugs and advance their efficiency is the development of so-called nanoantibiotics. These nano-sized structures meet criteria to overcome biological barriers, target the site of infection passively and actively, release high doses of drug close to and within their target and thus can prevent the development of antimicrobial resistance. In this work, we took a non-synthetic, biogenic avenue and utilized extracellular vesicles (EVs) to develop a new therapeutic against one of the most challenging gastrointestinal (GI) pathogens *Shigella* spp. We established an ecologically friendly protocol that makes it possible to isolate EVs on a large scale while reducing plastic waste and saving space for cultivation, drawing attention to sustainable EV research. Further, we were able to produce a carrier system that induced a low cytokine response in primary immune cells and contained endotoxin concentrations below 0.25 EU/mL, obtaining criteria for injectables. A three-dimensional cell model of the human intestinal wall was used to understand the spatial distribution of vesicles under healthy or inflamed conditions. They were mainly found within the epithelial layer, highlighting the potential use as a therapeutic against epithelial cell invading GI pathogens such as *Shigella*. Further, the vesicles were successfully loaded with the fluoroquinolone ciprofloxacin (CPX), an antibiotic of which resistant rates have been drastically increasing within the last years. Evaluating different loading techniques, the most efficient method was a passive-incubation approach, with CPX concentrations raging between 26 to 87 ng/vesicle × 10^{-12}. Potential toxicity of (un-) loaded vesicles was further assessed *in vivo* in zebrafish larvae. The carrier systems alone were not toxic to the larvae, and the embryological development comparable to controls. However, we observed a formation of heart edema when free CPX was injected into fish. Yet, the CPX loaded vesicles induced fewer incidences compared to the free drug. Finally, loaded vesicles were tested on a *Shigella flexneri* model, showing effective elimination of the pathogens after an overnight exposure. With this, a new biocompatible carrier system was established with promising properties, in particular for treating GI infections.

Introduction

Before the commercialization of the first antibiotic, infectious diseases were the leading cause of death, specifically pneumonia, tuberculosis and gastrointestinal (GI) infections (1). By bringing penicillin onto the market, the golden age of antibiotics began and the threat of infections diminished. New drugs were discovered with different modes of actions or pharmaceutical characteristics. However, several years later, the number of new approved antibiotics declined and pathogens continued to progressively develop resistances, such as the methicillin resistant *Staphylococcus* or the vancomycin resistant *Enterococcus* (2). If this recent trend continues, we will face a new era where the risk of complications after surgeries will critically increase, simple injuries will develop into sepsis and GI infections will, once again cost the lives of many, especially the elderly and children. As a consequence, the World Health Organization assigned ten issues, demanding attention and solutions, with antimicrobial resistance being one of them (3). At present, GI-infections caused by *Shigella* spp. result in 164,000 deaths worldwide annually with increasing incidence of antimicrobial resistance against azithromycin and ciprofloxacin (4, 5). Since the development of new antibiotics is stagnating however, there is an urgent need to further develop those antibiotics in order to increase their efficacy while at the same time prevent or prolong the development of resistance. One way to address this problem is the use of so-called nanoantibiotics (6). Besides improving the solubility and bioavailability, demonstrated for example with ciprofloxacin submicrocarrier (7), these systems can fuse with cellular membranes, releasing high dosages of drug into target cells and pathogens, combating resistance mechanisms on a multi-dimensional level. Chlaritromycin PLGA nanocapsules for instance, were able to inhibit intracellular growth of *Staphylococcus aureus* and *Mycobacterium absessus*, preventing these pathogens to escape antimicrobial treatment (8). Among these promising avenues, synthetic nanocarrier also bare the potential to induce immunogenicity and depleted efficacy throughout long-term therapy (6). Although the safety of commonly used materials has already been proven, the introduction of new, more advanced synthetic compositions poses new challenges in terms of biocompatibility and toxicity (9). Thus, a biogenic alternative, such as nano-sized, cell-derived vesicles would be desirable.

In this study, we introduce two different types of extracellular vesicles (EVs): 1) those derived from human B-lymphoid cells and 2) outer membrane vesicles (OMVs) obtained from gram-negative non-pathogenic myxobacteria. EVs are nano-sized structures, which originate from various different cell types, such as cancer, immune or epithelial cells and can be found in different tissues and fluids of the human body. Different origins of EVs within the cell have been discovered, for instance exosomes which are formed in the endosomal system and microvesicles formed by budding of the cell membrane (10). While ascertaining the exact

biogenesis of these vesicles is extraordinarily difficult, the umbrella term of EVs will be used respectively (11). In general, these vesicles consist of a phospholipid bilayer and contain nucleic acid, proteins or enzymes. The main biological function is to deliver content, enabling the cargo to be transported for longer distances, protected from the environment (12). This enables EVs to be involved in tissue repair or immune modulation by transporting miRNA or antigens (13, 14) and many other roles regarding maintenance, protection or development of the human body.

Outer membrane vesicles (OMVs) on the other hand are one type of vesicles derived from gram-negative bacteria. They generate by budding of the outer membrane of the pathogen (15). Hence, the structure and content of the vesicle is similar to that of their origin. In some cases, in addition to periplasmic proteins and nucleic acids, secondary metabolites have been identified to be incorporated within OMVs (16, 17). They play a crucial role in the transfer of resistances, whether in transporting degrading enzymes or genetic information (18, 19). They are also involved in biofilm formation and ensure the survival of the colony by eliminating competing bacteria and assist in nutrient acquisition (20).

EVs and OMVs present a new field of research for elucidating more insights on the pathology of diseases and its therapeutic prospects. Besides utilizing vesicles in non-invasive biomarker recovery, the possibility of using them as carrier systems gained great interest in drug-delivery research due to their potential inherent targeting properties (21). While EVs derived from human mesenchymal stem cells have been proposed as therapeutics to prevent scar formation, improve the recovery after cortical injury or inhibit tumor growth (22-24), other types of EVs have been introduced in cancer therapy (25) or the treatment of neurological disorders (26). Additionally, loading EVs with different compounds improved several pharmaceutical properties of the drug, such as solubility, bioavailability and enhanced specific targeting and delivery of the drug (27-29).

OMVs have been successfully used as vaccine adjuvants (30, 31). Moreover, due to their biological role in ensuring the colonies survival in a competitive environment by eliminating competing bacteria, OMVs showed great potential as therapeutics against infectious diseases (17). OMVs derived from different pathogens such as *Shigella* and *Staphylococcus aureus* (*S.aureus*), can be loaded with antimicrobial agents, showing effective elimination of intracellular *Shigella*, *Pseudomonas* or *S.aureus* (32-34). However, it remains unclear whether the use of these systems will provide sufficient therapeutic benefit, due to their potentially strong immunogenicity. By utilizing OMVs derived from commensal or non-pathogenic bacteria these problems can be avoided (35). For instance, Myxobacteria, a gram-negative family of δ-proteobacteria, mainly living in soil and non-pathogenic to humans, pray on other competitive bacteria, thus produce bacteriolytic compounds. In a recent study, we discovered

that OMVs derived from *Cystobacter velatus* are inherently loaded with the topoisomerase inhibitor cystobactamid 919-1 and found that they are able to inhibit growth of *Escherichia coli* and even reduce spreading of intracellular *S.aureus* (17, 36).

In this study, we evaluated the non-toxic properties and biocompatibility of OMVs derived from the myxobacterial strain SBSr073 (SB-OMVs) and EVs derived from B-lymphoid RO cells (RO-EVs) by determining endotoxin levels and cytokine release of peripheral blood mononuclear cells (PBMCs). To estimate their potential in fighting GI pathogens, the prospective localization of the vesicles in an advanced three-dimensional GI cell culture model, containing three significantly involved cell types was investigated and found to be co-localized within the epithelial barrier. We assessed different loading methods for the model antibiotic ciprofloxacin, ranging from passive to active loading avenues. The compatibility of vesicles was further tested on a *Danio rerio* embryo model. Due to their pronounced similarities to humans, with a genetic disposition of more than 80 % and similar behavioral patterns in host defense, potential side effects could be predicted and monitored (37). Finally, the loaded vesicles were successfully tested on a *Shigella flexneri* model, capturing their growth inhibition abilities. With this work, we create the fundamental basis for developing vesicles as well-tolerated and flexible platform technology to counterbalance growing bacterial resistance.

Results and Discussion

Vesicles were efficiently isolated and showed promising biocompatibility with low cytokine release in primary immune cells

Two different vesicles, derived from the myxobacterial strain SBSr073 and B-lymphoid RO cells were used as carrier systems to treat gastrointestinal infections. These two vesicles were chosen a) due to low immunogenicity, as MHC class II negative RO cells were isolated from a severe combined immunodeficiency patient (38) and b) because SBSr073 non-pathogenic myxobacteria are an unlimited and easily scaled up sources of biogenic OMVs, recently characterized (17). As previously described, we were able to create a platform to efficiently produce high volumes of conditioned media for vesicle isolation (39). RO cells were cultured in serum free medium for several passages (**Figure S 1 a, b**), without alterations in their morphology or cell viability and, averting unnecessary medium exchange or time-consuming serum depletion (40). Additionally, cells were cultured in an upright position with volumes up to 70 mL, reducing plastic waste and storage capacity compared to common culturing techniques (39). Furthermore, vesicles were isolated twice a week, before splitting and feeding

cells, with no significant difference in yield and physico-chemical properties (**Figure S 2 d,e**). SBSr073 myxobacteria were cultured in glass flasks up to 500 L. In addition to this, non-expensive media were used, paving the way for a sustainable upscale production of vesicles. Differential ultracentrifugation, a common and approved method in the field of EV research, was used to isolate vesicles (11). To remove non-EV components, a size exclusion chromatography using a 35 mL sepharose column was used, respectively. Vesicles typically eluted after 12 to 15 mL. The fraction with the most abundant concentration of vesicles at approximately 10^{12}/mL, determined by nanoparticle tracking analysis was then used for further experiments. To obtain equivalent particle concentrations, 390 mL of conditioned RO medium compared to 65 mL of conditioned SBSr073 medium had to be obtained for vesicle isolation. Hence, myxobacteria produced higher yields of vesicles per cell, which meant that the volume for the EV isolation had to be increased six fold (17, 28).

SB-OMVs have been recently characterized towards their size, size distribution, protein concentration and zeta potential (17). For a better comparison, **Figure S2** summarizes data acquired in the recent publication and newly obtained results. RO-EVs were additionally characterized towards surface marker CD9 and CD63 according to MISEV regulations (**Figure S 3**) (11). Compared to SB-OMVs, RO-EVs had a lower zeta potential of -12.8 and -6.8, respectively. This may be a result of higher protein concentrations associated with RO-EVs with 6.5 µg protein per vesicle × 10^{-10} compared to 3.6 µg per vesicle but might also be related to their lipid composition or other components (41).

To assess the biocompatibility of the vesicles, we first performed an endotoxin gel clot assay, a method generally recommended by the Food Drug Administration and the European Medicines Agency and anchored in several pharmacopoeia for evaluating the quality and safety of pharmaceutical products (42). Endotoxins, also known as lipopolysaccharides (LPS) are particularly associated with gram-negative bacteria and their outer membrane. These O-antigen, oligosaccharide and lipid A structures induce, by activating Toll-like-receptor 4 decorated on immune cells, the production of pro-inflammatory cytokines and thus trigger a severe immune response. Hence, detecting low levels of endotoxin are crucial towards the evaluation of safety and immunogenicity of pharmaceutical products. For injectables, regulatory agencies allow an endotoxin concentration below 0.25 EU/mL or 5 EU/kg (43). In our gel clot assay both aseptically prepared vesicle pellets did not infuse a firm gel formation, even at the highest possible vesicle concentration (**Figure S 4**). Indeed, in a recent study where a chromogenic endotoxin assay was used, we also observed a very low concentration of endotoxin associated with SB-OMVs (17). Although, LPS is part of the outer membrane of gram-negative bacteria and a distinct part of myxobacterial OMVs, the concentrations seem to be exceptionally low for SB-OMVs (20, 44, 45). This phenomenon has also been observed in

literature. Gujrati et al. were able to produce OMVs derived from a mutant *E.coli* strain with lower LPS concentrations compared to the wild type (46). This indicates that, while LPS is a component of OMVs, the concentration can be highly variable, depending on the vesicle producing bacteria. In our hands, the low LPS concentration of SB-OMVs reduces the risk of an unwanted immune reaction.

In order to understand the immunogenic potential of the vesicles in detail, we incubated primary immune cells isolated from whole blood with both vesicles at different dilutions. Peripheral blood mononuclear cells (PBMCs) consist of lymphocytes (T-, B- and NK-cells), monocytes or dendritic cells, which are primary involved in the innate immune response (47). These cells give detailed information on potential immunogenic effects connected with pathogen associated molecular patterns (PAMPs). These molecules are recognized by Toll-like receptors, leading to an activation of an immune response cascade and the release of pro-inflammatory cytokines. Consequently, the body reacts with fever and swelling, which can finally lead to an aseptic shock (48). Cytokine storm is an extreme, sudden and uncontrolled release of pro-inflammatory mediators, causing multi-organ failure and death (49). Thus studying the release of cytokines is of great importance in the development of new therapeutics. Here, we quantified interleukins produced by activated immune cells, which are part of an acute phase response of the immune system, such as IL-6, IL-8 and IL-1 beta and tumor necrosis factor alpha (TNF-alpha). A dose response of cytokine concentration in relation to particle concentration was detected during all experiments (**Figure S 5**). Vesicles induced a moderate to low release of pro-inflammatory cytokines compared to a 1 µg/mL positive LPS control. SB-OMVs, compared to RO-EVs triggered the release of higher cytokine levels *e.g.,* with 15.9 pg/mL of TNF-alpha compared to 10.6 pg/mL or 30.2 pg/mL compared to 16.8 pg/mL of IL-6 (**Figure 1 a, b**). Whereas TNF-alpha is produced by all different kinds of cells such as macrophages, lymphoid, mast or endothelial cells, Il-6 is predominantly secreted by macrophages activated by PAMPs (48). In addition, IL-8 was analyzed, as it also induces chemotaxis to trigger migration of immune cells to the side of infection. RO-EVs again, caused a lower release with 210 pg/mL compared to SB-OMVs with 264 pg/mL and LPS with 621 pg/mL (**Figure 1 c**).

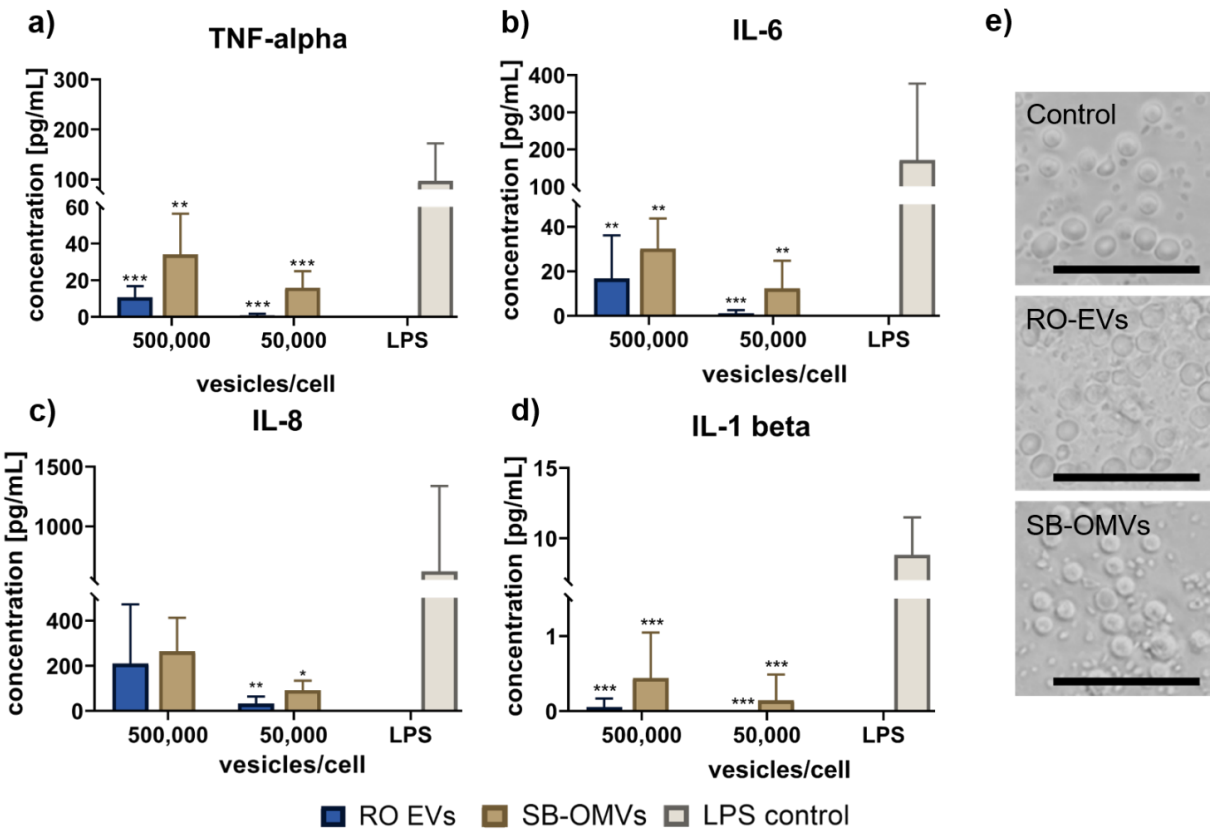

Figure 1 Cytokine release of PBMCs incubated with RO-EVs and SB-OMVs. a) Quantification of TNF-alpha after an incubation of PBMCs with RO-EVs, SB-OMVs and a LPS control for 4h b) Quantification of IL-1 beta c) IL-8 and d) IL-6 e) Microscopic images of PBMCs after vesicle exposure or control. Scale bar 50 µm. n = 3 - 6, n_{donor} = 3 - 4

The moderately low release of IL-1 beta by RO-EVs with 0.05, SB-OMVs with 0.44 and LPS with 8.83 pg/mL can be explained with a second pathway of cytokine production (**Figure 1 d**). The activation of the inflammasome by different caspases cannot be accomplished by LPS, thus the subsequent processing of IL-1 to IL-1 beta was not as abundant (50).

EVs are considered, due to their cellular origin to have a low immunogenicity, which has similarly been demonstrated, for cardiac-derived adherent proliferating cells as a new therapeutic to improve cardiac regeneration (51). In contrast to EVs, OMVs have frequently been shown to be immunogenic. For instance, OMVs derived from pathogenic bacteria such as *Porphyromonas gingivalis*, inducing chronic periodontitis, activated inflammasome complexes with high IL-1 beta secretion (52). Further, Avila-Calderón et al. investigated OMVs derived from *Brucella*, a gram-negative bacterium, that causes a zoonosis transmitted by contaminated milk (53). They found that these OMVs induced particularly high concentrations of pro-inflammatory cytokines, with levels up to 1000 pg/mL of TNF-alpha, which is 70 times higher compared to concentrations induced by our SB-OMVs. IL-6 concentrations increased

to 40,000 pg/mL after an overnight incubation, while here, SB-OMVs induced 1,300 times less the amount of IL-6 release.

In our hands and despite high exposure concentration, the cytokine response was marginal and cell morphology as well as the cell concentration after the vesicle exposure appeared to be healthy, advocating the applicability of RO-EVs and SB-OMVs in a therapeutic setting.

In a three-dimensional GI cell culture model vesicles mainly localized in the epithelial layer

To analyze the potential of the vesicles in tackling GI-infections, a recently published three-dimensional GI cell culture model was used (Hartwig et al. manuscript in preparation). Due to their well-controlled conditions, advanced cell culture models, are advantageous in predicting *in vivo - in vitro* correlations for a better assessment of therapeutic efficiency and safety of *i.e.,* nanoparticles (54-56). This 3D co-culture model was used to mimic the gastrointestinal tract with three essentially involved cell types: epithelial (CaCo-2) and two immune cell types, macrophages (*d*THP-1) and dendritic cells (MUTZ-3) (**Figure 2**). CaCo-2 cells were used to form the epithelial barrier present in the GI. Both immune cell types play a crucial role in inflammatory responses and present a link between innate and adaptive immune system. In this model, four different scenarios were simulated: i) a leaky epithelial barrier in an inflamed and ii) healthy setting, and iii) a tight barrier with an inflamed and iv) healthy setting. After 24 h exposure with vesicles, the cells were fixed, stained and analyzed using confocal scanning microscopy. To avoid the detection of false positive cells in the model, the intensity of exposure and emission filter settings to visualize fluorescently labeled vesicles was not altered for all conditions.

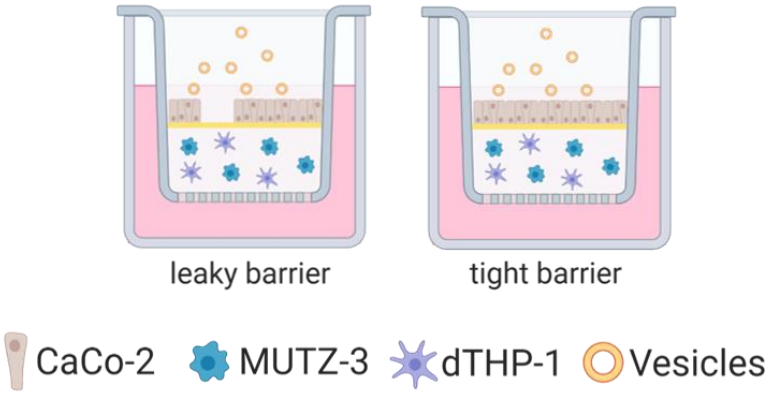

Figure 2 Schematic illustration of the three-dimensional GI co-culture model. CaCo-2 epithelial cells were added on top of a collagen layer containing immune cells MUTZ-3 and

*d*THP-1. While the “leaky” barrier model was cultured for 6 days to take advantage of a leaky epithelial layer, the “tight” barrier was cultured until a firm monolayer was established. Fluorescently labeled vesicles were added for 24h, respectively.

Prior to taking images of the co-culture, the trans-epithelial electric resistance (TEER) was measured before and after the vesicle treatment, to evaluate the effect of vesicles on the barrier function of the co-culture. TEER is a measure for resistance that is influenced by specific tight junction proteins, located between epithelial cells (57). Both vesicles did not affect the barrier function, on the contrary even improved it (**Figure S 6**). In the inflamed model, vesicles were able to increase TEER values up to 33 % ± 2.5 for RO-EVs and 24 % ± 7.9 for SB-OMVs compared to the untreated control with only 23 % ± 2.1. In a recent publication, the barrier function of CaCo-2 cells was investigated when exposed to *Bacillus subtilis* OMVs (58). It was shown that, TEER values were not affected by OMVs. In a different publication, the barrier function was even enhanced by probiotic OMVs and the vesicles had no effects on cell integrity and permeability (35). In **Figure 3**, confocal images with side view of the co-culture allow visualization of the epithelial layer and underneath embedded immune cells. The top view shows the leaky or tight regions of the epithelial barrier, assembled by CaCo-2 cells. The merged image shows the cytoskeleton (green), nucleus (blue) and vesicles (red), whereas the image next to it shows only the signal of DiI-labeled vesicles. In the tight barrier model, vesicles accumulated in the epithelial cell layer, independent of LPS stimulation. Using the leaky barrier model, vesicles were able to penetrate through collagen, occasionally reaching immune cells (**Figure S 7**). Further, uptake in *d*THP-1 was seen in a mono-culture embedded in collagen (**Figure S 8**). Uptake in dendritic-like cells was not observed (**Figure S 9**). Indeed, several attempts to investigate cellular uptake of EVs and OMVs has been taken, primarily studying individual cell lines with presumable specificity. Cancer cells, for example communicate with stromal cells via EVs through which efficient uptake is required (59). EVs derived from neural cells are able to exchange information either specifically to each other or target information towards glial cells (60, 61). An example of OMV uptake in cells demonstrates, that vesicles derived from *Streptococci*, showed increased uptake in dendritic and keratinocyte cells and comparably minor uptake in macrophages (62). However, to the best of our knowledge, the uptake of vesicles has not been investigated in co-culture models including different cell types embedded in a physiologically relevant extracellular matrix. Our models, give better insights into the interaction of EVs with epithelial and immune cells, representing a correlation between *in vitro* and *in vivo*. The simplified context of *in vitro* systems compared to animal models makes it easier to evaluate those pharmaceutical characteristics, such as size and surface charge of individual drug delivery systems, reducing unnecessary animal testing (54-56). Especially, size and surface charge of nanoparticles play significant roles in cell-nanoparticle interaction, promoting or averting cellular uptake (63, 64). Visualizing the localization of RO-EVs and SB-

OMVs in this *in vitro* co-culture model indicates the potential behavior of these vesicles encountering the intestinal mucosa under healthy or diseased conditions. The accumulation of the vesicles in the epithelial barrier is to this point advantageous, as this is the main replication site of *Shigella* and other GI pathogens (65). Furthermore, the investigation of the localization of vesicles in the leaky model shows, that the vesicles are able to penetrate the collagen layer, and can be taken up by macrophages. This demonstrates the advantage of a biomimetic co-culture system, as the interaction of different cell types with the vesicles was observed. At the same time, it also shows how the vesicles might behave in a diseased GI tract with an impaired epithelial barrier, as a result of ongoing inflammation and bacterial infection. The fact that the vesicles were also taken up successfully by macrophages makes us optimistic that in a persistent bacterial infection that also involves immune cells, the vesicles can be used as efficient drug delivery systems, attaining even sub epithelial tissue with different target cells.

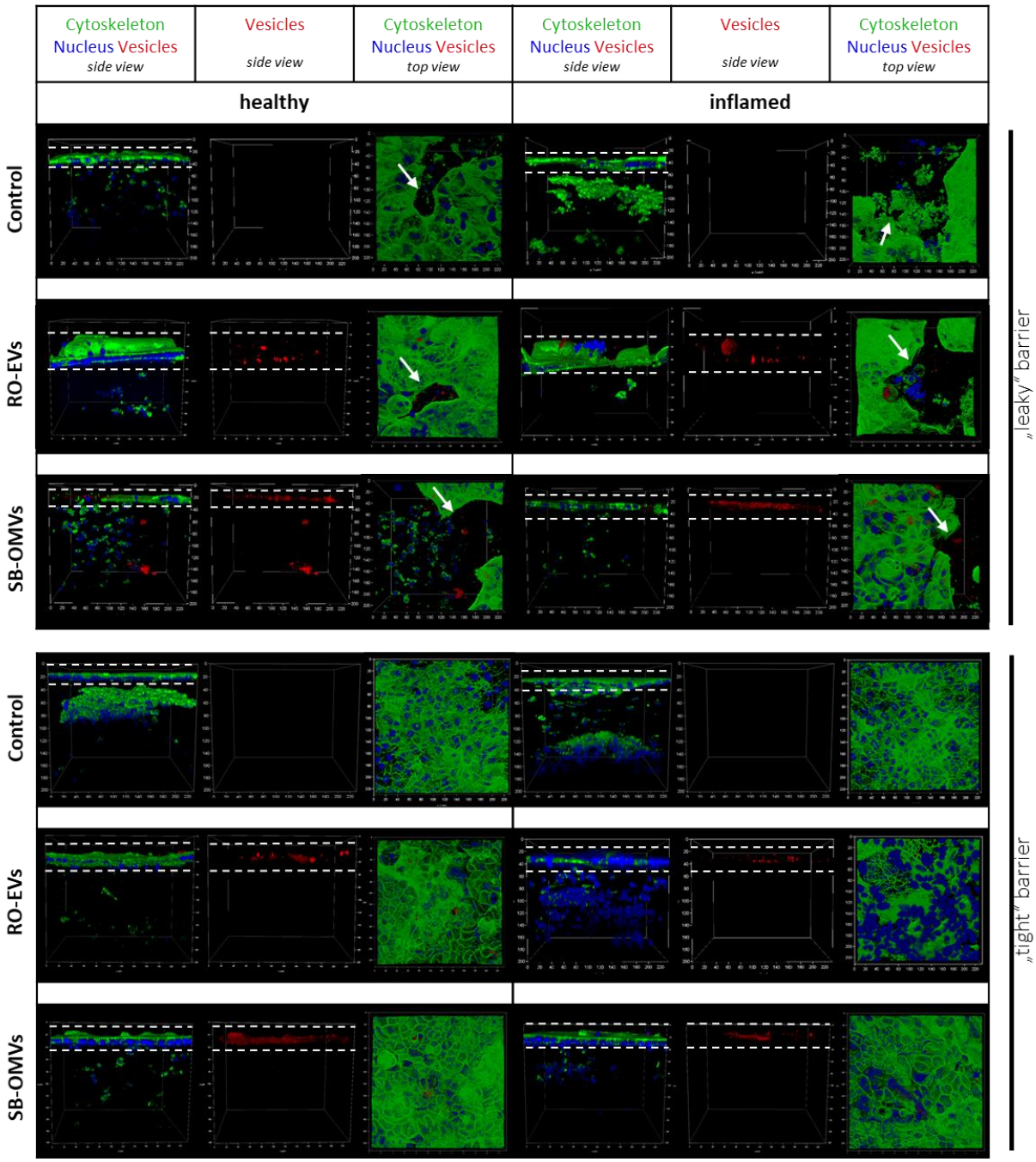

Figure 3 Confocal images of the co-culture model with a leaky and tight epithelial barrier. The cytoskeleton was labeled using phalloidin-FITC and is represented in green. Nuclei were stained with DAPI and vesicles labeled with DiI, seen in red. The left two images represent the side view of the 3D culture, the last image a top view. White arrows highlight holes in the epithelial layer. White dashed lines frame the epithelial layer.

Vesicles were successfully loaded with ciprofloxacin using different loading techniques

To efficiently load vesicles with the desired compound is one of the major challenges associated with EVs and OMVs as drug delivery systems. Ciprofloxacin (CPX) was used, as a model antibiotic to be encapsulated into RO-EVs and SB-OMVs. There is increased evidence of resistance development of this broad spectrum antibiotic, accentuating the urgent need to introduce an effective nanoformulation (66, 67). Four different loading techniques were used to evaluate the most effective method for loading RO-EVs and SB-OMVs: i) passive incubation, ii) saponin-assisted, iii) electroporation and iv) a combination of passive and saponin-assisted loading. Whereas the passive incubation method takes advantage of the ability of a compound to diffuse into a membrane, active loading techniques such as saponin or electroporation open the membrane chemically by pore formation or physically by applying an electrical field for a short amount of time (68).

To remove non-encapsulated drug and residual saponin, size exclusion chromatography (SEC) was the most efficient method. Although ultrafiltration (UF) and tangential-flow-field-fractionation (TFF) were tested, none of these methods were able to completely remove free CPX (**Figure S 10**).

The two most efficient loading methods were the passive incubation with 70 ng/vesicle for RO-EVs and 50 ng/vesicle × 10^{-12} for SB-OMVs and the saponin-assisted method with 53 ng/vesicle for RO and 28 ng/vesicle × 10^{-12} for SB-OMVs, respectively (**Figure 4 a**).

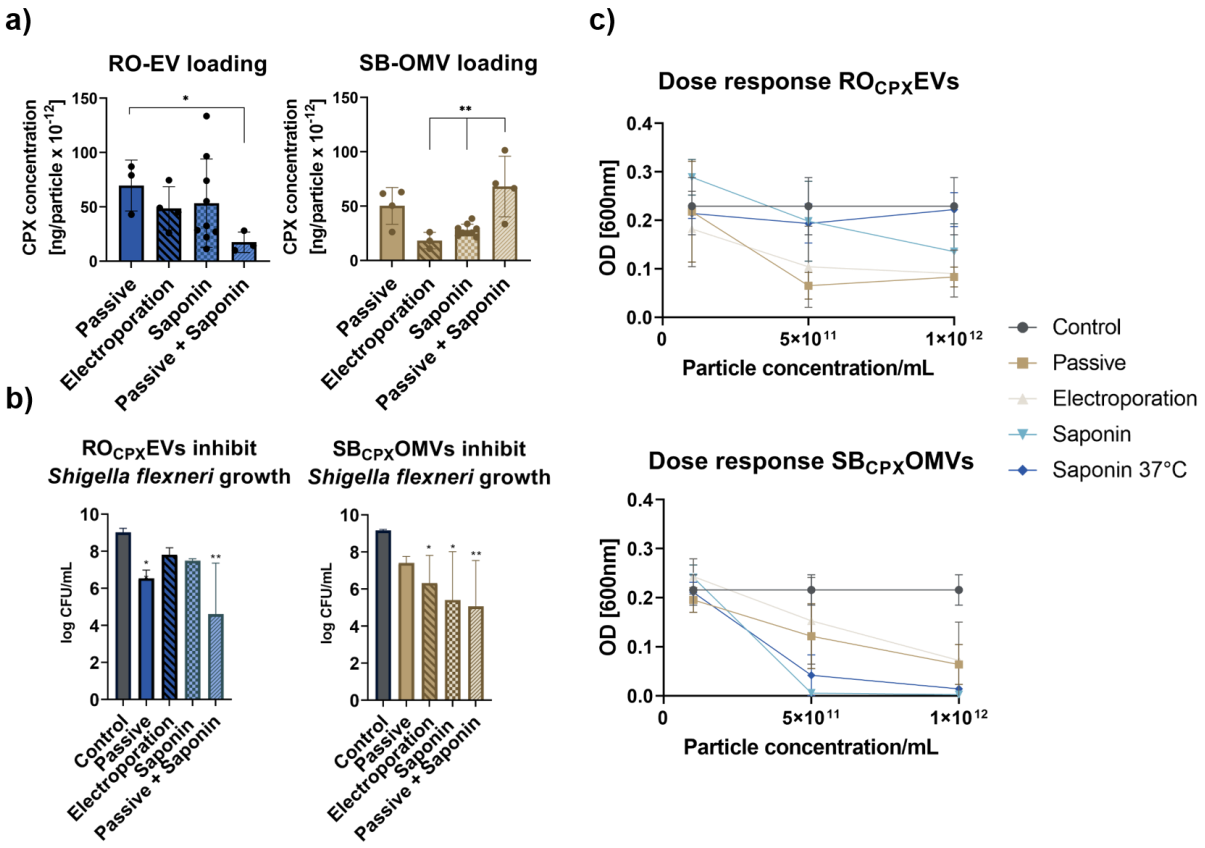

Figure 4 Loading of RO-EVs and SB-OMVs with the model antibiotic ciprofloxacin. a) CPX loading efficiency using different loading techniques and both types of vesicles. n = 3 - 9 b) Growth inhibition of *Shigella flexneri* using differently loaded vesicles but the same vesicle concentration of 10^{12} particles/mL. n = 3 – 4 c) Dose response of Shigella flexneri incubated with differently loaded vesicles and different particle concentrations. n = 3 - 4

Indeed, passive-incubation appeared to be one of the preferred methods when it comes to loading small molecules. Pascucci et al., for instance used this method to load paclitaxel into hMSC (24). Sun et al. and Caroolante et al. also used the passive-incubation method to load curcumin into EVs from RAW cells, CaCo-2 cells and cow milk (27, 69). When the saponin-assisted method was applied, loading efficiency increased for both, hydrophilic drugs and large molecules, whereby the loading efficacy of lipophilic compounds did not change considerably (27, 28). As ciprofloxacin has an intermediate lipophilicity, introducing the saponin-assisted method did not increase encapsulation efficiencies significantly compared to passive-incubation. Electroporation was the method with the lowest encapsulation efficiency with 49 ng/vesicle for RO-EVs and 18 ng/vesicle × 10^{-12} for SB-OMVs. Although electroporation has been shown to induce precipitation of large molecules, improved methods have demonstrated that this method is also efficient in loading vesicles with small and large compounds (28, 70, 71). Neither could we detect any evidence of percipitation in cryo-electron images, nor did this method improve the encapsulation efficiency of CPX. (**Figure 5**). Combining passive

incubation with the saponin method, increased the encapsulation efficiency of ciprofloxacin 1.36 fold for SB-OMVs. Conversely, the amount of encapsulated CPX for RO-EVs decreased almost 75 % compared to passive incubation alone.

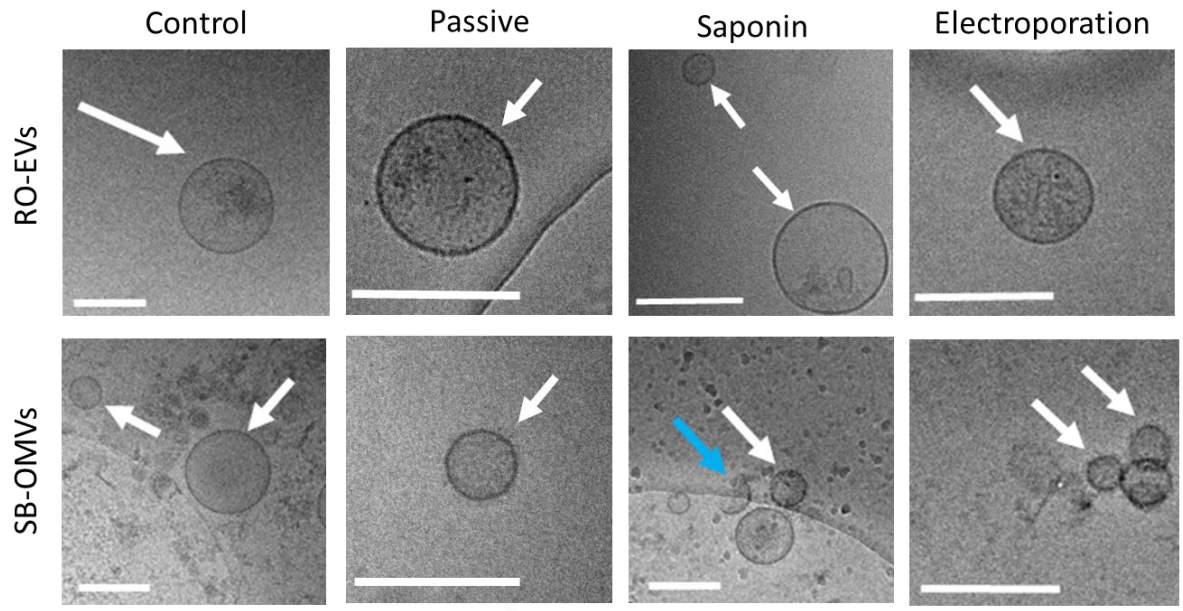

Figure 5 Cryo-EM images of native and loaded RO-EVs and SB-OMVs. White arrows show intact vesicles. The blue arrow indicates a disrupted membrane. Scale bar 200nm.

Comparing the overall amount of encapsulated CPX into EVs and OMVs, we observed higher CPX concentrations for RO-EVs with an average of 47 ng/particle compared to SB-OMVs with only 41 ng/particle × 10^{-12} (**Figure 6 a**). As Fuhrmann et al. discussed previously, the zeta-potential and the composition of the vesicle might play a role in loading efficiency (28). Indeed, RO-EVs typically had lower zeta-potential (-12.8 mV), but higher associated protein concentrations (6.5 µg/particle × 10^{-10}), which seemingly implied that more CPX was encapsulated (**Figure S 13**).

Besides endogenous loading of the isolated vesicles, a different, exogenous approach can be taken by incubating cells or bacteria with a desired compound to drive its encapsulation. Huang et al. incubated *Acinetobacter baumannii* with different sub-toxic concentrations of different antibiotics and isolated vesicles via ultracentrifugation (72). Kadurugamuwa et al used the same approach for loading *Shigella* OMVs with gentamicin (32). However, this method needs individual optimization according to the bacteria obtained and it remains unclear, if this method can be adapted to different species, respectively.

Drug loaded vesicles were able to inhibit Shigella flexneri growth

To evaluate the anti-infective potential of ciprofloxacin loaded RO_{CPX}EVs and SB_{CPX}OMVs, a *Shigella flexneri* model was applied. Different concentrations of loaded vesicles were incubated with planktonic *Shigella* overnight, whereby after, the optical density (OD) was measured and colony forming units conducted.

Vesicles were able to inhibit the growth of *Shigella* independent of the loading method and by at least 1.21 and at most 4.09 log units/mL (**Figure 4 b**). Further, growth inhibition was shown to be dose dependent, with the highest concentrations showing no turbidity in exposed *Shigella* cultures, resulting in close to zero OD values (**Figure 4 c**). The two most effective SB-OMVs were the ones loaded with either the saponin-assisted, reducing the growth of *Shigella* down to 5.41 log CFU/mL or the combined method of passive-incubation and saponin-assisted with 5.06 log CFU/mL. For RO-EVs, the passive-incubation was the most effective one in terms of growth inhibition, whereas the saponin-assisted was able to reduce the growth of *Shigella* down to 7.48 log CFU/mL. However, if vesicles were not diluted to a certain particle concentration and the most abundant SEC fraction with particle concentrations higher than 10^{12}/mL was used, the growth reduction was even more profound with a reduction down to 2.8 log CFU/mL for SB_{CPX}OMVs and 4.66 log CFU/mL for RO_{CPX}EVS (**Figure 6 a,b**).

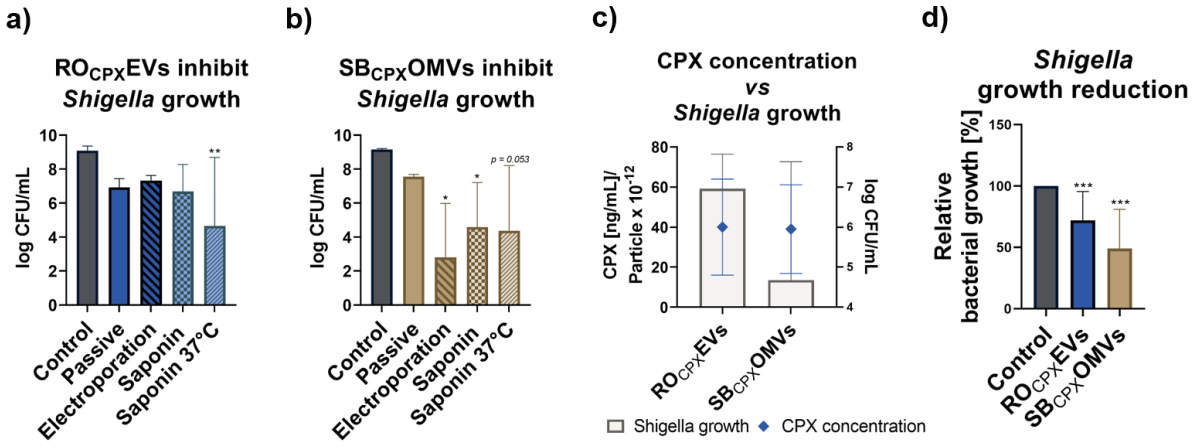

Figure 6 Growth inhibition of RO_{CPX}EVs and SB_{CPX}OMVs depending on their particle concentration. a) Growth inhibition of *Shigella flexneri* after an overnight exposure of undiluted RO_{CPX}EVs with 1.82e12 ± 7.1e11 vesicles/mL b) Growth inhibition after SB_{CPX}OMV incubation with 3.2e12 ± 1.1e12 vesicles/mL c) Ciprofloxacin concentration (blue dots) versus colony forming units (white bars) of *Shigella flexneri* after an overnight incubation with the vesicles. d) Relative bacterial growth after RO_{CPX}EVs, SB_{CPX}OMVs and PBS (control) incubation.

To the best of our knowledge, a few attempts have been taken in loading an antibiotic into EVs to create an anti-infective drug delivery platform. Yang et al. loaded linezolid, an antibiotic of the oxazolidinone family into RAW264.7 EVs via passive-incubation and tested them on intracellular *S.aureus* (73). With that, they were able to reduce intracellular growth from 10^6 CFU/mL down to 10^4 CFU/mL, leaving a log 2 difference in intracellular growth. However, it is doubtful, that centrifuging the loaded vesicles at 10,000 × g for 10 min in enough to remove the free drug completely and the killing effect of *S.aureus* is only due to vesicle encapsulated linezolid. Kadurugamuwa et al. loaded OMVs derived from *Shigella flexneri* with gentamicin to treat *Shigella flexneri* infected epithelial cells (33). Here, a reduction of bacterial growth of 1 log CFU/mL was achieved. Huwang et al. loaded ceftriaxone, amikacin, azithromycin, ampicillin, levofloxacin and ciprofloxacin into *A.baumanii* OMVs. However, they only measured the OD in treated pathogen controls, which might mask the ultimate effect of the loaded OMVs (74). In both of the latter cases, OMVs were loaded using endogenous methods with sub-toxic concentrations of antibiotics. It remains unclear, whether this method might provoke the encapsulation of resistance genes or other harmful bacterial components, due to defense mechanisms, increasing the risk of resistance transfer. In our hands, we were able to reduce bacterial growth down to 77 % with RO-EVs and even 53 % with SB-OMVs in a planktonic *Shigella flexneri* model (**Figure 6 d**). Interestingly, although the concentration of encapsulated CPX was higher in RO_{CPX}EVs, their effect on *Shigella* was not as effective towards their growth inhibition compared to SB_{CPX}OMVs (**Figure 6 c,d**). Although, the mechanism of EV and OMV uptake in eurakyotic cells has been studied intensively, pointing out several uptake mediated mechanisms, there is little known on the specific mechanisms of EV and OMV uptake in bacterial cells (75). Most likely, their uptake is fusion-mediated, which was demonstrated by Kadurugamuwa et al. where OMVs derived from *P.aeruginosa* rapidly fused with *S.aureus* and *E.coli* (76). Here, LPS might play a role in OMV and outer membrane recognition via cell surface proteins (77). Although it is not proven, whether vesicle uptake is exclusively dependent on membrane composition, strong evidence in liposomal formulation indicate that this might play a role in the efficiency of membrane fusion (78). In this case, two mechanisms might, potentially simultaneously influence the uptake and efficacy of SB_{CPX}OMVs in *Shigella*: i) LPS mediated fusion of OMV with OM of *Shigella* and ii) similar composition of the OMV and the OM of *Shigella* facilitating their uptake via fusion. In conclusion, we were able to load two different types of vesicles with similar amounts of CPX yet, the effect on growth inhibition on *Shigella flexneri* was differentially effective.

In a Danio rerio larvae model high concentration of vesicles showed no toxic effects

The biocompatibility of EVs was further assessed *in vivo*, monitoring the cytotoxicity of ciprofloxacin loaded and unloaded SB-OMVs and RO-EVs in a *Danio rerio* larvae model. These models provide the opportunity to study the toxicity, efficacy and biodistribution of nanoformulations, gaining insight of the pathophysiology of a therapeutic in a real time manner (79). We first incubated loaded and unloaded vesicles with one day post fertilization (1dpf) and three days post fertilization (3dpf) larvae. As a control, different concentrations of pure CPX were added to the water. The development of larvae exposed to SB-OMVs, RO-EVs, as well as SB_{CPX}OMVs and RO_{CPX}EVs was not impaired or changed at any time (**Figure S 16**). In comparison, bovine milk derived EVs reduced the survival of zebrafish larvae when exposed to EVs in water with comparable concentrations (80). Matsuda et al, even saw altered hatching behavior due to tetraspanin destabilization of the chorion. In our study, the hatching rate was similar to controls with no delay nor premature hatching (data not shown). To increase the exposure of vesicles to the larvae, we injected 1.5 nL of the vesicles into the blood island, mimicking a systemic administration. Here again, the development of the larvae was not impaired (**Figure S 16**). However, we observed heart edema in fish that were injected with drug loaded RO_{CPX}EV and SB_{CPX}OMV (**Figure 7 a, b**). Incidences of heart edema due to free CPX injection were, nevertheless higher with 13 % for 200 ng/mL or 17 % for 150 ng/mL compared to 5 % for SB_{CPX}OMVs and 7 % for RO_{CPX}EVs.

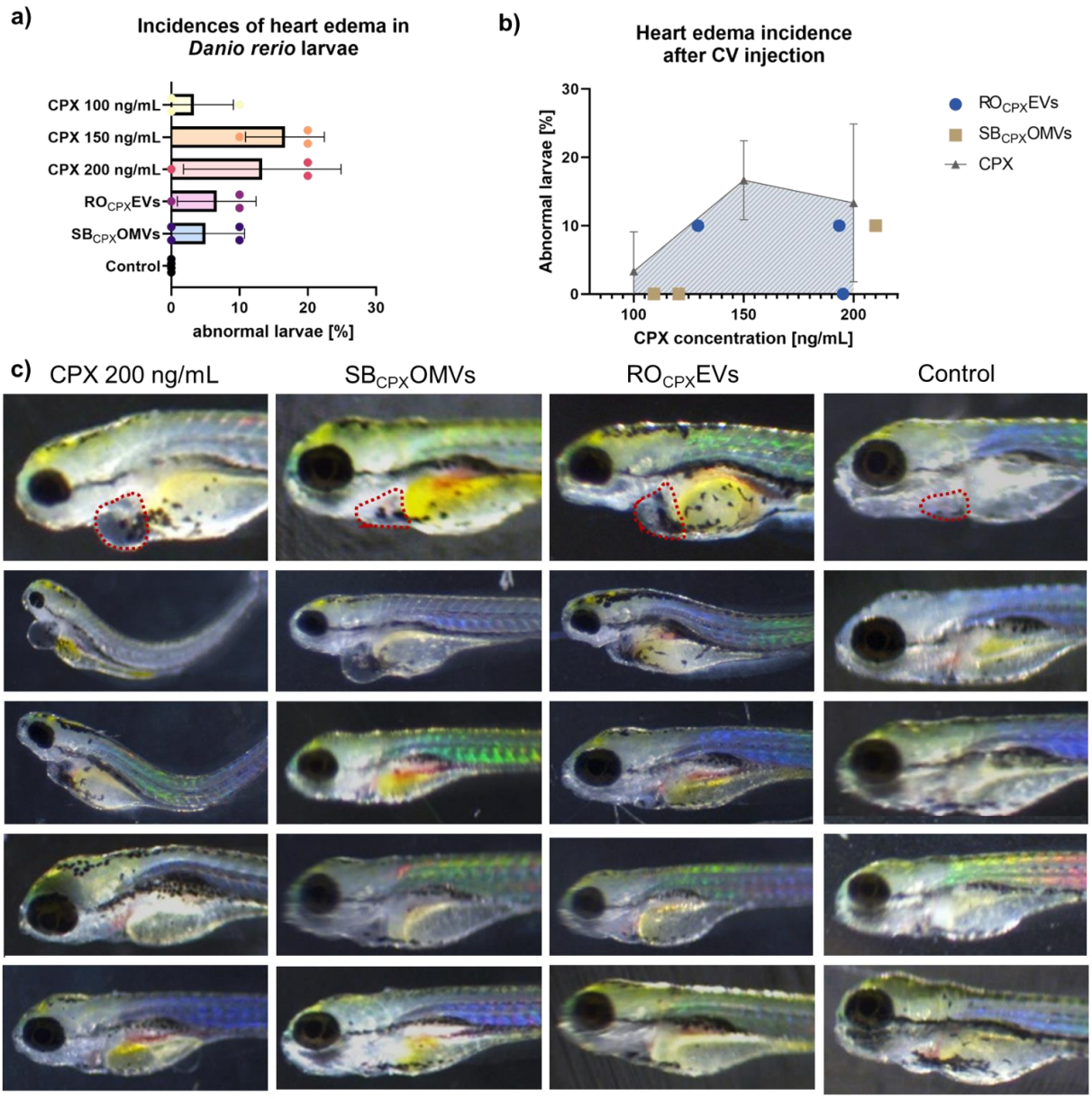

Figure 7 Cardio toxic effect of CPX and loaded vesicles. a) Percentage of incidences of heart edema development in zebrafish larvae after free CPX, RO_{CPX}EV (~172.6 ng/mL CPX) or SB_{CPX}OMV (~127.8 ng/mL CPX) injection b) percentage of development of heart edema compared to CPX concentration, free or encapsulated into vesicles. Individual dots represent individually loaded vesicles with CPX concentration and the percentage of abnormal larvae. The blue area is the area under the number of abnormal larvae due to CPX injection. c) Microscopic images of healthy and abnormal larvae 4 days after injection. The red dashed line frames the pericardium. n = 3 – 4, N = 10

Although CPX has already been tested in zebrafish larvae, the exact mechanism on cardiotoxicity has not been assessed yet (81). The development of the heart is a complex

process involving a variety of different gene expressions and regulations (82). However, it appears that encapsulating CPX into RO-EVs and SB-OMVs seems to reduce the risk of cardiotoxicity almost threefold. This might be due to specific targeting of the loaded vesicles and accumulation on the side of infections. Confirmation of this, however, must be investigated by means of precise biodistribution studies.

Loaded vesicles were not able to significantly reduce bacterial burden in Shigella flexneri infected zebrafish larvae

A zebrafish *Shigella flexneri* model was established to evaluate the potential of loaded vesicles in curing infected larvae. Different concentrations of *Shigella flexneri* GFP were injected into the blood island of 1dpf larvae. With 6.6×10^4 CFU per injection, a stable and persistent infection was generated. After 4 h of spreading, *Shigella* were already detectable by fluorescence microscopy (**Figure 8 c**). Larvae survived up to 72 h post infection with concentrations of up to 7.6 log CFU/mL per larvae (**Figure 8 a**). Mostowy et al. injected similar concentrations in zebrafish larvae but observed lower survival rates and all infected fish died after 48 h (83). However, they were able to show that *Shigella* infected macrophages and neutrophils, escaped cytosolic digestion and progressively spread through the entire fish, representing the zebrafish larvae as a valuable new model to study *Shigella* infections. We utilized this model to evaluate the therapeutic potential of the loaded vesicles *in vivo*. Unfortunately, we were not able to reduce the bacterial load of infected larvae (data not shown). The concentration of either water adjoined or injected ciprofloxacin was not enough to have any effect on infected larvae. Indeed, only high concentrations of up to 1000 × MIC values of ciprofloxacin were able to eradicate bacteria in 4 h post infected fish.

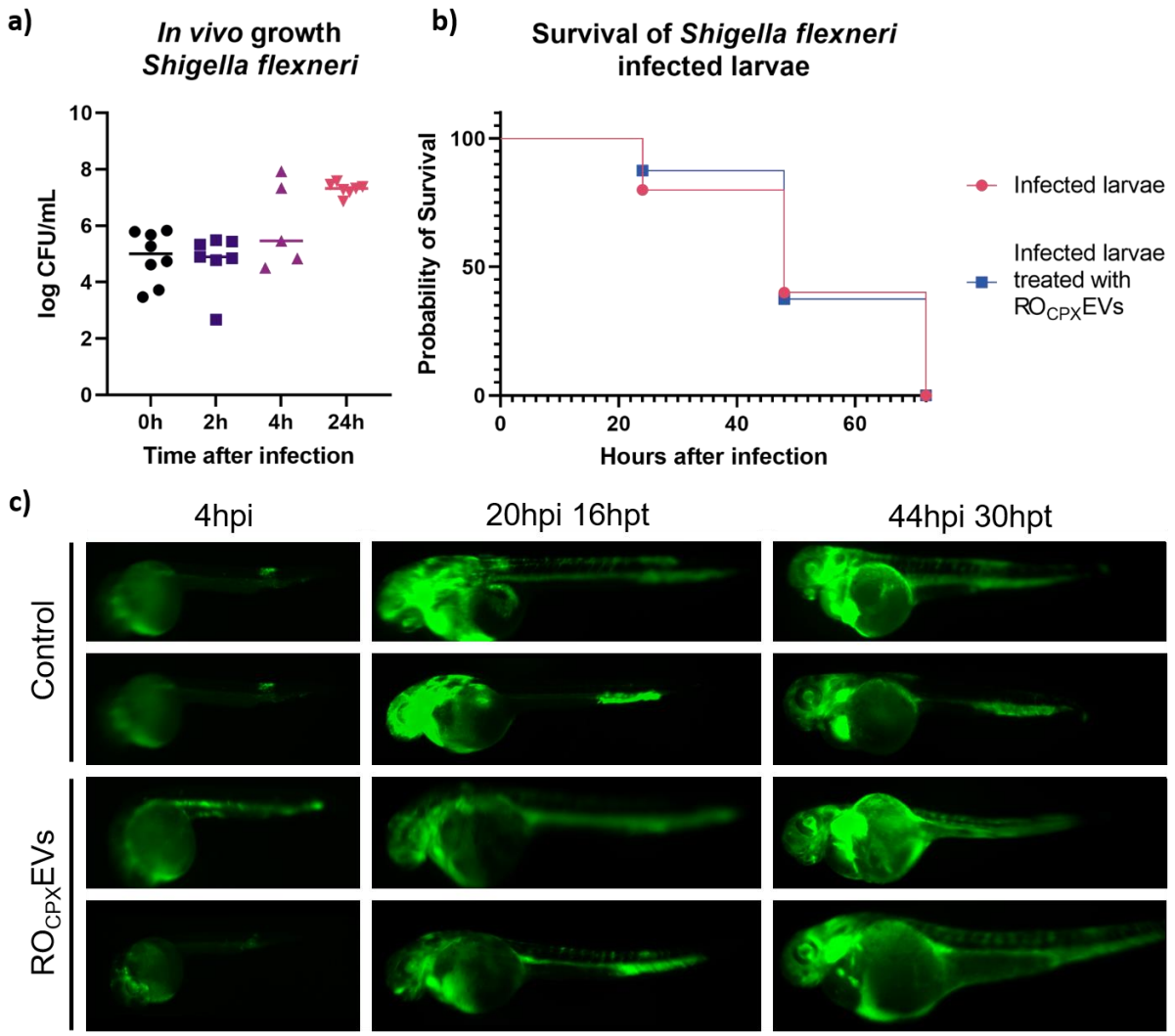

Figure 8 Zebrafish Shigella infection model. a) *in vivo* growth of *Shigella flexneri* in zebrafish after injection, 2 h, 4 h and 24 h. n = 5 - 8 b) Survival of *Shigella* injected larvae. n = 8 - 10 c) Fluoresce microscope images of *Shigella* GPF infected larvae. After 4 h post infection, larvae were treated by RO_{CPX}EV injection. Controls did not receive any treatment.

Although *Shigella flexneri* were eradicated, side effects towards the development of heart edema were observed (**Figure S 17**). This development was not noted in non-infected larvae, where only particularly high concentrations of CPX had an impact on embryonal development and survival (**Figure S 14 b, Figure S 15**).

Interestingly, the treatment of infected zebrafish in general seems to carry its difficulties also in other infection models. Despite increasing survival rates of mycobacteria infected fish, a successful eradication of the pathogens could not be achieved (84). The same applies to *S. agalactiae*, *A. hydrophila*, or *V. vulnificus* infected larvae, where liposome-encapsulated cinnamaldehyde was able to increase the survival and not eradicate the infection itself (85). In order to finally observe a therapeutic effect of the loaded vesicles, the concentration would

have needed to be increased drastically. In conclusion, a *Shigella* infection in zebrafish acts severe and rapidly spreading, minimizing and challenging the options of treatment. Different models such as a *Staphylococcus aureus* infection in zebrafish might be more effective towards evaluating the therapeutic effect of the vesicles, as the bacterial load can be lower and physiologically relevant (86).

Conclusion

In this work, we present two new biogenic drug delivery systems isolated from B-lymphoid cells and non-pathogenic myxobacteria to treat *Shigella flexneri* infections. We were able to efficiently load these vesicles with the model antibiotic ciprofloxacin and demonstrated that they evidently inhibit the growth of the GI pathogen.

Although different attempts in designing a vesicle-based antimicrobial carrier system have been taken (33, 72, 73), the two new vesicles presented in this work show profound advantages towards a successful application. We were able to introduce vesicle cultures for a scaled up economically friendly production with minimized expenses and reduced storage space. The isolated vesicles showed little to no immunogenic potential, tested on primary immune cells. Especially RO-EVs showed promising biocompatible results. As RO cells were isolated from a patient with severe combined immunodeficiency and cells expressed no MHC class II molecules, which are involved in initiating immune responses, their EVs naturally express low immunogenicity (38). Further, we efficiently removed non-encapsulated drug using size exclusion chromatography, leaving no traces of contamination and manipulated effective growth inhibitory effects on pathogens. Finally, the loaded vesicles were tested on a clinically relevant GI-pathogen *Shigella flexneri*. By conducting colony forming units, the unmasked antimicrobial effect compared to simple OD measurements was detected and showed promising growth inhibition qualities.

In the near future, supplementary evaluations of the loaded vesicles towards curing *Shigella* infected animal models and their biodistribution will be conducted. In addition to GI-infection models, further attempts using different pathogens in zebrafish larvae will be taken. As the broad spectrum antibiotic ciprofloxacin was used, the possibility of eradicating other (GI) pathogens is evidently. For instance, different zebrafish models mimicking a tuberculosis infection are present, paving the way to evaluate the potential of the loaded vesicles to be taken up into mycobacteria infected macrophages (87). The treatment of *S.aureus* infected larvae, gives another opportunity to test their potential (86). These targeting characteristics could also be improved by introducing targeting moieties specific for various pathogens (88).

With this work, the first steps in establishing a biocompatible vesicle-based carrier system to treat bacterial infections was achieved. In addition to effective loading, we were able to cover the chain of effects sustainably and ecofriendly, from production, *in vitro* and *in vivo* studies.

Materials and Methods

Bacterial and cell culture

SBSr073 were cultured as previously described (17, 39). *Shigella flexneri* M90T (DSM 4782, DSMZ) was cultured in tryptic soy broth (Thermo Fisher) at 37°C or on tryptic soy agar (Thermo Fisher) at 30°C. *Shigella flexneri* GFP (ATCC 12022GFP) was cultured in nutrient broth or agar (Thermo Fisher) with 100 µg/mL ampicillin (Carl Roth).

RO cells (DSMZ, ACC 452) were obtained in RPMI (Gibco) with 1 % (v/v) insulin-transferrin-selinium-ethanolamine (Thermo Fisher) as previously described (39). Briefly, cells were inoculated with a density of 0.75×10^6 cells with a total volume of 45 mL medium in an upright T75 flask. After 4 days, cells were maintained by exchanging 25 mL cell culture supernatant with 50 mL new medium.

CaCo-2 HTB37 (DSMZ, 169) were cultured in DMEM (Gibco) with 1 % (v/v) non-essential amino acids (Thermo Fisher) and 10 % (v/v) foetal calve serum (FCS). THP-1 (DSMZ, ACC16) grew in RPMI with 10 % (v/v) FCS. MUTZ-3 (DSMZ, ACC 295) were cultured in alpha-MEM (Gibco) with 20 % FCS.

Vesicle isolation

Vesicles were isolated as recently described (17, 39). Briefly, RO cell supernatants were centrifuged at 300 × g for 8 min, SBSr073 supernatants at 9,500 × g for 10 min. Subsequently, both vesicle supernatants were centrifuged at 9,500 × g for 15 min. Vesicles were isolated by differential centrifugation at 100,000 × g for 2 h at 4°C. Both pellets were resuspended in 500 µL residual supernatant.

Vesicle characterization

Particle concentrations were measured using nanoparticle tracking analysis. With a camera level of 15, a detection threshold of 5 and 20 to 120 particles per frame. The size and

concentration was calculated using the NanoSight 3.3. software. The zeta potential was measured using the Zetasizer Nano (Malvern) and folded capillary cells (Malvern), analyzed with Zetasizer software 8.01.4906. Protein concentrations were conducted using a bicinichonic assay kit (Sigma Aldrich) according to manufacturers specifications.

Gel clot- Endotoxin detection

Vesicles were isolated as described in 2.2., under aseptic conditions. After determining the particle concentration a gel clot assay (Toxin Sensor Endotoxin detection system, GenScript) was performed according to manufacturer's specifications with two different dilutions of the vesicle pellet, LAL reagent water and an *E.coli* endotoxin standard. A positive reaction was confirmed by a firm gel formation, indicating an equal or higher endotoxin concentration of 0.25 EU/mL, which is the allowed limit for sterile water for injection according to the federal drug and food administration.

Cytokine detection of vesicle treated PBMC

Buffy coats were obtained from three different donors from the Blood Donation Center, Saarbrücken, Germany, under the authorization by the local ethics committee (State Medical Board of Registration, Saarland, Germany; permission no. 173/18). With a seeding density of 100,000 cells per well in a 96 well plate, cells were incubated with either 5×10^5 or 5×10^4 particles per cell for 4 h in RPMI 1640 (Sigma Aldrich). Cell supernatants were collected and stored at -80°C until cytokine quantification. To determine IL-6, IL-8, IL-10, IL-1 beta, IL-12p70 and TNF-alpha a BD cytometric bead array human inflammatory cytokine kit was used according to manufacturer's specifications. Cytokine quantification and sample analysis was analyzed with FCAP array.

Localization of vesicles in a GI co-culture model

The leaky gut model, was further optimized towards a chronic inflamed state mimicking IBD conditions, based on the previously established co-culture system in our group (55). In brief, monocytic-THP-1 cells were differentiated into macrophage-like cells (*d*THP-1) using 50 nM phorbol 12-myristate 13-acetate (PMA, Sigma-Aldrich, Taufkirchen, Germany) for 72 h. For co-culture, *d*THP-1 (20.000/well) and MUTZ-3 (10.000/well) cells were embedded in 80% (v/v) collagen type I (3 mg/mL, PureCol; Advanced Biomatrix, Tucson, USA) solution containing 10% 10X RPMI + 20mg/mL $NaHCO_3$ (Gibco) and 10% human AB serum (Sigma). A total

volume of 150 µL was placed to the apical chamber of the insert (Transwell® Permeable Supports 3460, Corning). After 1 h of solidification at 37°C and 5% CO_2, Caco-2 cells (100.000/well) were seeded on top, in a total volume of 0.5 mL DMEM with 10% FCS and 1% penicillin/streptomycin (Pen/Strep, Gibco). Afterwards, 1.5 mL of RPMI with 10% FCS and 1% Pen/Strep was added to the basolateral side. Cells were cultured under submerged conditions and medium was exchanged every 2 to 3 days. For the inflamed state, the co-culture was stimulated on day 6 (leaky Caco-2 barrier) or on day 11 (tight Caco-2 barrier) apically with 10 µg/mL LPS (Sigma). After 24 h of stimulation, 200 µL on the apical side were removed and 100 µL Vybrant DiI (Thermo Fisher) labelled vesicles were added. Vesicles were labelled according to previous protocols and purified using a 40 mL sepharose CL-2B SEC (39). After 24 h, cells were fixed with 4% (v/v) paraformaldehyde (Electron Microscopy Sciences), washed, stained with fluorescein phalloidin (Thermo Fisher) and 4',6-Diamidino-2-Phenylindole, Dihydrochloride (DAPI) (Thermo Fisher) according to manufacturer's specifications. Confocal microscope (Leica TCS SB8) images were acquired using the following settings with a 20x objective: DiI (Ex/Em 561nm/ 588-609 nm), DAPI (Ex/Em 405nm/ 420-503 nm), FITC (Ex/Em 488nm/ 511-550 nm); 1024 × 1024 pixel. Leica Application Suite X was used to process images.

Loading vesicles with ciprofloxacin

After vesicle isolated via ultracentrifugation, the pellet was resuspended in residual supernatant and incubated with 17 mM ciprofloxacin-hydrochloride monohydrate (CPX) (Sigma Aldrich) using the following loading methods. During passive loading, vesicles were incubated with CPX for 30 min at 37°C. For electroporation, vesicles were mixed with CPX in Gene pulser cuvettes (0.4 cm cell electrode), where settings with 200 Ω, 500 µF and 200 mV with a pulse time of 9 – 18 ms were used (BioRad Gene Pulser). The saponin-assisted technique was performed by adding 0.1 mg/mL saponin (Sigma Aldrich) and incubation at RT for 20 min. The combination of passive and saponin was conducted by incubating the vesicles pellet at 37°C for 30 min with 0.1 mg/mL saponin. To remove non-encapsulated drug, all samples were purified by a size exclusion chromatography, using a glass column packed with 35 mL of sepharose CL-2B and filtered PBS as eluent. Vesicles typically eluted after 12-15 mL and particle concentrations were determined by nanoparticle tracking analysis. CPX was quantified via liquid chromatography coupled mass spectrometry (EVOQ LC-TQ Elite ER, Bruker). Briefly, vesicles were mixed 1:1 with a mixture of acetonitrile, 25 mM cinnarizin and triton-X (0.1% v/v). A linear gradient-based method with a Waters Acquity BEH C18 50 x 2.1 mm, 1.7 µm column heated up to 45°C was established. The gradient processed from (A) H_2O (0.1% FA) to (B) acetonitrile (0.1% FA); precisely from 0 – 0.1 min 100% (A) to 0.1 – 2.5 min

100 % (B) and further 0.9 min constant 100% (B). Retention times of 1.28 min for CPX and 2.10 min for cinnarizin were constant. Mass spectra were acquired in multiple-reaction-monitoring mode, scanning for masses of 332 and 288 m/z. Chromatograms were analyzed and processed using TASQ 4.0 software.

Growth inhibition of Shigella flexneri

Bacteria were cultured in liquid conditions until late log or early stationary phase. In order to have similar conditions, *Shigella* was diluted to a final concentration of $2.2 \times 10^5 \pm 9.3 \times 10^4$ CFU/mL (89). One hundred millilitre of either loaded vesicles, vesicle dilution, control (sterile PBS) or free CPX was incubated with 100 µL bacterial suspension at 37°C overnight. Subsequently, colony-forming units were conducted, incubating samples at 30°C and counted after an overnight incubation.

Zebrafish husbandry

According to standard operating procedures, AB wild-type zebrafish were raised in Danieau's medium (17 mM NaCl, 2 mM KCl, 0.12 mM $MgSO_4$, 1.8 mM $Ca(NO_3)_2$, 1.5 mM HEPES, 1.2 µM methylene blue at pH 7.1-7.3) with continuous water circulation as described previously (90).

Toxicity evaluation of vesicles on zebrafish larvae

1dpf and 3dpf larvae were transferred to 96 well plates, with one larvae per well. Residual medium was removed and loaded vesicles (25 % in Danieau's), free CPX with different concentrations or PBS (25 % in Danieau's) as a control added to the well. Each day the moto function, heartbeat, pigmentation and overall appearance of the fish was monitored using a Stemi 508 KMAT (Zeiss). For the toxicity assessment after injection, 1dpf larvae were dechorinated with 1 mg/mL pronase (Sigma), washed in Danieau's and anesthetized with 0.25 mg/mL tricaine (Sigma). Samples or controls, mixed 1:1 with phenol red (Sigma) were injected into the blood island with a volume of 1.5 nL for a systemic administration, using a FemtoJet Microinjector (Eppendorf). Larvae were washed and transferred to 96 well plates to study toxicity. All larvae were sacrificed at 5dpf.

Development of a Shigella flexneri model in zebrafish larvae

1dpf larvae were dechorinated and anesthetized before they were infected with $6.6 \pm 2.6 \times 10^4$ CFU. Larvae were kept in 0.03 mg/mL 1-phenyl 2-thiourea (Sigma) in Danieau's. After 4 h, 24 h and 48 h fluorescence microscope (Leica MZ 10 F) images were taken. To conduct the *in vivo* growth of *Shigella*, larvae were washed twice with 100 µg/mL ampicillin in PBS and transferred to an Eppendorf tube with one glass bead. Larvae were vortexed for several minutes. The suspension was diluted accordingly and plated on ampicillin nutrient agar plates, where colony forming units were counted the next day.

Statistical analysis

Data is displayed as mean ± standard deviation (SD) and n as the number independent experiments. Statistical analysis was performed by applying One-way ANOVA followed by Tukey or Dunnett post-hoc tests, using SigmaPlot. Significant p-values were displayed either as the exact value, * for $p < 0.05$ or ** for $p < 0.01$ or *** for $p < 0.001$.

Author Contributions

E.H. conducted all experiments on RO-EVs, SB-OMVs isolation, characterization, biocompatibility testing and loading, bacterial growth inhibition, zebrafish toxicity assays and zebrafish *Shigella* infection. O.H. established the three-dimensional co-culture and help with confocal imaging. B.L. and C.M.L supervised and revised the three-dimensional co-culture model. C.W. quantified ciprofloxacin concentrations. M.K. took cryo-electron microscopy images. A.K.K. supervised and revised cytokine detection experiments. R.M. kindly provided myxobacterial strains and zebrafish larvae and advised on their culture and handling. G.F received the study, supervised the project and wrote the manuscript together with E.H.

Funding

This work was supported by the NanoMatFutur Junior Research programme from the Federal Ministry of Education and Research, Germany (grant number 13XP5029A, BEVA).

Notes

The authors declare no competing financial interests. Illustrations were created with BioRender.com.

Abbreviations

EVs extracellular vesicles, OMVs outer membrane vesicles, SEC size exclusion chromatography, IL interleukin, TNF tumor necrosis factor, CPX ciprofloxacin, TEER transepithelial electrical resistance, GI gastrointestinal

Acknowledgements

The authors would like to thank Ronald Garcia for providing SBSr073 myxobacterial cultures. Verena Qallaku for maintaining the zebrafish husbandry and providing fertilized eggs. Susanne Kirsch-Dahlem and Jennifer Herrmann for the support and introduction to the zebrafish facilities. Miriam Jaki for her help in determining physico-chemical differences between loaded and unloaded vesicles and Charlotte Dahlem for her help in PBMC isolation.

References

1. Browne KC, S.; Chen, R.; Willcox, M.D.; Black, D.S.; Walsh, W.R.; Kumar, N. . A New Era of Antibiotics: The Clinical Potential of Antimicrobial Peptides. Int J Mol Sci. 2020;21(7047).
2. Graham CJ. The global threat of antibiotic resistance: what can be done? Journal of Global Health Reports. 2017;1(e2017002).
3. Organization WH. Ten threats to global health in 2019 [
4. Kotloff KL, Riddle MS, Platts-Mills JA, Pavlinac P, Zaidi AKM. Shigellosis. The Lancet. 2018;391(10122):801-12.
5. Bardsley M, Jenkins C, Mitchell HD, Mikhail AFW, Baker KS, Foster K, et al. Persistent Transmission of Shigellosis in England Is Associated with a Recently Emerged Multidrug-Resistant Strain of Shigella sonnei. Journal of Clinical Microbiology. 2020;58(4):e01692-19.
6. Huh AJ, Kwon YJ. “Nanoantibiotics”: A new paradigm for treating infectious diseases using nanomaterials in the antibiotics resistant era. Journal of Controlled Release. 2011;156(2):128-45.
7. Ho D-K, Costa A, De Rossi C, de Souza Carvalho-Wodarz C, Loretz B, Lehr C-M. Polysaccharide Submicrocarrier for Improved Pulmonary Delivery of Poorly Soluble Anti-infective Ciprofloxacin: Preparation, Characterization, and Influence of Size on Cellular Uptake. Molecular Pharmaceutics. 2018;15(3):1081-96.
8. Anversa Dimer F, de Souza Carvalho-Wodarz C, Goes A, Cirnski K, Herrmann J, Schmitt V, et al. PLGA nanocapsules improve the delivery of clarithromycin to kill intracellular Staphylococcus aureus and Mycobacterium abscessus. Nanomedicine : nanotechnology, biology, and medicine. 2019.
9. Hua S, de Matos MBC, Metselaar JM, Storm G. Current Trends and Challenges in the Clinical Translation of Nanoparticulate Nanomedicines: Pathways for Translational Development and Commercialization. Frontiers in Pharmacology. 2018;9(790).

10. van Niel G, D'Angelo G, Raposo G. Shedding light on the cell biology of extracellular vesicles. Nature Reviews Molecular Cell Biology. 2018;19(4):213-28.
11. Théry C, Witwer KW, Aikawa E, Alcaraz MJ, Anderson JD, Andriantsitohaina R, et al. Minimal information for studies of extracellular vesicles 2018 (MISEV2018): a position statement of the International Society for Extracellular Vesicles and update of the MISEV2014 guidelines. Journal of Extracellular Vesicles. 2018;7(1):1535750.
12. Woith E, Fuhrmann G, Melzig MF. Extracellular Vesicles-Connecting Kingdoms. International journal of molecular sciences. 2019;20(22):5695.
13. Latifkar A, Hur YH, Sanchez JC, Cerione RA, Antonyak MA. New insights into extracellular vesicle biogenesis and function. Journal of Cell Science. 2019;132(13):jcs222406.
14. Robbins PD, Morelli AE. Regulation of immune responses by extracellular vesicles. Nature reviews Immunology. 2014;14(3):195-208.
15. Deatherage BL, Lara JC, Bergsbaken T, Barrett SLR, Lara S, Cookson BT. Biogenesis of bacterial membrane vesicles. Molecular Microbiology. 2009;72(6):1395-407.
16. Berleman JE, Allen S, Danielewicz MA, Remis JP, Gorur A, Cunha J, et al. The lethal cargo of Myxococcus xanthus outer membrane vesicles. Frontiers in Microbiology. 2014;5(474).
17. Schulz E, Goes A, Garcia R, Panter F, Koch M, Müller R, et al. Biocompatible bacteria-derived vesicles show inherent antimicrobial activity. Journal of Controlled Release. 2018;290:46-55.
18. Kim SW, Park SB, Im SP, Lee JS, Jung JW, Gong TW, et al. Outer membrane vesicles from β-lactam-resistant Escherichia coli enable the survival of β-lactam-susceptible E. coli in the presence of β-lactam antibiotics. Scientific Reports. 2018;8(1):5402.
19. Fulsundar S, Harms K, Flaten GE, Johnsen PJ, Chopade BA, Nielsen KM. Gene transfer potential of outer membrane vesicles of Acinetobacter baylyi and effects of stress on vesiculation. Applied and environmental microbiology. 2014;80(11):3469-83.
20. Kuehn AJMaMJ. Outer Membrane Vesicles. 2005.
21. Sil S, Dagur RS, Liao K, Peeples ES, Hu G, Periyasamy P, et al. Strategies for the use of Extracellular Vesicles for the Delivery of Therapeutics. 2019.
22. Zhu Y-z, Hu X, Zhang J, Wang Z-h, Wu S, Yi Y-y. Extracellular Vesicles Derived From Human Adipose-Derived Stem Cell Prevent the Formation of Hypertrophic Scar in a Rabbit Model. Annals of Plastic Surgery. 2020;84(5).
23. Medalla M, Chang W, Calderazzo SM, Go V, Tsolias A, Goodliffe JW, et al. Treatment with mesenchymal-derived extracellular vesicles reduces injury-related pathology in pyramidal neurons of monkey perilesional ventral premotor cortex EVs reduce injury-related pathology in vPMC. The Journal of Neuroscience. 2020:JN-RM-2226-19.
24. Pascucci L, Coccè V, Bonomi A, Ami D, Ceccarelli P, Ciusani E, et al. Paclitaxel is incorporated by mesenchymal stromal cells and released in exosomes that inhibit in vitro tumor growth: A new approach for drug delivery. Journal of Controlled Release. 2014;192:262-70.
25. Garofalo M, Saari H, Somersalo P, Crescenti D, Kuryk L, Aksela L, et al. Antitumor effect of oncolytic virus and paclitaxel encapsulated in extracellular vesicles for lung cancer treatment. Journal of Controlled Release. 2018;283:223-34.
26. Haney MJ, Klyachko NL, Zhao Y, Gupta R, Plotnikova EG, He Z, et al. Exosomes as drug delivery vehicles for Parkinson's disease therapy. Journal of Controlled Release. 2015;207:18-30.
27. Sun D, Zhuang X, Xiang X, Liu Y, Zhang S, Liu C, et al. A Novel Nanoparticle Drug Delivery System: The Anti-inflammatory Activity of Curcumin Is Enhanced When Encapsulated in Exosomes. Molecular Therapy. 2010;18(9):1606-14.
28. Fuhrmann G, Serio A, Mazo M, Nair R, Stevens MM. Active loading into extracellular vesicles significantly improves the cellular uptake and photodynamic effect of porphyrins. Journal of Controlled Release. 2015;205:35-44.
29. Tian Y, Li S, Song J, Ji T, Zhu M, Anderson GJ, et al. A doxorubicin delivery platform using engineered natural membrane vesicle exosomes for targeted tumor therapy. Biomaterials. 2014;35(7):2383-90.

30. li Z, ye X, Liu M, Xia C, Zhang L, Luo X, et al. A novel outer membrane β-1,6-glucanase is deployed in the predation of fungi by myxobacteria. The ISME Journal. 2019;13:1-13.
31. Tan K, Li R, Huang X, Liu Q. Outer Membrane Vesicles: Current Status and Future Direction of These Novel Vaccine Adjuvants. Frontiers in microbiology. 2018;9:783-.
32. Kadurugamuwa JL, Beveridge TJ. Membrane vesicles derived from Pseudomonas aeruginosa and Shigella flexneri can be integrated into the surfaces of other Gram-negative bacteria. Microbiology. 1999;145(8):2051-60.
33. Kadurugamuwa JL, Beveridge TJ. Delivery of the Non-Membrane-Permeative Antibiotic Gentamicin into Mammalian Cells by Using Shigella flexneri Membrane Vesicles. Antimicrob Agents Chemother. 1998;42(6):1476-83.
34. Gao F, Xu L, Yang B, Fan F, Yang L. Kill the Real with the Fake: Eliminate Intracellular Staphylococcus aureus Using Nanoparticle Coated with Its Extracellular Vesicle Membrane as Active-Targeting Drug Carrier. ACS Infectious Diseases. 2019;5(2):218-27.
35. Kuhn T, Koch M, Fuhrmann G. Probiomimetics—Novel Lactobacillus-Mimicking Microparticles Show Anti-Inflammatory and Barrier-Protecting Effects in Gastrointestinal Models. Small. 2020;16(40):2003158.
36. Goes A, Lapuhs P, Kuhn T, Schulz E, Richter R, Panter F, et al. Myxobacteria-Derived Outer Membrane Vesicles: Potential Applicability Against Intracellular Infections. Cells. 2020;9(1):194.
37. Gomes MC, Mostowy S. The Case for Modeling Human Infection in Zebrafish. Trends in Microbiology. 2019.
38. Préval Cd, Hadam MR, Mach B. Regulation of Genes for HLA Class II Antigens in Cell Lines from Patients with Severe Combined Immunodeficiency. New England Journal of Medicine. 1988;318(20):1295-300.
39. Schulz E, Karagianni A, Koch M, Fuhrmann G. Hot EVs – How temperature affects extracellular vesicles. European Journal of Pharmaceutics and Biopharmaceutics. 2020;146:55-63.
40. Lehrich BM, Liang Y, Fiandaca MS. Foetal bovine serum influence on in vitro extracellular vesicle analyses. Journal of Extracellular Vesicles. 2021;10(3):e12061.
41. Midekessa G, Godakumara K, Ord J, Viil J, Lättekivi F, Dissanayake K, et al. Zeta Potential of Extracellular Vesicles: Toward Understanding the Attributes that Determine Colloidal Stability. ACS Omega. 2020;5(27):16701-10.
42. Department of Health EaW, Public Health Service, Food and Drug Administration. Bacterial Endotoxins/ Pyrogens 2014 [Available from: https://www.fda.gov/inspections-compliance-enforcement-and-criminal-investigations/inspection-technical-guides/bacterial-endotoxinspyrogens.
43. Li Y, Boraschi D. Endotoxin contamination: a key element in the interpretation of nanosafety studies. Nanomedicine. 2016;11(3):269-87.
44. RUIZ C, RUIZ-BRAVO A, DE CIENFUEGOS GA, RAMOS-CORMENZANA A. Immunomodulation by Myxospores of Myxococcus xanthus. Microbiology. 1985;131(8):2035-9.
45. Shimkets LJ, Dworkin M, Reichenbach H. The Myxobacteria. In: Dworkin M, Falkow S, Rosenberg E, Schleifer K-H, Stackebrandt E, editors. The Prokaryotes: Volume 7: Proteobacteria: Delta, Epsilon Subclass. New York, NY: Springer New York; 2006. p. 31-115.
46. Gujrati V, Kim S, Kim S-H, Min JJ, Choy HE, Kim SC, et al. Bioengineered Bacterial Outer Membrane Vesicles as Cell-Specific Drug-Delivery Vehicles for Cancer Therapy. ACS Nano. 2014;8(2):1525-37.
47. Kleiveland CR. Peripheral Blood Mononuclear Cells. In: Verhoeckx K, Cotter P, López-Expósito I, Kleiveland C, Lea T, Mackie A, et al., editors. The Impact of Food Bioactives on Health: in vitro and ex vivo models. Cham: Springer International Publishing; 2015. p. 161-7.
48. Zhang J-M, An J. Cytokines, inflammation, and pain. Int Anesthesiol Clin. 2007;45(2):27-37.

49. Tisoncik JR, Korth MJ, Simmons CP, Farrar J, Martin TR, Katze MG. Into the eye of the cytokine storm. Microbiol Mol Biol Rev. 2012;76(1):16-32.
50. Swanson KV, Deng M, Ting JPY. The NLRP3 inflammasome: molecular activation and regulation to therapeutics. Nature Reviews Immunology. 2019;19(8):477-89.
51. Beez CM, Haag M, Klein O, Van Linthout S, Sittinger M, Seifert M. Extracellular vesicles from regenerative human cardiac cells act as potent immune modulators by priming monocytes. Journal of Nanobiotechnology. 2019;17(1):72.
52. Cecil JD, O'Brien-Simpson NM, Lenzo JC, Holden JA, Singleton W, Perez-Gonzalez A, et al. Outer Membrane Vesicles Prime and Activate Macrophage Inflammasomes and Cytokine Secretion In Vitro and In Vivo. Frontiers in immunology. 2017;8:1017-.
53. Avila-Calderón ED, Medina-Chávez O, Flores-Romo L, Hernández-Hernández JM, Donis-Maturano L, López-Merino A, et al. Outer Membrane Vesicles From Brucella melitensis Modulate Immune Response and Induce Cytoskeleton Rearrangement in Peripheral Blood Mononuclear Cells. Frontiers in Microbiology. 2020;11(2500).
54. Leonard F, Collnot E-M, Lehr C-M. A Three-Dimensional Coculture of Enterocytes, Monocytes and Dendritic Cells To Model Inflamed Intestinal Mucosa in Vitro. Molecular Pharmaceutics. 2010;7(6):2103-19.
55. Susewind J, de Souza Carvalho-Wodarz C, Repnik U, Collnot E-M, Schneider-Daum N, Griffiths GW, et al. A 3D co-culture of three human cell lines to model the inflamed intestinal mucosa for safety testing of nanomaterials. Nanotoxicology. 2016;10(1):53-62.
56. Bouwmeester H, Poortman J, Peters RJ, Wijma E, Kramer E, Makama S, et al. Characterization of Translocation of Silver Nanoparticles and Effects on Whole-Genome Gene Expression Using an In Vitro Intestinal Epithelium Coculture Model. ACS Nano. 2011;5(5):4091-103.
57. Chen S, Einspanier R, Schoen J. Transepithelial electrical resistance (TEER): a functional parameter to monitor the quality of oviduct epithelial cells cultured on filter supports. Histochem Cell Biol. 2015;144(5):509-15.
58. Rubio APD, Martínez J, Palavecino M, Fuentes F, López CMS, Marcilla A, et al. Transcytosis of Bacillus subtilis extracellular vesicles through an in vitro intestinal epithelial cell model. Scientific Reports. 2020;10(1):3120.
59. Peinado H, Alečković M, Lavotshkin S, Matei I, Costa-Silva B, Moreno-Bueno G, et al. Melanoma exosomes educate bone marrow progenitor cells toward a pro-metastatic phenotype through MET. Nat Med. 2012;18(6):883-91.
60. Janas AM, Sapoń K, Janas T, Stowell MHB, Janas T. Exosomes and other extracellular vesicles in neural cells and neurodegenerative diseases. Biochimica et Biophysica Acta (BBA) - Biomembranes. 2016;1858(6):1139-51.
61. Frühbeis C, Fröhlich D, Kuo WP, Amphornrat J, Thilemann S, Saab AS, et al. Neurotransmitter-Triggered Transfer of Exosomes Mediates Oligodendrocyte–Neuron Communication. PLOS Biology. 2013;11(7):e1001604.
62. Mehanny M, Koch M, Lehr C-M, Fuhrmann G. Streptococcal Extracellular Membrane Vesicles Are Rapidly Internalized by Immune Cells and Alter Their Cytokine Release. Frontiers in Immunology. 2020;11(80).
63. He C, Hu Y, Yin L, Tang C, Yin C. Effects of particle size and surface charge on cellular uptake and biodistribution of polymeric nanoparticles. Biomaterials. 2010;31(13):3657-66.
64. Moore TL, Urban DA, Rodriguez-Lorenzo L, Milosevic A, Crippa F, Spuch-Calvar M, et al. Nanoparticle administration method in cell culture alters particle-cell interaction. Scientific Reports. 2019;9(1):900.
65. Philpott D, Edgeworth J, Sansonetti P. The pathogenesis of Shigella flexneri infection: Lessons from in vitro and in vivo studies. Philosophical transactions of the Royal Society of London Series B, Biological sciences. 2000;355:575-86.
66. Gu B, Cao Y, Pan S, Zhuang L, Yu R, Peng Z, et al. Comparison of the prevalence and changing resistance to nalidixic acid and ciprofloxacin of Shigella between Europe–America and Asia–Africa from 1998 to 2009. International Journal of Antimicrobial Agents. 2012;40(1):9-17.

67. Ali SQ, Zehra A, Naqvi BS, Shah S, Bushra R. Resistance pattern of ciprofloxacin against different pathogens. Oman Med J. 2010;25(4):294-8.
68. Stewart MP, Langer R, Jensen KF. Intracellular Delivery by Membrane Disruption: Mechanisms, Strategies, and Concepts. Chem Rev. 2018;118(16):7409-531.
69. Carobolante G, Mantaj J, Ferrari E, Vllasaliu D. Cow Milk and Intestinal Epithelial Cell-Derived Extracellular Vesicles as Systems for Enhancing Oral Drug Delivery. Pharmaceutics. 2020;12(3):226.
70. Kooijmans SAA, Stremersch S, Braeckmans K, de Smedt SC, Hendrix A, Wood MJA, et al. Electroporation-induced siRNA precipitation obscures the efficiency of siRNA loading into extracellular vesicles. Journal of Controlled Release. 2013;172(1):229-38.
71. Pomatto MAC, Bussolati B, D'Antico S, Ghiotto S, Tetta C, Brizzi MF, et al. Improved Loading of Plasma-Derived Extracellular Vesicles to Encapsulate Antitumor miRNAs. Molecular Therapy - Methods & Clinical Development. 2019;13:133-44.
72. Huang W, Zhang Q, Li W, Yuan M, Zhou J, Hua L, et al. Development of novel nanoantibiotics using an outer membrane vesicle-based drug efflux mechanism. Journal of Controlled Release. 2020;317:1-22.
73. Yang X, Shi G, Guo J, Wang C, He Y. Exosome-encapsulated antibiotic against intracellular infections of methicillin-resistant Staphylococcus aureus. International journal of nanomedicine. 2018;13:8095-104.
74. Beal J, Farny NG, Haddock-Angelli T, Selvarajah V, Baldwin GS, Buckley-Taylor R, et al. Robust estimation of bacterial cell count from optical density. Communications Biology. 2020;3(1):512.
75. O'Donoghue EJ, Krachler AM. Mechanisms of outer membrane vesicle entry into host cells. Cellular microbiology. 2016;18(11):1508-17.
76. Kadurugamuwa JL, Beveridge TJ. Bacteriolytic effect of membrane vesicles from Pseudomonas aeruginosa on other bacteria including pathogens: conceptually new antibiotics. Journal of Bacteriology. 1996;178(10):2767-74.
77. Berleman J, Auer M. The role of bacterial outer membrane vesicles for intra- and interspecies delivery. Environmental Microbiology. 2013;15(2):347-54.
78. Wang Z, Ma Y, Khalil H, Wang R, Lu T, Zhao W, et al. Fusion between fluid liposomes and intact bacteria: study of driving parameters and in vitro bactericidal efficacy. International journal of nanomedicine. 2016;11:4025-36.
79. Sieber S, Grossen P, Detampel P, Siegfried S, Witzigmann D, Huwyler J. Zebrafish as an early stage screening tool to study the systemic circulation of nanoparticulate drug delivery systems in vivo. Journal of Controlled Release. 2017;264:180-91.
80. Matsuda A, Moirangthem A, Angom RS, Ishiguro K, Driscoll J, Yan IK, et al. Safety of bovine milk derived extracellular vesicles used for delivery of RNA therapeutics in zebrafish and mice. Journal of Applied Toxicology. 2020;40(5):706-18.
81. Shen R, Yu Y, Lan R, Yu R, Yuan Z, Xia Z. The cardiovascular toxicity induced by high doses of gatifloxacin and ciprofloxacin in zebrafish. Environmental Pollution. 2019;254:112861.
82. Zhang Y, Wang X, Yin X, Shi M, Dahlgren RA, Wang H. Toxicity assessment of combined fluoroquinolone and tetracycline exposure in zebrafish (Danio rerio). Environmental Toxicology. 2016;31(6):736-50.
83. Mostowy S, Boucontet L, Mazon Moya MJ, Sirianni A, Boudinot P, Hollinshead M, et al. The Zebrafish as a New Model for the In Vivo Study of Shigella flexneri Interaction with Phagocytes and Bacterial Autophagy. PLOS Pathogens. 2013;9(9):e1003588.
84. Chang CT, Doerr KM, Whipps CM. Antibiotic treatment of zebrafish mycobacteriosis: tolerance and efficacy of treatments with tigecycline and clarithromycin. J Fish Dis. 2017;40(10):1473-85.
85. Faikoh EN, Hong Y-H, Hu S-Y. Liposome-encapsulated cinnamaldehyde enhances zebrafish (Danio rerio) immunity and survival when challenged with Vibrio vulnificus and Streptococcus agalactiae. Fish & Shellfish Immunology. 2014;38(1):15-24.
86. Zhang X, Song J, Klymov A, Zhang Y, de Boer L, Jansen JA, et al. Monitoring local delivery of vancomycin from gelatin nanospheres in zebrafish larvae. International journal of nanomedicine. 2018;13:5377-94.

87. Fenaroli F, Westmoreland D, Benjaminsen J, Kolstad T, Skjeldal FM, Meijer AH, et al. Nanoparticles as Drug Delivery System against Tuberculosis in Zebrafish Embryos: Direct Visualization and Treatment. ACS Nano. 2014;8(7):7014-26.
88. Gudbergsson JM, Jønsson K, Simonsen JB, Johnsen KB. Systematic review of targeted extracellular vesicles for drug delivery - Considerations on methodological and biological heterogeneity. J Control Release. 2019;306:108-20.
89. Wiegand I, Hilpert K, Hancock REW. Agar and broth dilution methods to determine the minimal inhibitory concentration (MIC) of antimicrobial substances. Nature Protocols. 2008;3:163.
90. Richter LHJ, Herrmann J, Andreas A, Park YM, Wagmann L, Flockerzi V, et al. Tools for studying the metabolism of new psychoactive substances for toxicological screening purposes - A comparative study using pooled human liver S9, HepaRG cells, and zebrafish larvae. Toxicol Lett. 2019;305:73-80.

Supplementary Information

A biocompatible carrier system against GI infections: Ciprofloxacin loaded Extracellular Vesicles inhibit the growth of *Shigella flexneri*

Eilien Heinrich, Olga Hartwig, Christine Walt, Marcus Koch, Alexandra K. Kiemer, Brigitta Loretz, Claus-Michael Lehr, Rolf Müller and Gregor Fuhrmann*

Figure S 1. RO cell culture during vesicle isolation
Figure S 2. Physico-chemical characteristics of RO-EVs and SB-OMVs.
Figure S 3. Surface marker identification of RO-EVs
Figure S 4. Gel clot endotoxin test
Figure S 5. Cytokine concentrations of PBMC incubated with SB-OMVs and RO-EVs normalized to cytokine concentration after LPS exposure.
Figure S 6. TEER values of the healthy and inflamed co-culture after vesicle or control incubation.
Figure S 7. Zoom in of the 3D co-culture exposed to SB-OMVs.
Figure S 8. Vesicle positive macrophages.
Figure S 9. Mono-cultures of dendritic cells in a 3D model.
Figure S 10. Different methods to remove free CPX.
Figure S 11. Cryo-electron microscopy of native and loaded RO-EVs.
Figure S 12. Cryo-electron microscopy of native and loaded SB-OMVs.
Figure S 13. Difference in physico-chemical properties after loading.
Figure S 14. Maximal tolerated concentration on 1dpf or 3dpf zebrafish larvae.
Figure S 15. Danio rerio larvae exposed to different concentration of ciprofloxacin.
Figure S 16. Danio rerio larvae exposed to vesicles at 1dpf, 3dpf or injected into the blood island at 1dpf.
Figure S 17. Infected larvae treated with 1000 x MIC CPX.

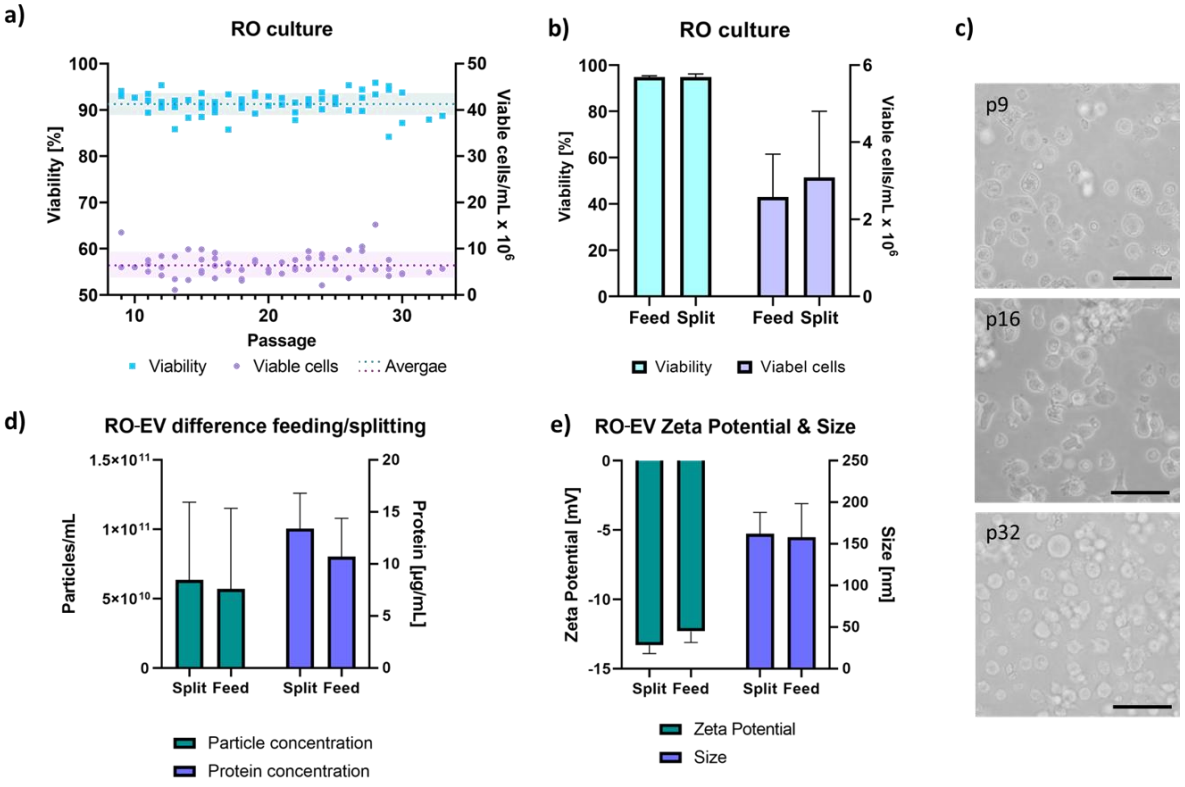

Figure S 1 RO cell culture during vesicle isolation. a) Cell viability and cell count from passage 8 to 35. b) Average cell viability and viable cell count on feeding and splitting days, before vesicle isolation. c) Microscopic images of different passages of RO cells. Scale bar 50 µm d) Difference of RO-EVs in particle concentration and protein concentration when isolated on a feeding or splitting day. e) Difference in zeta potential and size between RO-EVs isolated on a feeding or splitting day.

a)

Vesicle type	Protein/vesicle [µg/particle × 10^{-10}] n = 6 - 7	Size [nm] n = 6 - 7	Zeta potential [mV] n = 3 - 6
SB-OMVs	3.6 ± 2.9	194.0 ± 18.2	-6.8 ± 0.6
RO-EVs	6.5 ± 1.5	160.1 ± 2.0	-12.8 ± 0.5

b)

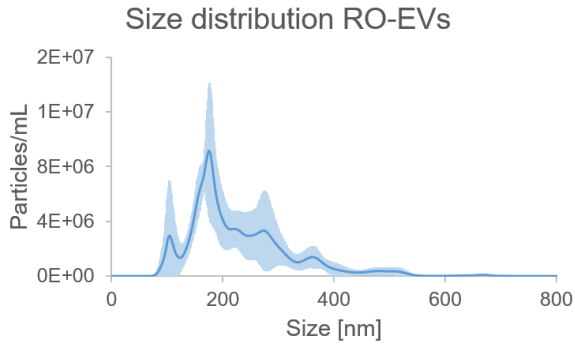

c)

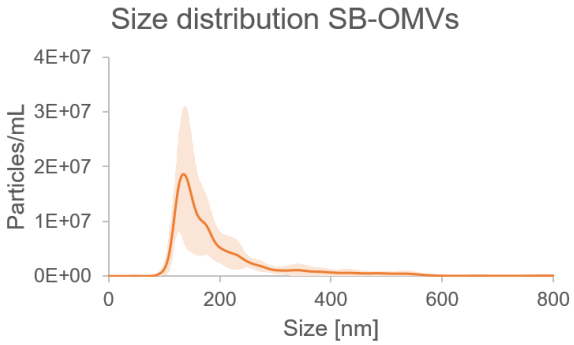

Figure S 2 Physico-chemical characteristics of RO-EVs and SB-OMVs. The protein concentration was measured using a bicinchoninic assay kit, the zeta potential using a zetasizer and the size as well as the size distribution using nanoparticle tracking analysis.

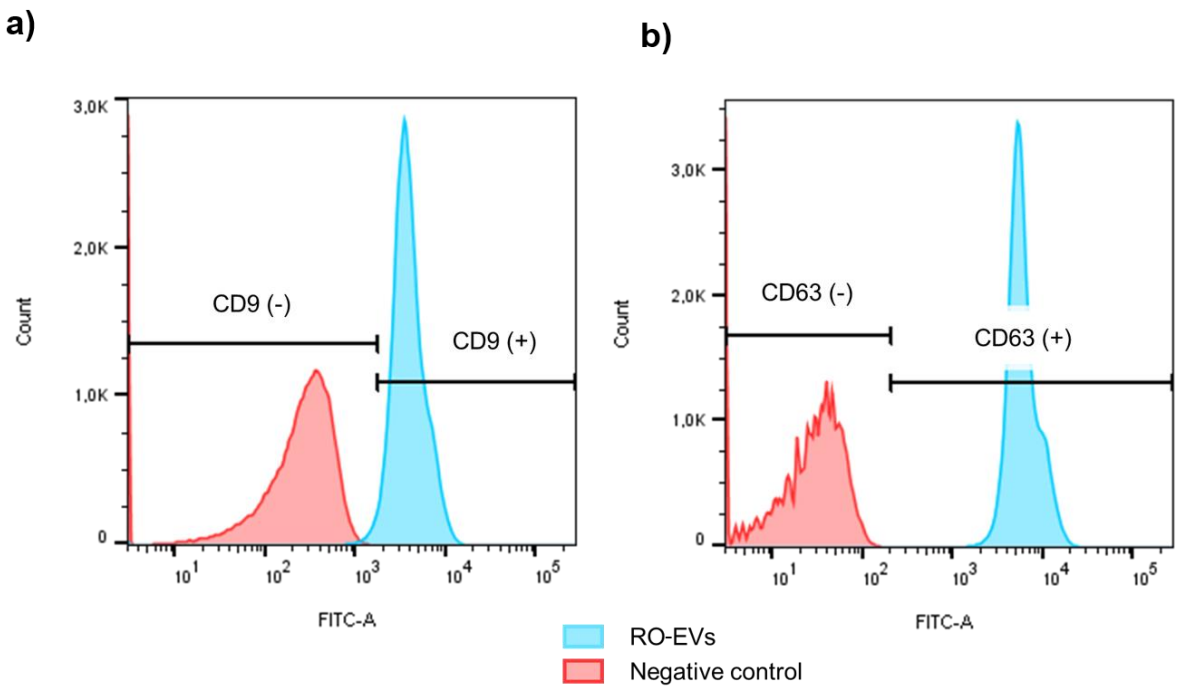

Figure S 3 Surface marker identification of RO-EVs. a) Detection of CD9 b) Detection of CD63 using flow cytometry and latex aldehyde beads (Richter et al. manuscript submitted)

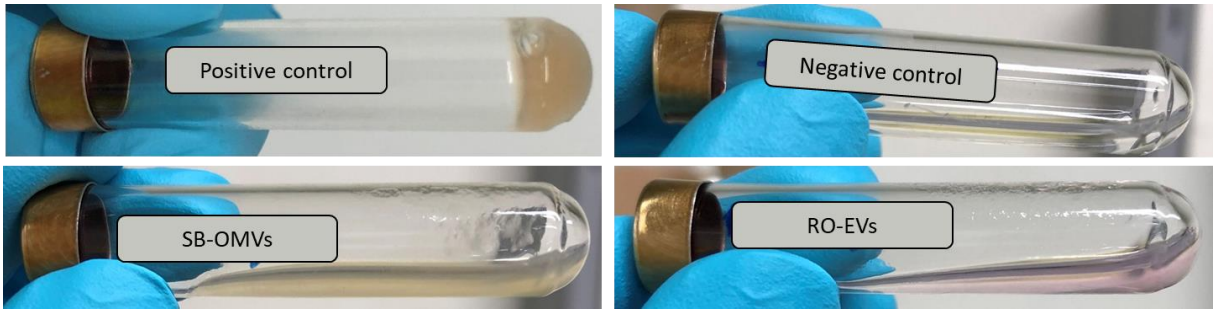

Figure S 4 Gel clot endotoxin test. Vesicles pellets did not show any firm gel formation, similar to the negative control.

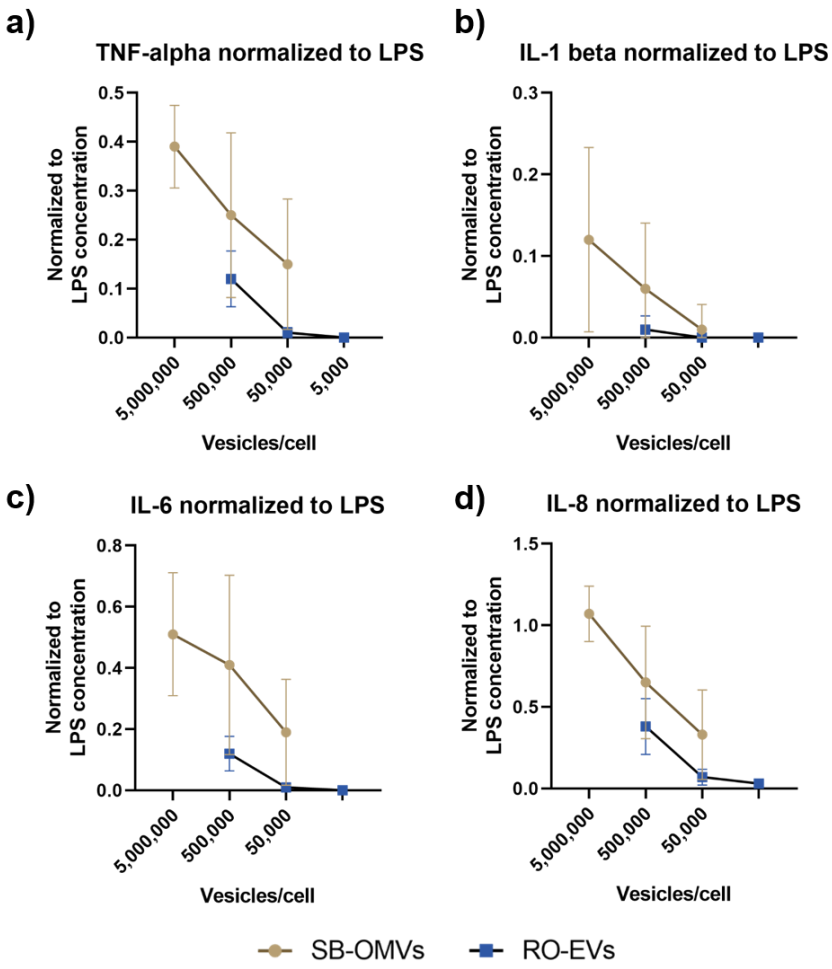

Figure S 5 Cytokine concentrations of PBMC incubated with SB-OMVs and RO-EVs normalized to cytokine concentration after LPS exposure.

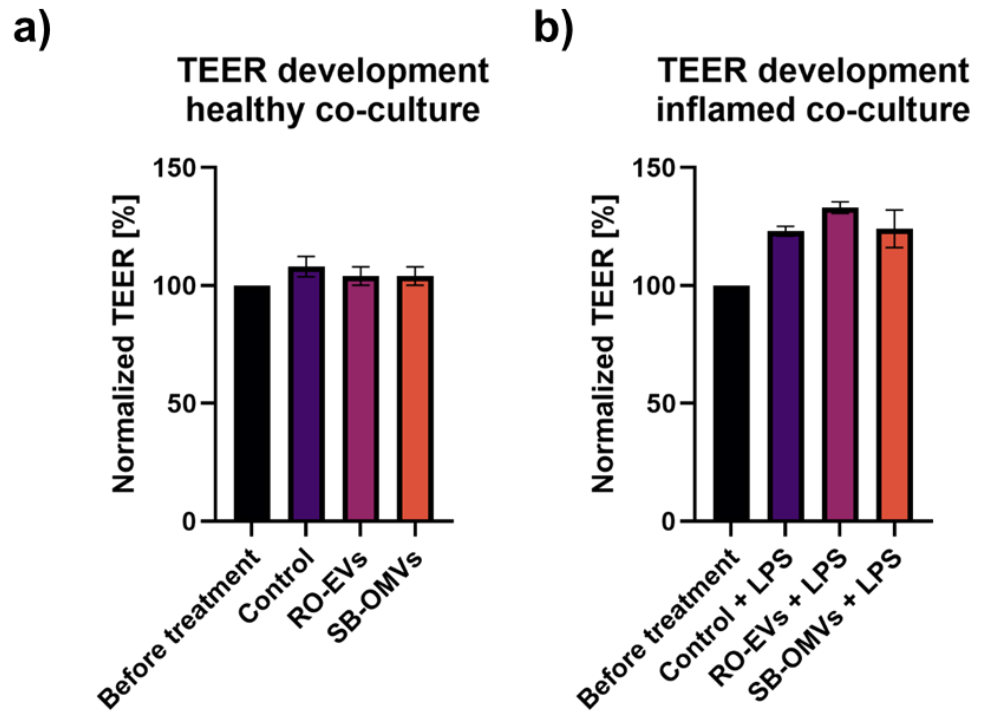

Figure S 6 TEER values of the healthy and inflamed co-culture after vesicle or control incubation. Values were normalized to TEER values before the treatment. n = 2, N = 3

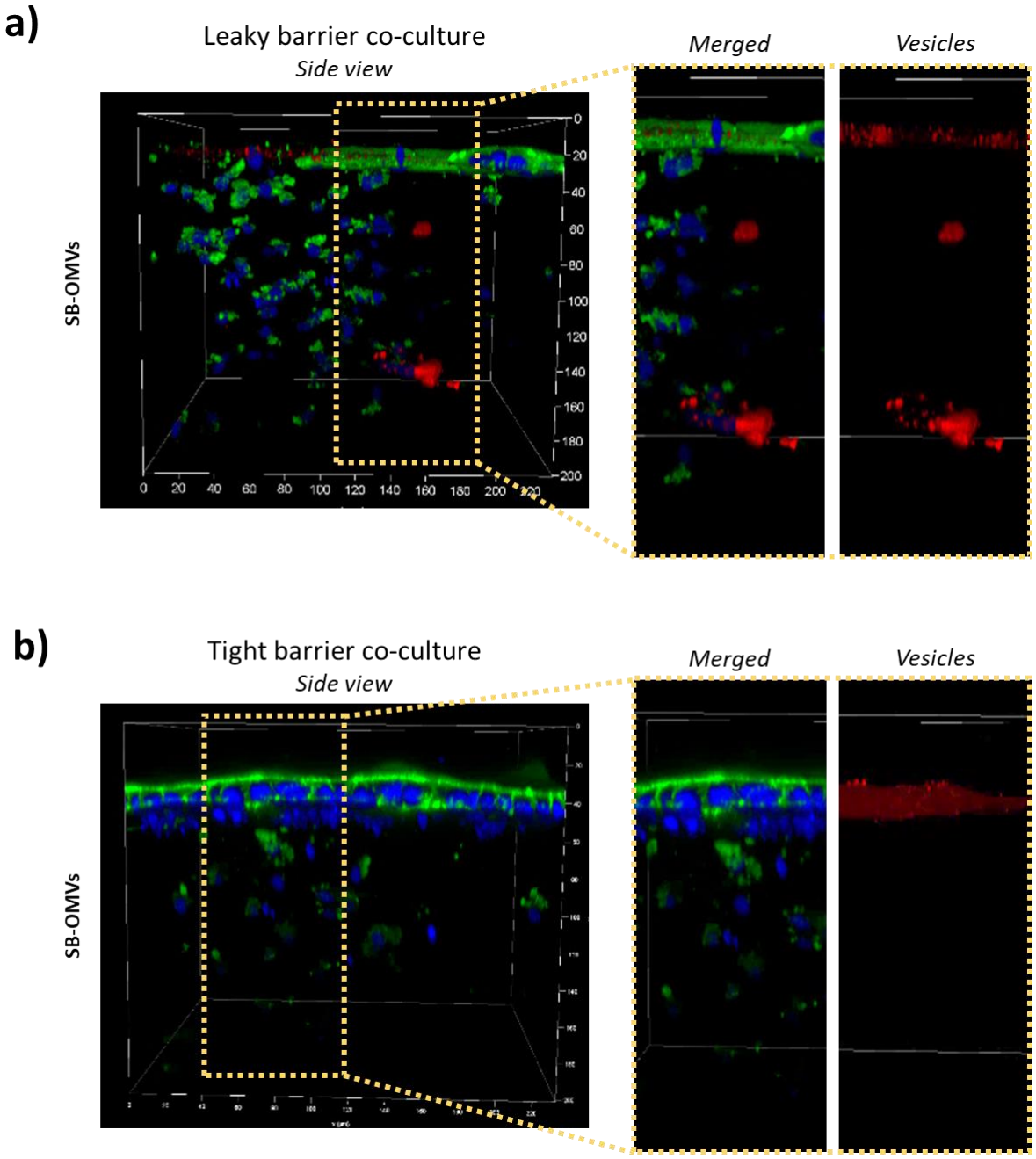

Figure S 7 Zoom in of the 3D co-culture exposed to SB-OMVs. a) Leaky epithelial barrier revealed vesicle positive immune cells b) No vesicle positive cells were detected in the tight barrier model.

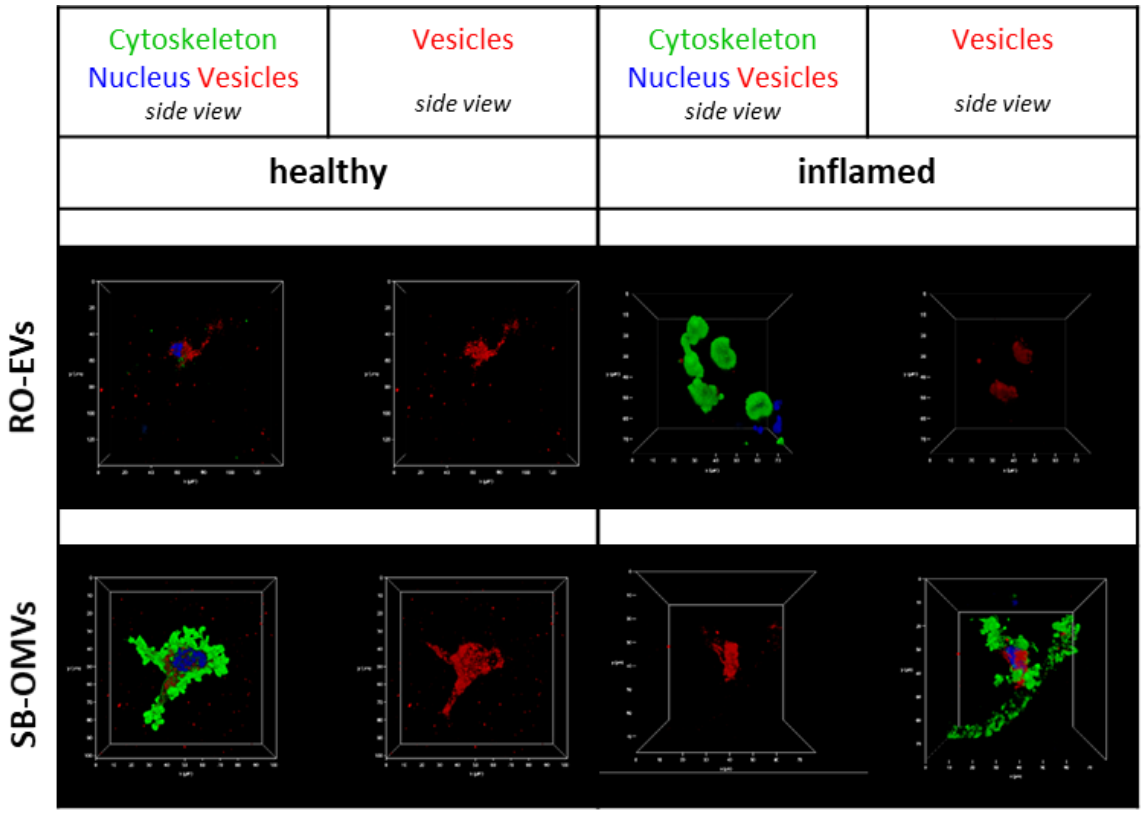

Figure S 8 Vesicle positive macrophages. Images were taken using confocal scanning microscopy. The cytoskeleton was labeled using FITC-phalloidin, DAPI for labeling the nucleus and the vesicles were stained using DiI.

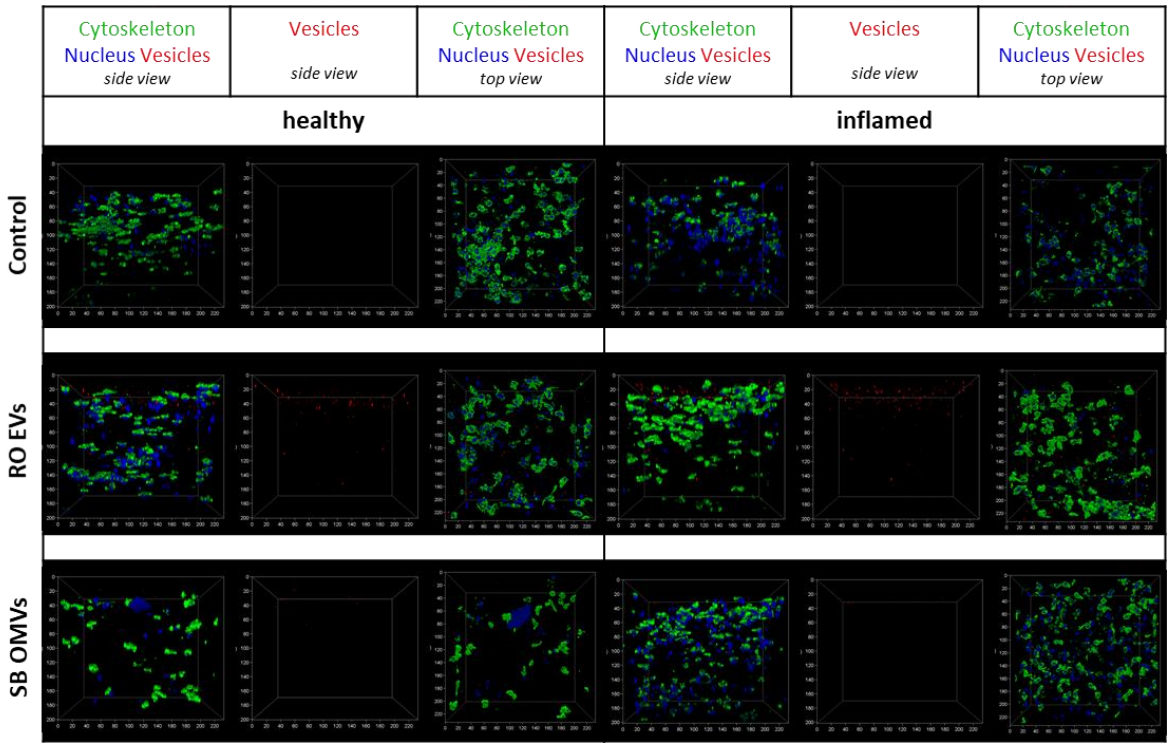

Figure S 9 Mono-cultures of dendritic-like cells in a 3D model. Confocal scanning microscopy revealed no vesicles positive cells as no co-localization was seen.

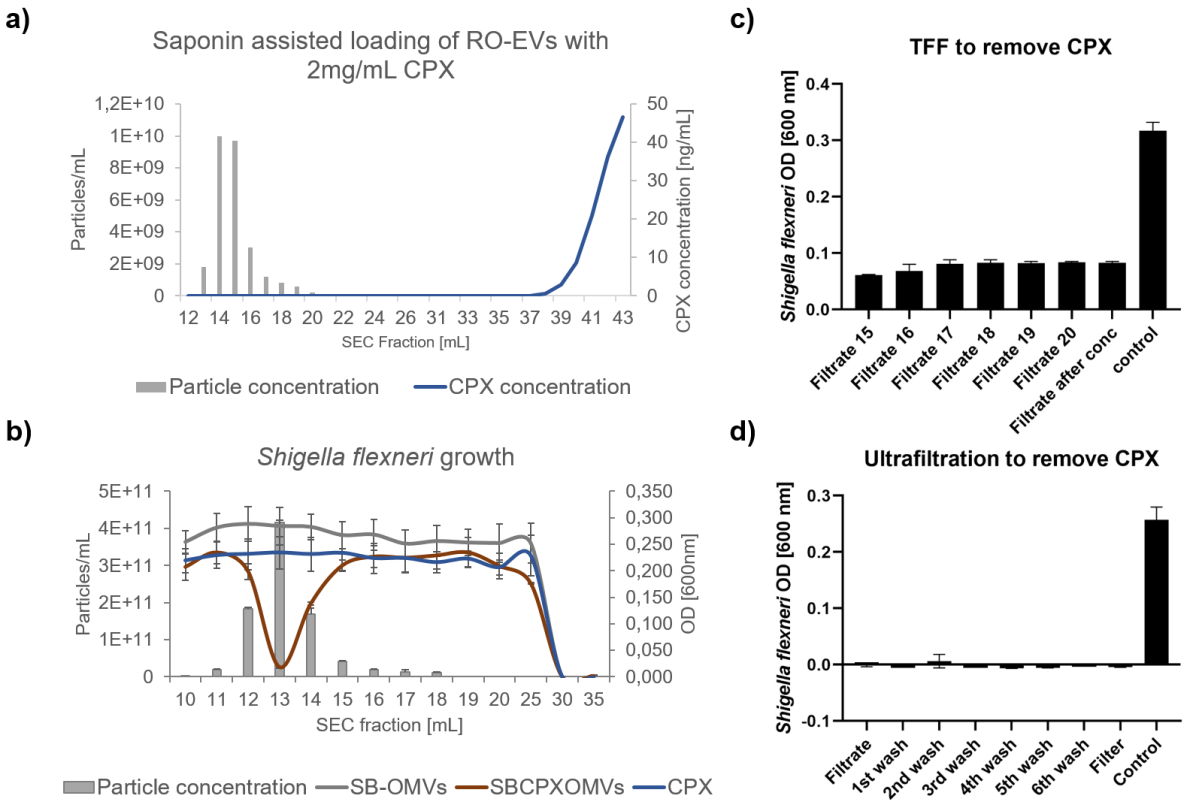

Figure S 10 Different methods to remove free CPX. a) Loading RO-EVs with 2 mg/mL CPX was not successful, as no CPX in vesicles could be quantified b) Growth inhibition of *Shigella flexneri* using SB-OMVs, SB_{CPX}OMVs and CPX loaded onto a SEC column and their respective collected fractions c) Removal of CPX using tangential flow field fractionation. Collected filtrates after several washing steps with 20 mL PBS were still able to inhibit the growth of *Shigella*, thus free CPX was still present. d) Removal of CPX using ultrafiltration. Collected filtrates of washing steps still inhibited the growth of *Shigella*.

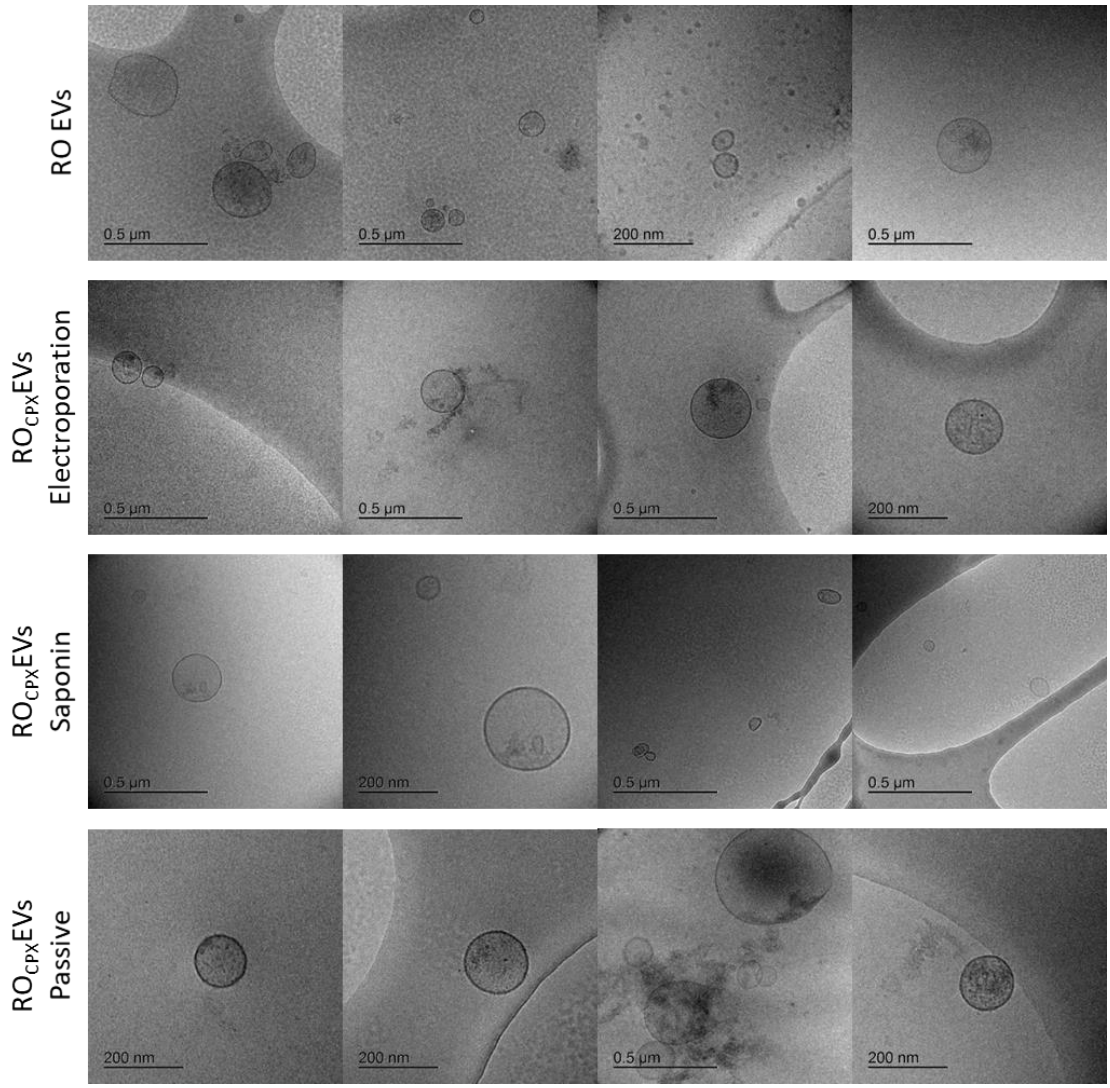

Figure S 11 Cryo-electron microscopy of native and loaded RO-EVs.

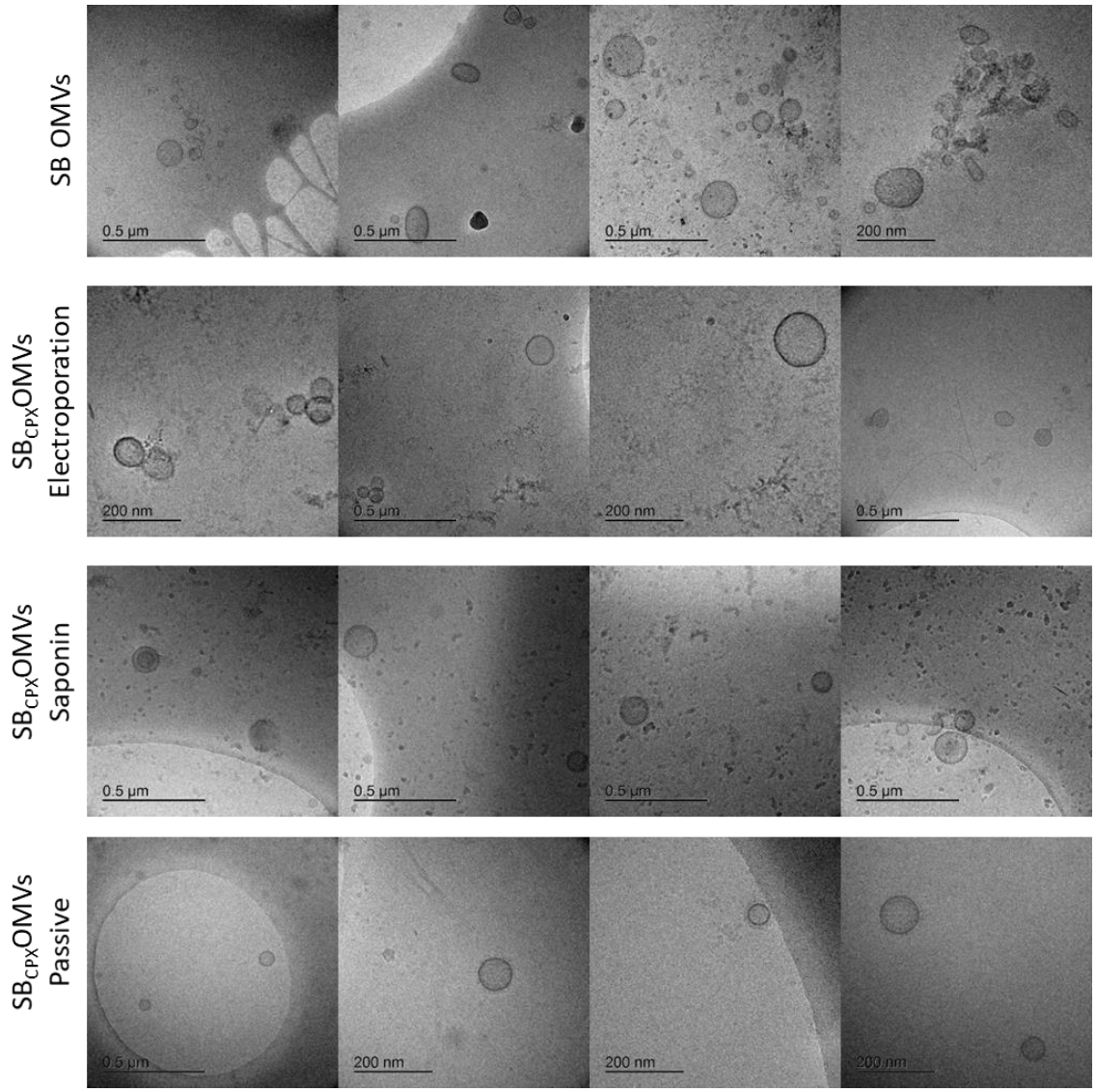

Figure S 12 Cryo-electron microscopy of native and loaded SB-OMVs.

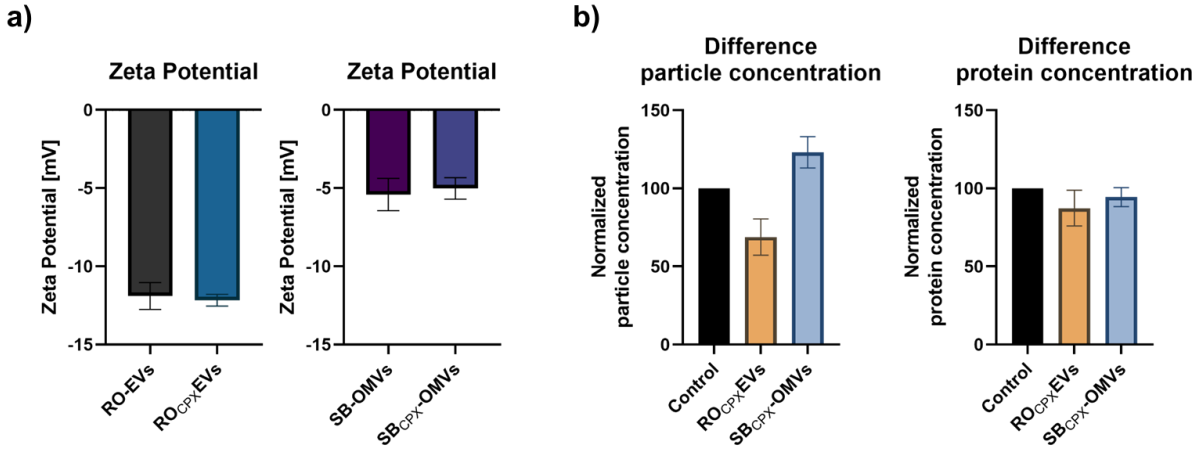

Figure S 13 Difference in physico-chemical properties after loading. a) Difference in zeta potential normalized to unloaded vesicles b) Difference in particle concentration and protein concentration normalized to respective unloaded vesicle types.

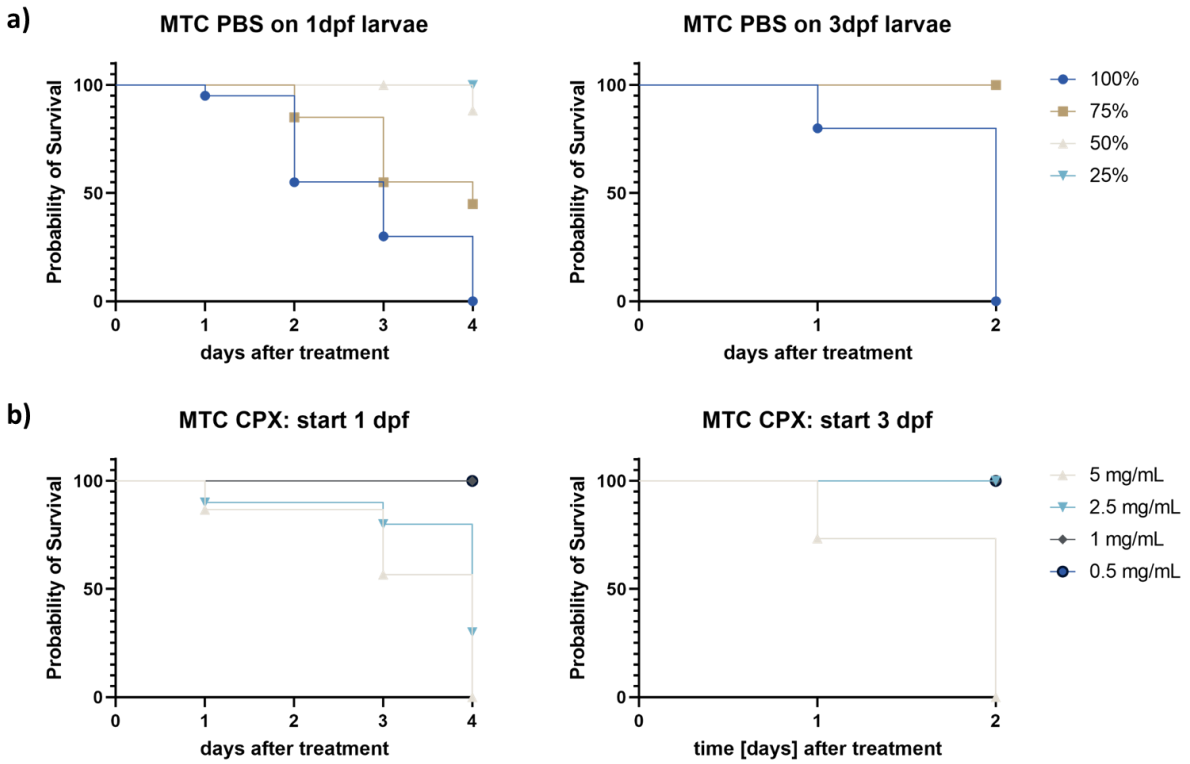

Figure S 14 Maximal tolerated concentration on 1dpf or 3dpf zebrafish larvae. a) Survival of larvae incubated with different concentration of PBS in water b) survival of larvae incubated with different concentration of ciprofloxacin in water. n = 3, N = 10

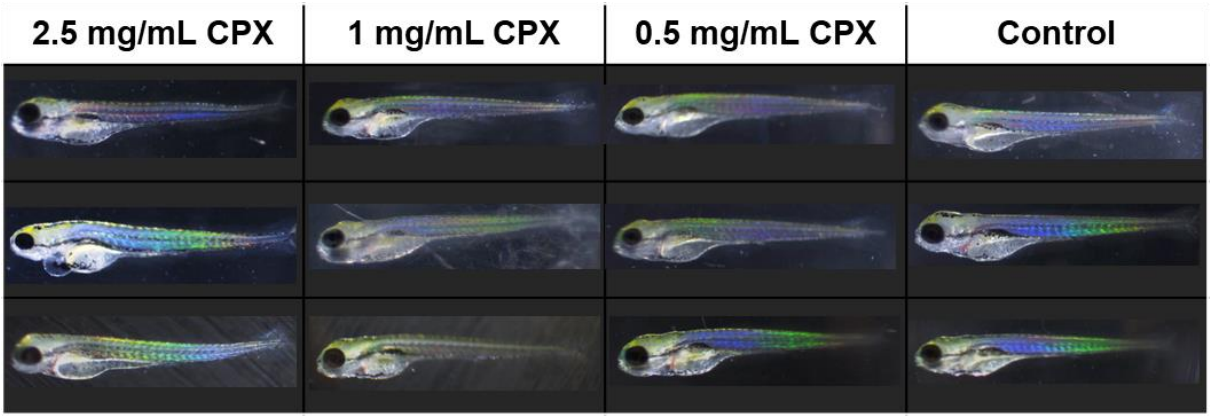

Figure S 15 *Danio rerio* larvae exposed to different concentration of ciprofloxacin.

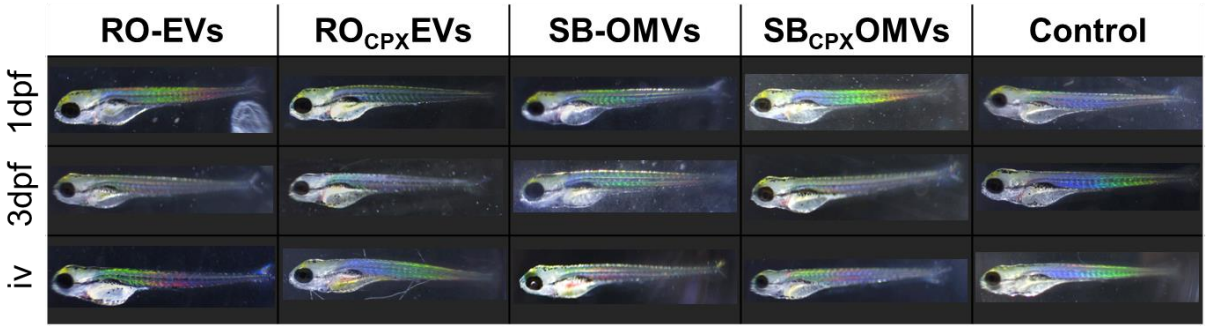

Figure S 16 *Danio rerio* larvae exposed to vesicles at 1dpf, 3dpf or injected into the blood island at 1dpf.

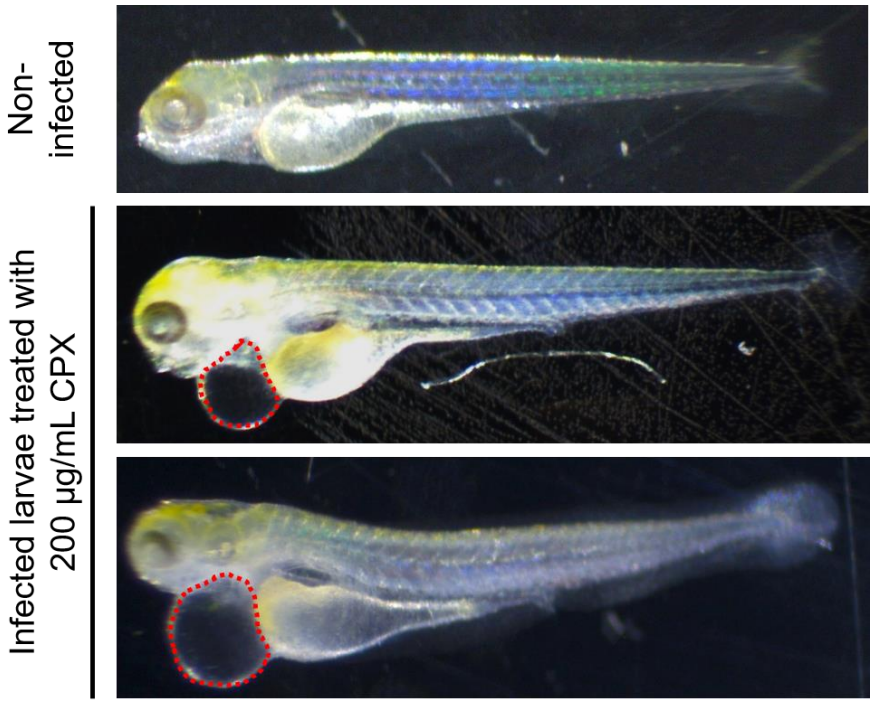

Figure S 17 Infected larvae treated with 1000 x MIC CPX. After 4 h of infection, larvae were treated with 200 µg/mL CPX. After 24 h no infection was observed, however, after 3 days at 5dpf all larvae developed heart edema, whereas the control (not infected larvae treated with 1000 x MIC of CPX) showed no abnormalities.

8. Acknowledgements

After three years of hard work, I would like to express my gratitude to all the people who made this project possible and supported me throughout the entire process.

I would like to thank my supervisor Junior Prof. Dr. Gregor Fuhrmann, who trusted me with this great project and gave me the opportunity to work in his group. He always supported me and my ideas and encouraged, as well as inspired me to think out of the box.

Further, I would like to thank the whole BION team, especially my fellow PhD colleagues, Adriely Goes, Thomas Kuhn, Maximilian Richter, Cristina Zivko and Mina Mehanny. Thank you for all your support, helpful ideas and just for listening when I needed someone to talk to. I will genuinely treasure the memories of decorating the Christmas tree, having dinner together, discussing the newest Netflix series and chatting in our gossip office. My special thanks goes to Adriely Goes, who supported me in the bacterial culture, Dr. Kathrin Fuhrmann who performed the viability assays and Anna Karagianni, who worked tremendously on studying the impact of heat on the vesicles.

Moreover, I would like to thank Prof. Dr. Rolf Müller for co-supervising this work, his input from a different perspective and helpful ideas. Dr. Ronald Garcia, who supplied me with new myxobacteria and for the support in maintaining their culture. Dr. Susanne Kirsch-Dahmen and Dr. Jennifer Herrmann for their support with the zebrafish; Sari Rasheed, Felix Deschner and Anastasia Andreas, who introduced me to the zebrafish facility and showed me the particulars in handling them. Special thanks goes to Christine Walt, who always managed to measure ciprofloxacin concentrations. I also want to thank Stephanie Schmidt for her support and help from the very beginning.

I also want to thank Prof. Dr. Alexandra Kiemer, Dr. Jessica Hoppstädter and Dr. Charlotte Dahlem, who helped design and perform the cytokine and PBMC assays. Moreover, I would like to thank Marcus Koch at INM for taking great cryo-EM images of the vesicles.

I would like to express my gratitude to the entire DDEL team for their help and support throughout these three years. At this point, I especially thank Jana Westhues and Petra König, who took care of my cells, when I could not, who always had an open ear when I needed help and who continuously supplied me with sweets and pasta. Special thanks goes to the girls team, Jana Westhues, Rebekka Christmann and Olga Hartwig. They always made me smile and I am grateful to call them friends. Moreover, I especially would like to thank Olga for her inspirations, contagious enthusiasm in confocal microscopy and attributing the co-culture to this work.

I would also like to thank the excellence program for women in science for introducing me to extraordinary and inspiring women.

Zum Schluss möchte ich noch meiner Familie danken, vor allem meinen Eltern. Vielen Dank an meinem Vater, der mich von klein auf an für Naturwissenschaften begeistern konnte und der nie die Geduld mit mir verloren hat. Ich danke auch meiner Mutter, die immer ein offenes Ohr für mich hat und die mich stets motiviert mein Bestes zu geben. Zu guter Letzt danke ich meinem Ehemann. Er hat mich von Anfang an unterstützt diesen Weg zu gehen. Er bringt mich jeden Tag zum Lachen und zeigt mir die Welt von einer ganz besonderen Seite.